UNIVERSITY OF CALIFORNIA

SANTA CRUZ

LIGHT-OXYGEN-VOLTAGE (LOV) DOMAINS FROM *ERYTHROBACTER LITORALIS*, A BIOCHEMICAL AND PHOTOCHEMICAL STUDY

A dissertation submitted in partial satisfaction
Of the requirement for the degree of

DOCTOR OF PHILOSOPHY
in

CHEMISTRY AND BIOCHEMISTRY

by

Farzin Bolourchian

June 2014

The Dissertation of Farzin Bolourchian
is approved:

_____
Professor Roberto Bogomolni, Advisor

_____
Professor Glenn Millhauser, Chair

_____
Professor David Kliger

_____
Tyrus Miller
Vice Provost and Dean of Graduate Studies

Table of Contents

LIST OF FIGURES

INTRODUCTION

CHAPTER 1

CHAPTER 2

CHAPTER 3

CHAPTER 4

ABSTRACT

LIGHT-OXYGEN-VOLTAGE (LOV) DOMAINS FROM *ERYTHROBACTER LITORALIS*, A BIOCHEMICAL AND PHOTOCHEMICAL STUDY

Farzin Bolourchian

Sunlight powers all living things on earth, either directly or indirectly. Plants use light for photosynthesis and pass on the energy to animals that consume them. In order to use light to manufacture food or signal other processes, living beings have to sense and react to light and they do this with a variety of photoreceptors that are sensitive to different spectrum of light. Many studies have been done on the plant photoreceptors and although the list is still incomplete, several have been identified and characterized. Phytochromes absorb mainly red/far-red light with some shown to even respond to UV-A/blue light. The main purpose of this study is to focus on blue light sensing segment of phototropin called LOV2 (in plants) and simply LOV domain in bacteria. We follow the light activation of LOV-HTH domain of *Erythrobacter Litoralis* bacterium and follow the events upon light activation using many spectroscopic tools available to study such event. It is the aim of this study to show that upon light activation, movement of a segment of this molecule causes LOV domain to activate the effector domain downstream. The kinetics of adduct formation and dark state relaxation of the other two LOV domains in this bacterium named EL346 and EL368 are also studied.

This thesis is dedicated to my beloved parents Mohammad Ali and Khanomtaj, my brother Ramin, my wife Farnaz, and my greatly indebted mentor, Professor Roberto Bogomolni

Acknowledgments:

I consider myself very fortunate to have been able to spend my years as a graduate student with great scientists that I admire and look up to. They provided an environment that helped me grow as a person and as a scientist. The main reason I consider myself so fortunate is being mentored by Dr. Roberto Bogomolni. I cannot express my true appreciation of the amount of support, help and knowledge he has given me during my time here at UCSC and completion of this thesis is my way of thanking him. He is always calm, patient and supportive of his students which is priceless as you deal with the stress of the graduate school. His great knowledge of spectroscopy and passion about science makes him an amazing mentor to have. I was also fortunate to learn from one of the great scientists of our time, Dr. Winslow Briggs of the Carnegie Institute of Washington at Stanford. I have the deepest appreciation for his invaluable guidance and support and for allowing me the pleasure to work in his lab. His enthusiasm and love of science is infectious and although he had no obligation to be my mentor, he treated me as one of his students and offered guidance and help whenever I asked him. You always feel great about what you are doing whenever you are around Dr. Briggs.

There are several great scientists that I need to thank for their help and mentorship. My committee members, Professor David Kliger and Professor Glenn Millhauser were great advisors and I am fortunate to have had their guidance. Dr. Jim Lewis offered his time, his spectroscopy equipment and his expertise to help me with

much of the work in this thesis. Dr. Istvan Szundi thought me kinetic data analysis which required a lot of his time and it is much appreciated. Dr. Hokenson and Dr. Swartz taught me how to do research and be a successful graduate student. Dr. Swartz was always more than willing to explain techniques and listen to ideas and really helped me prepare for my orals. Dr. Tong-Seung Tseng is an amazing biologist at Stanford that taught me molecular biology techniques. I also like to thank our collaborators; Dr. Heyn and Dr. Hoersch for their time and help. I also want to thank Professor Tom Schleich, Professor Bakthan Singaram, Dr. Eefei Chen, Dr. Chie Funatogawa, and Dr. Ruby Chan.

Finally, I would like to give thanks to my family and friends who each helped me greatly during my years as graduate student. I want to thank my father, Mohammad Ali Bolourchian and mother, Khanomtaj Shahinzad for their encouragement, love and never ending support. I want to thank my brother, Ramin Bolourchian for his love and support that made this possible for me. I want to thank my wife, Farnaz Abrishami who cheered, supported and loved me through this process. I also want to thank Jessica Jonoud for reading the thesis and helping me edit it.

Thank you from bottom of my heart, advisors, colleagues, friends, and family. You support and encouragement made not only all of this possible, it also made the journey fun and valuable. Thank you.

GENERAL INTRODUCTION

Historical Background

Light is a source of energy and information for all living things. Plants and some bacteria have evolved to harvest the rich energy of light in a highly regulated process. They have also developed photosensory systems that detect the light for other processes such as solar tracking, leaf expansion, phototropism (directional growth toward the light source), chloroplast movement, and stomatal opening. Since plants use the light directly, they have been the subject of study for many years and a diverse group of photosensory proteins have been discovered and studied over the years. Some of the first findings that focused on the blue light response in higher plants are as early as year 1817 [1]. In a paper by Sebastiano Peggioli, he reported that certain colors of light might be more favorable for the growth of *Mimosa Pudica*. Several other papers came along the way that measured the intensity of light needed as well as the spectrum of light required for growth, movement, and water loss in plants. In 1880, Charles Darwin had noted: "no one can look at the plants growing on a bank or on the borders of a thick wood, and doubt that the young stems and leaves place themselves so that the leaves may be well illuminated" [2]. Francis Darwin in 1898 showed that blue light had an effect on stomatal opening [1] but his work was not followed for many more years by any scientists. The story of blue light though became very interesting during the study of phototropism. The earliest work regarding blue light was reported by Blaaun in 1909 that concluded the 466nm and 478nm as the best wavelength for causing phototropism in *Oat Coleoptiles* [3].

Phototropism is unique because carotenoids could be excluded as a photosensor from it but not others, since carotenoids are present in both the stomatal opening and the chloroplast movement. The evolution of this field of study was with much controversy and disagreement. Based on the action spectra, it was first thought and reported by Galston and Baker in 1949 that riboflavin was responsible for phototropism [4], but Briggs demonstrated in 1957 that riboflavin did not affect the total amount of plant growth hormone, auxin [5]. The Winslow Briggs experiments, without intending to do so fueled the "flavin/carotenoid controversy" by excluding the riboflavin and therefore leaving the carotenoid as the only other possible alternative. Thimann and Curry produced a high resolution action spectra for the curvature of Avena Coleoptiles [6] in 1960 that showed maximum at 420, 445, and 475nm and a peak at 365nm (fig I-1). This action spectrum containing the 365 nm peak did not end the controversy but restored the flavins as possible receptors and helped guide the successful search for a blue light receptor responsible for the action.

It was the discovery of *Arabidopsis* mutants that lacked phototropism by Liscum and Briggs in 1995 [7] that helped isolate the receptor responsible. Using the same *Arabidopsis* mutants, John Christie identified the gene responsible [8], then cloned it and purified the receptor protein, later named phototropin [9], which contained two LOV domains and a Ser/Thr Kinase (fig I-2). A component of the identified protein named LOV (**L**ight, **O**xygen, and **V**oltage) which non-covalently binds to Flavin-mono-nucleotide (FMN) molecule is the photoreceptor for

phototropism. Phototropin was later named phototropin 1 (phot1) when a second one was discovered and was named phot2.

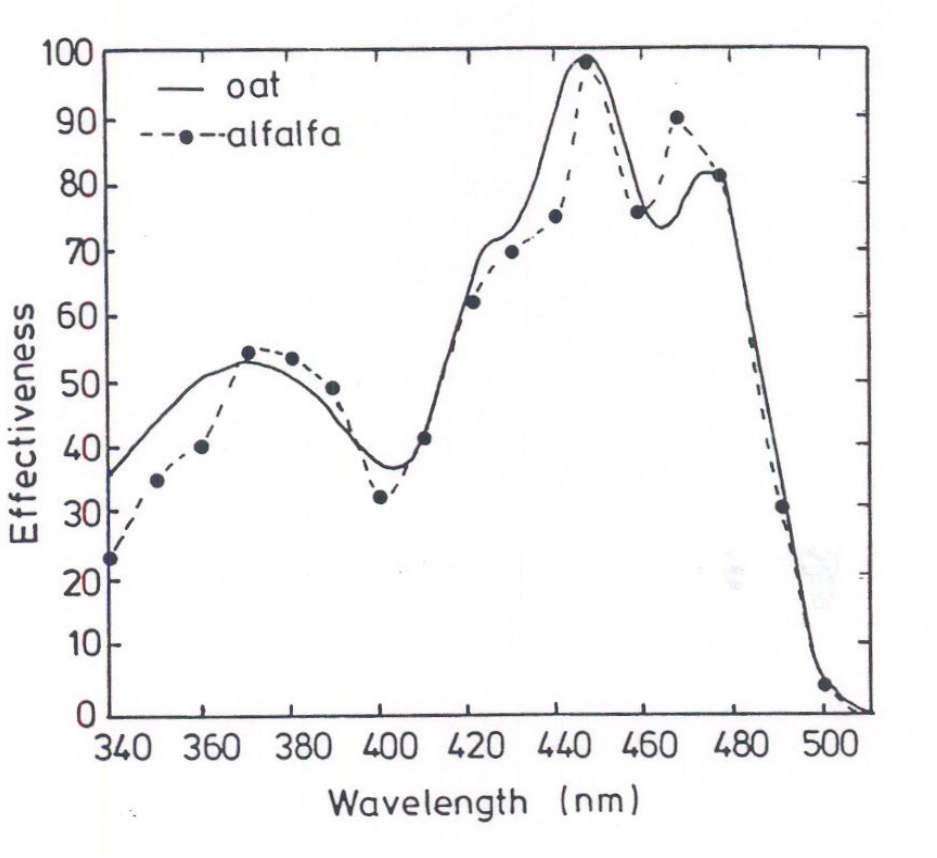

Figure I-1 Action spectra for first-positive phototropic curvature in the oat coleoptiles and alfalfa hypocotyls (Adapted from Thimann and Curry 1960, from Baskin and Iino 1987)

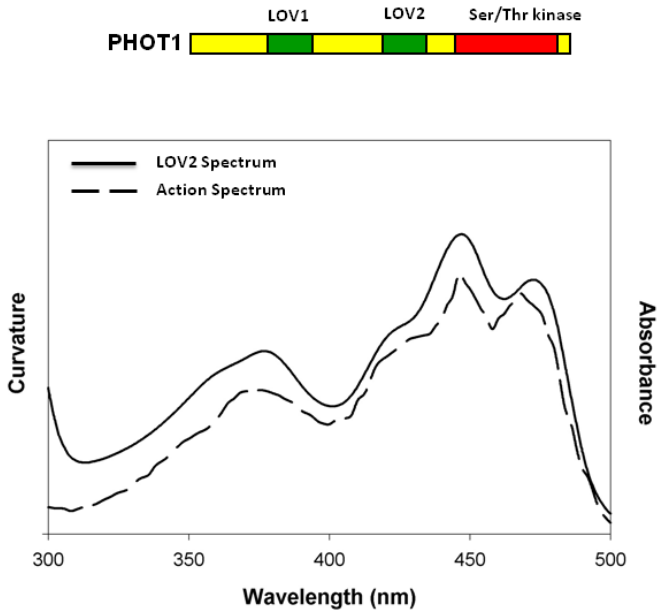

Figure I-2 Schematic representation of the CBP-LOV domain fusion proteins and Spectral analysis of the LOV2 domain and the action spectrum for first positive curvature in the *alfalfa* hypocotyls (adapted from Baskin and Iino 1987) showing a very close match.

Like phot1, phot2 has two LOV domains and a kinase domain [10] and undergoes light activated auto-phosphorylation much like phot1. Phot2 however seem to respond to high intensity blue light irradiation [11]. Since phot2 is less sensitive to light, it indicates that phot1 is the primary photoreceptor for blue light induced phototropism and chloroplast movement. These result brought much of the focus to phot1 and its two light sensors. LOV domains were isolated and shown to contain FMN and absorb blue light (fig I-2). Blue light irradiation causes spectral

changes that are characteristics of loss of absorption in the blue region of spectrum and formation of new peak near 390nm (fig I-3) and appearance of isosbestic points at 330, 375, and 410nm [12]. These changes are fully reversible when left in darkness in minutes and are indicative of a cysteine and flavin adduct formation. Mutation of a highly conserved cysteine to alanine completely removes photochemical reactivity demonstrating that cysteinyl-adduct formation is the mechanism of light detection by the phototropins [10]. LOV1 and LOV2 show different quantum efficiencies and photochemical reaction kinetics which suggest they have different roles in regulating phototropin light sensing activity [13]. LOV2 has a higher quantum efficiency for cysteinyl-adduct formation than LOV1 and mutagenesis studies show that LOV2 is required for phot1 autophosphorylation and phototropism in *Arabidopsis* [14]. The exact role of LOV1 therefore is still unknown although one study seems to suggest that LOV1 increases the lifetime of phototropin activation [15] and another study suggesting that phototropin dimerization is mediated by LOV1 [16]. Most of research have been then directed toward the study of LOV2 with crystal structure [17], mutagenesis analysis on mode of activation [10], and downstream signaling [18].

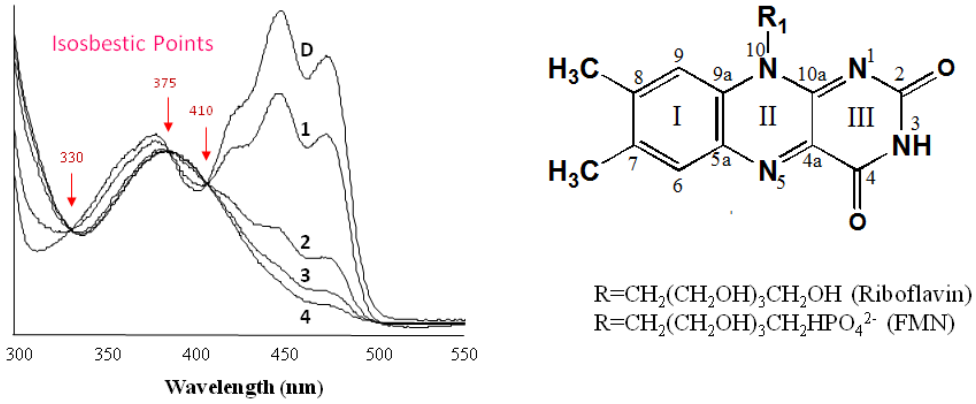

Figure I-3 LOV domain showing blue light absorption in dark (marked with a D) and blue light irradiation every second, causing loss of absorption in the blue region and formation of new peak near 390nm. The appearance of Isosbestic points are shown in red. On the right, flavin chromophore with the numbering of atoms of the isoalloxazine ring is shown.

LOV DOMAINS ARE SUBSET OF THE PAS DOMAIN SUPERFAMILY

LOV domains belong to PAS domain super family which is a group of proteins that play roles in the detection of environmental changes and adaption to them. The term PAS comes from the first letter of each of the three family members: PER, ARNT and SIM [19].

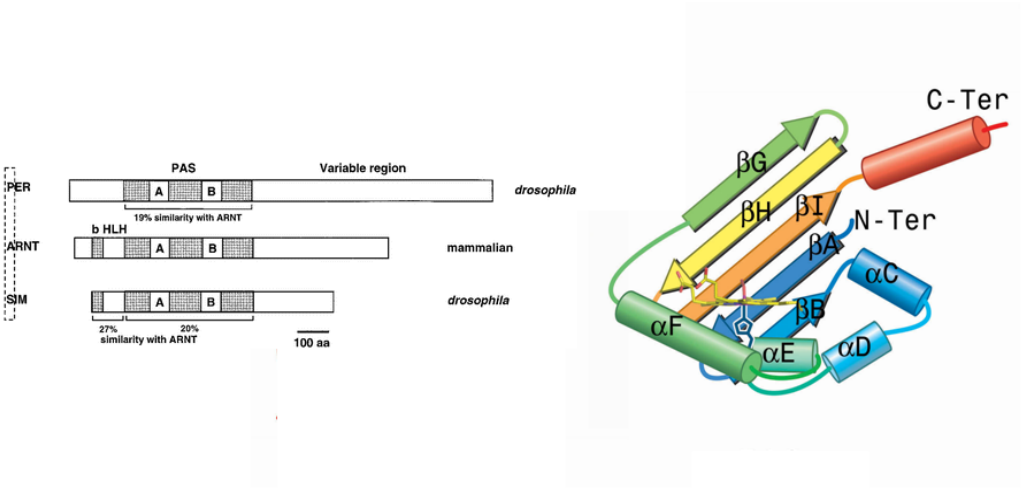

Figure I-4 The founding PAS family members. Domain structures of the founding PAS proteins PER, ARNT, and SIM are shown. The name PAS stems from the first letters of PER, ARNT, and SIM (*boxed*). The basic region (b), helix-loop-helix (HLH), PAS, and C-terminal variable domains are labeled on *top*. The percentage amino acid similarities of SIM and PER, as compared with ARNT, are labeled *beneath* their respective domains. On the right a cartoon representation of typical PAS domain is shown. It consists of conserved α/β fold.

PER is Drosophila clock protein, ARNT (arylhydrocarbon receptor nuclear translocator) is a helix turn helix containing transcription factor and SIM (Single-Minded protein) is a regulator midline cell lineage in Drosophila [19]. PAS domains are best described as regions of approximately 100 to 120 amino acids (fig I-4) in a conserved α/β-fold (several helical segments alongside of five β-antiparallel strands) although no conservation is detected at the amino acid sequence level among them

[20]. In PAS domains signals are generated typically in the core and create structural and dynamic changes in the β-sheet which then transfers to the attached effector domain via an α-helical linker [21]. These domains have been identified in proteins from all three kingdoms of life (although 81% of 21,000 PAS domains in database are bacterial) but unlike most other sensors, they are located in the cytosol. They bind to wide variety of co-factors including flavin, ρ-coumaric acid, heme, ions, and in case of HERG protein to no co-factor at all. This ability makes them versatile and able to monitor changes in light, redox potential, oxygen, small ligands, and overall energy level of a cell [21].

When the crystal structure of first LOV domain was solved, the structure superposed well with the particular subset of the PAS photosensors and therefore it was determined to be a PAS domain. The name LOV (Light, Oxygen, and Voltage) was introduced to reflect that this protein was a member of this group of PAS domains [12]. Determination of this new class of photoreceptors as PAS domain, streamlined the further development in this field since for PAS domains that bind co-factors, such molecules directly mediate signal detection (in this case blue light) so the attention was given to the non-covalently bound FMN molecule inside the LOV domain [12]. It was determined quickly that a cysteine in a highly conserved amino acid region of the LOV domain (GXN**C**RFLQ) is the molecule that interacts with the FMN [10] and this sequence is now used as a signature region to find new LOV domains among the newly annotated PAS domains.

PHOTOCYCLE OF LOV DOMAINS

For the many years that the flavins have been studied, it has become well known that they are extremely sensitive to light. It is therefore not surprising to find FMN as the blue light detector bound inside LOV domains. It is therefore extremely important to understand the chemistry of FMN and its excited states. Electronic excitation energy at upper excited states in flavins can dissipate in two ways: either the electron decays to the lowest singlet state by internal conversion or by intersystem crossover transfers to a lower energy triplet state and these two processes may compete with each other (fig I-5). The triplet state that has a maximum absorption at 650nm for the lumiflavin and 660nm for FMN was first observed using flash spectroscopy [22]. The lifetime of the flavin singlet state is approximately 5ns, while that of a triplet state is around 1ms. The lifetime of the triplet in practice is reduced due to interactions with O_2 or other environmental factors to around 10 to 50 μs [22]. The probability of a reaction occurring via a triplet state is three orders of magnitude higher than that of the singlet state because of its extended lifetime as well as its effect on the electron density distribution in the isoalloxazine ring, which greatly increases around N5 and shifts its pKa from about 0 to 5 [22]. This pK shift will be a key element in the mechanism proposed for the photochemistry of phototropins.

The FMN inside the LOV2 interacts with the protein through hydrogen bonding especially with N3, O2, and O4 of the isoalloxazine ring. Also the

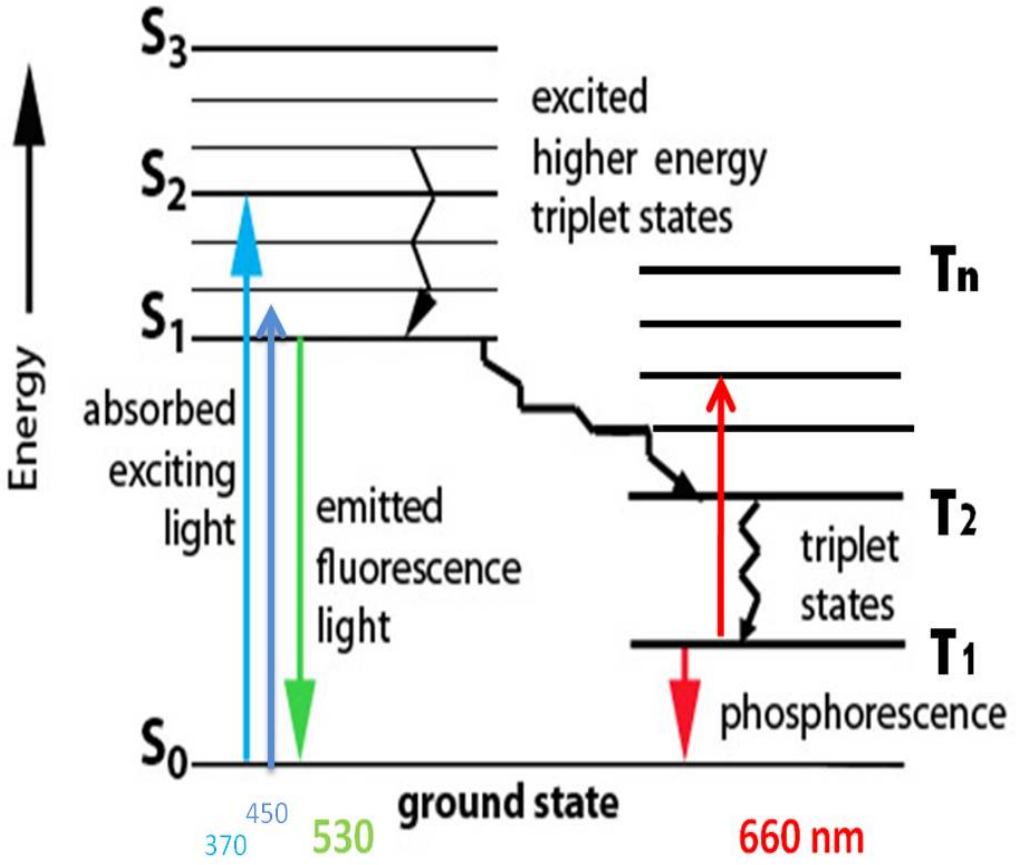

Figure I-5 Jablonski diagram for the visible range electronic transitions of FMN. For simplicity only few vibrational bands are shown and energy levels represented are approximates. Straight arrows represent photon absorption or emission and wavy arrows represent internal conversion or inter system crossing. Colors represent the wavelengths of maximum effect which is shown with the same color.

phosphate group on the FMN ribityl chain hydrogen bonds with a glutamine and two argentine residues. There are several water molecules around the chromophore that might be important in the photocycle of LOV2. The signature absorption of LOV domain in the dark has a band around 370nm which is associated with the $S_0 \rightarrow S_2$ transition and a 450nm band which is associated with the first singlet state transition of $S_0 \rightarrow S_1$ [22-23]. There are vibronic structures at around 360, 380, 425, and

475nm [23]. These vibronic structures, which are not seen in free FMN, are due to reduction of the vibronic bands of FMN due to restriction of motion in the pocket of LOV2. The FMN associated with LOV2 has a sulfur atom of a cysteine group within 4 Angstrom of its isoalloxazine ring that moves closer upon the light activation to less than 2 Angstrom distance. The primary photophysical event involves intersystem crossing from the singlet excited state to the triplet state (fig I-6). This intersystem conversion is the result of a heavy atom effect of the sulfur from the nearby cysteine with an efficiency of 60 to 80% [24]. The presence of the conserved cysteine is also responsible for shortening the singlet excited state lifetime to about 2-3 ns [25] by

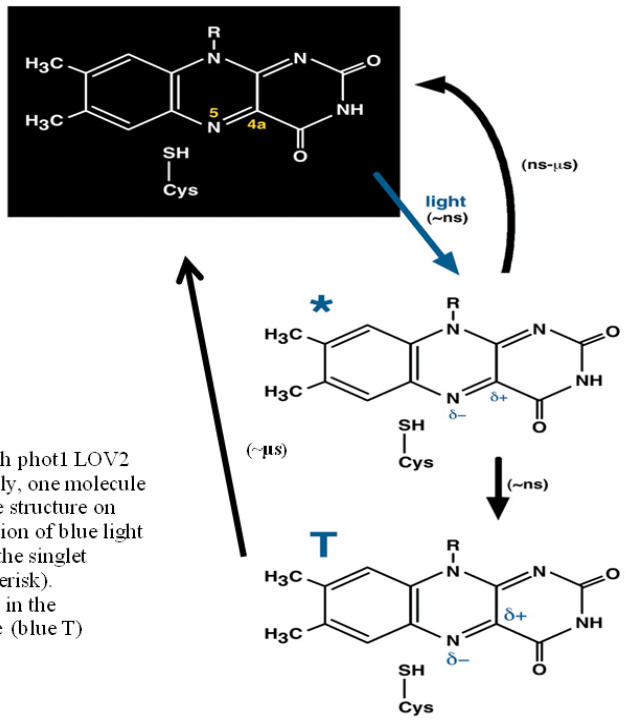

Figure I-6 In darkness, each phot1 LOV2 domain binds, non-covalently, one molecule of ground-state FMN (white structure on black background). Absorption of blue light results in the generation of the singlet excited state FMN (blue asterisk). Intersystem crossing results in the formation of the triplet-state (blue T)

enhancing the rate of intersystem crossing. The proximity of the sulfur of the cysteine to the isoalloxazine ring of the FMN also enables the rapid covalent thio-adduct formation with the C4a atom of the FMN within 2-4 µs [23]. The global kinetic analysis (for explanation refer to chapter 2) of the data collected by laser flash absorption spectroscopy on LOV2, indicates a linear kinetics scheme with the triplet and the species is the covalent thio-adduct bond formed (named LOV^{S}_{390} by Dr. Trevor Swartz and Dr. Roberto Bogomolni). The laser flash spectroscopy experiments also showed that there was 1:1 split between the triplet going thermally back to the ground state and forward to the LOV^{S}_{390} [23]. This LOV^{S}_{390} specie decays spontaneously in the dark back to the ground state to make this a photocycle (fig I-7).

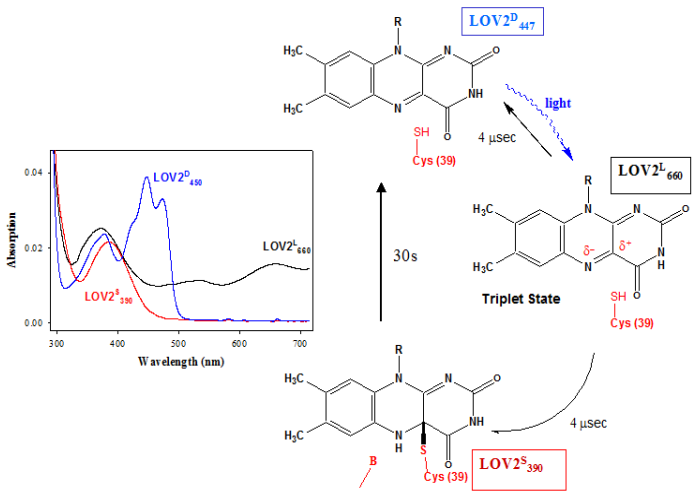

Figure I-7 Photocycle scheme and proposed reaction mechanism for LOV2. Also shown is the ground state LOV2 spectrum and calculated intermediate spectra.

This return is variable from 30 seconds in LOV2 to many minutes in EL346 which is the LOV-histidine kinase of the bacterium *Erythrobacter Litoralis*, to not returning to ground state at all (truncated photocycle) in Brucella LOV domain [26]. LOV2 is a stable protein and will decay back to the ground state even after many flashes with light if kept in the dark after. For some spectroscopic work, continuous illumination is used which converts most of the sample into LOV^{S}_{390} since it forms in the microsecond range and decays in many seconds. The recovery of LOV^{S}_{390} to the dark state by base catalyzed reaction is widely accepted and has even shown to have a faster recovery in the presence of imidazole [27]. Also pH, deuterium effect studies have indicated that a proton transfer reaction from N(5) of the FMN, is the rate limiting step for this reaction [28]. The details of formation of LOV^{S}_{390} though are still a matter of debate and there are several proposed pathways. The first two pathways only differ in their explanation of how and when the proton transfer to N5 of the FMN takes place. The first proposal (fig I-8) suggests a proton transfer to the triplet state of FMN from an acidic group nearby, then followed by reaction of C4a carbon-cation with the cysteine thiolate [23]. Another suggested pathway proposes direct transfer of a proton from the thiol to the N5 of the triplet state of FMN followed by the C-S bond formation [17, 25]. These groups all propose an ionic pathway to adduct formation through a triplet state that has a more basic N5 because of the correlation that exists between the net charge distribution (which happens between N5-C4a double bond of FMN in triplet state) and the pka values for isoalloxazine ring of the FMN [29]. Actually major pka change occurs upon singlet-

singlet excitation for N5 and it decreases slightly upon intersystem crossing from the S_1 to T_1 state [29]. Swartz et al. proposes that cysteinyl group is de-protonated in the LOV2 on the basis of the pH titration fluorescence work done on FMN, LOV2 and LOV2C39A mutant where the active cysteine is removed and no adduct is formed. The Crosson and Kennis proposal is based on femtosecond transient absorption spectroscopy where they see that the majority of the FMN triplets in the LOV2 domain exist in the protonated form (fig I-8).

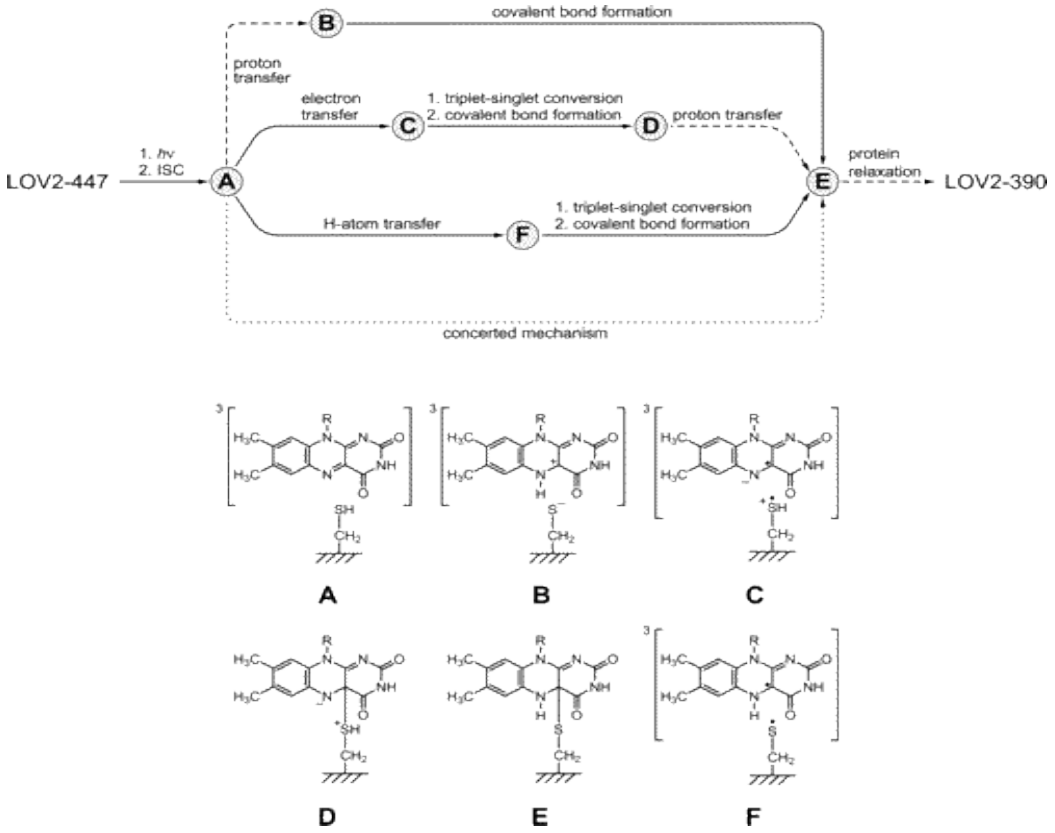

Figure I-8 Suggested reaction pathway (top) and intermediates (bottom) of photo-adduct (LOV-390) formation in wild-type LOV2 domains.

The other proposed reaction pathway is very different. It offers FMN semiquinone (free radical) in a reaction with a sulfur radical of cysteine as an explanation for the LOV^{S}_{390} formation [30]. In their view, adduct formation in the triplet state is unlikely and they favor a two step radical mechanism that starts with a hydrogen atom transferring from the cysteine to the N5 of FMN. It is also possible that the initial electron transfer from the sulfur and then protonation by an unidentified donor which then is followed by the semiquinone reacting with the cysteine radical to form the C-S covalent bond [31]. Although there is not enough evidence to exclude any of the discussed mechanisms, a few glaring problems with the radical pair formation needs to be discussed in order to show it is the least likely of the possible mechanisms proposed. At physiological light intensities, the formation of a neutral flavosemiquinone was not observed in LOV2C39A [23]. We do not see the formation of this radical with a flash or one minute of blue light irradiation during our experiments but we do observe the formation of semiquinone at very high light intensities or continuous flashing of the sample. Kay et al. illuminates the sample for 40 minutes with light from a Xe lamp for their experiment [31] and Kottke et al. irradiates the sample with a 100W tungsten lamp until the absorbance at 570nm (indication of neutral radical) reaches its maximum [30]. Kottke et al. also conduct their experiments on a C57M mutant which renders a proton or hydrogen atom transfer from the thiol group to FMN impossible. The question is of course with such intense light illumination and a mutant where the active cysteine missing, are those results relevant for the wild type LOV2 protein under physiological light

settings? Another problem in the mechanism is the adduct formation and triplet decay times. In their samples, the yield of flavin radical differs each time and when left in the dark, the flavin radical is completely re-oxidized under aerobic conditions in around 7 minutes, which does not match the reported times for the decay of triplet state back to the ground state. On formation, when the radical pairs of FMN and sulfur form, FMN is still in triplet form and since pairing happens in the singlet state, FMN has to go through interconversion which has relaxation times of nanoseconds in the presence of a sulfur-centered radical because of its strong spin orbit coupling between them. If spin mixing occurs on this time scale, the covalent bond formation is expected to form in nanoseconds but the reported time for this reaction is in microseconds. Femtosecond transient absorption spectroscopy experiments do not detect any radicals [23] but FTIR work on this matter has not been very conclusive. Iwata et al. can detect S-H bonds in the light minus dark infrared difference spectra of phy3-LOV2 [32] but they could not distinguish between an SH or $SH^{+\bullet}$ (which is proposed to be involved in one mechanism of radical pair formation) at 77K temperature [33]. They also raise the possibility that SH can be de-protonated at higher temperatures.

LIGHT INDUCED CHANGES IN LOV2

X-ray crystal structure of isolated, short LOV domain constructs from *Adiantum Capillus-Veneris* [34], *Chlamydomonas reinherdtii* [35] in their light state provided the first evidence for formation of photoproduct with small structural change around FMN. Spectroscopic data, provided information showing structural

changes in longer LOV domain constructs [28] which was demonstrated to be in the C-terminal of core LOV2 domain at Jα-helix [36-37]. The interaction between core LOV2 domain and Jα-helix (fig I-9) seems to change upon light activation causing the unraveling of the helix that is docking to a β-sheet [28] which in turn may play a role in the propagation of the initial signal from the photosensor to the output domain (fig I-10). This discovery brought significant attention and much research in the modes of downstream signaling cascade and raised several interesting questions. How does the LOV domain actually activate a wide variety of attached output domains, including histidine kinases [26, 38-39], DNA binding domain (subject of this study), and the STAS domains [40]? If the Jα-helix is the major contributor in downstream activation, why is there no conserved sequence motif observed in that segment?

We will review the studies that suggest possible answers to these questions here. The formation of adduct disrupts the planarity of the flavin isoalloxazine ring causing a tilt or puckering of it in the pocket of LOV2 protein. The N5 position of the ring and its altered hydrogen bonding is the main contributor of the response [18]. A highly conserved glutamine in the β-strand rotates to form a hydrogen bond with the protonated N5 [34] which then alters the hydrogen bonding between β-sheet and the Jα-helix (fig I-11). This perturbation eventually releases the Jα-helix from the LOV-core and causes it to open, exposing the hidden hydrophobic protected part of the effectors domain (fig I-10). In the LOV multi-domain proteins that include kinases, these light induced exposed areas, are shown to be the active site of the

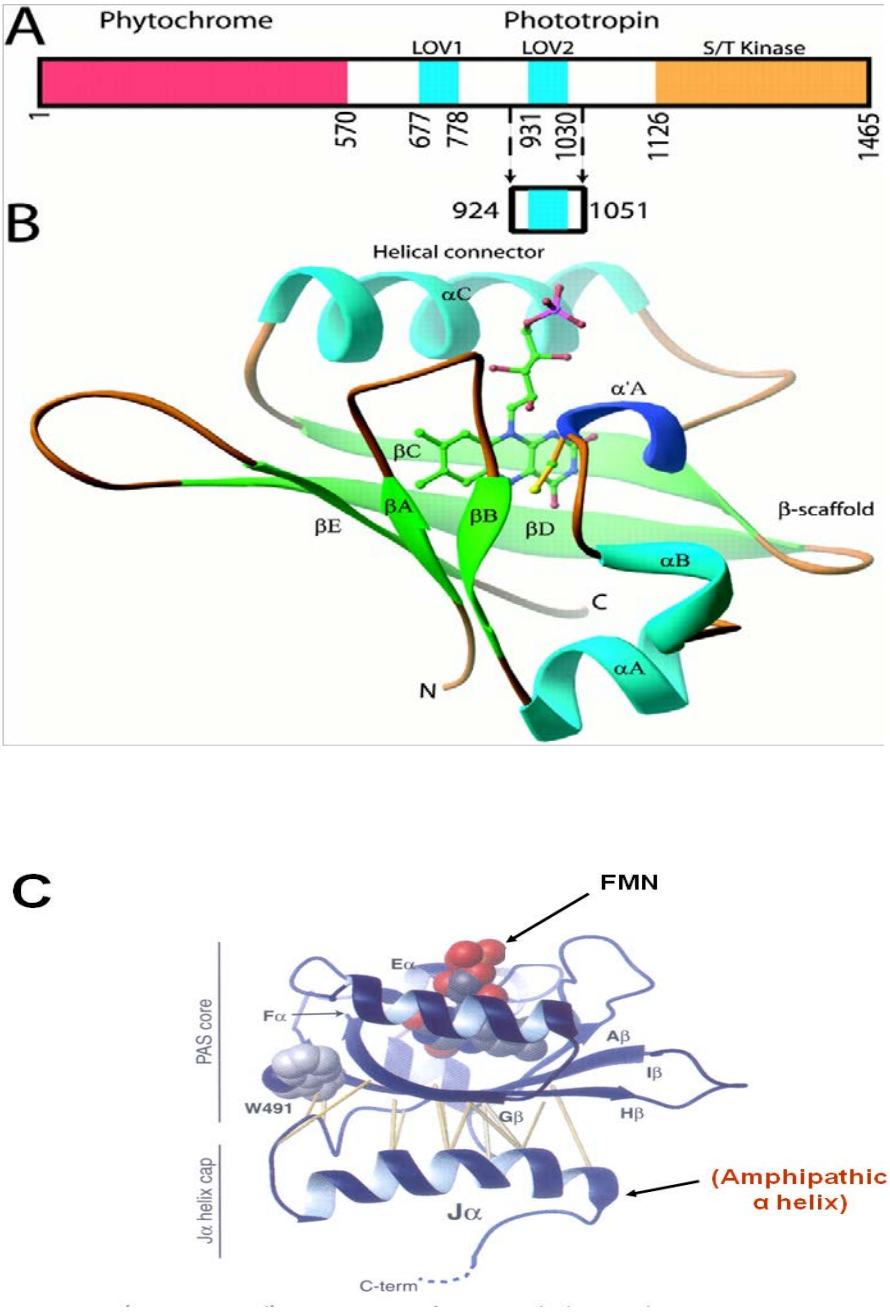

Figure I-9 A) Schematic representation of *Adiantum* phy3 LOV2 domain proteins **B)** Overall fold of phy3 LOV2. Ribbon diagram of *Adiantum* phy3 LOV2 in its ground state. The 3_{10} helical turn, which contains the photoactive cysteine, is denoted as α'A and colored in dark blue. **C)** Structural model of the LOV2 domain from oat phot1 in the dark state as determined by NMR analysis and homology modeling. Positions of the FMN chromophore and the Jα-helix are indicated.

enzyme [41]. There is also evidence which shows that other residues like a conserved phenyl-alanine on a different β-sheet in LOV2 also plays a role in regulating conformational dynamics happening within the β-sheet preceding the Jα-helix displacement [42]. The magnitude of Jα-helix movement is variable (fig I-10) among various phototropins [43] as it does in fungal photoreceptor VVD [44] and the bacterial photoreceptor YtvA [45]. This variation can explain why the Jα-helix region is much less conserved than the LOV-core part. Although not very similar in their sequence, a similar structural organization to that in the Oat phot1 LOV2 Jα-helix is seen in all the LOV domains studied so far [46]. Such terminal helices are also seen in most of the PAS domains studied so far in both the single and multi-

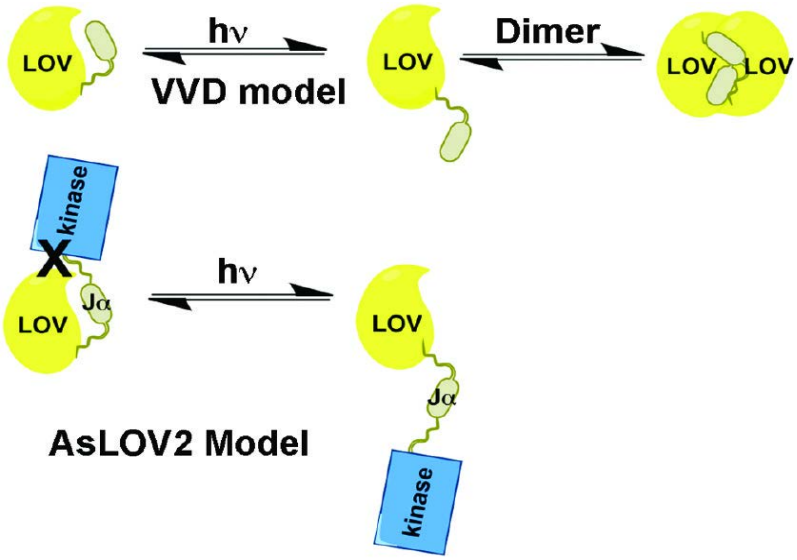

Figure I-10 In VVD,conformational changes at the LOV domain induce dimerization involving the LOV. In AsLOV2, the N-terminus LOV locks the signaling domain (kinase blue) in an inactive conformation. Changes in Jα docking relieve inhibition by exposing the active site of enzyme.

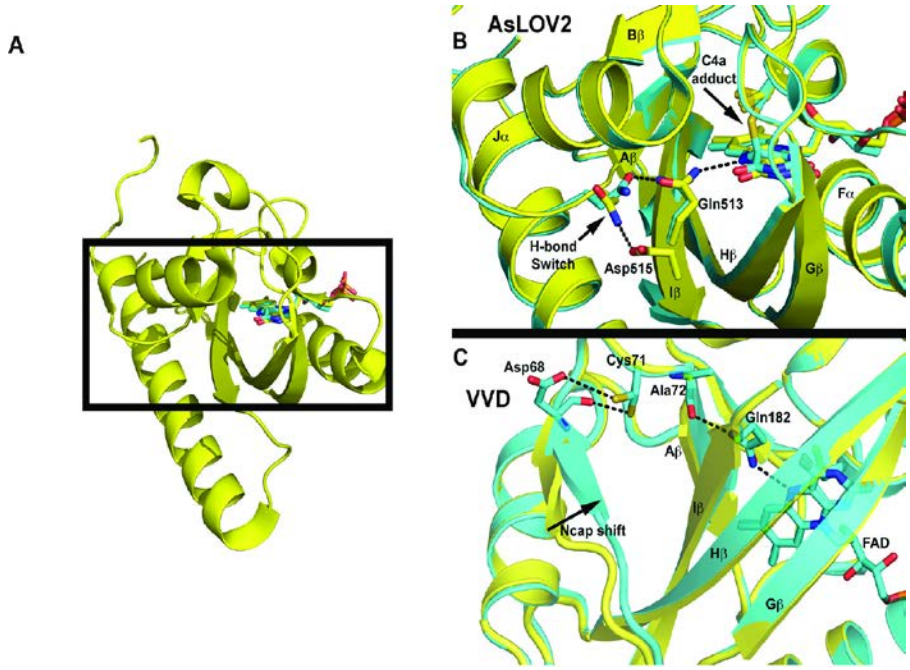

Figure I-11 Models of signal propagation in LOV domains. Both AsLOV2 (A and B) and VVD (C) initiate signal propagation from rotation of a conserved Gln in the Iβ strand (Q513 inAsLOV2 andQ182 inVVD). The interaction between core LOV domain and Jα-helix changes based on hydrogen bonding changes that occur due to light activation.

domain proteins [47]. The phylogenic analysis now suggests that the ancient LOV signaling module retained its photosensitivity from Archaea to plants (fig I-12) and spread from the prokaryotic to the eukaryotic kingdom of life [48-50]. Both plant phot-LOV and fungal WC-1 LOV show an affinity toward the α-proteobacterial class of the phylogenic tree [50] and it is therefore reasonable to conclude that their appearance in eukaryotes originates from the endosymbiosis of an ancient proteobacterium that could have also led to the appearance of the mitochondria.

As the result of these studies, LOV-domain can be considered a new mechanism of

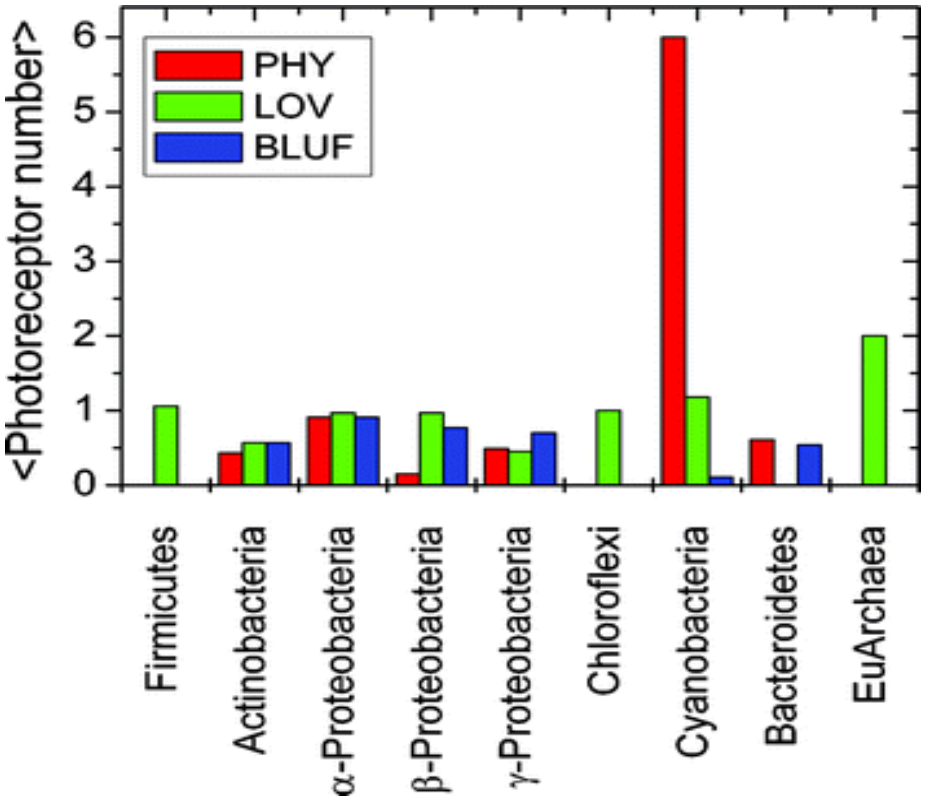

Figure I-12 Percentage of fully sequenced bacteria having PHY, LOV or BLUF proteins. For the phylum Proteobacteria, the three major classes (α, β, and γ) have been separated.

blue light sensor or more plainly a light switch for turning on or off a function in a cell. As of the completion of this dissertation, LOV genes have been found in 227 bacteria species with the highest concentration seen in α-proteobacteria and in 11 archaea species [48]. Out of the 322 total LOV domains that have been analyzed, 171 have a kinase as an effectors domain, 31 STAS (Sulfate Transporter and Anti-Sigma factor antagonist), 9 HtH (Helix-turn-Helix) and 62 GGDEF domains.

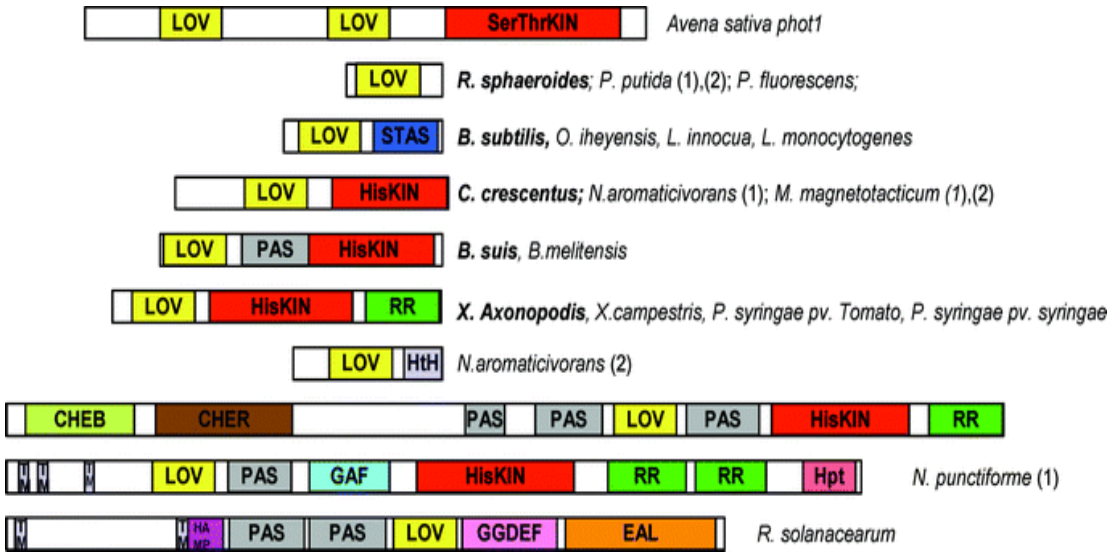

Figure I-13 Domain architecture of selected bacterial LOV proteins and plant phot. The proteins are named after the bacterium of origin. TM: transmembrane helices; STAS: Sulfate transporter/anti-sigma factor antagonist domain; HisKIN: histidine kinase; RR: response regulator, receiver domain; HTH: Helix-Loop-Helix transcriptional regulator domain; Hpt = Histidine phosphotransfer domain; CheB: CheB methylesterase domain; CheR: CheR methyltransferase domain; GGDEF, EAL =domains named after their conserved aa motifs, found in diguanylate cyclases and phosphodiesterases; HAMP = domain found in Histidine kinases, Adenylyl cyclases, Methyl binding proteins, Phosphatases [48].

Since many of these LOV domains started to show up in organisms that were not thought to show any reaction to light, our lab decided to tackle the study of bacterial LOV domain in parallel to phot1 LOV2 which is still the subject of much study. The lab concentrated on studying the modes of activation and photochemistry of LOV domain with different effectors domains. *Listeria* containing LOV-STAS, *Brucella* containing LOV-Histidine Kinase, and *Erythrobacter Litoralis* containing both LOV-HtH and LOV-Histidine Kinase domains have been the subject of the intense study in our lab with interesting results. *Erythrobacter Litoralis* HTCC2594 genome has been sequenced (accession number CP000157) showing that genes for bacteriochlorophyll a (Bchla) biosynthesis and photosynthetic reaction center proteins

are missing [51]. This confirms negative spectroscopic measurements for Bchla both seen by Hyun et al. [51] and our lab. The genus *Erythrobacter* were known before this to be an aerobic, anoxygenic phototrophs [52] and shown to form red/orange pigmented colonies. The HTCC2594 strain was isolated from a depth of 10 meter in the Sargosso Sea, Atlantic ocean and were grown on a low nutrient medium [51]. *Erythrobacter* shows high level resistance to tellurite and accumulation of metallic tellurium crystals and has resistance to penicillin and streptomycin [53]. The size of *Erythrobacter* bacterium is 0.5 to 0.7 μm in diameter and 0.7 μm in length but can form long thread-like formation of cells up to 5 μm. They contain a large amount of Zeaxanthin carotenoids not engaged in photosynthetic activity [51]. Blue light is shown to inhibit carotenoids production in *Erythrobacter* Och1114 specie [54] and authors conclude that there has to be a blue light absorbing pigment system which regulates the biosynthesis of carotenoids as well as Bchl in this bacterium. We observe the same phenomenon with the HTCC2594 strain and the carotenoids production in our lab (data not shown) and since there are four different LOV domain multi-protein domains in this bacterium, we suggest that a LOV domain may be responsible for regulation of carotenoid production in *Erythrobacter Litoralis* HTCC2594.

This research involves the characterization and complete photochemistry of *Erythrobacter Litoralis* LOV domains that include: a 346 amino acid and a 368 amino acid sequences both contain a LOV domain at the N-terminus and a Histidine Kinase at the C-terminus (named EL346 and EL368). It also contains a 222 amino

acid sequence that contains a LOV domain at the N-terminus and a DNA binding HtH domain at the C-terminus (named EL222). EL222 light activated structural changes are studied in detail using Absorption Spectroscopy, FTIR, CD, and Fluorescence Spectroscopy. Various mutants are designed and studied to gain understanding into photochemistry, detail of activation, and tuning the photocycle of EL222 by altering the hydrogen bonding network with the FMN chromophore.

References:

1. Briggs, W.R., *Blue/UV-A receptors: Historical overview*, in *Photomorphogenesis in plants and bacteria*. 2006, Springer. p. 171-197.

2. Darwin, C., *Power of Movement in plants (John Murray: London)*. 1880, London.

3. Briggs, W.R., *The Phototropic Responses of Higher Plants.* Annual Review of Plant Physiology, 1963. **14**(1): p. 311-352.

4. Galston, A.W. and R.S. Baker, *Studies on the physiology of light action. II. The photodynamic action of riboflavin.* American Journal of Botany, 1949: p. 773-780.

5. BRIGGS, W.R., R.D. TOCHER, and J.F. WILSON, *Phototropic Auxin Redistribution in Corn Coleoptiles.* Science, 1957. **126**(3266): p. 210-212.

6. Thimann, K.V., Curry, G.M., *Phototropism and Phototaxis.* Comparative Biochemistry 1960. **1**: p. 63.

7. Liscum, E. and W.R. Briggs, *Mutations in the NPH1 Locus of Arabidopsis Disrupt the Perception of Phototropic Stimuli.* Plant Cell, 1995. **7**(4): p. 473-485.

8. Christie, J.M., et al., *Arabidopsis NPH1: a flavoprotein with the properties of a photoreceptor for phototropism.* Science, 1998. **282**(5394): p. 1698-701.

9. Briggs, W., et al., *The phototropin family of photoreceptors.* PLANT CELL, 2001. **13**(5): p. 993-997.

10. Salomon, M., et al., *Photochemical and mutational analysis of the FMN-binding domains of the plant blue light receptor, phototropin.* BIOCHEMISTRY, 2000. **39**(31): p. 9401-9410.

11. Briggs, W. and J. Christie, *Phototropins 1 and 2: versatile plant blue-light receptors.* TRENDS IN PLANT SCIENCE, 2002. **7**(5): p. 204-210.

12. Christie, J.M., et al., *LOV (light, oxygen, or voltage) domains of the blue-light photoreceptor phototropin (nph1): binding sites for the chromophore flavin mononucleotide.* Proc Natl Acad Sci U S A, 1999. **96**(15): p. 8779-83.

13. Kasahara, M., et al., *Photochemical properties of the flavin mononucleotide-binding domains of the phototropins from Arabidopsis, rice, and Chlamydomonas reinhardtii.* PLANT PHYSIOLOGY, 2002. **129**(2): p. 762-773.

14. Christie, J., et al., *Phototropin LOV domains exhibit distinct roles in regulating photoreceptor function.* PLANT JOURNAL, 2002. **32**(2): p. 205-219.

15. Kagawa, T., *The phototropin family as photoreceptors for blue light-induced chloroplast relocation.* J Plant Res, 2003. **116**(1): p. 75-80.

16. Salomon, M., U. Lempert, and W. Rüdiger, *Dimerization of the plant photoreceptor phototropin is probably mediated by the LOV1 domain.* Febs Letters, 2004. **572**(1): p. 8-10.

17. Crosson, S. and K. Moffat, *Structure of a flavin-binding plant photoreceptor domain: Insights into light-mediated signal transduction.* PROCEEDINGS OF THE NATIONAL ACADEMY OF SCIENCES OF THE UNITED STATES OF AMERICA, 2001. **98**(6): p. 2995-3000.

18. Crosson, S., S. Rajagopal, and K. Moffat, *The LOV domain family: Photoresponsive signaling modules coupled to diverse output domains.* BIOCHEMISTRY, 2003. **42**(1): p. 2-10.

19. Gu, Y.-Z., J.B. Hogenesch, and C.A. Bradfield, *The PAS Superfamily: Sensors of Environmental and Developmental Signals.* Annual Review of Pharmacology and Toxicology, 2000. **40**(1): p. 519-561.

20. Taylor, B.L. and I.B. Zhulin, *PAS domains: internal sensors of oxygen, redox potential, and light.* Microbiol Mol Biol Rev, 1999. **63**(2): p. 479-506.

21. Moglich, A. and K. Moffat, *Engineered photoreceptors as novel optogenetic tools.* Photochemical & Photobiological Sciences, 2010. **9**(10): p. 1286-1300.

22. Müller, F., *Chemistry and biochemistry of flavoenzymes*. 1991, Boca Raton: CRC Press. v. <1-3 >.

23. Swartz, T., et al., *The photocycle of a flavin-binding domain of the blue light photoreceptor phototropin.* JOURNAL OF BIOLOGICAL CHEMISTRY, 2001. **276**(39): p. 36493-36500.

24. Alexandre, M.T.A., et al., *Electronic and Protein Structural Dynamics of a Photosensory Histidine Kinase.* Biochemistry, 2010. **49**(23): p. 4752-4759.

25. Kennis, J., et al., *Primary reactions of the LOV2 domain of phototropin, a plant blue-light photoreceptor.* BIOCHEMISTRY, 2003. **42**(12): p. 3385-3392.

26. Swartz, T.E., et al., *Blue-light-activated histidine kinases: Two-component sensors in bacteria.* Science, 2007. **317**(5841): p. 1090-1093.

27. Alexandre, M., et al., *A Base-Catalyzed Mechanism for Dark State Recovery in the Avena sativa Phototropin-1 LOV2 Domain.* BIOCHEMISTRY, 2007. **46**(11): p. 3129-3137.

28. Corchnoy, S., et al., *Intramolecular proton transfers and structural changes during the photocycle of the LOV2 domain of phototropin 1.* JOURNAL OF BIOLOGICAL CHEMISTRY, 2003. **278**(2): p. 724-731.

29. Song, P.S., *On the basicity of the excited state of flavins.* Photochemistry and Photobiology, 1968. **7**(3): p. 311-3.

30. Kottke, T., et al., *Irreversible photoreduction of flavin in a mutated Phot-LOV1 domain.* BIOCHEMISTRY, 2003. **42**(33): p. 9854-9862.

31. Kay, C., et al., *Blue light perception in plants - Detection and characterization of a light-induced neutral flavin radical in a C450A mutant of phototropin.* JOURNAL OF BIOLOGICAL CHEMISTRY, 2003. **278**(13): p. 10973-10982.

32. Iwata, T., S. Tokutomi, and H. Kandori, *Photoreaction of the cysteine S-H group in the LOV2 domain of adiantum phytochrome3.* JOURNAL OF THE AMERICAN CHEMICAL SOCIETY, 2002. **124**(40): p. 11840-11841.

33. Iwata, T., et al., *Light-induced structural changes in the LOV2 domain of Adiantum phytochrome3 studied by low-temperature FTIR and UV-visible spectroscopy.* BIOCHEMISTRY, 2003. **42**(27): p. 8183-8191.

34. Crosson, S. and K. Moffat, *Photoexcited structure of a plant photoreceptor domain reveals a light-driven molecular switch.* Plant Cell, 2002. **14**(5): p. 1067-1075.

35. Fedorov, R., et al., *Crystal structures and molecular mechanism of a light-induced signaling switch: The Phot-LOV1 domain from Chlamydomonas reinhardtii.* BIOPHYSICAL JOURNAL, 2003. **84**(4): p. 2474-2482.

36. Harper, S., L. Neil, and K. Gardner, *Structural basis of a phototropin light switch.* SCIENCE, 2003. **301**(5639): p. 1541-1544.

37. Harper, S.M., J.M. Christie, and K.H. Gardner, *Disruption of the LOV-J alpha helix interaction activates phototropin kinase activity.* Biochemistry, 2004. **43**(51): p. 16184-16192.

38. Purcell, E.B., et al., *A photosensory two-component system regulates bacterial cell attachment.* Proceedings of the National Academy of Sciences of the United States of America, 2007. **104**(46): p. 18241-18246.

39. Correa, F., et al., *Blue Light regulated two-component systems: Enzymatic and functional analyses of Light-Oxygen-Voltage (LOV)-histidine kinases and downstream response regulators.* Biochemistry, 2013. **52**(27): p. 4656-4666.

40. Avila-Perez, M., K.J. Hellingwerf, and R. Kort, *Blue light activates the sigma(B)-dependent stress response of Bacillus subtilis via YtvA.* Journal of Bacteriology, 2006. **188**(17): p. 6411-6414.

41. Salomon, M., et al., *Mapping of low- and high-fluence autophosphorylation sites in phototropin 1.* BIOCHEMISTRY, 2003. **42**(14): p. 4217-4225.

42. Yamamoto, A., et al., *Light Signal Transduction Pathway from Flavin Chromophore to the J[alpha] Helix of Arabidopsis Phototropin1.* Biophysical journal, 2009. **96**(7): p. 2771-2778.

43. Koyama, T., et al., *Different Role of the Jα Helix in the Light-Induced Activation of the LOV2 Domains in Various Phototropins.* Biochemistry, 2009. **48**(32): p. 7621-7628.

44. Zoltowski, B.D., et al., *Conformational Switching in the Fungal Light Sensor Vivid.* Science, 2007. **316**(5827): p. 1054-1057.

45. Möglich, A., et al., *Structure and Function of Plant Photoreceptors.* Annual Review of Plant Biology, 2010. **61**(1): p. 21-47.

46. Halavaty, A.S. and K. Moffat, *N-and C-terminal flanking regions modulate light-induced signal transduction in the LOV2 domain of the blue light sensor phototropin 1 from Avena sativa.* Biochemistry, 2007. **46**(49): p. 14001-14009.

47. Jones, M.A., et al., *Mutational Analysis of Phototropin 1 Provides Insights into the Mechanism Underlying LOV2 Signal Transmission.* Journal of Biological Chemistry, 2007. **282**(9): p. 6405-6414.

48. Losi, A., *The bacterial counterparts of plant phototropins.* Photochemical & Photobiological Sciences, 2004. **3**(6): p. 566-574.

49. Krauss, U., et al., *Initial characterization of a blue-light sensing, phototropin-related protein from Pseudomonas putida: a paradigm for an extended LOV construct.* Physical Chemistry Chemical Physics, 2005. **7**(14): p. 2804-2811.

50. Krauss, U., et al., *Distribution and phylogeny of light-oxygen-voltage-blue-light-signaling proteins in the three kingdoms of life.* Journal of bacteriology, 2009. **191**(23): p. 7234-7242.

51. Oh, H.-M., et al., *Complete Genome Sequence of Erythrobacter litoralis HTCC2594.* J. Bacteriol., 2009. **191**(7): p. 2419-2420.

52. Rathgeber, C., J.T. Beatty, and V. Yurkov, *Aerobic phototrophic bacteria: new evidence for the diversity, ecological importance and applied potential of this previously overlooked group.* Photosynthesis Research, 2004. **81**(2): p. 113-128.

53. Yurkov, V., J. Jappe, and A. Vermeglio, *Tellurite resistance and reduction by obligately aerobic photosynthetic bacteria.* Applied and environmental microbiology, 1996. **62**(11): p. 4195-4198.

54. Hellingwerf, K., et al., *Photobiology of bacteria.* Antonie van Leeuwenhoek, 1994. **65**(4): p. 331-347.

CHAPTER 1

PHOTOCHEMICAL AND BIOCHEMICAL STUDIES OF LIGHT-INDUCED CHROMOPHORE AND PROTEIN STRUCTURAL CHANGES IN A BACTERIAL LOV-HTH DNA-BINDING DOMAIN

1.1 Introduction

Phototropins, found in both plants and algae, are members of photosensory proteins that have evolved to sense and respond to light and its varying intensities. Phototropins sense light through two LOV (**L**ight-**O**xygen-**V**oltage) domains and control a range of biological responses, including, phototropism, stomatal opening, relocation of chloroplasts, and other photo-movements in plants [1-5]. LOV domains bind flavin mononucleotide (FMN) and upon absorption of blue light, use the energy to cause conformational changes that trigger downstream signal transduction [6-7]. This flavoprotein is a member of the PAS (Per-ARNT-Sim) superfamily [8], which usually have a five-stranded anti-parallel β-sheet core surrounded by several helical segments ($\beta_2\alpha_4\beta_3$). The discovery of LOV-domains in the bacterial world with diverse effector domains raises an interesting question. How can LOV domains with conserved motifs in their amino acid sequence and comparable structure, regulate such complex and diverse responses in the bacterial world? From the solved crystal structure of several LOV-domains [9-12] and from the biochemical and biophysical studies done on phot1-LOV2, it is determined that all LOV-domains have similar activation mechanism. This flavin containing protein forms a covalent adduct between the sulfur of a highly conserved cysteine residue and the C(4a) carbon of the

isoalloxazine ring of the flavin chromophore [7, 9, 13]. Structural studies reveal that that the blue light activation leads to the unfolding of a helix (named Jα-helix) connecting the LOV-domains to the effector domain [14]. This unfolding seems to separate the two domains which leads to the removal of inhibition from the effector domain, leading to a response.

Recently, 2.1 A° resolution dark state crystal structure of EL222, a 222 amino acid bacterial LOV-domain from bacterium *Erythrobacter Litoralis* HTCC2594 has been solved [15]. EL222 has a LOV-domain at the N-terminus and a C-terminus helix-turn-helix DNA binding protein. The DNA binding domain in EL222 is a member of the LuxR-type DNA binding proteins which are regulated with a sensor that detects environmental stimuli [15]. The gel shift assays using labeled DNA fragments, suggest that EL222 is a light-activated DNA binding protein, meaning that the LOV-domain represses the DNA binding of the HTH in the dark and that light illumination removes the inhibition [15]. Although the crystal structure is helpful for observing the interactions between the LOV and HTH domain, without a true light-state crystal structure, questions about the methods of activation and the light-induced structural changes remain. Here, we present FTIR, Raman, and CD spectroscopy studies to address the mechanism of light-activation and the structural changes following it.

1.2 Materials and Methods

1.2.1 EL222 Cloning, Cell Growth, Protein Expression, and Purification

The details of cloning, expression, and purification of EL222 will be covered in chapter 2. In short, DNA segment corresponding to the EL222 domain was PCR amplified and cloned into the pET/100D TOPO plasmids (Invitrogen) which adds a Histidine tag to the C-terminus of targeted protein. Successful colonies after transformation into BL21-DE3-pLysS competent cells were chosen and grown in sterilized Lauria Broth (LB) overnight. This was used to inoculate two one liter sterilized LB the next day and they were grown at 37℃ with a 250rpm shaking. When the bacterial culture growth reached an optical density (OD) of 0.8 at 600 nm, 1mM (final concentration) of IPTG was added to induce expression at 30℃ for three hours. After growth, cells were harvested, frozen at -20℃, thawed, broken with the French press, and purified using the gravity column that contained Talon cobalt resin. The collected samples were buffer exchanged, concentrated, and some were lyophilized for the FTIR experiments.

1.2.2 Chromophore Identification

The departmental LTQ mass spectrometer (Thermo Scientific, San Jose, CA) was used to identify the chromophore inside the EL222 protein. The purified sample was buffer exchanged into nanopure water using a Sephadex G-25 desalting column (GE Healthcare Life Sciences, UK). The Trichloroacetic acid, TCA, was used in a 2% final concentration to denature and precipitate the protein. The sample was centrifuged at a speed of 10,000 rpm for 10 minutes twice to remove the precipitate. The supernatant (yellow solution) contains the chromophore and was lyophilized

overnight and re-suspended in 35% ethanol for a final chromophore concentration of 1 µM (colorless solution). A 25 µl sample was injected into the machine and then compared with prepared standards of FAD, FMN, and riboflavin.

1.2.3 Absorption Spectroscopy

The kinetic measurement at 450nm and light induced changes at long times were collected using Hewlett Packard 8452A diode array spectrometer using software written in the LabVIEW environment for data acquisition and instrumental control. The light source was a fiber optics illuminator (V-Lux 1000, Volpi Manufacturing, USA). Samples were illuminated for one minute to create maximum adduct (excited state) population and greater signal.

1.2.4 Fluorescence Spectroscopy

Fluorescence spectra and kinetics were acquired using a Varian Carey Eclipse Fluorescence spectrometer with a scanning speed of 600 nm/min and medium detector sensitivity. Fluorescence emission was monitored between 400nm to 600 nm with the excitation at 350nm. The tryptophan fluorescence emission was monitored between 300 nm to 400 nm with the excitation at 280 nm. The scan speed of 600 nm/min and medium detector sensitivity was used. Fluorescence kinetic spectra were followed for three minutes with an emission wavelength of 340 nm.

The transient fluorescence spectroscopy measurements were performed with the same type of a set up as shown in figure 1.1. The three directions available in the

cuvette are used to excite the tryptophan, to excite the photocycle, and to observe the tryptophan emission. The tryptophan fluorescence is excited by an LED emitting at 280 nm with a half-width of 10 nm, and the emission is detected by a photomultiplier. The time course of the signal is recorded from 100 ns to seconds after exciting the sample with a 20 ns flash at 460 nm from a dye laser (coumarin 102, dissolved in ethanol) pumped by a XeCl-excimer laser (EMG 50; Lambda Physics). Filters were used to protect the photomultiplier from the LED emitted light and the excitation light. The cuvette containing the sample was placed in the thermostated sample holder.

1.2.5 Circular Dichroism (CD) Spectroscopy

Protein CD spectra were recorded using an AVIV 60DS CD spectrometer. Light source was a fiber optics illuminator (Dyonics, USA) that had a white 175W, 60Hz lamp filtered with a blue glass filter. The fiber optics was fitted through a hole on the lid in order to be positioned directly on top of the cuvette. Shutters were designed and fitted into the lid to block the CD lamp and detector to protect them from the exciting light.

A temperature control bath was used and full spectra were recorded at 3℃ in order to slow down the back reaction to take the spectra of the adduct form. Samples placed into the CD sample chamber were in complete darkness while the CD lamp and detector were blocked and the exciting light was turned off. The dark spectra was recorded first, followed by 30 seconds of light irradiation to induce the adduct

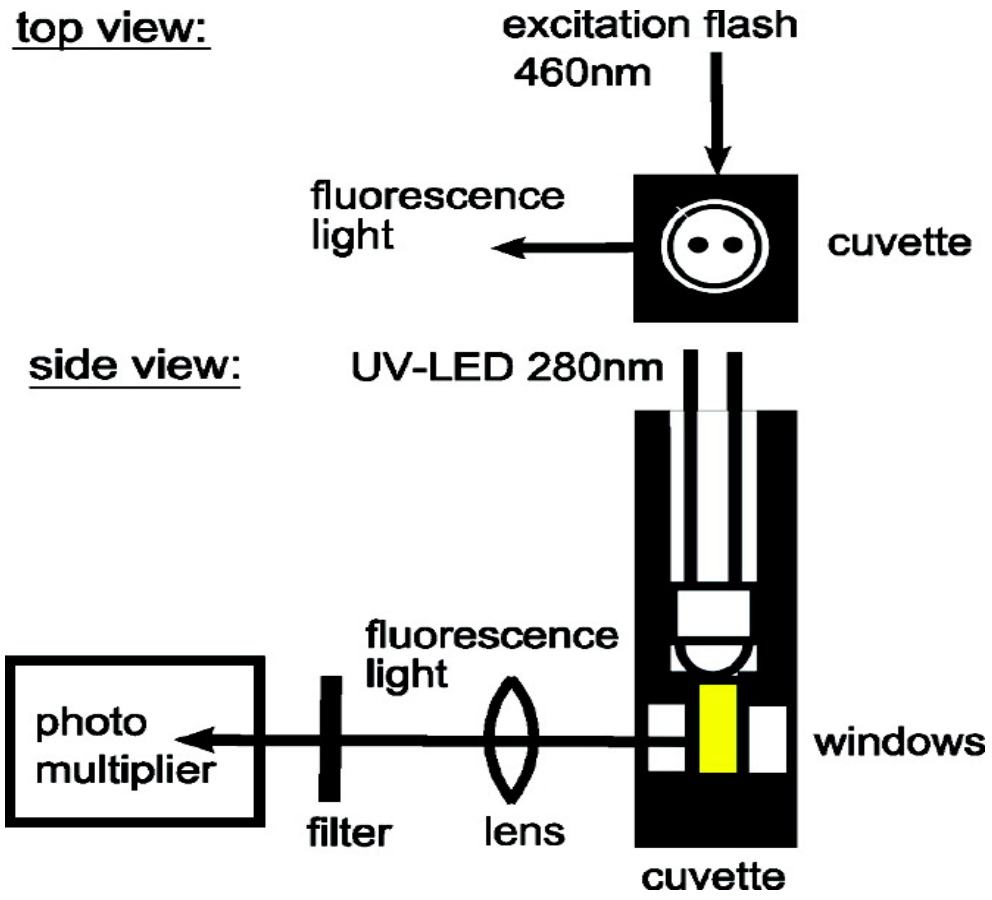

Figure 1-1 Set-up used for the measurement of the transient tryptophan fluorescence changes during the EL222 photocycle. The sample is illuminated by an LED emitting at 280 nm from above. The fluorescence light is collected under an angle of 90° and detected by a photomultiplier tube (PM).

formation. Full spectrum of the adduct was recorded, followed by more spectra to observe the spontaneous relaxation of the adduct to the dark state. In the far-UV region (190nm-250nm), a 0.1 cm pathlength, rectangular cuvette was used with a sample concentration of 6 µM. The data was transferred to a personal computer and the SigmaPlot (SPSS Science) program was used to plot and smooth the data.

1.2.6 Time-Resolved Optical Rotatory Dispersion (TRORD)

The schematic diagram of the TRORD instrument is shown in figure 2 and has already been described in detail [16]. In short, the TRORD system comprises two major components, the photo-excitation source for exciting the EL222 sample, which is a 355 nm light from a Q-switch Quanta Ray DCR-1 Nd: YAG laser. The second component is the probe beam which is initially an unpolarized light from a Xenon flash lamp passed through an MgF_2 polarizer to a mirror which focused the light at the sample [17]. After passing through the sample, the probe light then passes through a second UV-enhanced aluminum spherical mirror and a second MgF_2 polarizer. The light is then focused onto the slit of a spectrograph and detected with a CCD detector. The focused 3 mm laser beam intersects the probe light at an angle of 15° after entering the sample. Since the probe light passes through two polarizers (LP1 and LP2 from figure 2), ORD signals were obtained by measuring the intensities of the probe light after the first polarizer (LP1) has been rotated by angles of +β and –β off the crossed 90° angle of the two polarizers. The samples were kept at room temperature in a dark environment during the experiment. The EL222 sample was transferred to a 2mm quartz flow cell with a peristaltic pump, and flow through was collected in a collection vial and recycled for further data collection since the sample cycles in seconds. Far-UV TRORD data were collected at the following delays: 1.5 μs, 100 μs, 1 ms, 100 ms, and 1000 ms. An initial dark state ORD signal was collected before delay time points.

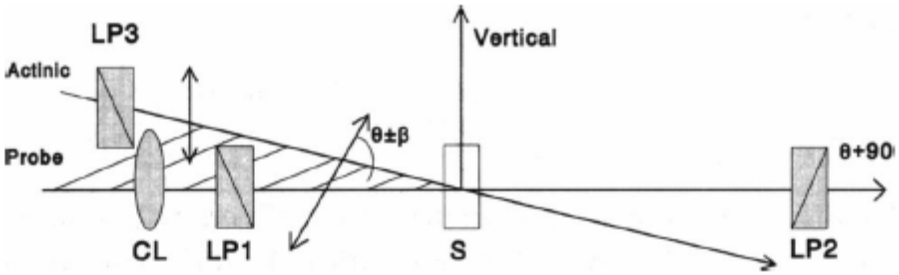

Figure 1-2 Schematic diagram of the TRORD instrument.

1.2.7 FTIR and Raman Data Collection and Analysis

FTIR measurements were performed on a Thermo Scientific spectrometer equipped with a microscope. 1-2 µl drop of nanopure water was placed on a silver coated FTIR microscope slide (Thermo Scientific, San Jose, CA) with a small amount of lyophilized sample added to the drop of water. The measurements were done under reflection mode with microscope light used to excite the photocycle of the EL222. The dark scan was taken first, followed by a scan after 30 seconds of white light illumination. The light minus dark difference spectrum was obtained by the subtraction of these two spectra. Following irradiation and the collection of data, a second dark spectrum was collected after several minutes to confirm that the sample had fully relaxed into its ground state and was behaving normally (photochemically active). The collected data was transferred to a personal computer and analysis of the spectra was carried out by OMNIC analysis software provided by manufacturer.

The Raman spectra were collected using Thermo Scientific spectrometer equipped with a microscope. Samples were prepared on a silver coated microscope slide as described above and used with the microscope to collect Raman data. The experiment was repeated with a sample in a sealed 3 mm glass capillary tube and comparable data were collected. Data was transferred to a personal computer and TQ analysis software (provided by manufacturer) was used to analyze the data.

1.3 Results

1.3.1 Sequence Analysis of EL222

Figure 1-3 shows the full sequence analysis of the EL222 which shows a 42% homology to the phot1-LOV2. The EL222, like all other LOV-domains studied, has a reactive cystiene (position 75) in a highly conserved flavin binding motif, GXNCRFLQ [18-19]. The EL222, unlike most other LOV-domains has alanine instead of glutamine (position 79) in the conserved binding motif which was used to explore the importance of hydrogen bonding in modulating the photocycle time constants of the EL222 (chapter 3). As the name indicates, full length EL222 has 222 amino acids with calculated molar mass of 24 kD. The histidine tag and antibody binding site adds another 0.5 to 1.0 kD. EL222 has an additional cysteine at position 70 which is not seen in LOV2. The presence of two tryptophans, both in the LOV-domain segment of the protein, allows us to follow the tryptophan fluorescence to probe the protein structural changes which is reported here. The N-terminus LOV-

domain spans residues 35-146 with a region of 18 amino acids following it that connects the LOV-domain to the HTH DNA binding domain at the C-terminus that spans residues 164-220 (fig 1-3). The 18 amino acid connecting region resembles the Jα-helix in LOV2 functionally.

```
         10          20          30          40          50          60
MGQDRPIDGS GAPGADDTRV EVQPPAQWVL DLIEASPIAS VVSDPRLADN PLIAINQAFT

         70          80          90         100         110         120
DLTGYSEEEC VGRNCRFLAG SGTEPWLTDK IRQGVREHKP VLVEILNYKK DGTPFRNAVL

        130         140         150         160         170         180
VAPIYDDDDE LLYFLGSQVE VDDDQPNMGM ARRERAAEML KTLSPRQLEV TTLVASGLRN

        190         200         210         220
KEVAARLGLS EKTVKMHRGL VMEKLNLKTS ADLVRIAVEA GI
```

Number of amino acids: 222
Molecular weight: 24381.7
Theoretical pI: 4.87

Amino acid composition:

Ala (A)	20	9.0%
Arg (R)	16	7.2%
Asn (N)	8	3.6%
Asp (D)	18	8.1%
Cys (C)	2	0.9%
Gln (Q)	8	3.6%
Glu (E)	17	7.7%
Gly (G)	16	7.2%
His (H)	2	0.9%
Ile (I)	10	4.5%
Leu (L)	24	10.8%
Lys (K)	10	4.5%
Met (M)	6	2.7%
Phe (F)	4	1.8%
Pro (P)	13	5.9%
Ser (S)	11	5.0%
Thr (T)	11	5.0%
Trp (W)	2	0.9%
Tyr (Y)	4	1.8%
Val (V)	20	9.0%

Total number of negatively charged residues (Asp + Glu): 35
Total number of positively charged residues (Arg + Lys): 26
Formula: $C_{1065}H_{1730}N_{302}O_{335}S_8$
Total number of atoms: 3440

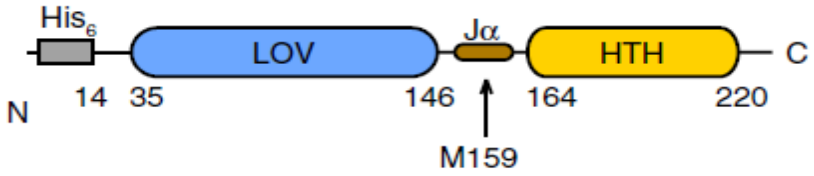

Figure 1-3 Sequence of EL222 and computation of various physical and chemical parameters using ProtParam tool from ExPASy bioinformatics resource portal [18-19]. Schematic illustration of the primary structure of full-length EL222 is also shown. Arrow represents position of chymotrypsin cut during light illumination studied by SDS-PAGE.

SDS-PAGE analysis of chymotrypsin limited proteolysis experiments show that upon illumination, EL222 gets cleaved within the Jα-linker at the methionine residue in position 159 (fig 1-3). This result suggests that light-induced conformational changes increase the accessibility of the Jα-linker by reorientation of the LOV and the HTH domains which happens through this linker.

1.3.2 FMN is the major chromophore inside the EL222

Although most LOV-domains, like the phot1-LOV2, have FMN (fig 1-4) as the flavin chromophore [7], a DNA-binding LOV-domain of *Neurospora Crassa* is reported to bind flavin adenine dinucleotide, FAD [20-21]. Phot1-LOV2 had been shown to bind FAD with chromophore exchange experiments and do photochemistry [22]. Also a fungal blue light photoreceptor named vivid (VVD) is reported to be capable of binding both FMN and FAD [23]. FMN, FAD, and riboflavin have similar absolute spectra therefore it is not possible to identify the chromophore by UV-Visible absorption spectroscopy. In order to determine the chromophore associated

with the LOV-domains, ethanol extraction at neutral pH and thin layer chromatography (TLC) method is usually used [7]. This method can hydrolyze the FAD into FMN by cleaving the phosphodiester bond therefore yielding only FMN as the chromophore observed in these studies. In order to avoid false results if the FAD is the chromophore, we decided to extract the associated chromophore under acidic

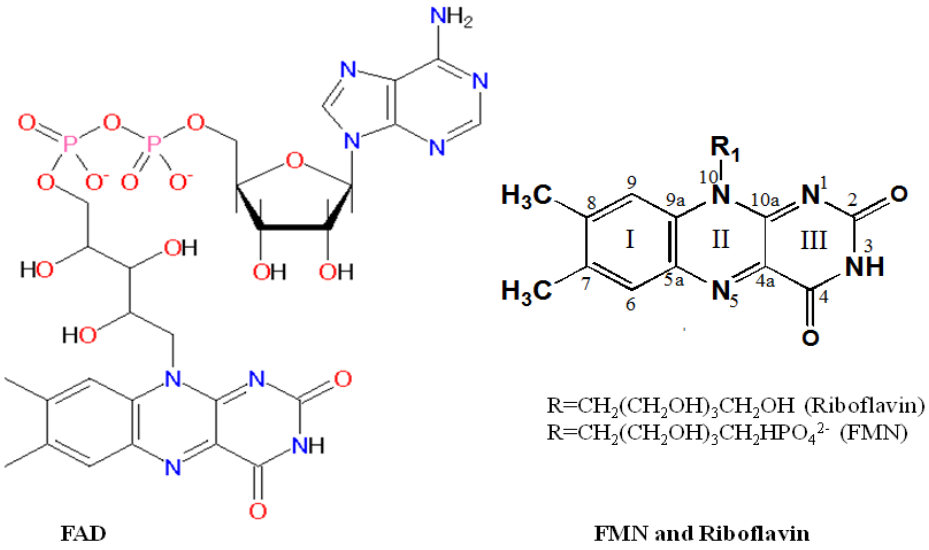

Figure 1-4 Flavin chromophores FMN, riboflavin, and FAD are shown. FMN and riboflavin have the same isoalloxazine ring and differ in their R-group. FAD has a ribose and adenine attached to the riboflavin by a diphosphate group. The numbering system of the isoalloxazine ring is also shown.

conditions using trichloroacetic acid (TCA) and run it through HPLC-MS to identify the flavin. FMN, under acidic conditions, can hydrolyze into riboflavin so observation of some riboflavin is expected if FMN is the chromophore. The TCA

extraction is a stable method for FAD and mass spectrometry can detect the presence of different flavins in our sample with high sensitivity. The standard solutions of riboflavin, FMN, and FAD show peaks of 377 g/mole, 456 g/mole, and 768 g/mole corresponding to their molecular weight. From the results of this experiment (fig 1-5) we conclude that the chromophore bound to EL222 is FMN. As expected, we also found riboflavin but according to our results, we have four times more FMN than riboflavin.

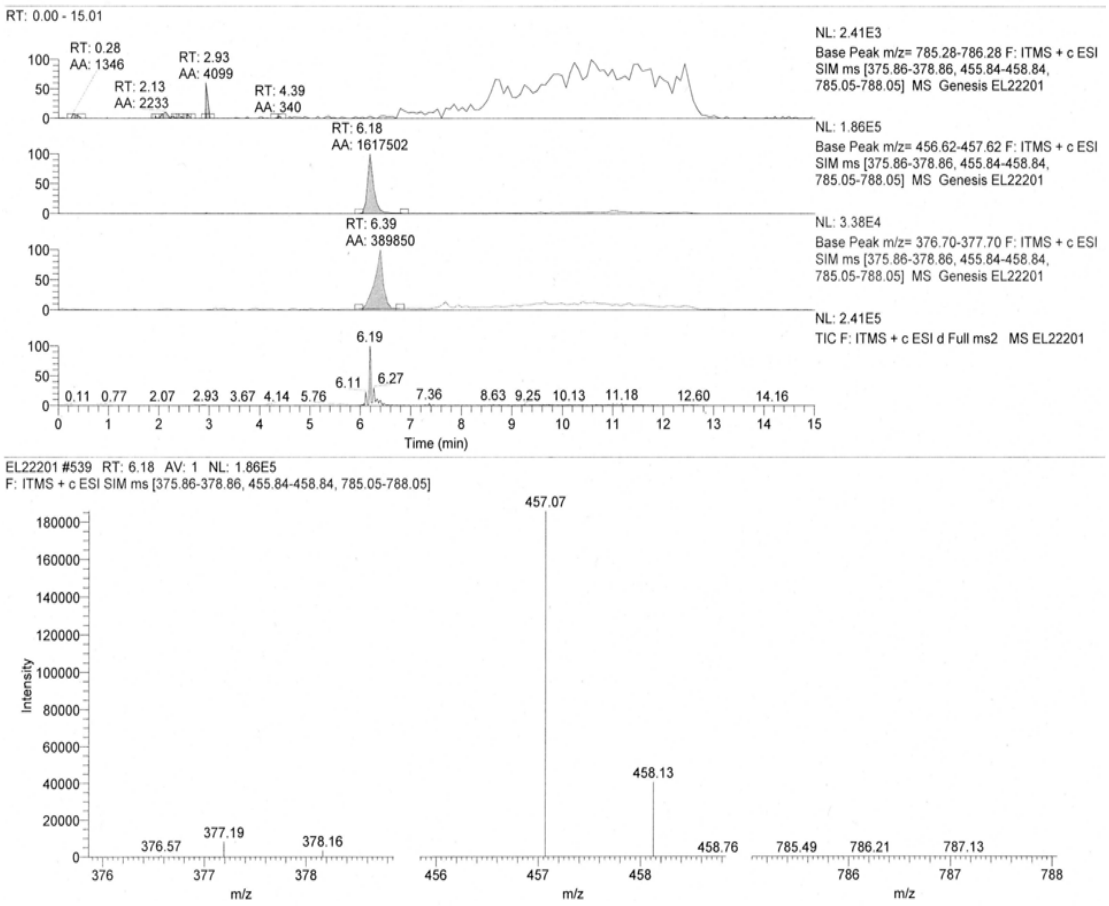

Figure 1-5 HPLC-MS of EL222 showing peaks with elution time and molecular masses correspond to those of riboflavin and FMN.

1.3.3 Kinetics of the adduct relaxation by UV-Visible spectroscopy

In order to establish that EL222 can do photochemistry and behave like LOV2, absolute spectra were taken which show a maximum at 450 nm with vibrational fine structures around it. Much like LOV2, EL222 loses blue light absorbance after illumination, which is characteristic of the formation of the cysteinyl adduct [13] which is named $EL222^{S}_{390}$ (signaling state with absorption at 390 nm). Upon removal of the light source, the sample relaxes back to the dark state spontaneously (fig 1-6). This observation is important since not all LOV-domains relax back to the dark state [24] so we needed to establish whether EL222 behaves like LOV2 or a non-cycler. After establishing that EL222 can undergo photochemistry, we performed kinetics at 450 nm for several minutes to find the half life of the relaxation back to the ground state. The recovery of the EL222 happens with a first order kinetics (fig 1-6) and half life is calculated to be 11 seconds at room temperature in a pH 7.0 buffer which is faster than the half life reported for LOV2 [13].

1.3.4 Time Resolved and Steady State Tryptophan Fluorescence and FMN fluorescence emission

Figure 1-7, shows the fluorescence emission spectra of EL222. The highest peaks are at 490 nm for the emission spectrum, with a shoulder near 530 nm. This is very similar to the fluorescence emission spectra previously reported for the LOV-domains from Oat and Arabidopsis [7, 9].

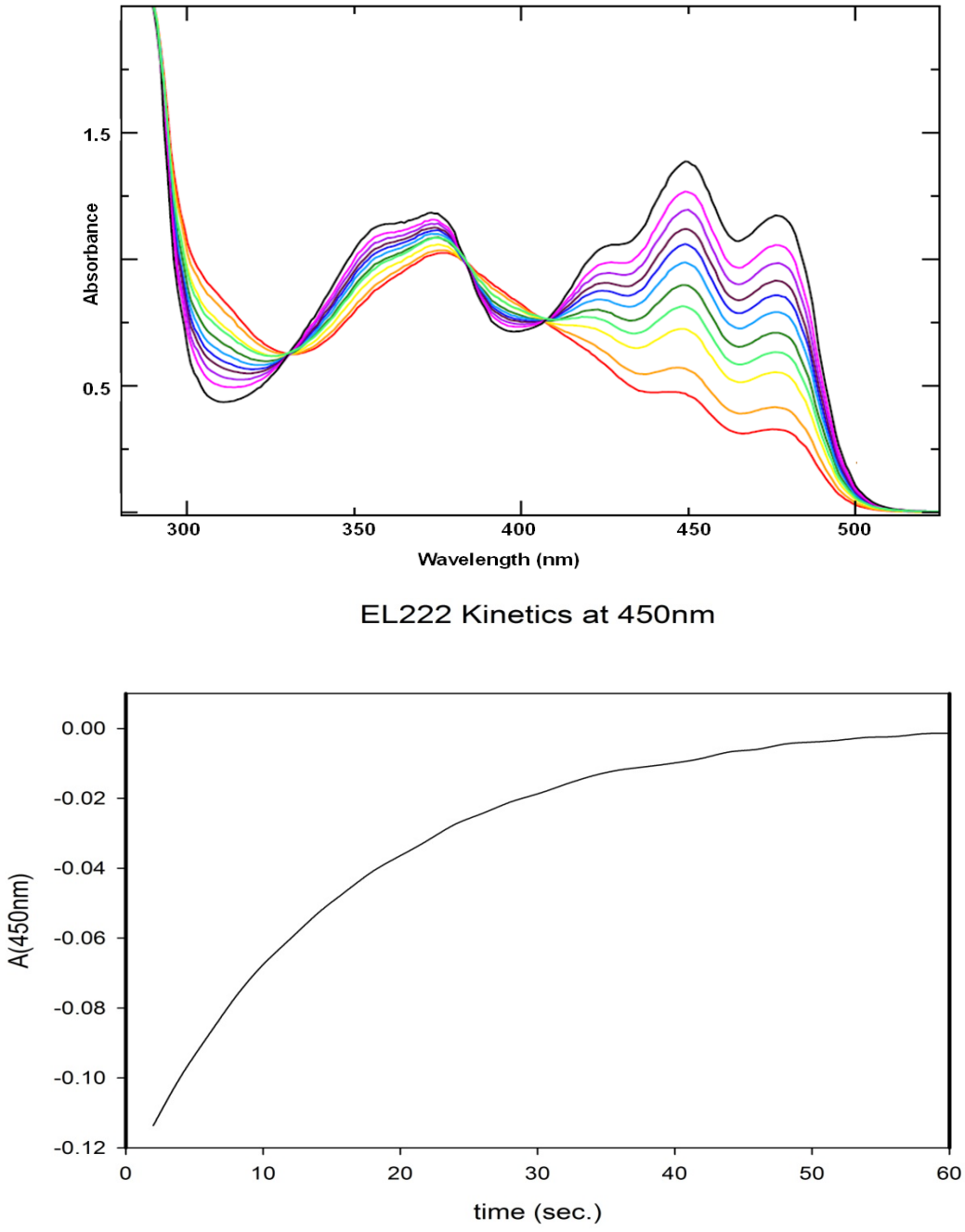

Figure 1-6 UV-Visible absorbance spectra of EL222 showing absorbance near 450 nm like other LOV domains and loss of blue light absorption after illumination and spontaneous recovery to the dark state. The kinetics of this recovery is has a first order kinetics and shows half-life of 11 seconds.

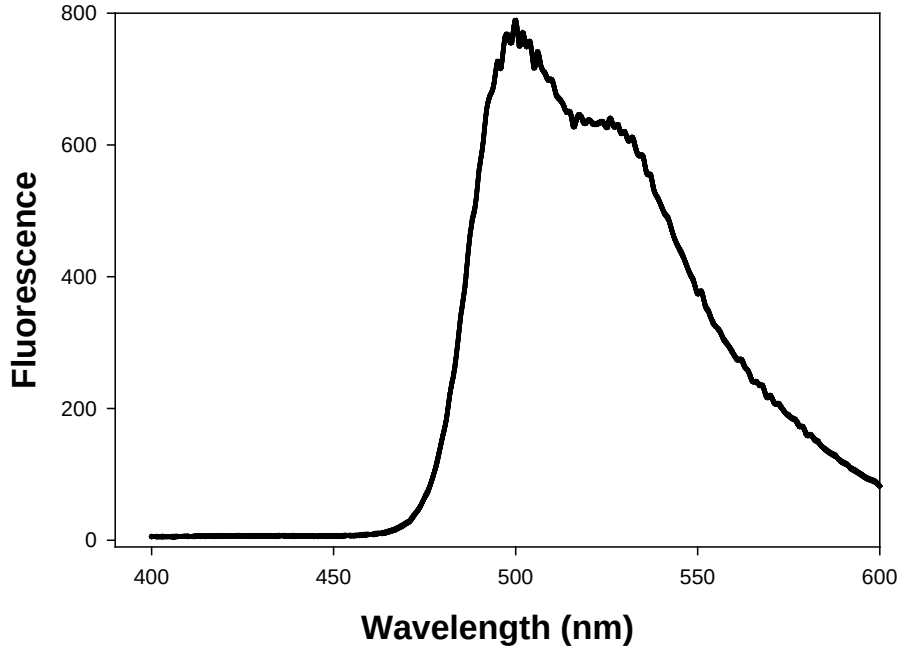

Figure 1-7 Fluorescence emission spectrum of the EL222 excited at 350nm. Emission spectrum is recorded from 400 nm to 600 nm.

As mentioned earlier, there are two tryptophans in the LOV-domain segment of the EL222 (fig 1-20) and since the indole side chain of tryptophan is highly fluorescent, it provides us with a natural site-specific fluorescent marker. Also, the wavelength maximum of the tryptophan is highly sensitive to the polarity of its environment [25] and is used to monitor the kinetics of conformational changes in proteins. This gives us the ability to monitor structural changes outside of the chromophore binding pocket. In order to observe if there are changes in tryptophan fluorescence of EL222, the steady state fluorescence measurements of both the dark

and the illuminated sample was performed (fig 1-8). The data indicates that blue light leads to an approximately 20% increase in the tryptophan fluorescence and a slight red shift from 339 nm to 341 nm. This result suggests that one or both tryptophan residues change their conformation or their environment with respect to their energy transfer partners. The increase in the fluorescence emission of the illuminated sample can suggest that the FMN is the likely energy transfer partner involved with tryptophan in fluorescence resonance energy transfer (FRET) in the ground state. While in the ground state, the singlet excited state of tryptophan (excited by 280 nm light, has a fluorescence emission of 340 nm that can overlap with the S_2 singlet excited state of FMN (fig 2-2) which is at 370 nm. This overlap (energy transfer) is lost after blue light illumination because the absorption maximum shifts from 370 nm to 390 nm. The loss of energy transfer is then seen as an increase in the tryptophan emission. Since in EL222 much like LOV2, we do not expect a big difference in the orientation of the FMN transition dipole moment between the dark and the adduct state, light induced movement of tryptophan residues relative to FMN is suspected. Also the red shift in the emission maximum of the illuminated sample can indicate that the tryptophans have entered into an even more polar environment since 340 nm emission in the dark state, already suggests a polar environment. The increase of fluorescence in this case is opposite of what is expected since water molecules quench tryptophan fluorescence and a decrease in fluorescence should be expected if tryptophans are exposed to more polar environment. This difference can be resolved by proposing that a yet unidentified amino acid quencher near tryptophan in the dark,

moves away from the tryptophan during light activated structural changes. The flexible loop connecting the LOV-domain and the HTH domain contains three aspartic acid residues and followed by a glutamine and a glutamic acid. All these amino acids are moderate to good tryptophan fluorescence quenchers [26] and are within a reasonable distance (10A°) to quench by excited state electron transfer. Glutamic and aspartic acids can quench by their carboxyl group and glutamine by its amide group [26].

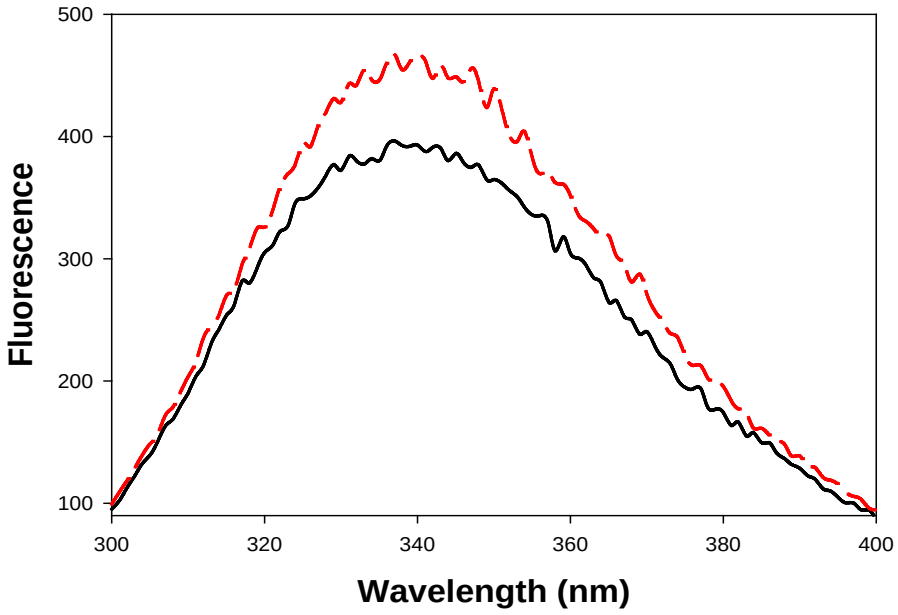

Figure 1-8 The Tryptophan Fluorescence of EL222 in dark (black solid line) and light (red dash line) was measured at room temperature. The excitation wavelength is 280nm and emission was followed between 300-400 nm.

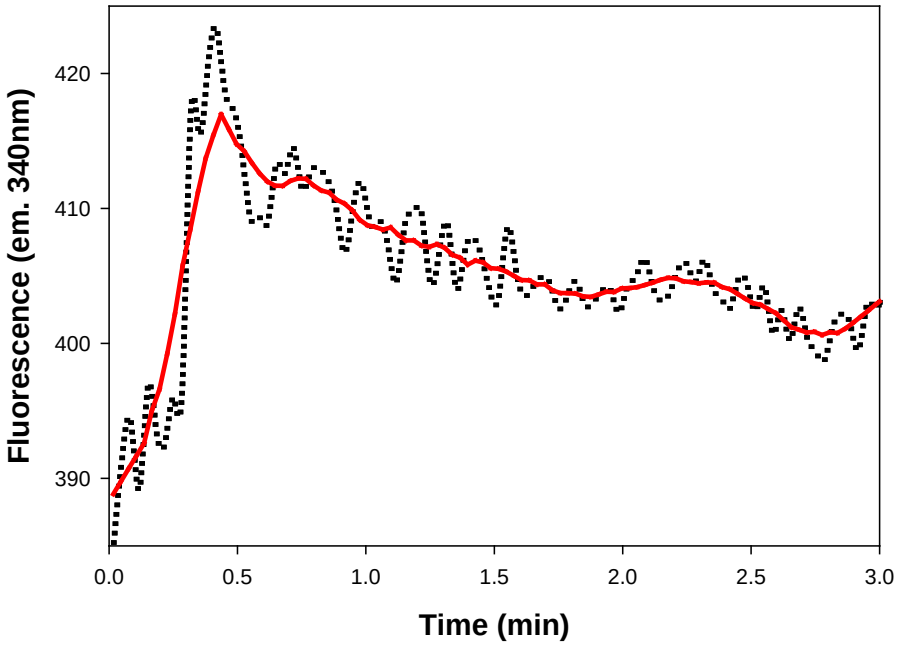

Figure 1-9 kinetics of tryptophan fluorescence studied. Excitation wavelength is 280 nm and emission wavelength is 340 nm and the kinetics is followed for three minutes. The dotted black line is the actual data and red solid line shows the smoothing of the data.

After establishing that there is a change in the tryptophan fluorescence of the EL222, the kinetics of this change was studied (fig 1-11) in seconds and then microsecond to millisecond using time resolved tryptophan fluorescence measurements (fig 1-10). Time resolved tryptophan fluorescence was used to monitor the dynamics of LOV2 conformational changes with 100 ns time resolution [27]. In LOV2, the fit curve of the transient fluorescence signal ($\Delta F/F_0$) is fitted using three exponentials which corresponds to time constants of 3.4 µs, 500 µs, and 4.3 ms.

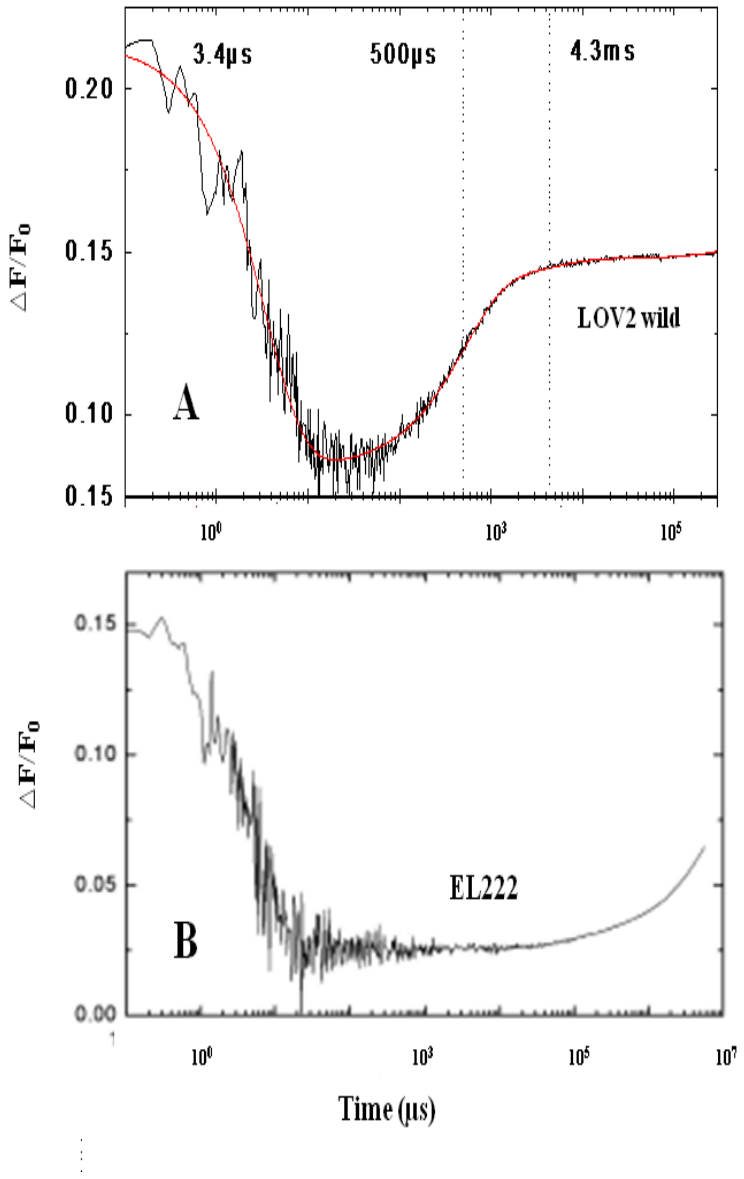

Figure 1-10 Transient tryptophan fluorescence of the LOV2 (A) and EL222 (B). Signal starts at 100 ns and with a large positive value and decreases in microsecond time range to a minimum that is around 20 µs.

As figure 1-10 shows, signal starts at 100 ns with a large positive value for both LOV-domains and then the signal decreases in microsecond time range to a minimum which is around 20 µs. The positive fluorescence change in the millisecond time range where adduct is the dominant species, is in agreement with the steady state tryptophan fluorescence change that we have seen (fig 1-8). In LOV2, the 3.4 µs phosphorescence emission signal is due to the phosphorescence of the flavin triplet state and two transitions at 500 µs and 4.3 ms are due to tryptophan emission (fig 1-10A). These two time constants indicate the light activated changes not sensed by the FMN and therefore not detected by UV-Visible spectroscopy [27]. In EL222, tryptophan fluorescence emission at microsecond time is not seen. Figure 1-10B shows that this fluorescence increase starts at about 200 ms and continues into seconds. This result was confirmed when this experiment was repeated in millisecond to seconds time range (data not shown).

1.3.5 Structural Changes during the photocycle of EL222 explored by Circular Dichroism (CD) Spectroscopy and Time-Resolved Optical Rotatory Dispersion Spectroscopy (TRORD)

The CD spectra of the EL222 ground state and adduct state in the far UV range (250 to 190 nm), which contains protein structural information is reported here (fig 1-11). The CD spectra show a maximum at 195 nm and a double minimum at 208 nm and 218 nm, which represents a helical secondary structure. The β-sheet conformation transitions occur at 175 nm, 198 nm, and 215 nm and are typically

smaller than α-helical conformations. The 195 nm and 208 nm bands represents the exciton split $\pi \rightarrow \pi^*$ transition and the 222 nm band represent the $n \rightarrow \pi^*$ transition of the peptide bond. It was shown in LOV2 that FMN does not make a significant contribution to the LOV2 far UV CD spectrum [28]. The CD spectrum for EL222 in the far UV range (fig 1-11) is therefore expected to show specially CD from the peptide bonds. This also means that the kinetic studies done at this region will reflect the light induced protein secondary structural changes. The double minima at 208 nm and 222nm suggest a well-folded protein with significant α-helical character in the ground state which is consistent with the crystal structure of this protein. Figure 1-11 shows the CD spectra of EL222 in the far UV range in dark and after light illumination. In LOV2, a 10-15% α-helicity loss is reported upon light activation [28] but in EL222, there is only a minimal change in the secondary structure content upon illumination. The minimal change is not unexpected, since recent studies of the histidine kinase LOVK indicates that the bacterial LOV-domain undergoes modest light-induced conformational changes [29]. Even with this information available, still the question remains: how do the peptide bonds of additional residues in EL222, which are not part of LOV-domain, contribute to the spectrum? There are 58 residues in EL222 that correspond to HTH DNA-binding domain with an additional 18 residues (Jα-helix) that are connecting the LOV-domain to the HTH domain.

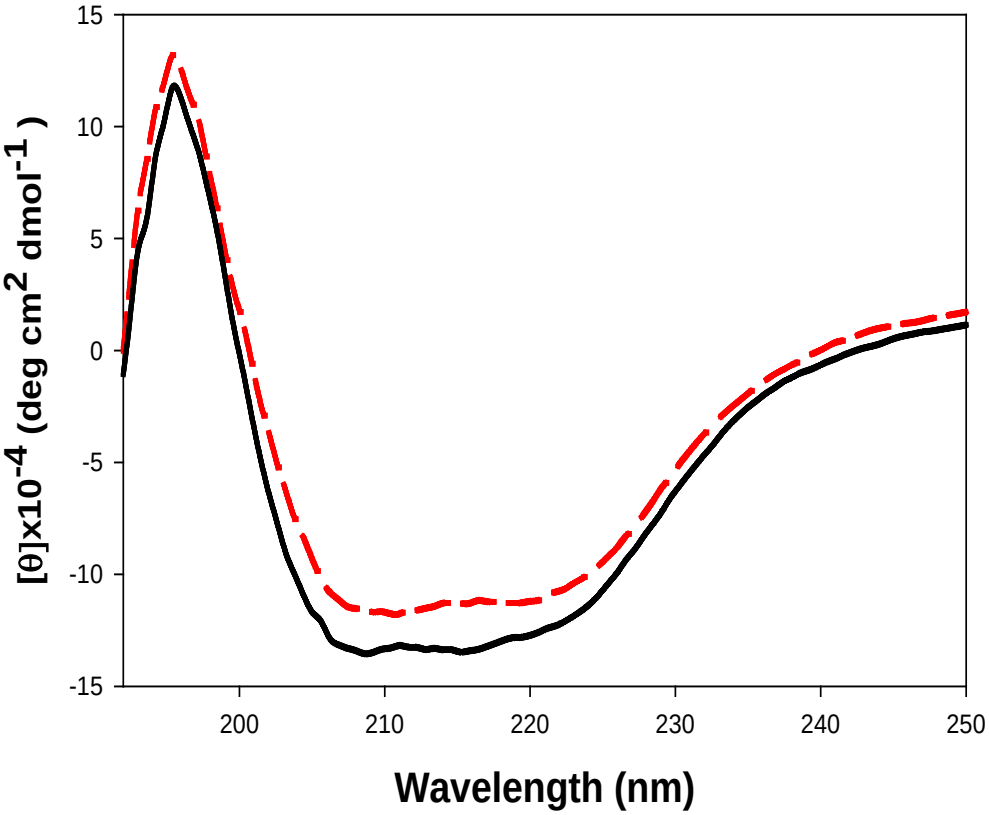

Figure 1-11 The CD spectrum for the EL222 in the far UV range reflect primarily CD from the peptide bond and thus reflects protein secondary structure (black solid line). The measurements were done at 3°C with 30 second illumination using Dyonics light source that had a white 175W 60Hz lamp. The observed double minimum at 208 and 218nm and the maximum around 195nm are signature features of helical secondary structure. Upon adduct formation, this spectrum loses some intensity (red dashed line) suggesting that very small amount of helicity is lost upon adduct formation.

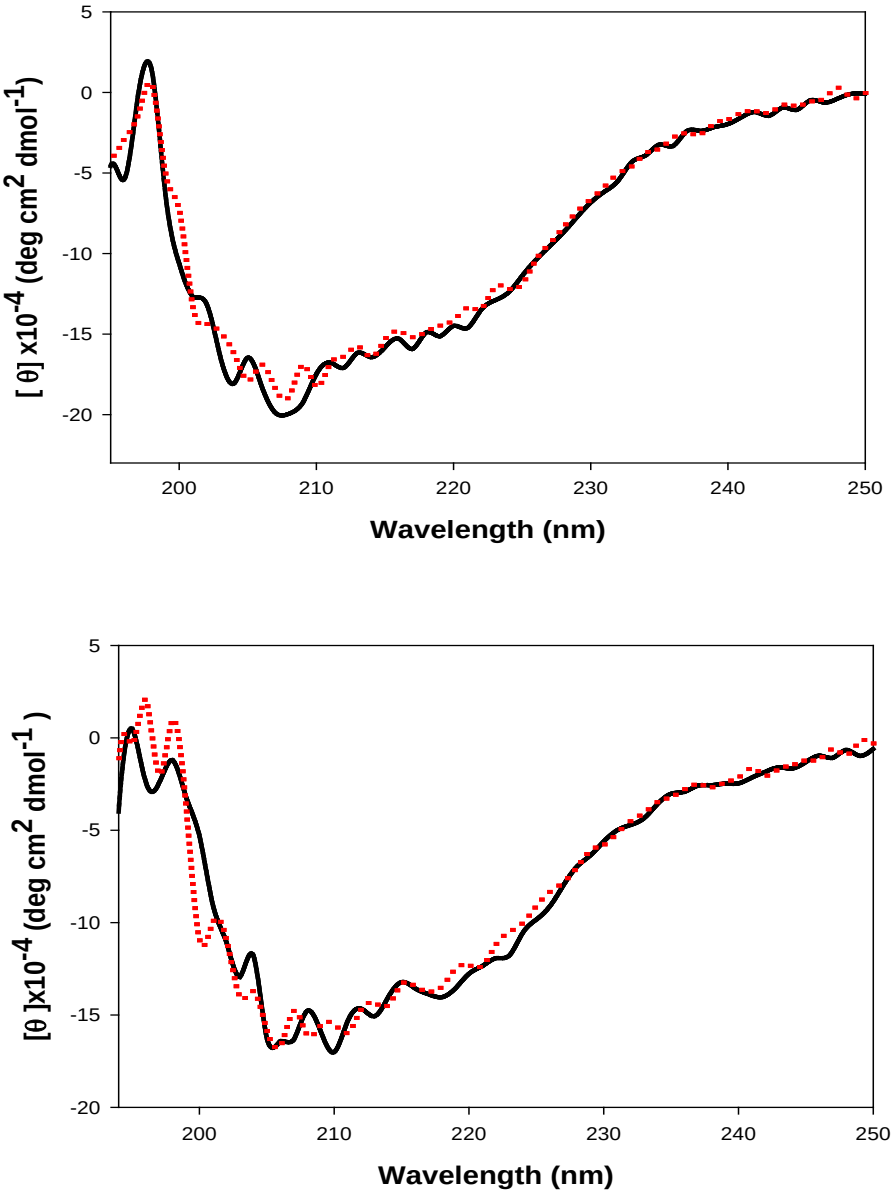

Figure 1-12 The CD spectrum for the EL222 LOV Jα-helix (top figure) and EL222 LOV-core (bottom figure) in the far UV range in dark state (black solid line) and in light state (red dotted line). The data for figures were not subjected to the smoothing function of the program to avoid errors.

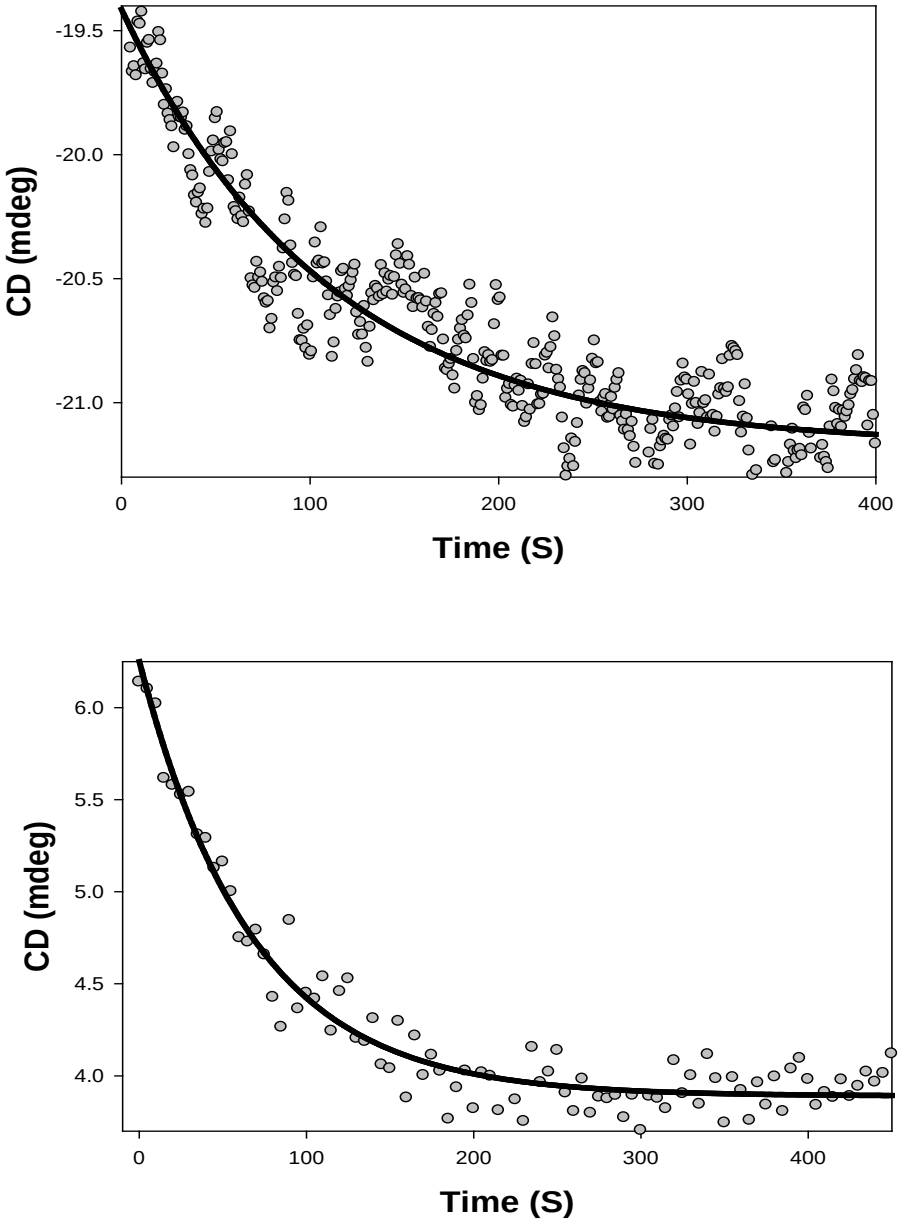

Figure 1-13 Dark relaxation of the EL222 adduct is followed for 450 seconds by circular dichroism at 218 nm (top figure) and 290 nm (bottom figure). Symbols represent raw data, and lines are first-order exponential fits. Experiment is performed at 3°C and first order exponential fit gave a half life 47 seconds.

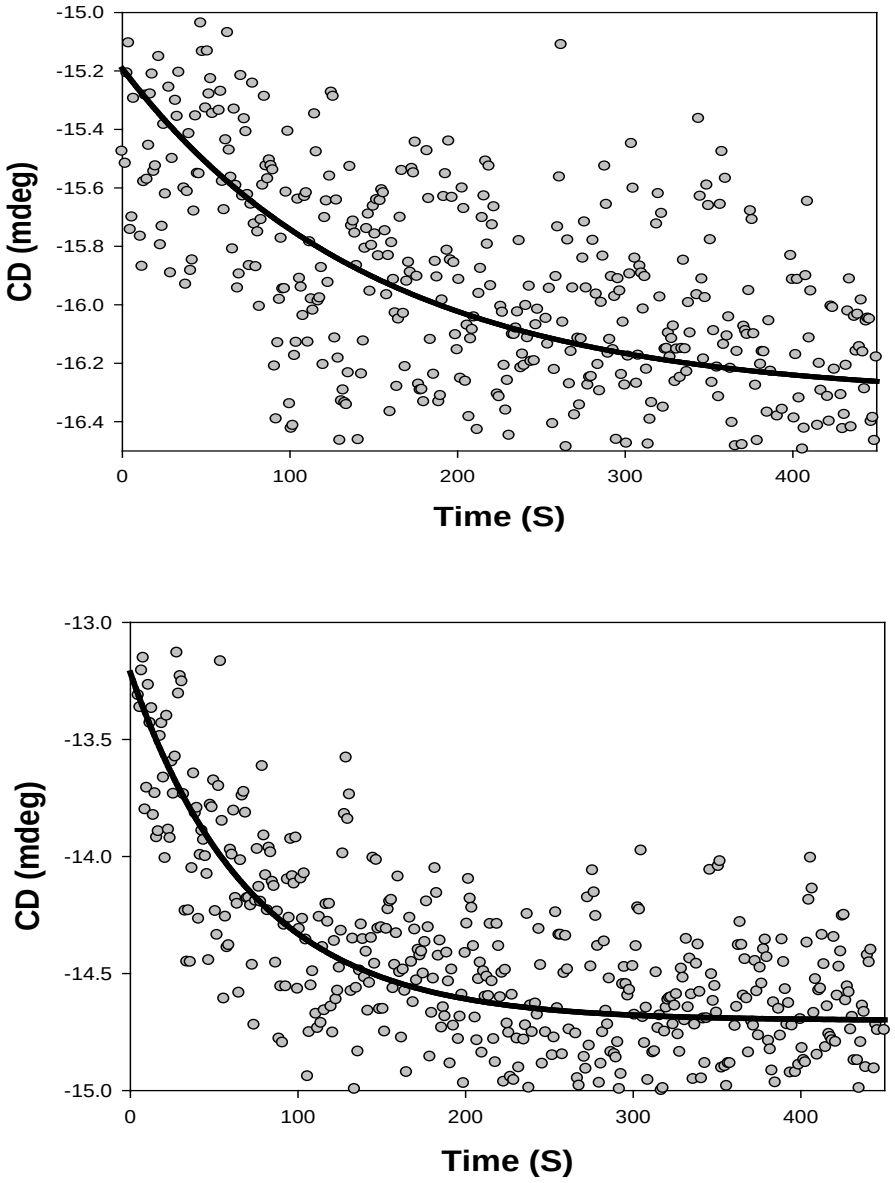

Figure 1-14 Dark relaxation of the EL222 LOV Jα-helix (top figure) and EL222 LOV-Core (bottom figure) adduct is followed for 450 seconds by circular dichroism at 218 nm. Symbols represent raw data, and lines are first-order exponential fits. Experiment is performed at 3°C.

In order to address the question, constructs of EL222 containing only the LOV-domain (EL222 LOV-core) and LOV domain with the Jα-helix (EL222 LOV Jα-helix) were prepared (see chapter 2 materials and methods). Figure 1-12 shows the far UV CD spectra of these two constructs and in both cases the change is still minimal. This observation means that although the peptide bonds of these additional residues contribute to the far UV CD spectrum, the change to the secondary structural content upon illumination remains minimal.

The CD spectroscopy was also used to detect whether protein structural changes could be separated kinetically from the chromophore during the photocycle. Since changes in the visible and near UV regions of the CD spectrum reflect mainly chromophore activity [28], and the far UV range of the CD spectrum indicates changes in protein secondary structure, one wavelength from each that show the changes with illumination was selected. We followed the dark relaxation of the EL222 adduct by CD spectroscopy to see whether the protein band of 218nm would show a different rate from the chromophore band of 290nm. As shown in figure 1-13, relaxation monitored at 218 nm and 290nm show single exponential decay with a half life of 47 seconds, at 3^0C. Additional wavelengths of 196nm and 330nm were then selected with different results. The 196nm wavelength did not show much change and 330nm showed a single exponential rise that did not match the study before (data not shown). Although we did not observe much changes in the far UV CD spectrum of the constructs, we still followed the adduct relaxation at 218 nm to see if the kinetics will be different than the full length EL222. In both cases (EL222

LOV Jα-helix, and EL222 LOV-Core), the dark relaxation followed first order exponential decay with half life comparable to the full length (fig 1-14). In both cases, constructs help clarify if the small changes we see are significant. Since HTH domain is all α-helical (4 helices), EL222 contains more helical structure than LOV2. One can hypothesize that smaller relative changes might be due to the large background CD of additional helices from the HTH domain. CD spectroscopy work showed that EL222 LOV domain still shows minimal change, meaning that the additional helical structure of HTH does not affect the percentage change and the LOV-domain from EL222 has smaller CD changes compared to LOV2.

In order to investigate the protein structural changes in more detail, nanosecond time-resolved optical rotatory dispersion (TRORD) spectroscopy was used. Figure1-15 shows the far-UV TRORD data of the EL222 adduct decay to the dark state. Data at only a few time points are shown because the change in the signal is very small. This result confirms our results obtained in time-resolved transient tryptophan fluorescence emission, where we see very small changes, if any in the microsecond and millisecond time range. It is important to add that tryptophan fluorescence emission indirectly probes protein conformational changes by monitoring the change in the environment of the tryptophans whereas TRORD method reports on the global secondary structural changes of the protein.

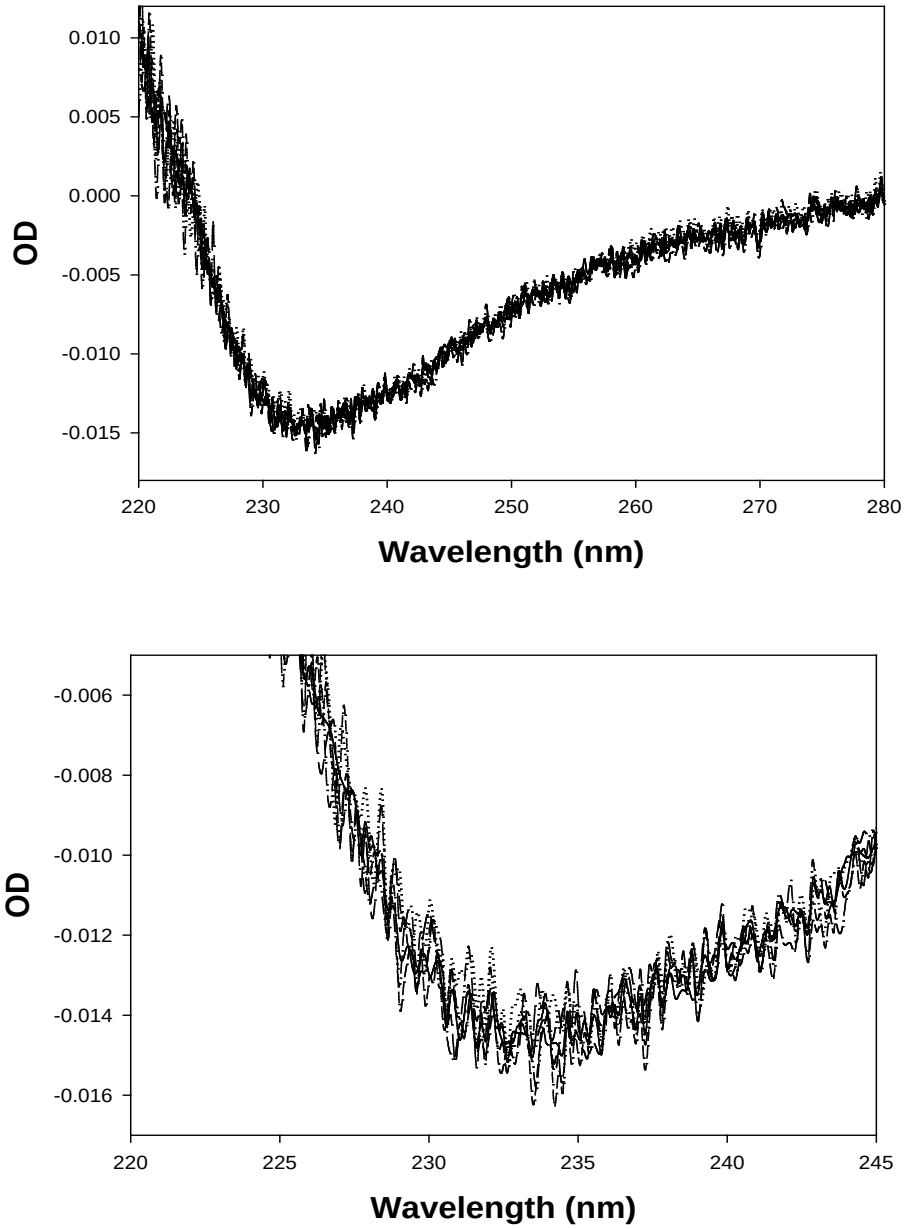

Figure 1-15 Far-UV TRORD data for the EL222 photocycle. Multichannel-detected ORD signals measured before illumination and delay times of 1.5 µs, 100 µs, 1 ms, 100 ms, and 1000 ms after illumination are shown (top figure). Data at only a few time points are shown because the change in signal is very small. The minimum area are zoomed (bottom figure) to show the small change.

1.3.6 FTIR reveals light induced chromophore and protein structural changes in the EL222

FTIR has been one of the most important tools in studying LOV-domain's intramolecular interactions in our lab [6] and elsewhere [30]. In order to further probe the structural changes that happen during the adduct formation, we measured the light-minus-dark FTIR difference spectra for the EL222 (fig 1-16). In the difference FTIR spectra, positive bands are assigned to the adduct state ($EL222^{S}_{390}$) and negative bands are assigned to the native dark state ($EL222^{D}_{450}$) vibrations. Many of the assigned bands are the vibration bands of FMN, which is based on the alignment of the FTIR bands of EL222 with the Resonance Raman bands of FMN [31]. In this study, we have also measured the Raman spectra of EL222 to compare with the difference FTIR spectra (fig 1-17). By comparing the resonance Raman bands of FMN [6] with the difference FTIR and Raman bands of EL222, we are able to assign these bands to chromophore and protein structural changes in the EL222. The findings in this study are summarized in table 1-1 and will be discussed here. FTIR provides the major evidence that the cysteinyl adduct is formed in EL222. Since the solved crystal structure of this protein is the dark state, FTIR is one technique that gives us direct evidence of the changes that happen to chromophore after illumination. The spectra shows the disappearance of bands at 1580, 1548, and 1350 cm^{-1} which originate from the disappearance of N5=C(4a) stretching vibrations [6]. This is consistent with the proposed model where the protonation of N5 and disappearance of this double bond leads to C(4a) adduct formation (fig 1-18). The

disappearance of these three prominent bands is also seen in the Resonance Raman of EL222. The adduct formation brings two notable positive bands of 1516 and 1537 cm^{-1} which are associated with symmetric and anti-symmetric stretching vibrations of C(10a)=N1 that is affected by disappearance of C(4a)=N5 double bond. These are coupled conjugated double bonds on the planer polar side of the FMN. These vibrations are expected to change after the adduct formation since the double bond disappears and C(4a) changes from a planer carbon (sp^2) to a tetrahedral carbon (sp^3). The protonation of N5 is represented by the appearance of 1375 cm^{-1} band which then causes C(4a) to become reactive carbocation, and then the sulfur of the cysteine 75 attacks it resulting in the formation of S-C(4a) bond. The loss of S-H bond of cysteine is seen as a negative band at 2570 cm^{-1} (fig 1-17, and table 1-1). We propose that the cysteine 75 of EL222 exists at an equilibrium between a thiol (-SH) and a thiolate ($-S^-$) form in the dark state. As the thiolate forms the thio-adduct with the C(4a) of the FMN, the equilibrium shift toward the ionized form of cysteine. We do see the disappearance of the S-H bond, which we observe in the FTIR difference spectra. The Raman S-C bond stretching in the adduct is predicted to be at 719 cm^{-1} [6] which is seen in the light illuminated sample. Although we cannot identify this band with complete certainty at this time without specific isotope substitution, the presence of this band only in the light illuminated sample allows us to predict that it may come from the S-C(4a) bond.

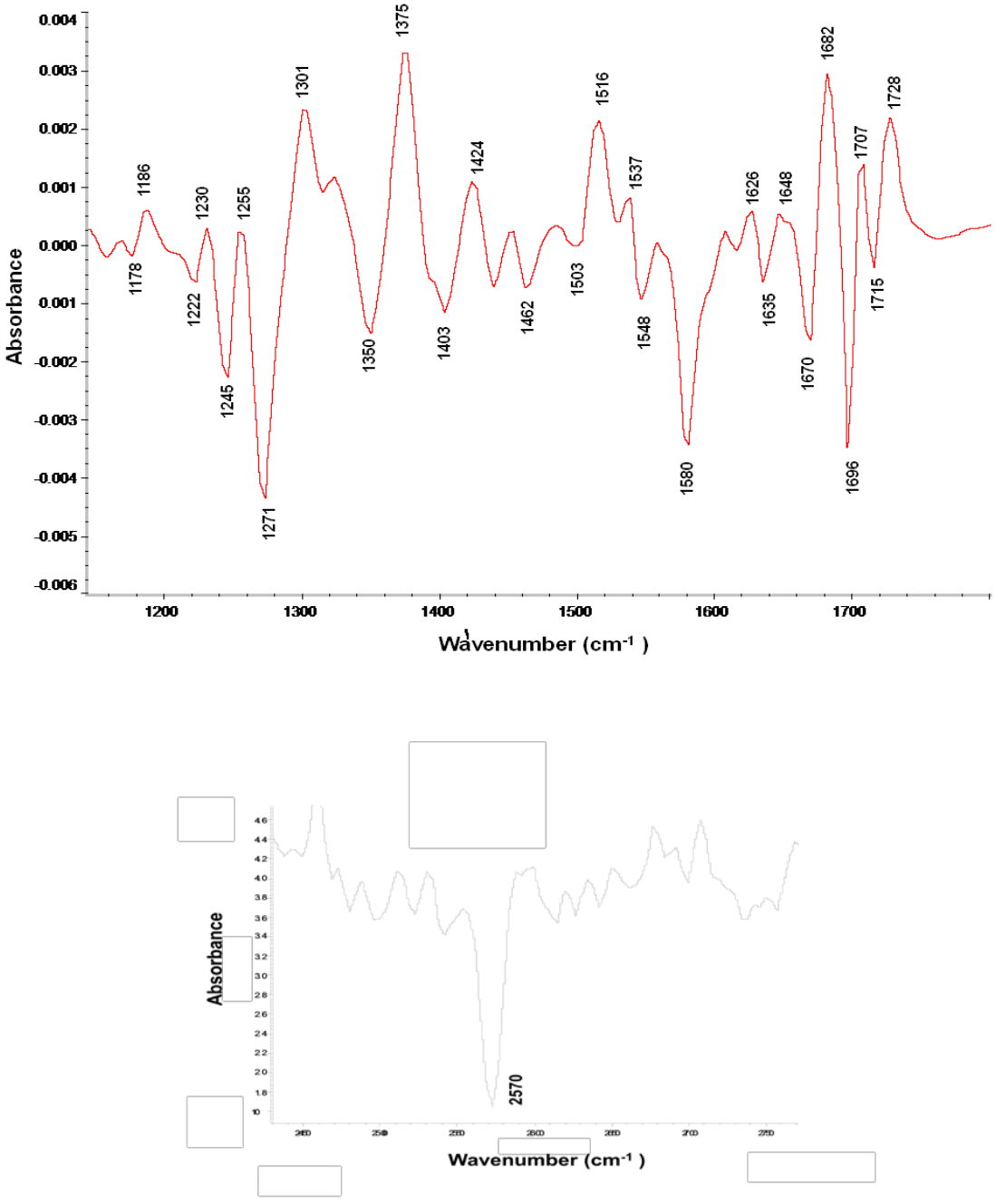

Figure 1-16 Difference between the FTIR spectra of EL222 adduct form and EL222 ground state (light minus dark). The bottom figure shows a negative band seen at 2570 cm^{-1} which is the S-H bond of the cysteine missing in adduct as expected.

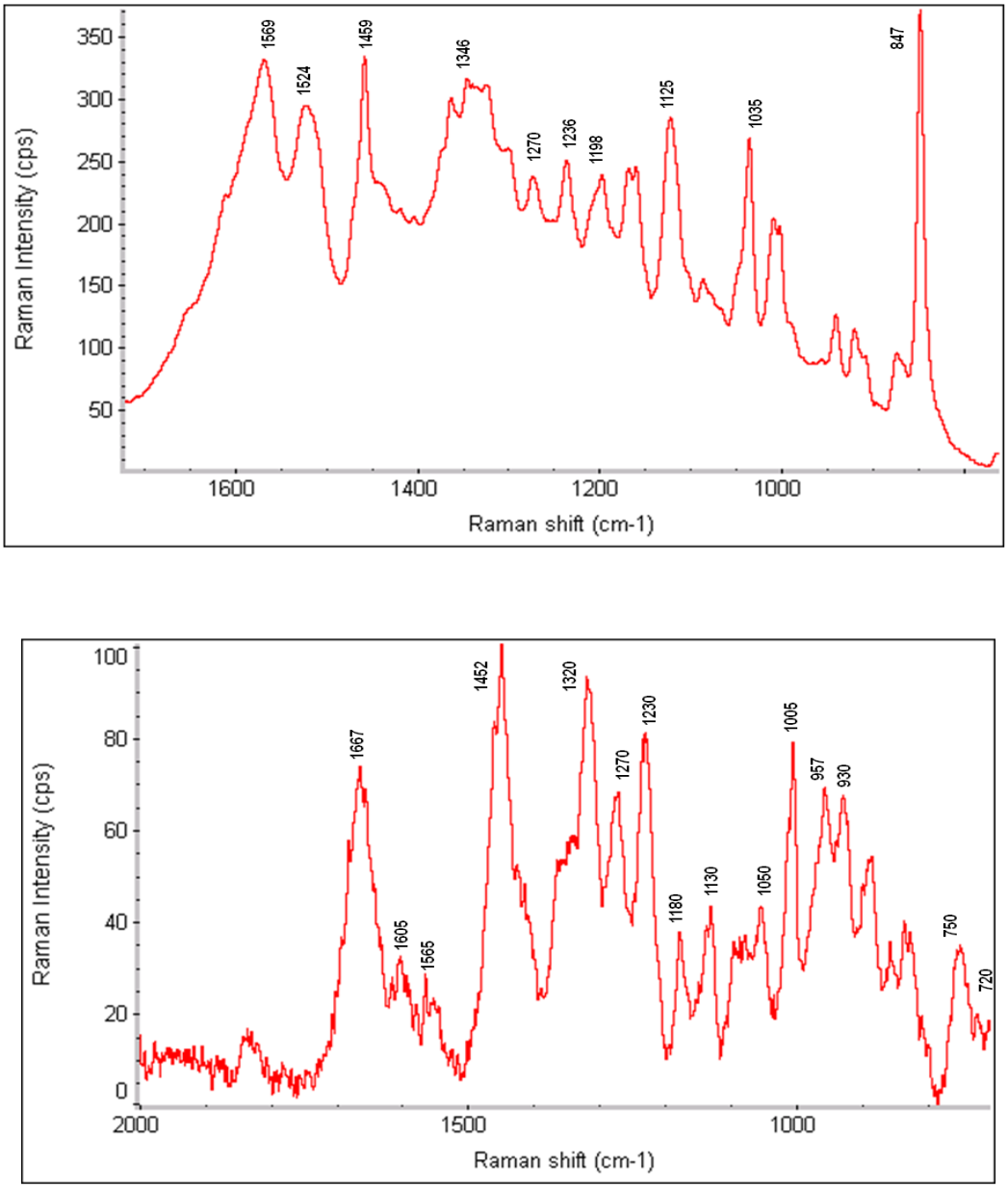

Figure 1-17 Raman spectra of the dark sample which is the ground state of EL222 (top figure) and the light illuminates sample which is the adduct state of EL222 (bottom figure).

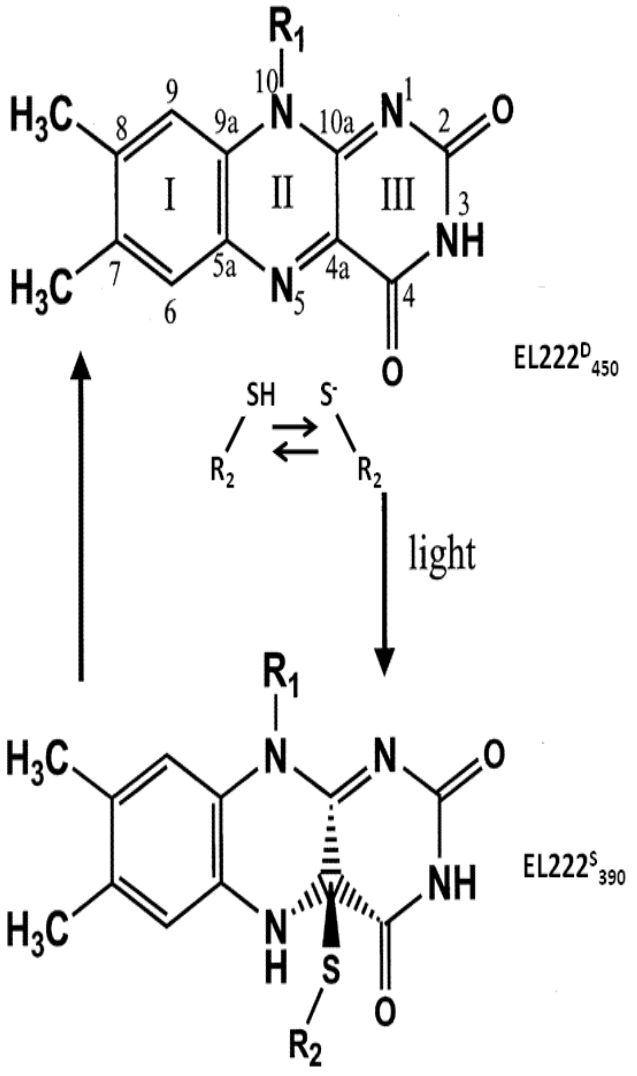

Figure 1-18 Simplified photocycle scheme of EL222 based on vibrational bands of the difference FTIR and Raman. The flavin chromophore with the numbering of atoms and rings of its isoalloxazine ring is shown. R_1 is the ribityl side chain of FMN and R_2 is the cysteine 75 of the EL222.

IR bands positive $EL222^{S}_{390}$	IR bands negative $El222^{D}_{450}$	Raman bands $EL222^{S}_{390}$	Raman bands $El222^{D}_{450}$	Raman bands of FMN	Vibrational assignment of EL222
	2570				ν(S-H)
1728					ν(C4=O), Amide I contribution
	1715				ν(C4=O), Amide I contribution
1707					ν(C4=O)
	1696				ν(C2=O), loop structure
1682		1667			Amide I of the turn structure
	1670				ν(C2=O), Amide I
1648					Amide I of loop structure
	1635			1632	ν(C=C) of ring I, Jα-helix contribution
1626					Amide I β-sheet
1608		1605			Amide I β-sheet
	1580		1569	1585	ν(C4a=N5), ν(C4a-C4)
1560		1565			
	1548		1524	1551	ν(N5=C4a), ν(C5a=C6), ν(C5a=N5)
1537					ν(C10a=N1), β-sheet amide II
1516					ν(C10a=N1)
	1503			1504	ν(C10a=N1), ν(C6=C7)
1485					Amide II
	1462		1459	1468	ν(C4a=N5), ν(C10a=N1)
1452		1452			
	1437				
1424					δ(C4-C4a), δ(C4=O)
	1403			1411	δ(C4=O), ν(C4-C4a)
1375					δ(N5-H), Ring I stretch
	1350		1346	1355	ν(C4a=N5), ν(C10a-C4a)
1322		1320			
1301					ν(C4-N3), ν(C10a=N1)
	1271	1270	1270		ν(N3-H)
1255					
	1245		1236	1259	δ(C2=O), ν(C2-N3), ν(C2-N1)
1230		1230			
	1222		1198	1229	ν(C10a-C4a), ν(C2-N3)
	1178	1180	1160	1185	ν(C10a-C4a)

Table 1-1 The vibrational bands of the EL222 domain detected by FTIR difference and Raman spectroscopy. The Raman bands of FMN in H_2O are introduced to assign the chromophore bands.

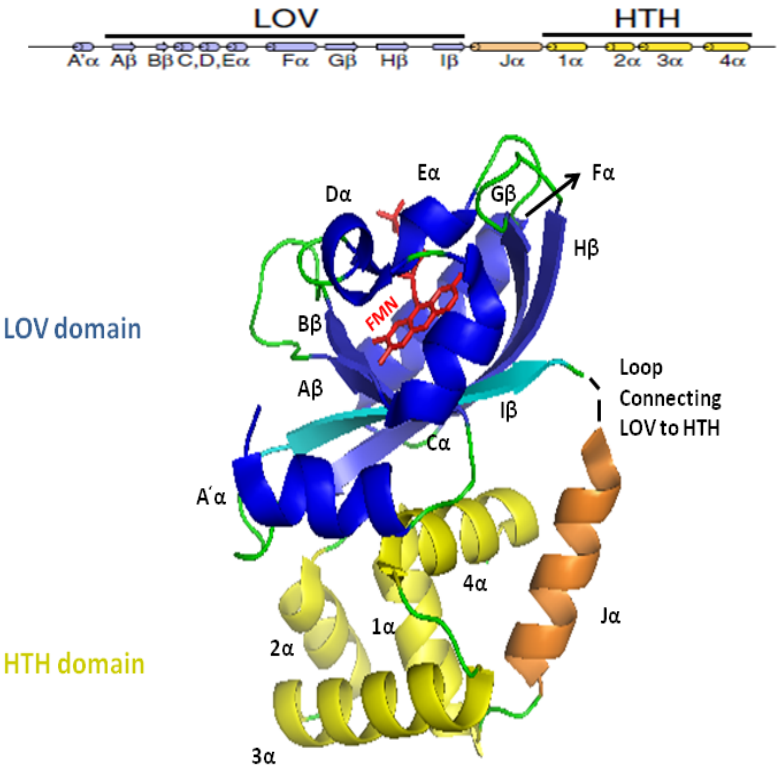

Figure 1-19 The dark-state crystal structure of EL222 reveals LOV-HTH interactions predicted to inhibit HTH DNA binding activity based on light induced DNA binding assay experiments. Overview of EL222 structure, showing locations of the LOV-domain (blue), HTH domain (yellow), and the Jα-helix (brown) which connects the two. The loop structure connecting the Jα-helix to the LOV domain was not resolved. It is predicted that the LOV domain binds to and interacts with the HTH domain using the LOV β-sheet surface (Iβ of the LOV shown in magenta interacting with 4α of the HTH domain). The light induced opening of the molecule removes the inhibition by LOV-domain and the HTH domain can bind to DNA to activate a transcription.

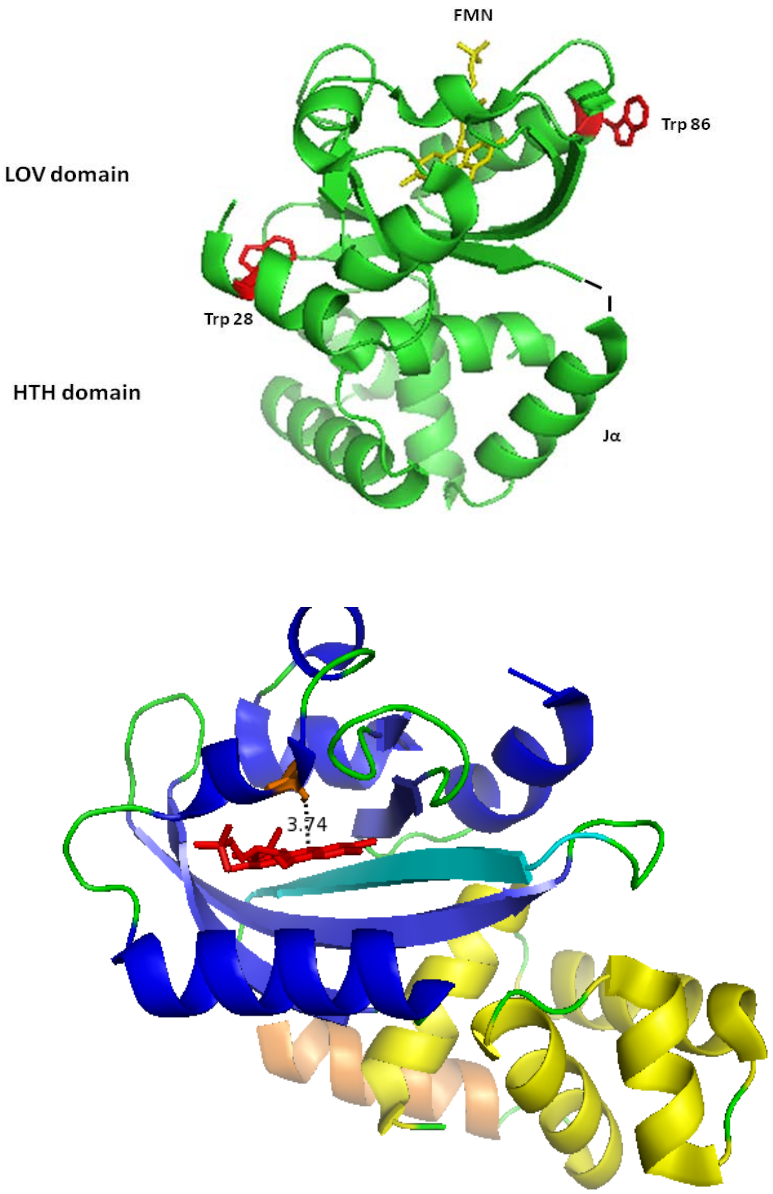

Figure 1-20 The structure of EL222 showing the two tryptophans both in the LOV-domain segment of the molecule. Tryptophans are used as markers for the tryptophan fluorescence spectroscopy. The bottom figure shows the view of the molecule from the top with active cysteine 3.7 Angstrom away from the N5 atom of the FMN.

1.4 Discussion

We have presented detailed biophysical and biochemical studies of the dark and light states of the EL222 to study the structural changes due to light activation. These studies define some of the molecular events associated with the formation and decay of the light state. In the absence of a light state crystal structure for EL222, the fluorescence emission spectrum of the EL222 exhibits the fluorescence properties of free flavins which mean EL222 is associated with a flavin. The extraction of chromophore and HPLC-MS studies of the extract showed the FMN is the chromophore inside the EL222. The FMN molecule is the light sensor inside the LOV-domain of EL222 and therefore the subject of much of our study. The UV-visible absorbance spectrum of the EL222 shows absorption at 450nm with vibronic structures around it, which is the result of the protein-FMN interactions in the dark state. EL222 shows loss of this absorbance upon illumination much like other LOV-domains and forms an adduct which relaxes spontaneously back to the ground state.

Light induced conformational changes in EL222 are very different from phot1-LOV2. Unlike LOV2, time resolved tryptophan fluorescence of EL222 did not show any conformational changes in either the microsecond or millisecond range but change was observed much later in seconds. In LOV2, the changes were attributed to the detachment of the relatively small J-helix present in these constructs. EL222 is a much bigger molecule than LOV2 (almost twice as large) and shows a much smaller light induced secondary structure change (results from the CD spectroscopy). These

small conformational changes in the LOV-domain are followed by changes in the much larger full length protein presumably transmitted via the J-helix linkage [14]. The movement of a larger molecule mass might explain the longer time it takes to see conformational changes in the full-length EL222. The 10 to 15% CD changes in the α-helical region of LOV2 comes from the unraveling of the Jα-helix (loss of helicity) which translates into the opening of the molecule [28]. We propose that the opening of the EL222 happens through a loop structure (residues 140-149) and not through the unraveling of Jα-helix which explains the small CD changes we observed. The crystal structure and light-minus-dark FTIR studies presented here help explain the small change in CD spectra in more detail. The PAS domain signaling usually happens via a β-sheet surface and many LOV-domains do the same [32]. The crystal structure of EL222 reveals extensive LOV-HTH interactions around Iβ-sheet of the LOV-domain and 4α-helix of the HTH domain (fig 1-19). The blue light activation of the light domain changes the hydrogen bonding between FMN chromophore and residues on the Iβ-sheet (specifically glutamine at position 138). The rearrangement of the LOV-domain in the adduct state then causes the interactions between Iβ and 4α to change and release the effector HTH domain without unfolding the Jα-helix as proposed in phot1-LOV2 ( ). Positive bands at 1626 and 1608 cm^{-1} of the difference FITR might be contributions from changes in the β-sheet interactions with the 4α-helix. This model not only explains the small change seen in CD spectra but may also explain the longer times seen in the tryptophan fluorescence emission experiments. We have shown here that the far-UV CD kinetics in the regions of the

protein change have the same profile as that of the CD changes corresponding to the FMN chromophore, suggesting that FMN and protein structural changes have a common rate limiting step. This small change in the area of Iβ-sheet of LOV-domain 4α-helix of the HTH domain might not have been felt by the two tryptophans (fig-20) at the same time frame as the adduct formation. This implies that there might be additional intermediates in the signaling state of this molecule. After the adduct formation and the rearrangement of the hydrogen bonding, which happens in the microsecond time range, the molecule then opens up as two domains separate. The opening of the EL222 molecule exposes the tryptophans (especially tryptophan at position 29) to the polar environment around the molecule, therefore increasing the tryptophan fluorescence and shifting the emission to the red. The observation of additional intermediate steps were also seen in phot1-LOV2 by CD spectroscopy [17] and fluorescence spectroscopy [27] in the microsecond and millisecond time range.

Light-minus-dark FTIR bands also provided information about the chromophore inside the EL222 with direct evidence for a light-induced adduct formation. As explained in the results section, bands of difference FTIR spectra show the disappearance of the C(4a)=N5double bond and the formation of N5-H band, which we believe to be the rate limiting step in the adduct formation (chapter 2). The disappearance of the S-H band of the cysteine, which is the necessary step to form the adduct, is also seen. With the results obtained in this study, we investigated the details of the adduct formation and relaxation back to the ground state (chapter 2) as

well as the effects of altering Iβ-sheet interactions with the chromophore on the photocycle of EL222 (chapter 3).

References:

1. Huala, E., et al., *Arabidopsis NPH1: a protein kinase with a putative redox-sensing domain.* Science, 1997. **278**(5346): p. 2120-3.

2. Jarillo, J., et al., *Phototropin-related NPL1 controls chloroplast relocation induced by blue light.* NATURE, 2001. **410**(6831): p. 952-954.

3. Kagawa, T., et al., *Arabidopsis NPL1: a phototropin homolog controlling the chloroplast high-light avoidance response.* Science, 2001. **291**(5511): p. 2138-41.

4. Sakai, T., et al., *Arabidopsis nph1 and npl1: blue light receptors that mediate both phototropism and chloroplast relocation.* Proc Natl Acad Sci U S A, 2001. **98**(12): p. 6969-74.

5. Briggs, W., et al., *The phototropin family of photoreceptors.* PLANT CELL, 2001. **13**(5): p. 993-997.

6. Swartz, T., et al., *Vibration spectroscopy reveals light-induced chromophore and protein structural changes in the LOV2 domain of the plant blue-light receptor phototropin 1.* BIOCHEMISTRY, 2002. **41**(23): p. 7183-7189.

7. Christie, J.M., et al., *LOV (light, oxygen, or voltage) domains of the blue-light photoreceptor phototropin (nph1): binding sites for the chromophore flavin mononucleotide.* Proc Natl Acad Sci U S A, 1999. **96**(15): p. 8779-83.

8. Gu, Y.-Z., J.B. Hogenesch, and C.A. Bradfield, *The PAS Superfamily: Sensors of Environmental and Developmental Signals.* Annual Review of Pharmacology and Toxicology, 2000. **40**(1): p. 519-561.

9. Salomon, M., et al., *Photochemical and mutational analysis of the FMN-binding domains of the plant blue light receptor, phototropin.* BIOCHEMISTRY, 2000. **39**(31): p. 9401-9410.

10. Harper, S.M., L.C. Neil, and K.H. Gardner, *Structural Basis of a Phototropin Light Switch.* Science, 2003. **301**(5639): p. 1541-1544.

11. Crosson, S., *LOV-domain structure, dynamics and diversity*, in *Handbook of Photosensory Receptors*, W. Briggs, Spudich, JL., Editor. 2005, Wiley VCH: Weinheim. p. 323-336.

12. Fedorov, R., et al., *Crystal structures and molecular mechanism of a light-induced signaling switch: The Phot-LOV1 domain from Chlamydomonas reinhardtii.* BIOPHYSICAL JOURNAL, 2003. **84**(4): p. 2474-2482.

13. Swartz, T., et al., *The photocycle of a flavin-binding domain of the blue light photoreceptor phototropin.* JOURNAL OF BIOLOGICAL CHEMISTRY, 2001. **276**(39): p. 36493-36500.

14. Harper, S.M., J.M. Christie, and K.H. Gardner, *Disruption of the LOV-J alpha helix interaction activates phototropin kinase activity.* Biochemistry, 2004. **43**(51): p. 16184-16192.

15. Nash, A.I., et al., *Structural basis of photosensitivity in a bacterial light-oxygen-voltage/helix-turn-helix (LOV-HTH) DNA-binding protein.* Proceedings of the National Academy of Sciences, 2011. **108**(23): p. 9449-9454.

16. Shapiro, D.B., et al., *Nanosecond optical rotatory dispersion spectroscopy: application to photolyzed hemoglobin-CO kinetics.* Biophysical journal, 1995. **68**(1): p. 326-334.

17. Chen, E., et al., *A LOV Story: The Signaling State of the Phot1 LOV2 Photocycle Involves Chromophore-Triggered Protein Structure Relaxation, As Probed by Far-UV Time-Resolved Optical Rotatory Dispersion Spectroscopy†.* Biochemistry, 2007. **46**(15): p. 4619-4624.

18. Arnold, K., et al., *The SWISS-MODEL workspace: a web-based environment for protein structure homology modelling.* Bioinformatics, 2006. **22**(2): p. 195-201.

19. Bordoli, L., et al., *Protein structure homology modeling using SWISS-MODEL workspace.* Nat. Protocols, 2008. **4**(1): p. 1-13.

20. Cheng, P., et al., *Functional conservation of light, oxygen, or voltage domains in light sensing.* PROCEEDINGS OF THE NATIONAL ACADEMY OF SCIENCES OF THE UNITED STATES OF AMERICA, 2003. **100**(10): p. 5938-5943.

21. He, Q., et al., *White collar-1, a DNA binding transcription factor and a light sensor.* SCIENCE, 2002. **297**(5582): p. 840-843.

22. Schwerdtfeger, C. and H. Linden, *VIVID is a flavoprotein and serves as a fungal blue light photoreceptor for photoadaptation.* EMBO JOURNAL, 2003. **22**(18): p. 4846-4855.

23. Dürr, H., M. Salomon, and W. Rüdiger, *Chromophore Exchange in the LOV2 Domain of the Plant Photoreceptor Phototropin1 from Oat†.* Biochemistry, 2005. **44**(8): p. 3050-3055.

24. Swartz, T.E., et al., *Blue-light-activated histidine kinases: Two-component sensors in bacteria.* Science, 2007. **317**(5841): p. 1090-1093.

25. Lakowicz, J., R., *Principles of Fluorescence Spectroscopy*. 2006.

26. Chen, Y. and M.D. Barkley, *Toward Understanding Tryptophan Fluorescence in Proteins†.* Biochemistry, 1998. **37**(28): p. 9976-9982.

27. Hoersch, D., et al., *Dynamics of Light-Induced Activation in the PAS Domain Proteins LOV2 and PYP Probed by Time-Resolved Tryptophan Fluorescence.* Biochemistry, 2010. **49**(51): p. 10811-10817.

28. Corchnoy, S., et al., *Intramolecular proton transfers and structural changes during the photocycle of the LOV2 domain of phototropin 1.* JOURNAL OF BIOLOGICAL CHEMISTRY, 2003. **278**(2): p. 724-731.

29. Alexandre, M.T.A., et al., *Electronic and Protein Structural Dynamics of a Photosensory Histidine Kinase.* Biochemistry, 2010. **49**(23): p. 4752-4759.

30. Bowman, W.D. and T.G. Spiro, *Normal mode analysis of lumiflavin and interpretation of resonance Raman spectra of flavoproteins.* Biochemistry, 1981. **20**(11): p. 3313-8.

31. Kasahara, M., et al., *Photochemical properties of the flavin mononucleotide-binding domains of the phototropins from Arabidopsis, rice, and Chlamydomonas reinhardtii.* PLANT PHYSIOLOGY, 2002. **129**(2): p. 762-773.

32. Crosson, S., S. Rajagopal, and K. Moffat, *The LOV domain family: Photoresponsive signaling modules coupled to diverse output domains.* BIOCHEMISTRY, 2003. **42**(1): p. 2-10.

CHAPTER 2

PHOTOCYCLE OF THE BLUE LIGHT ACTIVATED EL LOV-HTH PROTEIN: KINETICS AND SCHEME

2.1 Introduction

The genome of *Erythrobacter Litoralis* HTCC2594, a marine bacterium, codes for a 222 amino acid protein (EL222) that contains a 146 amino acid LOV-domain at the N-terminus and a helix-turn-helix (HTH) domain at the C-terminus. This DNA binding domain is a member of a Lux-R type DNA binding domain family that is regulated with an N-terminal regulatory domain. Lux-R is involved in quorum sensing, the process of cell-to-cell communication between bacteria via secreted signal molecules called autoinducers. The detection of these autoinducers ultimately leads to the production of LuxR, the quorum-sensing master regulator that controls expression of the genes (usually a large number of genes) in the quorum sensing regulon [1]. The LOV domain is a flavoprotein that functions as a light-sensory module in plants, algal, fungal, and bacterial blue light receptors [2]. LOV domains are associated with a wide variety of physiological responses [3-4] in all three kingdoms of life [5]. *E. coli* expressed LOV domain from plant blue light receptor (LOV2 from phototropin 1) binds riboflavin-5'-monophosphate (FMN) as a chromophore and shows major absorption peaks at 370 and 450 nm. The 450 nm absorption peak of LOV domain shows vibronic structure at 425 and 475 nm that are absent in the absorption of the free FMN in H_2O at room temperature. Upon

illumination, a flavin-cysteinyl adduct is formed between a sulfur of a highly conserved cysteine and C4a carbon of FMN. This covalent bond which is the signaling state spontaneously breaks in the dark, returning the plant photo-sensor to the ground state and completing the photocycle. EL222 shows absorption peaks very similar to LOV2 with a difference at the 370 nm absorption band (fig 2-1). This band is associated with the $S_0 \rightarrow S_2$ transition and the change in polarizability is much larger than the $S_0 \rightarrow S_1$ transition (450nm band) which makes it sensitive to the dielectric environment around the flavin binding pocket in proteins [6]. In LOV2, the 370 nm absorption band has a dome shaped structure with vibronic structure at 360 and 380 nm region [7]. In EL222 these two vibronic components are the same height which gives a flat top shape to the spectrum (fig 2-1).

In this chapter, we report the formation of adduct and return to the ground state measured by short and long time light-induced absorption changes and by globally analyzing the data, provide a photocycle scheme that fits the data. Several constructs and mutants will be presented to show that photocycle is the intrinsic property of the LOV domain and that cysteine at position 75 is the chromophore binding molecule. We also show thermodynamics of activation parameters of the adduct formation as well as effects of pH changes and imidazole effect.

2.2 Materials and Methods

2.2.1 Cloning, Mutagenesis, Protein Expression, and Purification

EL222 corresponding to 222 amino acids of a gene (Accession ID:

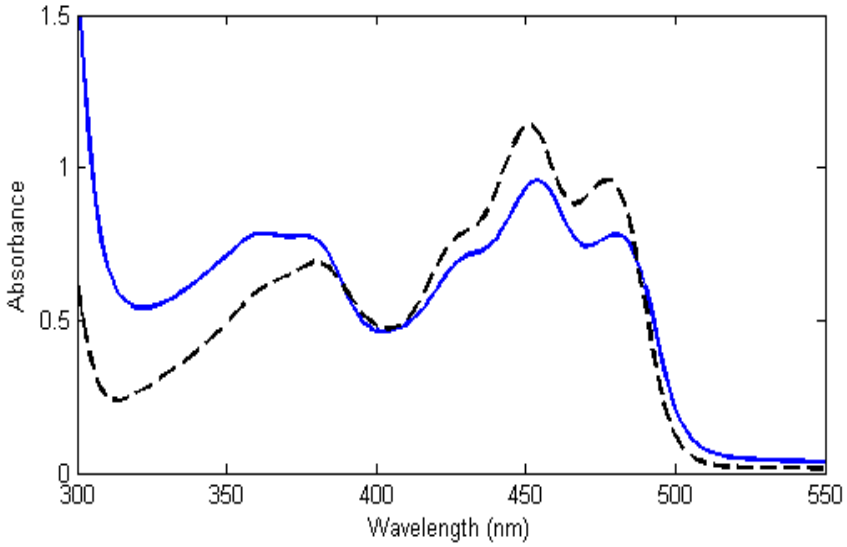

Figure 2-1 Absorption spectrum of the ground state of EL222 (blue) and Oat LOV2 (Black dash lines). Vibronics at 450 nm are similar for both proteins. However, spectral features at the 370 nm range which is associated with $S_0 \rightarrow S_2$ are different, presumably due to different electrostatics in the chromophore binding environment.

YP_457840 and pdb 3P7N_A) was PCR amplified and cloned into the pET-100D Topo directional vector (Invitrogen Inc.) according to the manufacturer's instructions. This vector adds a 6xHis fusion tag to the N-terminal that can be removed since it has an Enterokinase cleavage site. The vector takes advantage of the high activity and specificity of the bacteriophage T7 RNA polymerase to allow regulated expression of heterologous genes in *E. coli* from the T7 promoter. In this system, PCR products are directionally cloned by adding four bases (CACC) forward primer. This method ensures that PCR products anneal in the correct orientation with an efficiency of more than 90 percent. Mutagenesis of active cysteine into alanine (C75A) and the other cysteine (C70S) was carried out by PCR according to the instructions provided

by the Stratagne Quickchange site-directed mutagenesis kit. The primers for the reaction: 5'-AAGAATGCGTCGGCCGCAATG CCCGATTCCTGGC-3' forward and 5'-TGCCAGGAATCGGGCATTGCGGCCGA CGCATTCTT-3' reverse primer for the EL222C75A mutant and 5'CTATTCCGAAGAAGAATCCGTCGGCCGCAATT GCC-3' forward and 5'-GGCAATTGCGGCCGACGGATTCTTCTTCGGAATAG-3' reverse primer for the EL222C70S mutant were synthesized by Integrated DNA Technologies (San Diego, CA). The PCR products which are the cloned genes with mutations in pET-100D TOPO vector were transformed into XL-blue competent cells on Ampicillin plates and successful colonies were grown overnight in Luria Broth (LB) and plasmids were purified using StrataPrep plasmid mini-prep kit. Samples of plasmids were sent to UC Berkeley DNA Sequencing facility for confirmation of correct sequence. Plasmids containing the targeted mutation were then transformed into *E. coli* BL-21(DE3) pLysS competent cells and grown on an Ampicillin plates overnight. Selected colonies were transferred and grown in LB broth medium sterilized by 30 minutes of autoclaving with the addition of the correct amount of Ampicillin (100mg/ml) overnight. The grown cultures were used to inoculate 750ml of autoclaved growth media and grown under dark conditions in a shaker at 37°C and 250 rpm for approximately 2-3 hours until the OD_{600} of the culture was between 0.6-0.9 in 1 cm cuvette. Protein expression was induced by the addition of 1mM final concentration IPTG and left in the shaker for three more hours at 30°C or 16 more hours at room temperature (20°C) to maximize protein expression. Cells containing the EL222 were collected by centrifugation at 6K rpm for 10 minutes. Cells pellets

were frozen at -20°C, thawed the next day and re-suspended in 50mM sodium phosphate and 300mM NaCl, pH 7.0 buffer and then broken with a 2000 lbs/in^2 pressure using a French press machine. Protease inhibitor, PMSF, was added to the mix and centrifuged for 20 minutes at 19K rpm. The clarified supernatant containing our protein was loaded onto an affinity resin column containing Talon cobalt metal affinity resin. The mixture was stirred several times and left on ice in the dark for resin to settle. The resin was washed with 5 bed volumes of wash buffer three times and then another 5 bed volumes of wash buffer with 10mM imidazole to remove the non-specific binders and other cell components. The protein was then eluted with 5 bed volumes of elution buffer that contains 150 mM imidazole and 1 ml fractions were collected in several eppendorf tubes. Fractions were inspected for presence of our protein by UV-light and further checked by UV-Visible absorption spectroscopy. Several fractions containing high concentrations of our protein were selected (usually fractions 3,4, and 5) and were buffer exchanged using a Sephadex G25 PD-10 ml gravity desalting column (GE Healthcare) into a 10 mM phosphate and 20 mM NaCl buffer at pH 7. Proteins were then centrifuged at 10K for 10 minutes to remove any aggregates before any measurements were taken. Dialysis against 4L of low salt buffer (5 mM Tris/ 5 mM NaCl) or de-onized water was also used sometimes in combination with desalting columns to remove the imidazole from the samples. Concentrations of the buffer exchanged samples were checked one more time by taking the absolute spectrum of sample using UV-Visible absorption spectroscopy

and were used fresh for experiments. Liquid samples were kept in the dark at 4°C and the lyophilized samples were kept at -20°C in the dark.

2.2.2 Sample Preparation for PH Changes, D_2O, and Imidazole Effect Experiments

Samples were purified and buffer exchanged as described in section 2.2.1. For pH changes, a 0.1 M HCL and 0.1 M NaOH solutions were prepared and 1 µl aliquots of HCL were added to the pH 7 protein solution to lower it to pH 6 and 1 µl aliquots of NaOH was added to raise the pH to 8.0 and then 9.5 for the experiments. For D_2O and imidazole effect experiments, 500 µl of buffer exchanged samples were frozen in liquid nitrogen and then lyophilized in the dark to dry powder overnight. Samples were then rehydrated in D_2O or buffer containing 200 mM imidazole pH adjusted to 7.

2.2.3 UV-Visible Absorption Spectroscopy

In flavin chemistry, the mechanistically relevant moiety is the isoalloxazine ring that is involved in the covalent bonding to amino acid residues or hydrogen bonding to protein or structural waters. This is also the structural component of the flavin that is responsible for light absorption in the UV and visible spectral range. Absorption at the blue region gives the yellowish appearance to the flavin (complementary color) and flavoproteins (which is also the root of the name in Latin: flavus=yellow). Since the flavin is the light sensor in the LOV domain, UV-Visible spectroscopy is a very useful technique to study it. It can provide kinetic information

on formation and back reactions and detect the presence of absorbing species (intermediates) in the process. Time resolved absorption measurements on flavins are useful since the shape of the absorbance bands that are observed gives information about the homogeneity of the species present as a function of time [8].

Since light is a form of energy, absorption of light by the chromophore causes the energy content of the molecule to increase. Total potential energy of the molecule is the sum of its electronic, vibrational, and rotational energies:

$$E_{Total} = E_{Electronic} + E_{Vibrational} + E_{Rotational} \qquad (2.1)$$

The amounts of energies are in the order:

$$E_{Electronic} > E_{Vibrational} > E_{Rotational}$$

In flavins, photons of UV and visible light have enough energy to cause transitions between the different electronic energy levels. The isoalloxazine ring system has two transition dipoles as indicated by two UV-Visible absorption bands. These transitions should result in very narrow absorbance bands as it does in atoms (fig 2-2a) at wavelengths of 370 nm (S_2 excited state) and 450 nm (S_1 excited state). However, vibrational and rotational energy levels on molecules are superimposed on the electronic energy levels and because of this, the bands are broadened (fig 2-2b).

Light intensity decreases exponentially as it passes through an absorbing sample of flavin. The change in intensity between incident and transmitted light can be used to calculate the flavin concentration. Each LOV molecule contains one FMN molecule (1:1 ratio of FMN to LOV molecules); therefore the Beer-Lambert law (eq. 2-2) can also be used to find concentrations of our protein.

$$A = \log \frac{I_o}{I} = \mathcal{E}lc \qquad (2.2)$$

Where *A* is the absorbance measured as optical density (OD) of sample, I_0 is the intensity of light incident on the sample, *I* is the intensity of light transmitted from sample, *l* is the pathlength of the sample cell (cuvette), $\mathcal{E}$ is the molar absorption or extinction coefficient, and *C* is the concentration of the flavin. The extinction coefficient measures the extent of absorption at a certain wavelength and explains the probability of an electronic transition at that wavelength. It is the variation in the extinction coefficient at each wavelength that outlines the absorption spectrum. The extinction coefficient not only depends on wavelength, it also depends on solvent, temperature, and partially to the instrument used too.

Light Induced Absorption Changes at Long Times

The HP 8452A diode array spectrometer was used to take absolute spectra of the samples after each purification step to check for concentration and activity. This spectrophotometer was also used to take difference spectra in the 1-60 seconds region with a program written in the LabView software environment in Dr. Bogomolni's lab for automated control (via a GPIB interface, IEEE 488) and data acquisition (National Instruments, Austin, TX). The light source was a continuous beam provided by a fiber optic illuminator (V-LUX 1000, Volpi Manufacturing, USA) or by Dyonics light source with 175W 60Hz lamp. A blue corning glass filter was used to provide

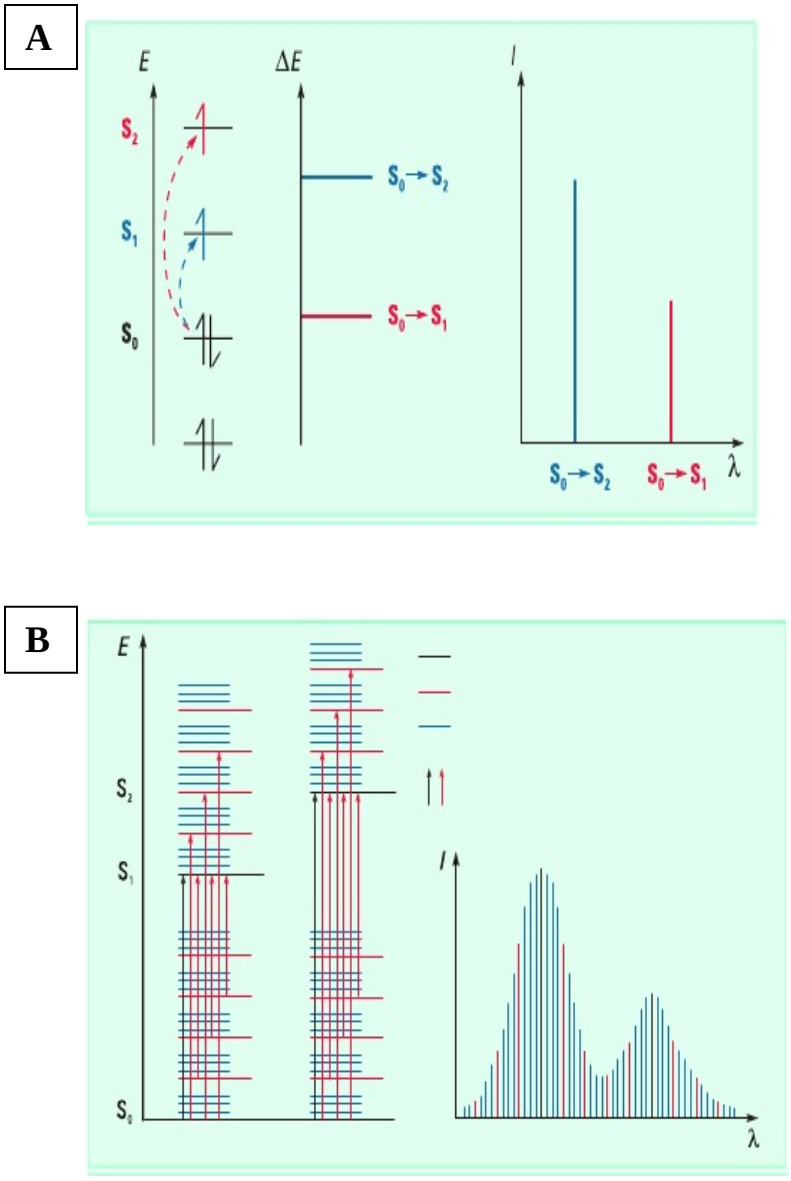

Figure 2-2 Electrical transitions and respective spectra. A) Electronic structure results in narrow bands in atoms B) However in molecules the vibrational and rotational energy levels are superimposed on the electronic energy levels.

blue light with maximum transmission at 420nm and samples were illuminated for one minute in order to create a possible maximum number of excited state molecules. Data was collected on a personal computer; temperature was not controlled but measured to be 20±2℃ with an optical pathlength of 1cm.

Light Induced Absorption Changes at Short Times

Difference spectra from nanosecond to millisecond time window were collected. The apparatus used for this experiment [9] uses 10 nanosecond duration, 80 μJ/mm^2 energy, 477 nm pulse from a dye laser pump by the third harmonic of a Nd:YAG laser (fig 2-3). Laser flash photolysis spectrometer has a microflow system which is used to provide a fresh sample for each laser flash. This system is automated by use of a syringe attached to a stopper motor. The syringe needle is inserted into the small hole in the toe of the Delrin insert [9] and the insert can then be fitted into a cuvette with optical pathlength of 2 mm. Individual stepper pulses are then used to fill the cell with one microliter of fresh sample followed by photo-lyzation with a pulse of vertically polarized 477 nm light in a 0.5 mm pathlength. Absorption changes were probed with polarized light from a short arc, microsecond Xe flash lamp (FXZ-856 white light, approximately 500 μsec duration) which was refocused onto a 1mm X 0.5mm rectangular aperture which photolyzed the 1 μl sample under the cuvette insert. Actinic and probing lights enter the sample in 90° geometry. Spectra at our targeted time intervals were acquired by delaying the probe flash polarized at the magic angle 54.7° relative to the laser polarization axis to

prevent rotational diffusion artifacts [10]. Light transmitted by the sample, was collected using an Andor DH520 intensified charge coupled device (ICCD) detector and the time resolution was provided by a 60 to 100 nanosecond gate on the detector to lower the noise. The detector has 1024 channels over a one inch width but since the image intensifier is 18mm wide, only the center 720 channels actually detect light. Data acquisition was done using the getdata 50 program which saved the absorbance difference spectra in files whose names start with a four letter file prefix followed by a number. The difference spectra represent the absorbance of an illuminated sample minus the absorbance of the sample prior to photo-excitation (blank).

$$\Delta A\ (\lambda,t) = A(\lambda,t) - A(\lambda)_{blank} \qquad (2.3)$$

The data analysis was carried out using programs written in MATLAB in collaboration with Dr. James Lewis.

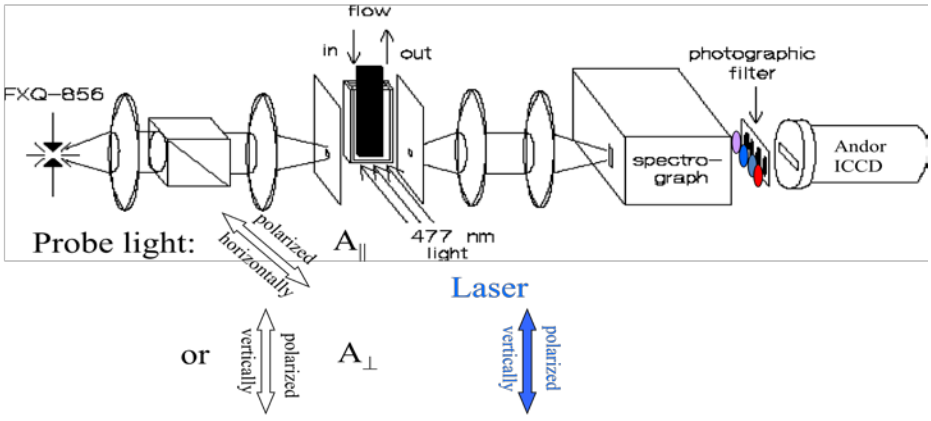

Figure 2-3 Schematic of a Laser flash photolysis spectrometer for measuring the time-resolved difference spectra at short times ( ). The 477nm laser pulse is provided by a Nd:YAG Laser. Probe light is provided by Xe flash lamp (FXZ-856 white light, approximately 500 µsec duration).

2.2.4 Kinetic Analysis Using Singular Value Decomposition and Global Exponential Fitting

The absorption difference spectra taken at each delay point following light excitation pulse were converted to the columns of a data matrix using MATLAB program. The matrix was subjected to singular value decomposition (SVD) followed by global exponential fitting [11]. The purpose of SVD is to reduce noise by reducing the size of the matrix with the elimination of the data that contribute to noise [6, 11-13]. After SVD treatment of the data, the matrix was subjected to global exponential fitting which assumes that the dark reactions followed by light excitation are first order processes. After the SVD treatment, the truncated matrix can be represented as $\Delta A = USV^T$ where U is the matrix with the singular spectral components (basis spectra), S is the diagonal matrix of significant values that represent how important each basis spectrum is in the original data matrix, and V is the time-dependent matrix describing the time evolution of the basis spectra. For the analysis of absorption changes in microseconds, two basis spectra were used to fit the data but for the absorption changes at long times three to four basis spectra were used (in some cases even two were used after realizing that in those cases more does not improve the results). Global exponential fitting follows the SVD and provides apparent lifetimes that are reported as well as the b-spectra. The b-spectra contain useful information about the kinetic scheme because it can be interpreted as difference spectra between decaying and forming intermediates. The b-spectra are calculated from the amplitudes of the fit which has a time dependent and time independent components. The time independent b-spectrum (b_0) is the difference

between the spectra of the final photoproduct and the initial state (dark state). In a cyclic process like LOV2, the b_0-spectrum becomes zero because the final photoproduct is the recovered material.

2.3 Results

2.3.1 Early Photocycle

Following the pattern of other LOV domains studied, EL222 LOV-HTH called EL222 for short, produces triplet state specie upon excitation by light. The rise of the triplet state was observed from 600 to 700 nm and decayed as the FMN either goes to form adduct or back to ground state. The time constant of formation of this triplet state was not measured by us since it is in times shorter than our earliest time resolution of 100 ns but in LOV2 was reported to be 2 ns [14]. As mentioned, the triplet state decays into a flavin-cysteinyl adduct which in EL222 has an absorption peak around 390 nm ($EL222^{S}_{390}$) and to find an apparent rate constant of formation, we chose eight delay points of (1, 2, 5, 10, 20, 50, 100, 1000 µsec). All of these points were chosen in microsecond region because LOV2 domain of phot1 has an apparent time constant (τ_{app}) of 2 µsec [6] but in our first try (fig 2-4) the global exponential fitting showed that EL222 has apparent time constant faster than one microsecond so we had to repeat the experiment with different delay times. In the next two experiments, we added delay times in nanosecond range (fig 2-5) and global exponential fitting analysis of data gave apparent time constant of 780 nanosecond at room temperature which was not controlled but measured to be 20 ± 2℃. From the

spectra, we can estimate the branching ratio (amount decaying to adduct versus percentage that go back to ground state) which will help us calculate the time constant for adduct formation (τ_f) and time constant for return to ground state (τ_R) from the apparent time constant(τ_{App}). This is possible because in our global kinetic analysis only one apparent rate was seen, which is similar to LOV2, where a linear scheme can explain the data at early times. We can explain the data in the following way.

$$EL222^{D}{}_{450}\ (\tau_R) \leftarrow EL222^{L}{}_{660} \rightarrow (\tau_F)\ EL222^{S}{}_{390}$$

With $EL222^{D}{}_{450}$ being the ground state $EL222^{L}{}_{660}$ being the light activated triple state and $EL222^{S}{}_{390}$ is the signally adduct state (subscript are the absorption maximums). Therefore the apparent single rate constant becomes

$$K_{app} = \frac{1}{\tau_{app}} = \frac{1}{\tau_f} + \frac{1}{\tau_R} = K_f + K_R \qquad (2.4)$$

$$\frac{1}{\tau_f} = K_f \quad \text{and} \quad \frac{1}{\tau_R} = K_R$$

To find the branching ratio, the bleaching at 450nm at the first time point delay (full bleach) was measured and then compared with the bleach at the longest time point delay. The total bleach at first delay represents the total population that was converted to triplet state and bleach at longest time delay represents the population that had gone to signaling adduct state. The difference of the two spectra is the population that has gone to back to the ground state (fig 2-6). The measurement of the spectra shows that 40% decays from triplet state into the signaling adduct state and 60% decays back to ground state which will be used as factors in rate constant determination. This is very different than phot1 LOV2 that was reported by Swartz

[6] which has a 50% forward and 50% reverse branching ratio which then with a τ_{app} = 2 µsec, each of the time constants are reported at 4 µsec ($\tau_f = \tau_R$ = 4 µsec).

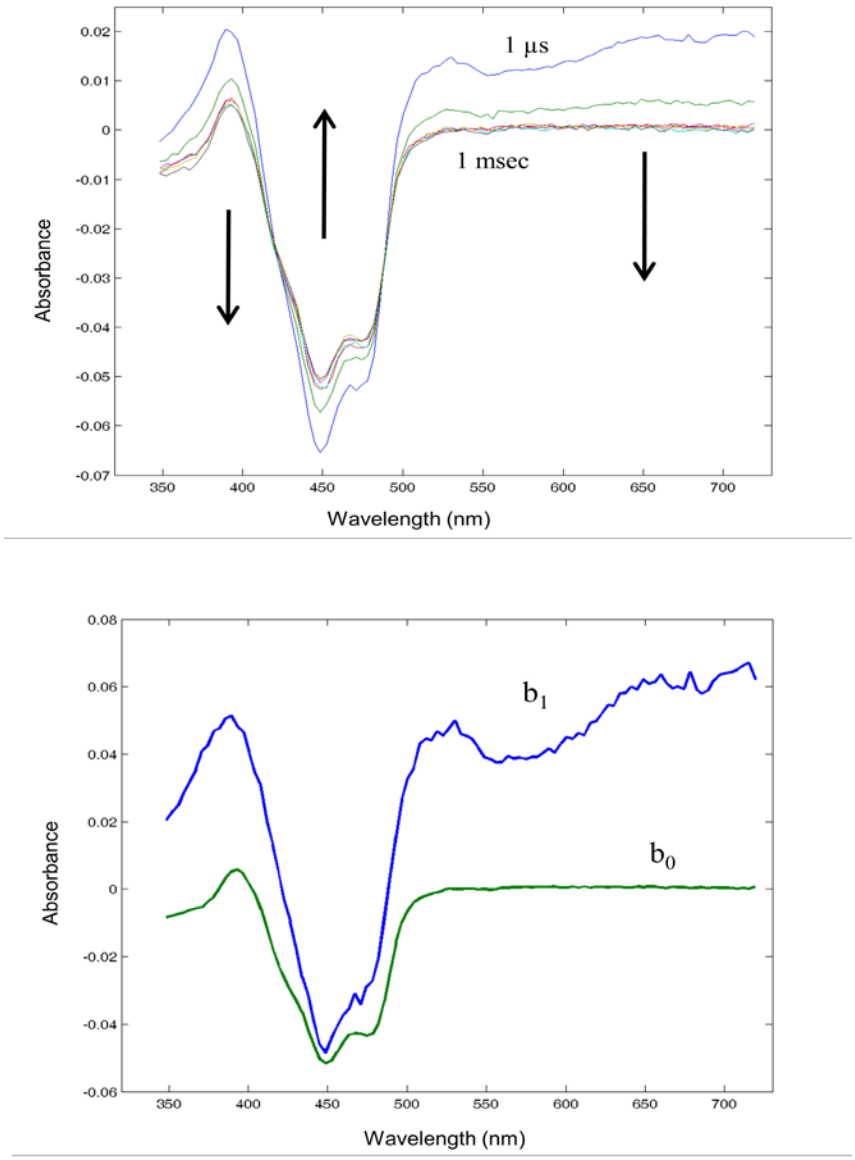

Figure 2-4 The absorption difference spectra of EL222 at room temperature after excitation with a 477nm laser pulse. Spectra were collected at 1, 2, 5, 10, 20, 50, 100, 1000 µsec. Arrows indicate spectral changes with time. Bottom graph shows the results of global multi-exponential fitting of difference absorption spectra from EL222. b_1 is the b-spectrum with an apparent rate constant of less than 1µsec, and b_0 is the spectrum of the product formed.

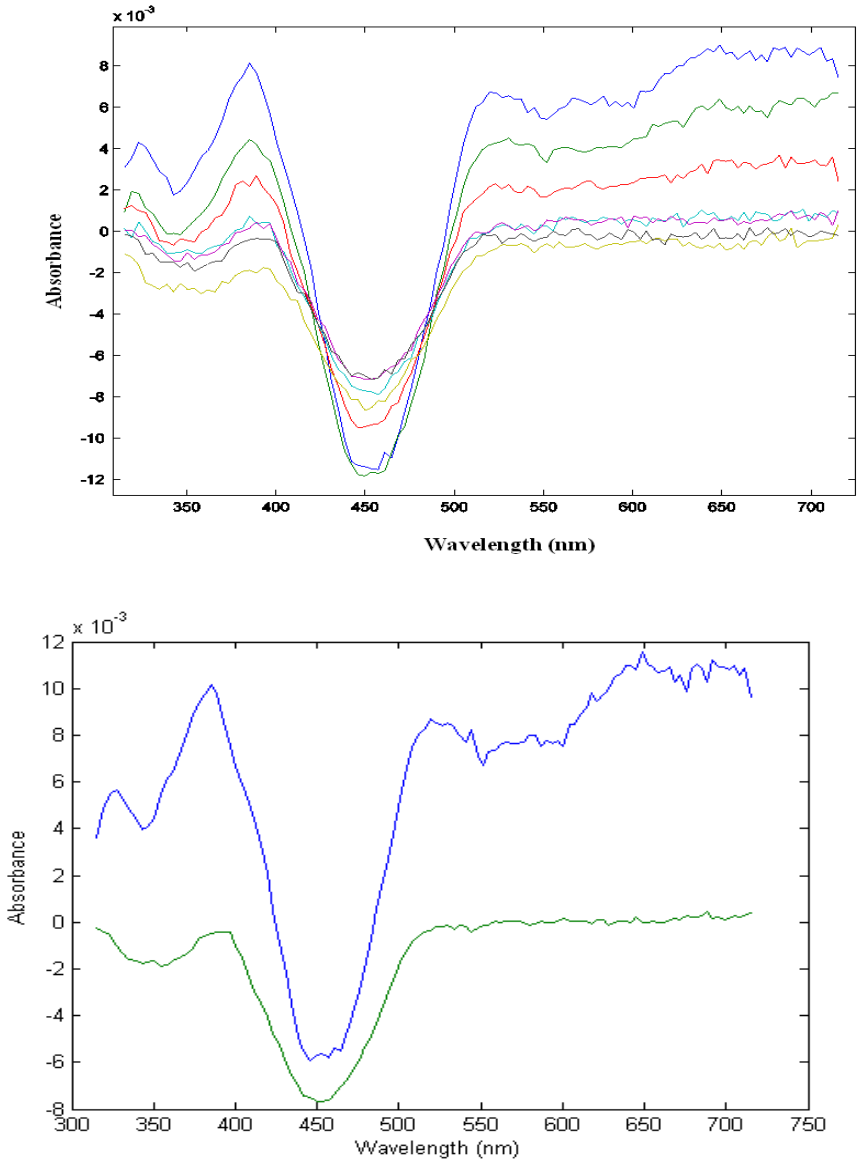

Figure 2-5 The absorption difference spectra of EL222 at room temperature after excitation with a 477 nm laser pulse. Spectra were collected at 0.2(blue), 0.4(green), 1(red), 3(cyan), 10(magenta), 30(yellow), 100(black) µsec. Bottom graph shows the results of global multi-exponential fitting of difference absorption spectra from EL222. b_1(blue) is the b-spectrum with an apparent rate constant of 780nsec, and b_0(green) is the spectrum of the product formed.

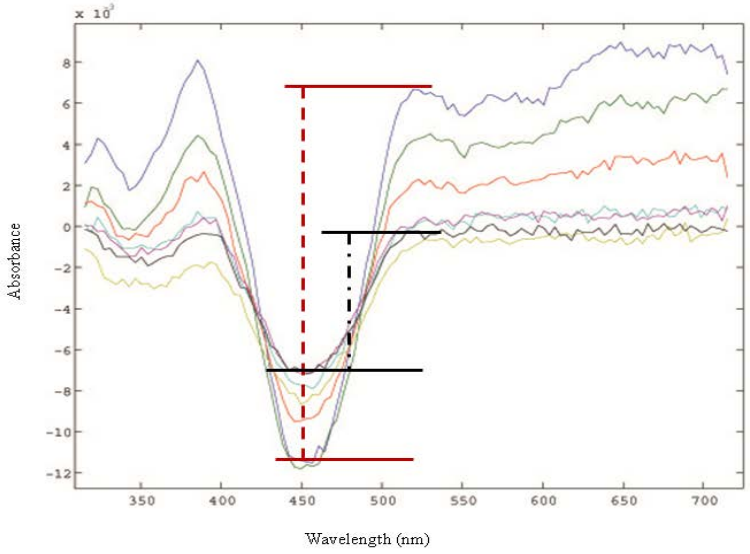

Figure 2-6 finding the branching ratio. The first time point delay (blue line) which is the full bleach is measured (red dash line). The longest time delay (black line) which is the population of signaling adduct state is measured (black dash line) and the ratio of them gives the percentage decaying from triplet to the signaling adduct (40%) and ratio of the difference to the total bleach gives the percentage that decays back to the ground state (60%).

In the case of EL222, using the measured branching ratio, we calculated that τ_f = 1.95 µsec and τ_R = 1.3 µsec. At that point, additional sets of experiments were designed to address basic questions regarding adduct formation of this molecule. The phot1 LOV2 fusion protein from pCAL-n-EK expression vector has calmodulin-binding peptide which adds 46 non-native residues to our LOV2 domain. The EL222 protein was Histidine tagged which adds a poly-histidine region (6 His.), EK recognition site (Asp Asp Asp Asp Lys) with a short antibody recognition site. Although we could not find any report of a Histidine tag interfering with the protein, we cut the tag and repeated the experiment under same conditions to be sure of our data. The apparent

time constant for the formation was 840 nanoseconds which we do not believe is any different than the apparent time constant measured before because it is within experimental error (fig 2-7). Based on the result of this experiment, following experiments were performed with the Histidine tag included.

In phot1 LOV2, it has been shown that the back reaction is based catalyzed so the addition of imidazole increases the rate of recovery [15]. The imidazole effect had not been tested on the formation of LOV2 or EL222 (we tested on the LOV2; imidazole does not affect the formation time constant in LOV2, data not shown). The experiment on EL222 was conducted with 200 mM concentration of imidazole added to the buffer (pH checked and adjusted to 7). The solution became turbid and protein started to precipitate in the middle of our run, so data became noisy (fig 2-8) but apparent time constant of 770 nanoseconds was obtained which shows that the imidazole does not affect the formation of adduct in EL222. This result is expected since the formation is not based catalyzed but an important lesson was learned about imidazole. Histidine tagged EL222 protein is eluted from the column using a 150 mM imidazole containing elution buffer. As the result of this experiment, it was realized that EL222 should be buffer exchanged as soon as it is eluted from the column because imidazole has a detrimental effect on the protein and causes it to precipitate. This effect was not observed in LOV2 so we cannot conclude that imidazole has the same effect on all the LOV proteins.

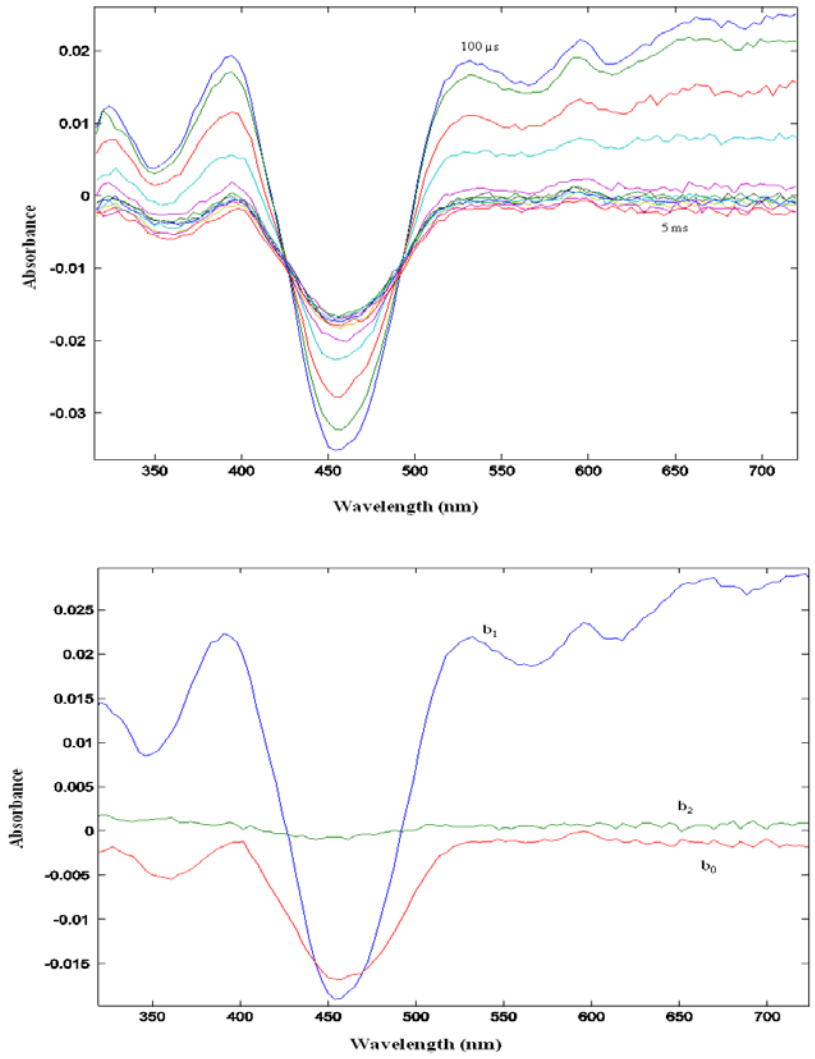

Figure 2-7 The absorption difference spectra of EL222 without a His-tag at room temperature after excitation with a 477nm laser pulse. Spectra were collected at 0.1, 0.2, 0.5, 1, 2, 50, 100, 200, 500, 1000, 2000, 5000 µsec. Longer time points at millisecond region are chosen to see if there are any late events that might have been missed before. Bottom graph shows the results of global multi-exponential fitting of difference absorption spectra from EL222. b_1 is the b-spectrum with an apparent rate constant of 840 nsec, and b_0 is the spectrum of the product formed. b_2 is the b-spectrum that was chosen because it might represent a second process at 1.3 ms but this is unlikely.

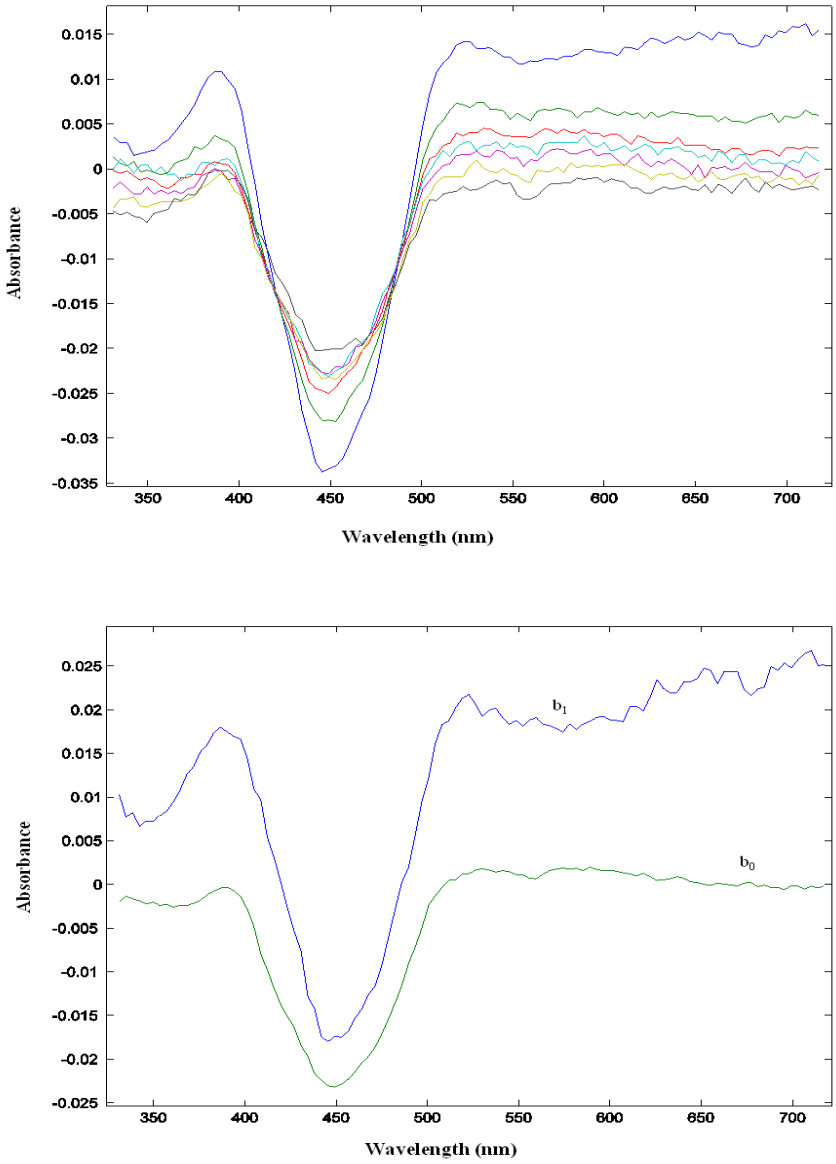

Figure 2-8 The absorption difference spectra of EL222 in 200mM imidazole containing buffer at room temperature after excitation with a 477nm laser pulse. Spectra were collected at 0.4, 1, 2, 4, 10, 20, 100 µsec. Data was analyzed up to 20 µsec point to reduce noise. Bottom graph shows the results of global multi-exponential fitting of difference absorption spectra from EL222. b_1 is the b-spectrum with an apparent rate constant of 770 nsec, and b_0 is the spectrum of the product formed.

Although cysteine at the position75 in the highly conserved NCRFLQ motif is suspected to be involved in flavin-cysteinyl adduct formation, there is another cysteine at position 70 that is not present in phot1 LOV2. Two different mutants were prepared, changing the cysteine in position 70 into serine (EL222C70S) and another mutant in which the conserved cysteine at position 75 into alanine (EL222C75A). EL222C70S showed formation time constant just like the EL222 wild type (fig 2-9) which is an important result since this mutant will be used as template for designing further mutants (double mutants) for EPR studies. The EL222C75A mutation resulted in a truncated photocycle as compared to the wild type (fig 2-10). Since the protein was missing the reactive cysteine, it did not form the adduct so $EL222^{S}_{390}$ intermediate was not seen after the FMN went to the excited triplet state. The excited state $EL222^{L}_{660}$ was measured to decay back to the ground state in 2 ms, which is three order of magnitude slower than the wild type and much different than phot1 LOV2 which was only one magnitude slower at 72 μs [6]. The interactions with FMN can greatly change the triplet lifetime and the proximity of a sulfur atom in the wild type EL222 has contributed by increasing the rate of spin flipping due to spin orbit coupling therefore shortening the triplet decay time constant. The absence of the sulfur atom in the EL222 LOV pocket and interactions with other residues in the pocket has greatly stabilized the triplet state more than the FMN in the solution which can be from 100 μs to 1 ms.

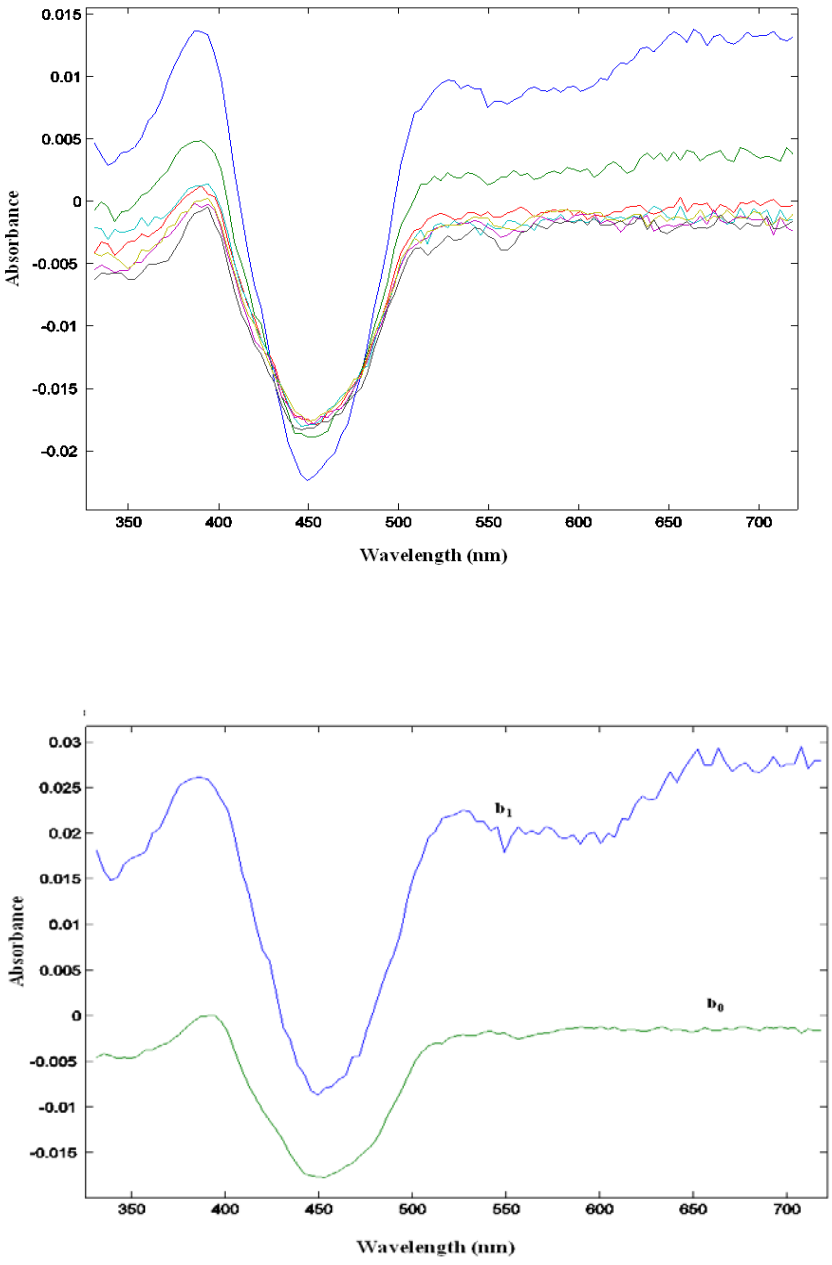

Figure 2-9 The absorption difference spectra of EL222C70S mutant at room temperature after excitation with a 477nm laser pulse. Spectra were collected at 0.4, 1, 2, 4, 10, 20, 100 µsec. Bottom graph shows the results of global multi-exponential fitting of difference absorption spectra from EL222. b_1 is the b-spectrum with an apparent rate constant of 620 nsec, and b_0 is the spectrum of the product formed.

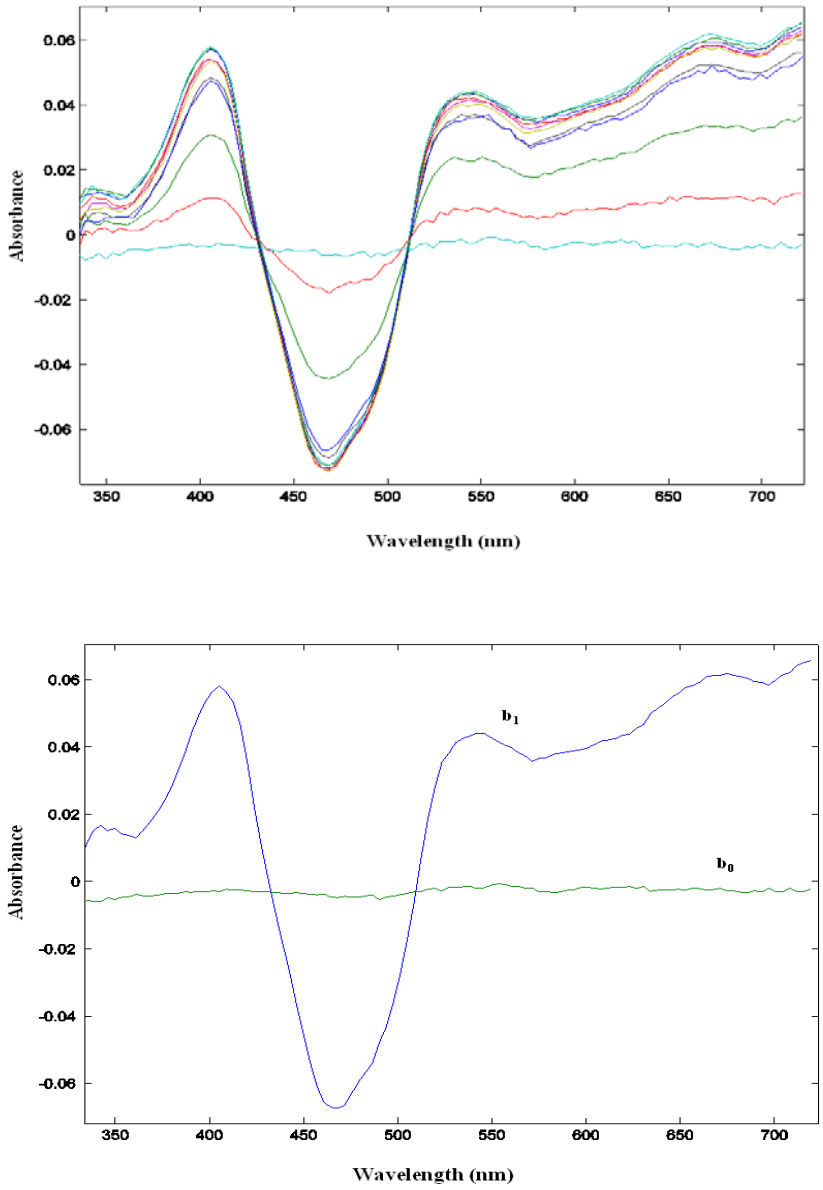

Figure 2-10 The absorption difference spectra of EL222C75A mutant at room temperature after excitation with a 477nm laser pulse. Spectra were collected at 0.4, 1, 2, 4, 10, 20, 100 µsec and 1, 3, and 10 ms time points are added to follow any late events. Bottom graph shows the results of global multi-exponential fitting of difference absorption spectra from EL222. b_1 is the b-spectrum with an apparent rate constant of 2 msec, and b_0 is the spectrum of the product formed. Since this is the cyclic process in which triplet state returns to the ground state b_0 spectrum is zero.

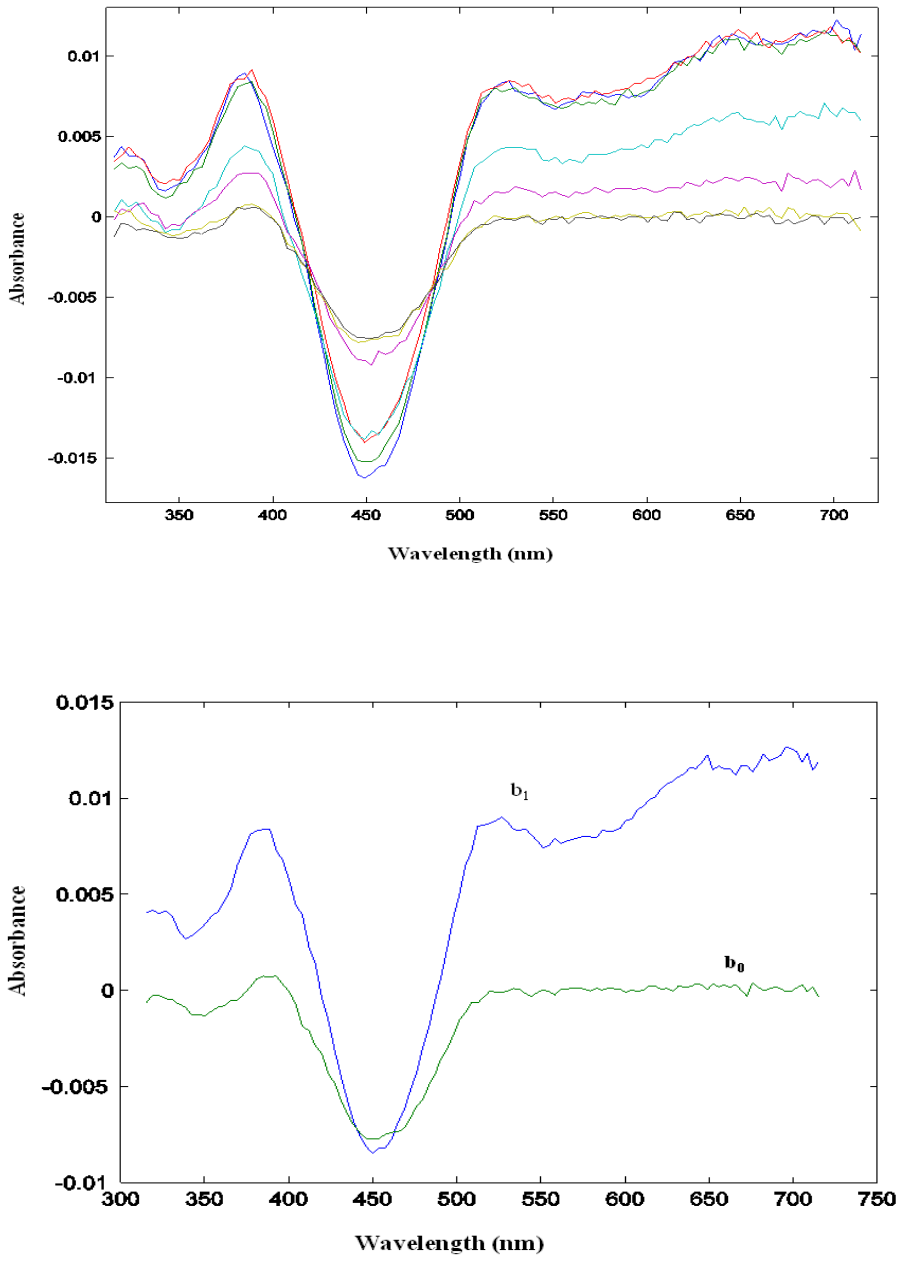

Figure 2-11 The absorption difference spectra of EL222 wild in D_2O at room temperature after excitation with a 477nm laser pulse. Spectra were collected at 0.2, 0.4, 1, 3, 10, 30, 100 µsec. Bottom graph shows the results of global multi-exponential fitting of difference absorption spectra from EL222. b_1 is the b-spectrum with an apparent rate constant of 5.5 µsec, and b_0 is the spectrum of the product formed.

In order to understand the adduct formation further; we measure the D_2O and pH effect on kinetics by nanosecond laser flash spectroscopy. Figure 2-11 shows the absorption difference spectra of EL222 in D_2O. Global exponential analysis of the measured difference spectra indicate a single first order process just like the EL222 in H_2O but with much slower apparent time constant of 5.5 µsec, which is more than 7 times slower. The ground state absorption spectrum of EL222 in D_2O is unchanged so the slowing down of this reaction means alteration of hydrogen bonds or proton transfer reaction is the rate limiting step in the reaction of the $EL222^{S}_{390}$ adduct formation. To probe the dependence of $EL222^{S}_{390}$ adduct formation on proton transfer, we studied the triplet decay into adduct from pH 6.0 to pH 9.5 (fig 2-12, 2-13, 2-14). EL222 sample precipitated at pH levels lower than 6.0 which can be the result of chromophore FMN loss and subsequently the instability of the protein without the chromophore (white precipitate and yellow solution that shows absorption spectrum of the free FMN). EL222 shows apparent rate constant of 660 nsec at pH 6.0 (fig 2-12), 890 nsec at pH 8.0 (fig 2-13), and 1.11 µsec at pH 9.5 (fig 2-14). The difference spectra and the b-spectra obtained were the same as the pH 7.0 studies and show a single first order process at various pH ranges. Although there are changes in the apparent time constants, they are very small so we conclude that the adduct formation is relatively insensitive to pH changes. This finding is consistent with the observation made on LOV2 that there is no change in the chromophore fluorescence intensity in the 4.5-9.5 pH range. This argues that the lack of pH sensitivity is consistent with either a cysteine (pK less than 4) where it remains as a thiolate ($-S^-$) at

higher pH or with a pK more than 10 where the cysteine molecule is a thiol (-SH) within the entire pH range [6].

In each of these measurements, the corresponding b-spectra that resulted from the global exponential analysis are also shown. In each case, the single exponential fit of the data indicates that two spectra (b_1 and b_0) exist over the time of the measurements and each of the spectra represents at least one species. The b_1 spectrum represents the difference between the spectra of the starting delay time (in most cases either 0.2 or 0.4 nsec) and final delay time (variable from 100 µsec to milliseconds) intermediates and provide us with the apparent time constants reported here. The b_0 spectrum is the spectrum of the final intermediate ($EL222^{S}_{390}$) minus the initial state ($EL222^{D}_{450}$) or the ground state. It was shown that b_1-spectrum resembles the difference spectrum of the FMN triple state and the b_0-spectrum resembles the flavin –cysteinyl adduct [6]. EL222 wild type in H_2O and D_2O follow this behavior like phot1 LOV2. EL222 without a His-tag is followed at much longer time delays to observe if there are any late events that we might have missed before. In the global exponential analysis of this data, we can add another b-spectrum (b_2) to the fit and although b_2 is nearly zero, it is persistently there and has a time constant of 1.3 ms. The b_0-spectrum in EL222C75A mutant (fig 2-10) is zero as expected. Since this mutant does not form the flavin–cysteinyl adduct and after producing the triplet state, relaxes back to the ground state. This is an indication that there are no spectrally observable intermediates are formed during triplet decay and since this is a

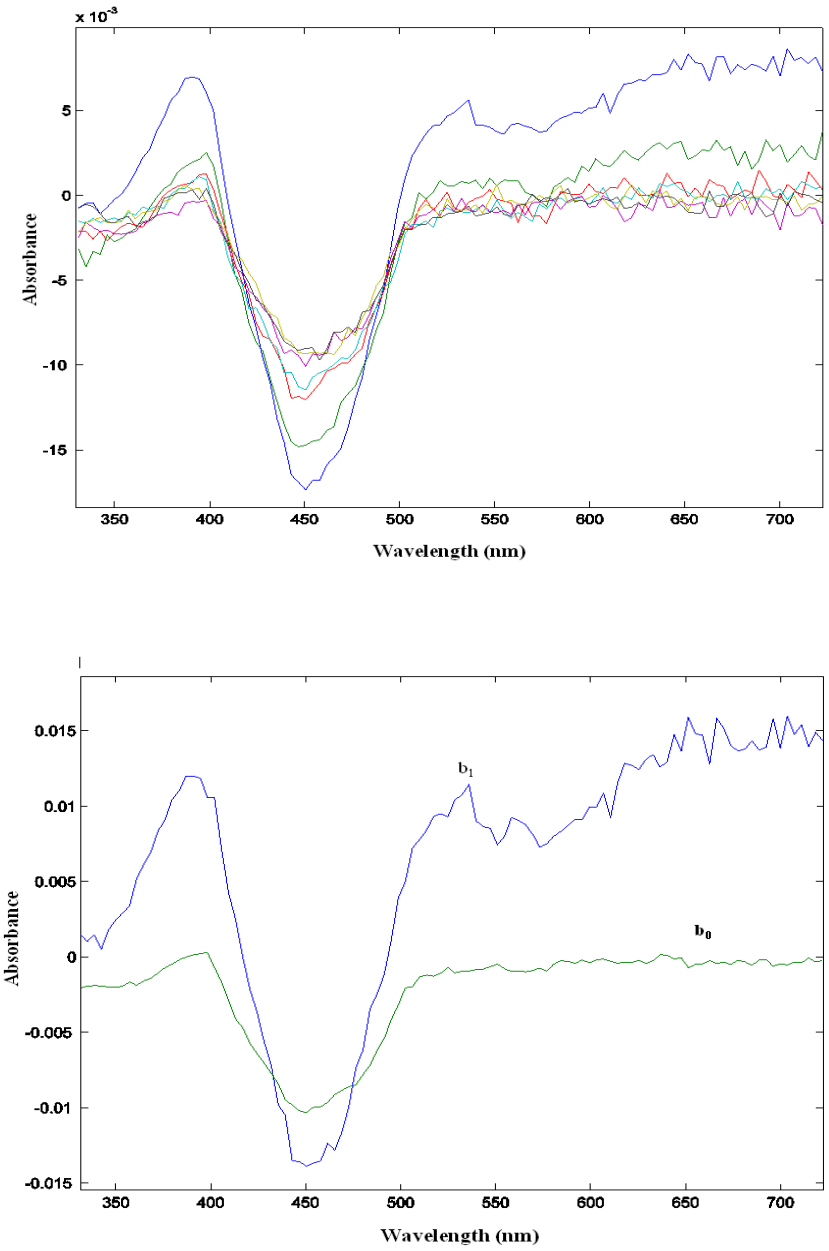

Figure 2-12 The absorption difference spectra of EL222 wild at pH 6.0 at room temperature after excitation with a 477nm laser pulse. Spectra were collected at 0.4, 1, 2, 4, 10, 20, 100 µsec. Bottom graph shows the results of global multi-exponential fitting of difference absorption spectra from EL222. b_1 is the b-spectrum with an apparent rate constant of 660 nsec, and b_0 is the spectrum of the product formed.

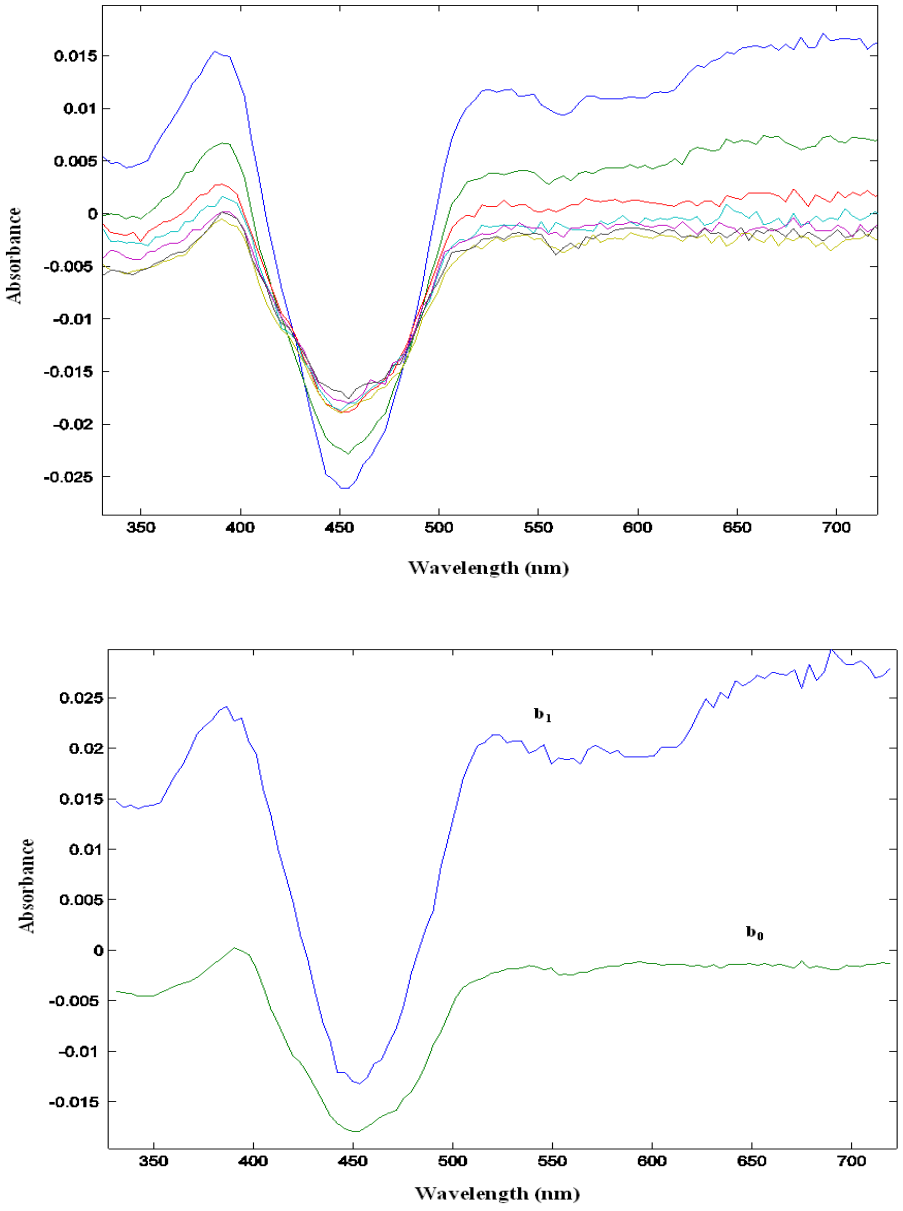

Figure 2-13 The absorption difference spectra of EL222 wild at pH 8.0 at room temperature after excitation with a 477nm laser pulse. Spectra were collected at 0.4, 1, 2, 4, 10, 20, 100 µsec. Bottom graph shows the results of global multi-exponential fitting of difference absorption spectra from EL222. b_1 is the b-spectrum with an apparent rate constant of 890 nsec, and b_0 is the spectrum of the product formed.

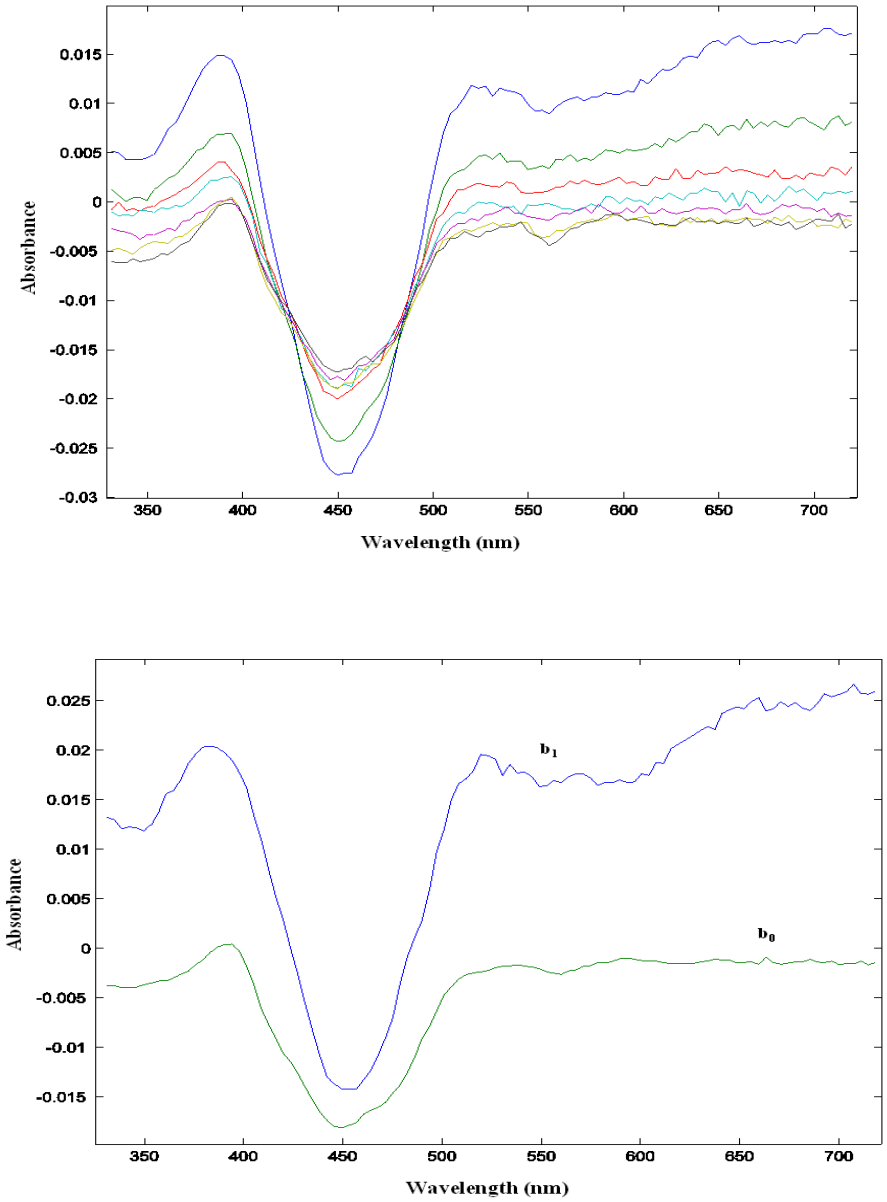

Figure 2-14 The absorption difference spectra of EL222 wild at pH 9.5 at room temperature after excitation with a 477nm laser pulse. Spectra were collected at 0.4, 1, 2, 4, 10, 20, 100 µsec. Bottom graph shows the results of global multi-exponential fitting of difference absorption spectra from EL222. b_1 is the b-spectrum with an apparent rate constant of 1.11 µsec, and b_0 is the spectrum of the product formed.

cyclic process, b_0-spectrum becomes zero. The b_1-spectrum is consistent with the EL222 wild type and shows the formation of triplet state intermediate. The branching ratios of the mutant EL222C70S remain the same as the wild type EL222 but changes slightly when EL222 is in the imidazole containing buffer (35% forward and 65% back). The branching ratio also changes when EL222 is in D_2O to 30% forward and 70% back which gives $\tau_R \approx 8\mu$sec and $\tau_r \approx 18$ μsec. The difference in the branching ratio makes τ_r of the EL222 in D_2O exactly 9 times slower than the wild types EL222. This branching change from the wild type might not be significant though since experiments done on samples of EL222 wild types with different delay times show slight difference in branching ratio (forward reaction changes within 30-40% range) so the branching ratio changes seen in EL222 containing imidazole or D_2O might not be different from the wild type EL222 at all.

In order to study the energetic of adduct formation reaction, temperature effect on the formation was studied at three additional temperatures of 15, 25, and 35^0C (figs 2-15, 2-16, 2-17). As expected, as the temperature increases, the adduct formation reaction becomes faster. At 15^0C, the apparent time constant is reported by us to be 970 nsec, at 25^0C, it is775 nsec, and at 35^0C the time constant becomes 535 nsec. This temperature dependence of τ_f which will be calculated from the apparent time constants and they follow the EL222 wild type since the branching ratio does not change (table 2-1).

Temp. (℃)	τ_{app} **(ns)**	τ_R **(µs)**	τ_F **(µs)**
15	970	1.62	2.4
20	780	1.3	2
25	775	1.3	1.9
35	535	0.89	1.34

Table 2-1.The apparent time constant, adduct formation, and return of the triplet to ground state time constants at various temperature calculated using single exponential fitting and branching ratios.

To find the activation energy, the Arrhenius equation is used. In 1899 Arrhenius showed that the rate constant of reactions increased in an exponential manner with T (in Kelvin) which can be rewritten as

$$K=Ae^{-E/RT} \qquad (2.5)$$

Where A is the proportionality constant, R is the gas constant (8.314 J/mole.K), E is the activation energy in joules/ mole and e is the base of the natural system of logarithms.

This equation can be rewritten as:

$$\ln k = lnA - \frac{\mathrm{E}}{\mathrm{RT}}$$

$$lnk = -\left(\frac{E}{R}\right)\left(\frac{1}{T}\right) + lnA \qquad (2.6)$$

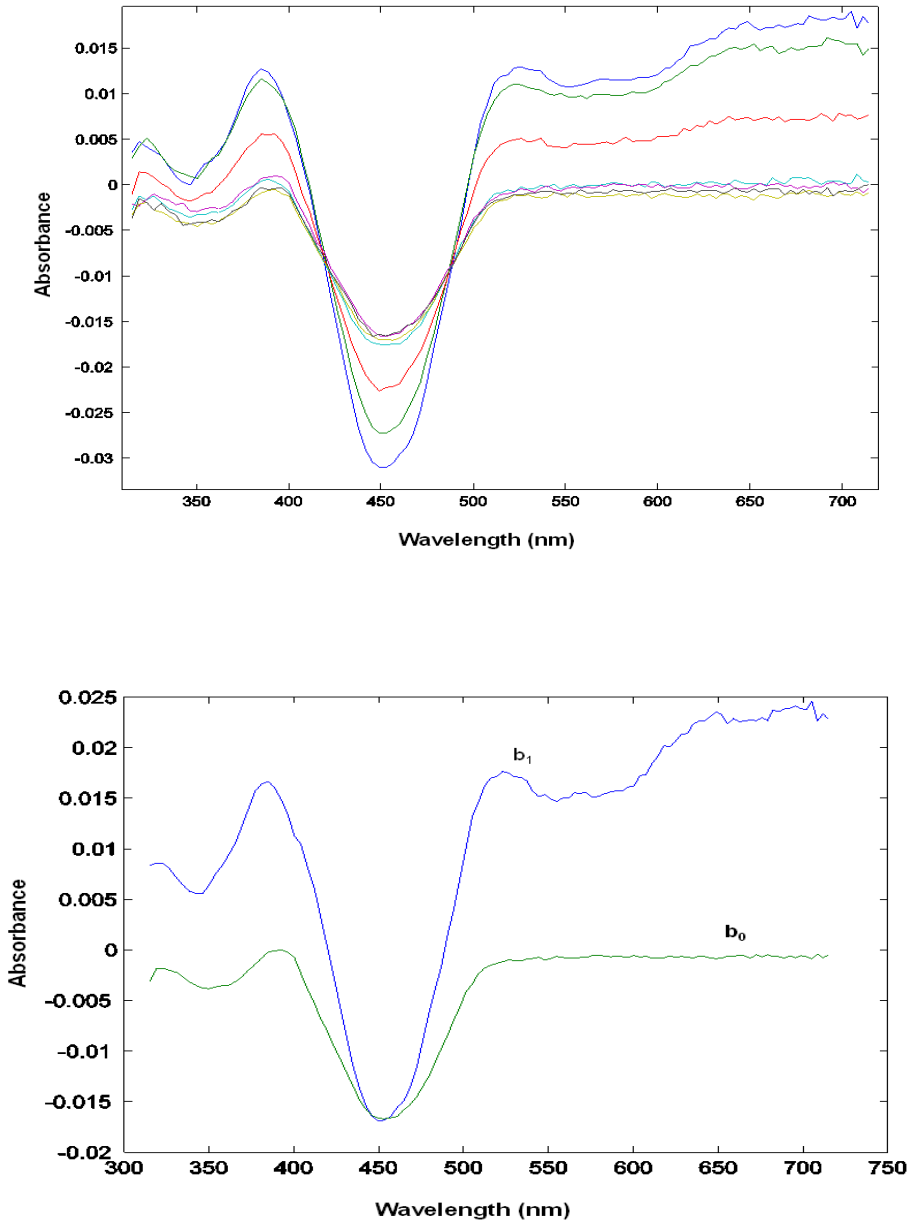

Figure 2-15 The absorption difference spectra of EL222 wild at 15℃ after excitation with a 477nm laser pulse. Spectra were collected at 0.2, 0.4, 1, 3, 10, 30, 100 µsec. Bottom graph shows the results of global multi-exponential fitting of difference absorption spectra from EL222. b_1 is the b-spectrum with an apparent rate constant of 970 nsec, and b_0 is the spectrum of the product formed.

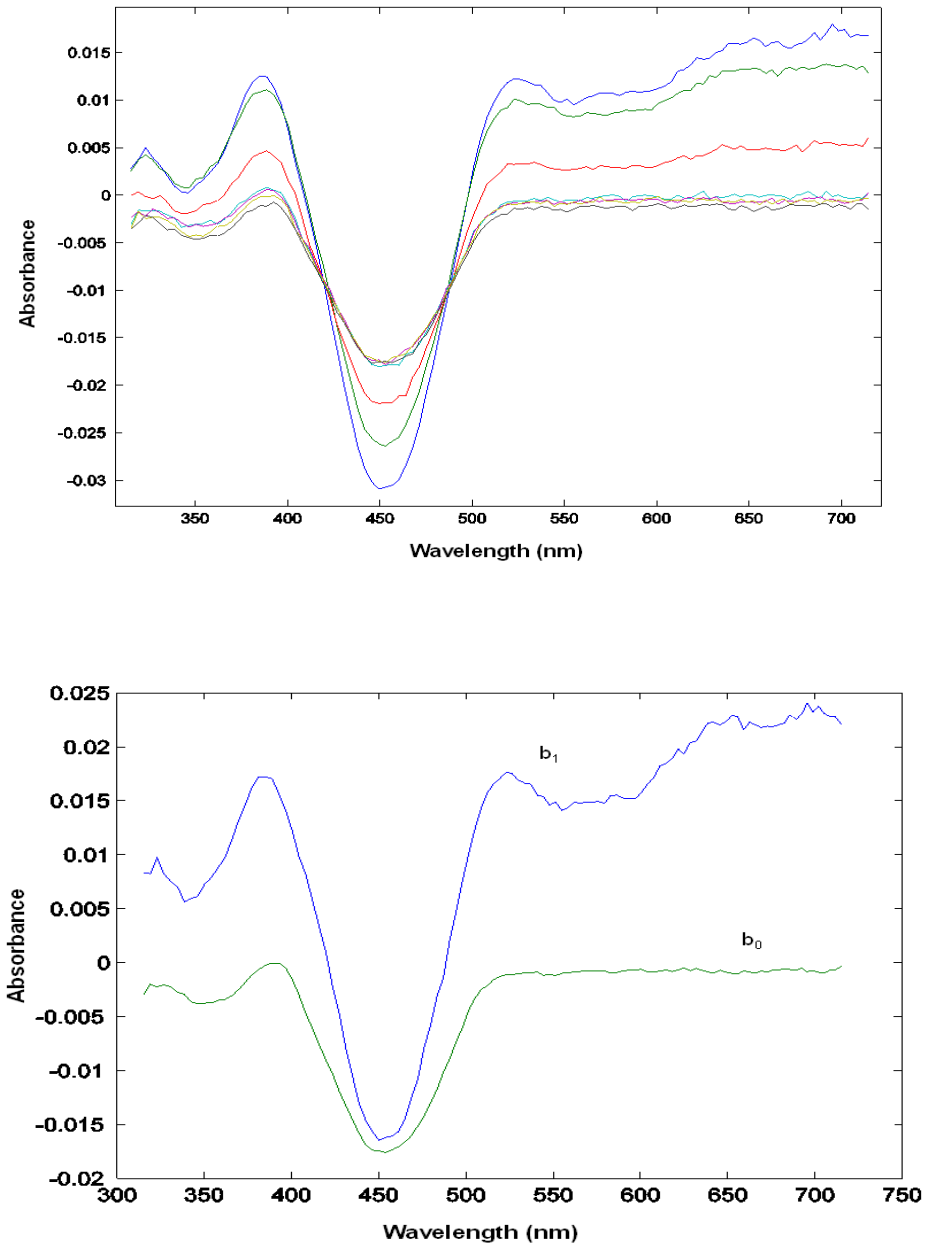

Figure 2-16 The absorption difference spectra of EL222 wild at 25℃ after excitation with a 477nm laser pulse. Spectra were collected at 0.2, 0.4, 1, 3, 10, 30, 100 µsec. Bottom graph shows the results of global multi-exponential fitting of difference absorption spectra from EL222. b_1 is the b-spectrum with an apparent rate constant of 775 nsec, and b_0 is the spectrum of the product formed.

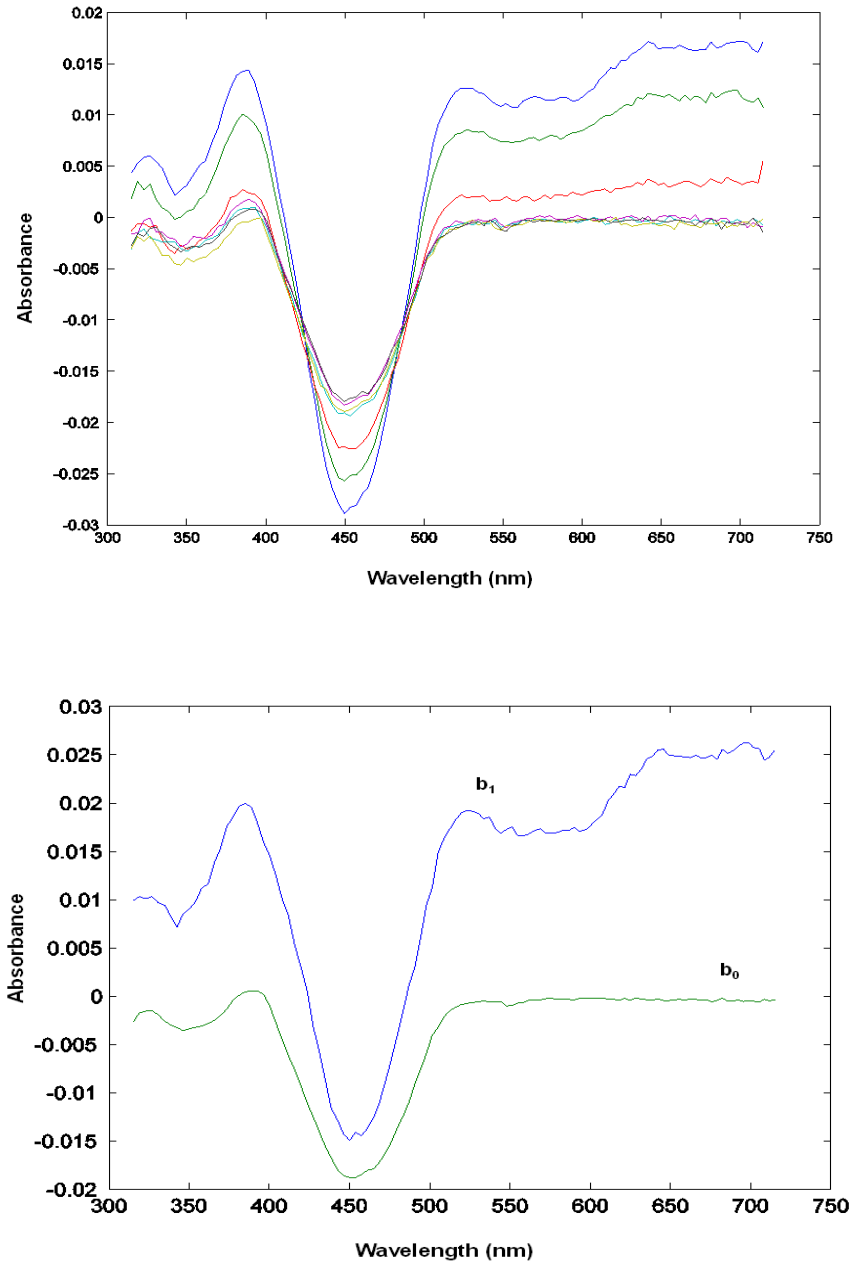

Figure 2-17 The absorption difference spectra of EL222 wild at 35℃ after excitation with a 477nm laser pulse. Spectra were collected at 0.2, 0.4, 1, 3, 10, 30, 100 µsec. Bottom graph shows the results of global multi-exponential fitting of difference absorption spectra from EL222. b_1 is the b-spectrum with an apparent rate constant of 535 nsec, and b_0 is the spectrum of the product formed.

If we plot (ln k) vs. (1/T), then the slop of the line will give (-*E/R*) value so from slope of the line, we can calculate the activation energy. From this information we can also calculate the entropy of activation for adduct formation of EL222 with the following equation.

$$\Delta S^{\ddagger} = R[lnA - \ln\left(k_b . \frac{T}{h}\right)] \qquad (2.7)$$

Where $\Delta S^{\ddagger}$ is called the entropy of activation (J/mole.K), K_b is the Boltzmann constant (1.38×10^{-34} J/K) and h is the plank constant (6.626×10^{-34} J.s). The y-intercept is (ln A) of our (ln k) vs. (1/T) plot.

The enthalpy of activation for the $EL222^{S}_{390}$ species formation is 22 KJ/mole (5.2 Kcal/mole) calculated from the slope of the plot (fig 2-18). The y-intercept of the plot is used to calculate the entropy of the activation. The entropy of adduct formation is -131.5 J/mole.K (-31.4 cal/mole.K) at room temperature (295K is used in calculations). The negative entropy value calculated suggests that the reaction is entropically unfavorable. This result was expected since changes in active site structure (movement of the helix containing the cysteine toward the FMN) and the hydrogen bonding rearrangement occurs before the adduct formation. These changes are required to overcome and generate the transition state.

Since phot1-LOV2 is a segment of a complete molecule, photochemical studies on LOV2 do not address whether the C-terminus effector domain influences the photocycle or not. In order to show that the adduct formation is the property of

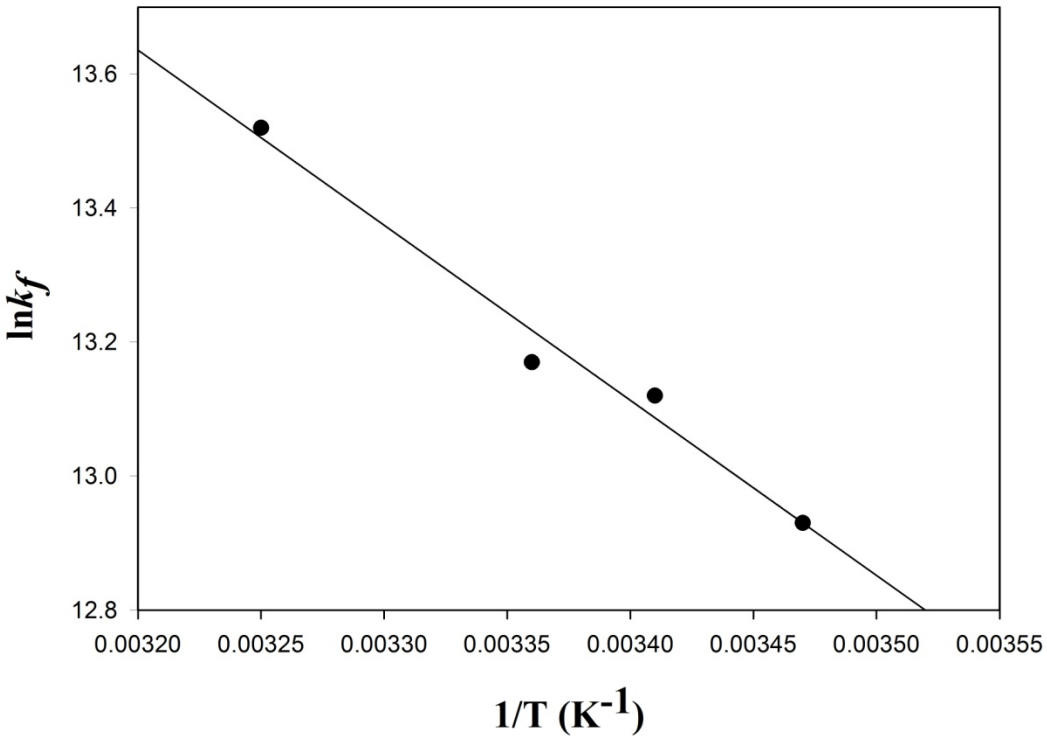

Figure 2-18 Arrhenius plot for the adduct formation kinetics of the El222.

the LOV domain, we made two different constructs where in the first one the HTH DNA binding C-terminus is missing (EL222 LOV Jα) and in the second construct the connector between the LOV and HTH domains that resembles the Jα helix in LOV2 and the HTH domain are missing (EL222 LOV-core). Both proteins were purified and shown to have the same absolute spectrum as the wild type EL222. The adduct formation time constant were studied with delay times into milliseconds to observe any possible late events that might have been there. EL222 LOV Jα helix showed an

apparent rate constant of 1.04 µsec (fig 2-20) and EL222 LOV-core shows an apparent rate constant of 1.3 µsec time constants (fig 2-21). In both cases, there is a second process that shows an apparent rate constant at about 260-300 µsec that we could not explain at first. Upon suggestion by Dr. James Lewis, we ran a sample of FMN in buffer in parallel to our samples and saw a process at the 100 µsec range that is very similar to the event that we see with both constructs. It is therefore our conclusion that the second time constant is not real since there is not any shape of triplet seen there and might be due to free FMN in the Solution (fig 2-19). It is also necessary to mention that resolving the second component by nanosecond absorption spectroscopy is extremely difficult and other studies are needed to explore this further. The branching ratio for both of the constructs is the same as the wild type EL222 but the formation times seem to be slower than EL222. This change can be explained by the changing environment around FMN. The FMN inside the wild type EL222 is protected from the environment around it but the FMN inside the constructs might be accessible and therefore ionic strength and PH change can affect the time constant of adduct formation. Still when we look at b-spectra no additional intermediates are observed and the constructs behave much like the wild type in the reaction scheme. This shows that photocycle of the EL222 is the inherent property of the LOV domain segment at the N-terminus of the protein and neither the presence of Jα-helix nor the helix-turn-helix segment affect the photocycle scheme of the EL222.

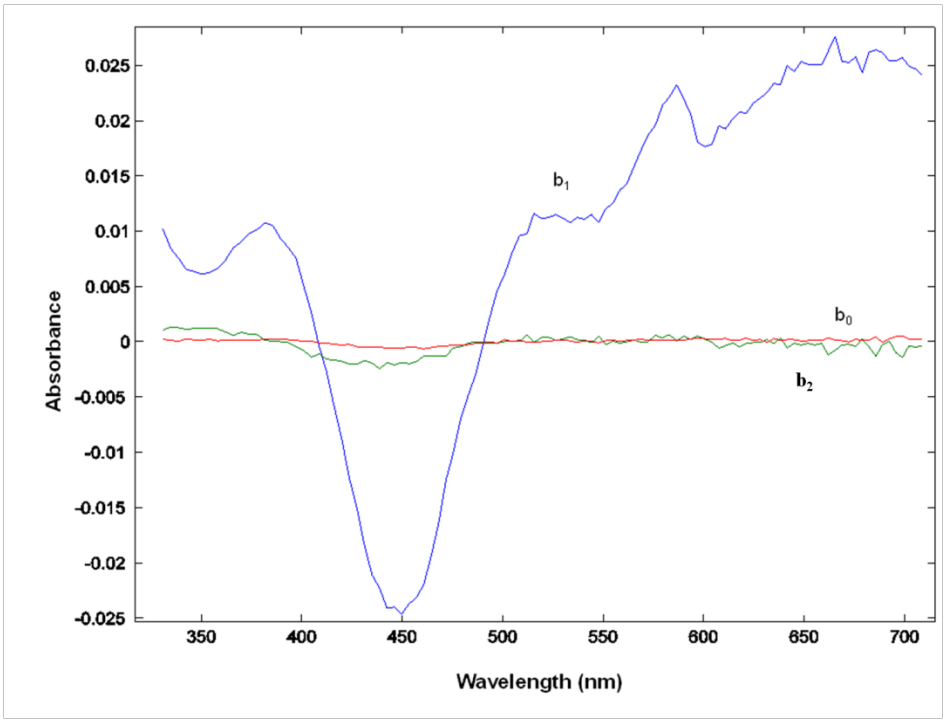

Figure 2-19 Spectra of the FMN were collected at 0.1, 0.2, 0.5, 1, 2, 50, 100, 200, 500, 1000, 2000, 5000 µsec. Spectra not shown. Longer time points at millisecond region are chosen to see if there are any late events that might have been missed before. This graph shows the results of global multi-exponential fitting of difference absorption spectra from FMN. b_1 is the b-spectrum with an apparent rate constant of 3.5 µsec, and b_0 is the spectrum of the product formed which is zero since FMN returns to the ground state in a cyclic process. b_2 is the b-spectrum that was chosen because it might represent a second process at 100 µs and this was seen again in the constructs of EL222.

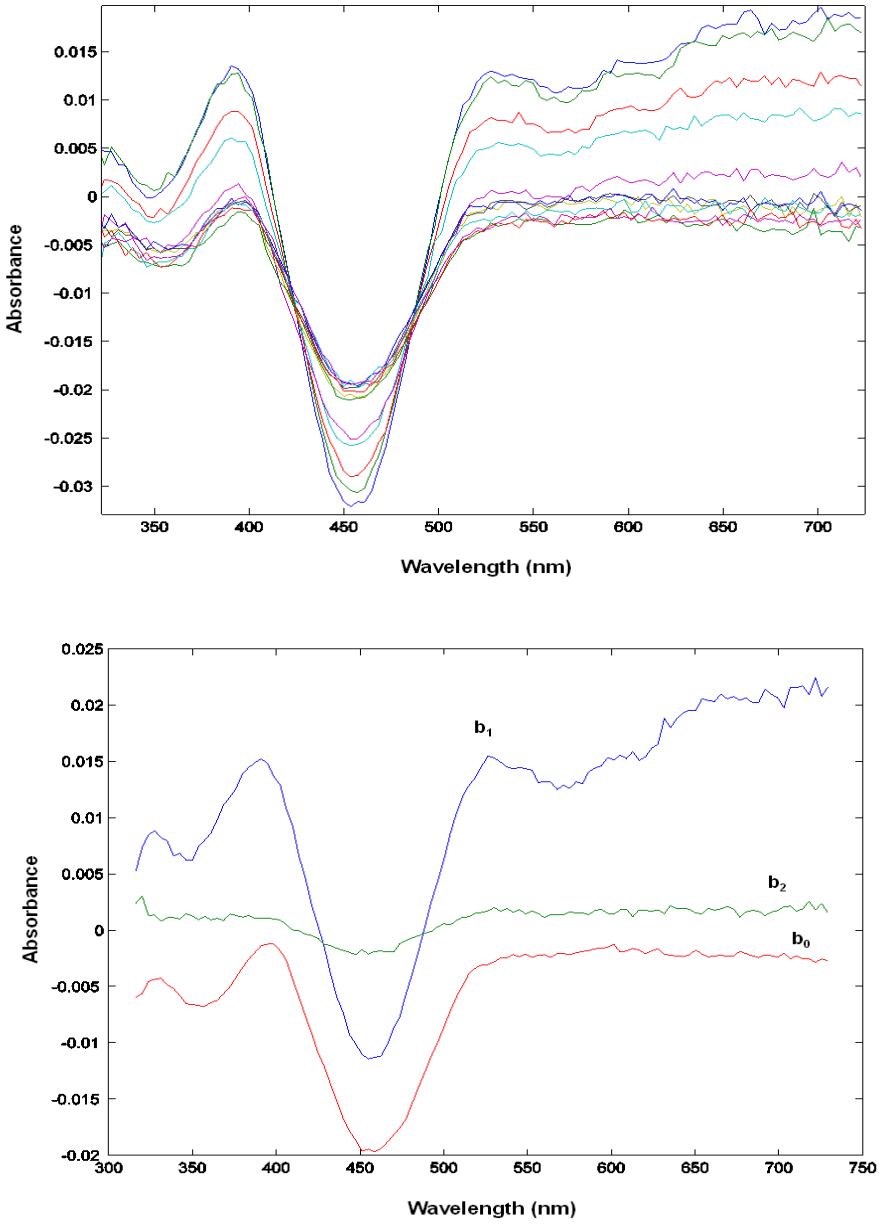

Figure 2-20 The absorption difference spectra of EL222 LOV Jα helix at room temperature after excitation with a 477nm laser pulse. Spectra were collected at 0.1, 0.2, 0.5, 1, 2, 50, 100, 200, 500, 1000, 2000, 5000 µsec. Longer time points at millisecond region are chosen to see if there are any late events that might have been missed before. Bottom graph shows the results of global multi-exponential fitting of difference absorption spectra from EL222 LOV Jα helix. b_1 is the b-spectrum with an apparent rate constant of 1.04 µsec, and b_0 is the spectrum of the product formed. b_2 is the b-spectrum that was chosen because it might represent a second process at 280 µs but this might be due to free FMN as the small peak at 520nm represents semiquinone (see figure 2-19).

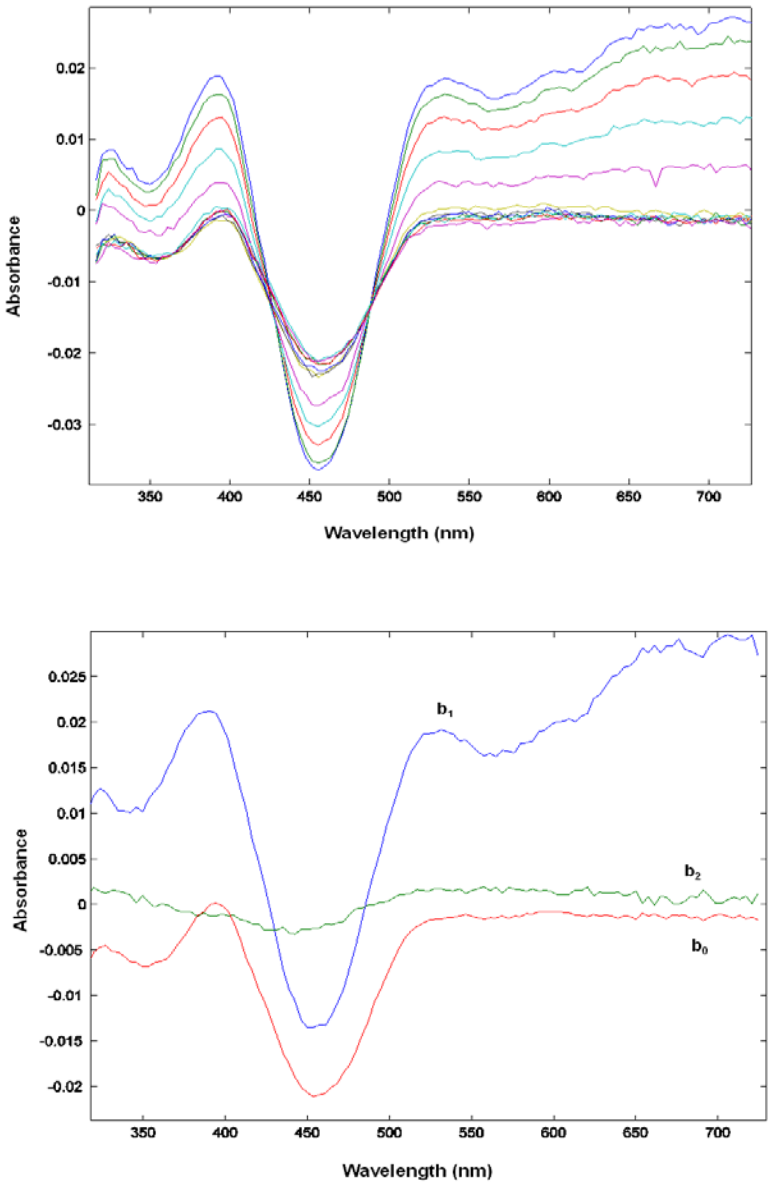

Figure 2-21 The absorption difference spectra of EL222 LOV-core at room temperature after excitation with a 477nm laser pulse. Spectra were collected at 0.1, 0.2, 0.5, 1, 2, 50, 100, 200, 500, 1000, 2000, 5000 µsec. Longer time points at millisecond region are chosen to see if there are any late events that might have been missed before. Bottom graph shows the results of global multi-exponential fitting of difference absorption spectra from EL222 LOV-core. b_1 is the b-spectrum with an apparent rate constant of 1.3 µsec, and b_0 is the spectrum of the product formed. b_2 is the b-spectrum that was chosen because it might represent a second process at 325 µs but this might be due to free FMN (see figure 2-19).

2.3.2 Late Photocycle

The data collected by nanosecond laser flash spectroscopy show that the spectral features after 10 μs are nearly identical to those at milliseconds. This observation indicated that like LOV2, $EL222^{S}_{390}$ decays back to the ground state in seconds. This result allows us to study the kinetics of adduct state decay back to the $EL222^{D}_{450}$ using the Hewlett Packard 8452A diode array spectrometer. The sample shows a spontaneous return to the ground state within 60 seconds after a period of 30 seconds to one minute of illumination. The b-spectra of the analyzed data show that one exponential is acceptable for satisfying the fitting of that data at room temperature (fig 2-22). Therefore analysis of the slow back reaction decay reveals only one apparent time constant of 16 seconds, where the half-life can be calculated by

$$t_{1/2} = \ln(2)\,\tau_{rec} \qquad (2.8)$$

where τ_{rec} is the recovery apparent time constant which yields to $t_{1/2}$ = 11 seconds. This time constant is associated with the b_1-spectrum that is the time dependent b-spectra and the time independent time spectra (b_0) is zero since this is a cyclic process. Time-resolved light induced absorption changes at long times for EL222 shows absorption at 390 nm and loss of absorption at 450 nm (indications of the formation of the stable intermediate $EL222^{S}_{390}$) and follows the return to the zero line which is the dark state ($EL222^{D}_{450}$).

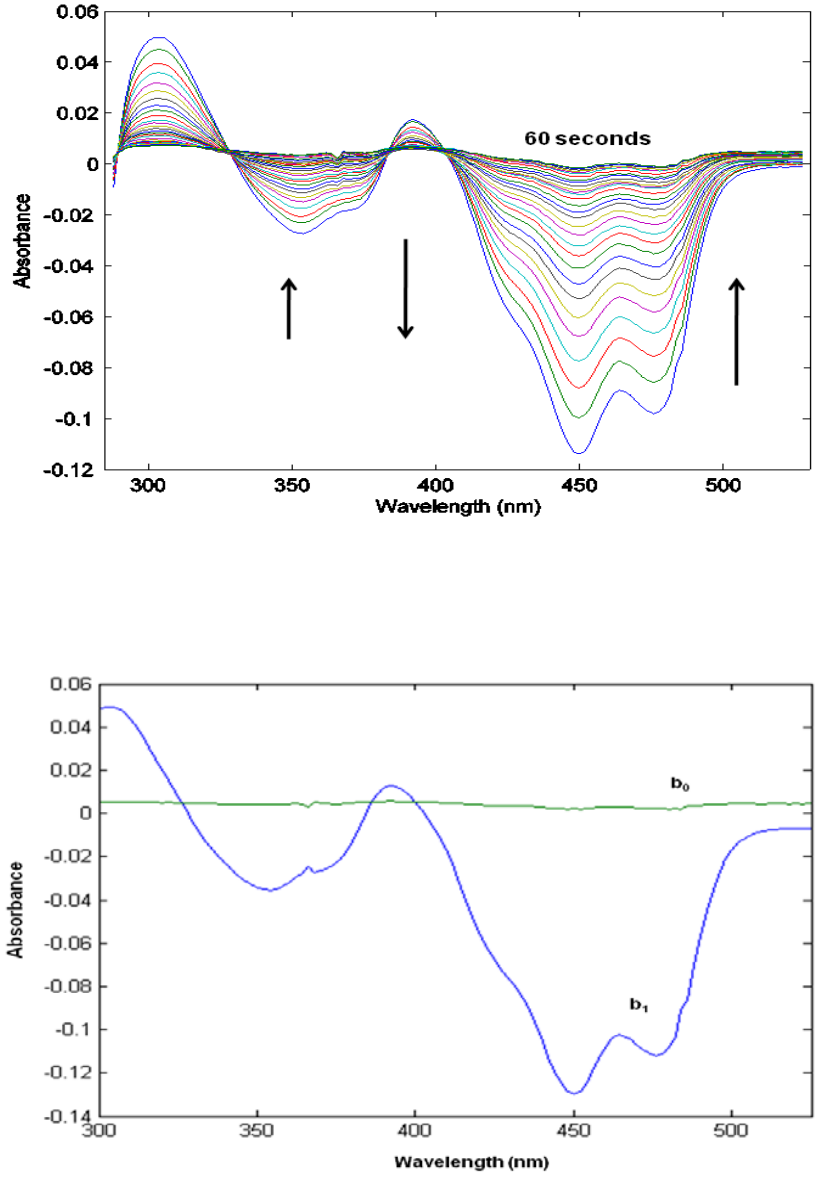

Figure 2-22 Time resolved, light induced absorption changes for EL222 at room temperature. Sample was illuminated for 60 seconds and spectra were taken every 2 seconds for 60 seconds. Formation of $EL222^{S}{}_{390}$ is seen by loss of blue light absorption and formation of the absorption band at 390 nm. Bottom figure shows b-spectra from single-exponential fitting with time constant of 16 sec. associated with b_1 (τ_{rec}). b_0 is the time-independent spectra and will become zero if the recovery is a complete cyclic process.

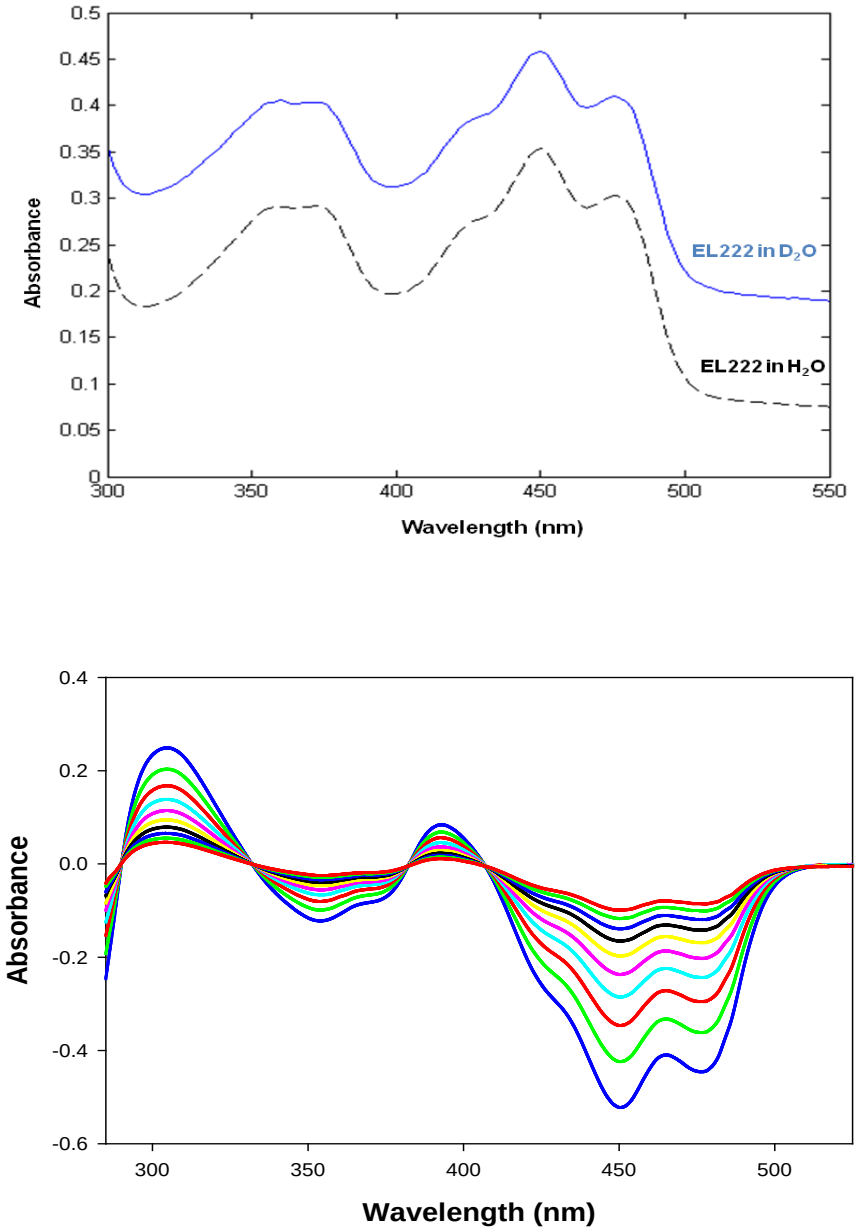

Figure 2-23 Ground-state absorption spectra of EL222 in H_2O and D_2O. Spectra are offset for clarity. Bottom graph is the time resolved, light induced absorption changes for EL222 in D_2O at room temperature. Sample was illuminated for 60 seconds and spectra were taken every 20 seconds for 200 seconds.

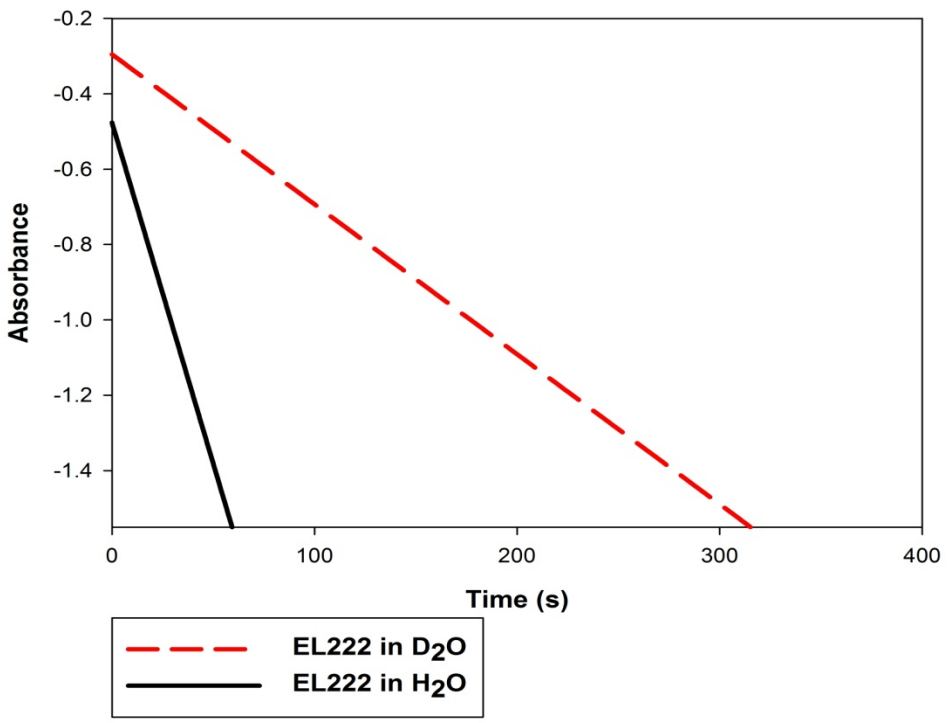

Figure 2-24 Back-reaction kinetics for EL222 in H_2O versus D_2O. EL222 in H_2O recovers with a time constant of 16 seconds, but EL222 in D_2O recovers with a time constant of 90 seconds. Recovery of the ground state was monitored at 450 nm.

In order to elucidate the photocycle mechanism and structural changes further, we measure D_2O and pH-dependencies of EL222 back reaction kinetics. As mentioned earlier, the ground-state absorption spectrum of EL222 in D_2O remain the same (fig 2-23) but the back reaction in D_2O is five times slower than in H_2O (fig 2-24). The slowing of the dark recovery due to the deuterium effect would suggest that a proton transfer reaction is the rate limiting step. This slowing could also reflect hydrogen bonds rearrangement or a hydrogen bond breakage as the rate limiting step

in the back reaction. Altering the hydrogen bonding does affect the formation of the adduct and the back reaction to the ground state in EL222 (see chapter 3). The next two experiments complicate the mechanism of the dark recovery of the ground state $EL222^{D}_{450}$ from $EL222^{S}_{390}$. In *Chlamydomonas* phot1-LOV, there is a large pH dependence of the decay rate between pH 3.0 to pH 8.0 in which the rate increases several fold [16] which indicates that the back reaction is base catalyzed. In oat phot1-LOV2, there is not a large pH-dependence seen but shows a slight rate increase with increased pH [17] which, combined with an imidazole effect also indicates a base catalyzed reaction [15]. These differences in pH-dependence indicate differences in chemical behavior among LOV domains that is also evident in EL222. Experiments with 200mM imidazole containing buffer show a clear increase in the time constant of the EL222 back reaction (fig 2-25). In imidazole, the time constant of the back reaction decreases from 16 seconds to 5.75 seconds which would indicate a base catalyzed reaction. The pH experiments of the EL222 yields surprising results in EL222 that are very different from other LOV domains (fig 2-29). Although EL222, much like LOV2, shows only a slight pH-dependence, unlike LOV2, the rate decreases with the increased pH (fig 2-26, 2-27, 2-28, and 2-29). This result is hard to explain since the proposed mechanism for the back reaction of LOV-domains involves the removal of the N(5) proton (acid-base catalysis) in the step that initiates the reaction.

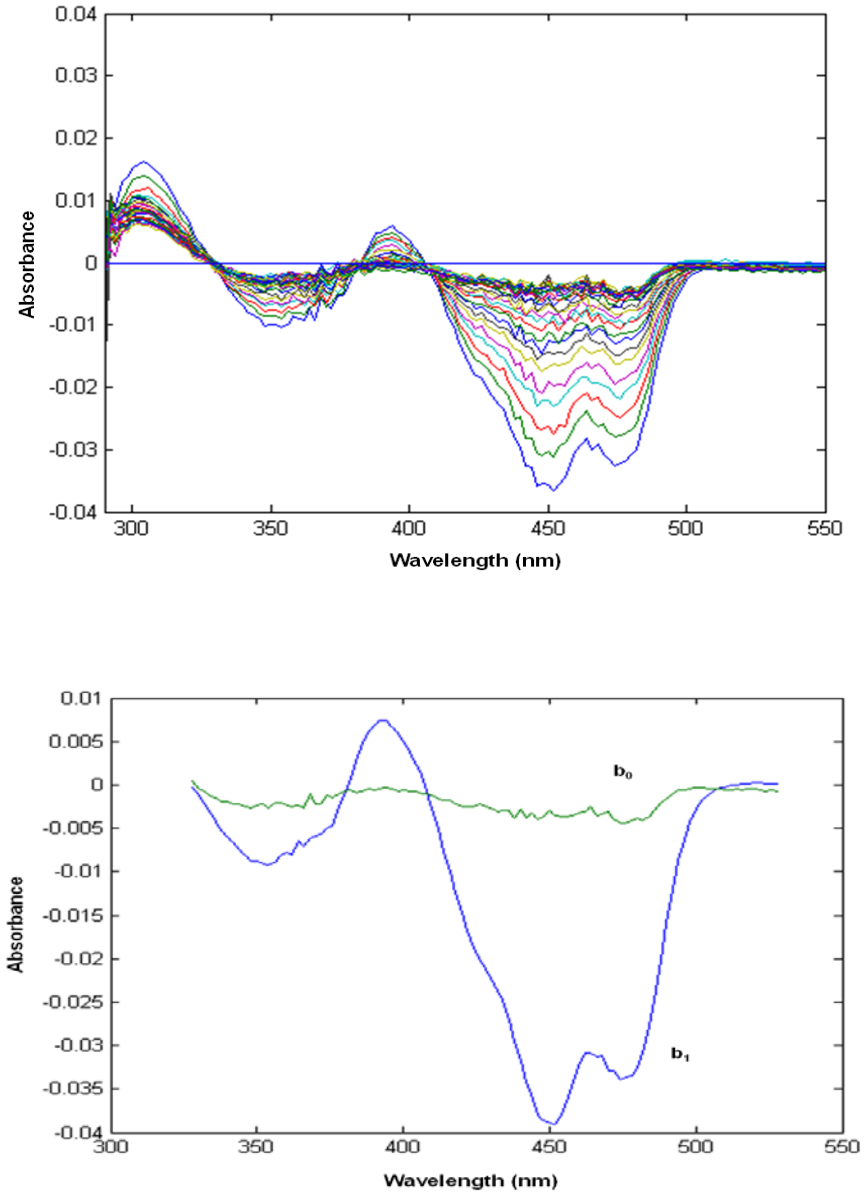

Figure 2-25 Time resolved, light induced absorption changes for EL222 in 200mM imidazole containing buffer at room temperature. Sample was illuminated for 60 seconds and spectra were taken every second for 30 seconds. Protein started to show precipitation which resulted in noisy spectra and a b_0 spectrum that is not zero. The single-exponential fitting shows a time constant of 5.75 sec. associated with b_1 (τ_{rec}).

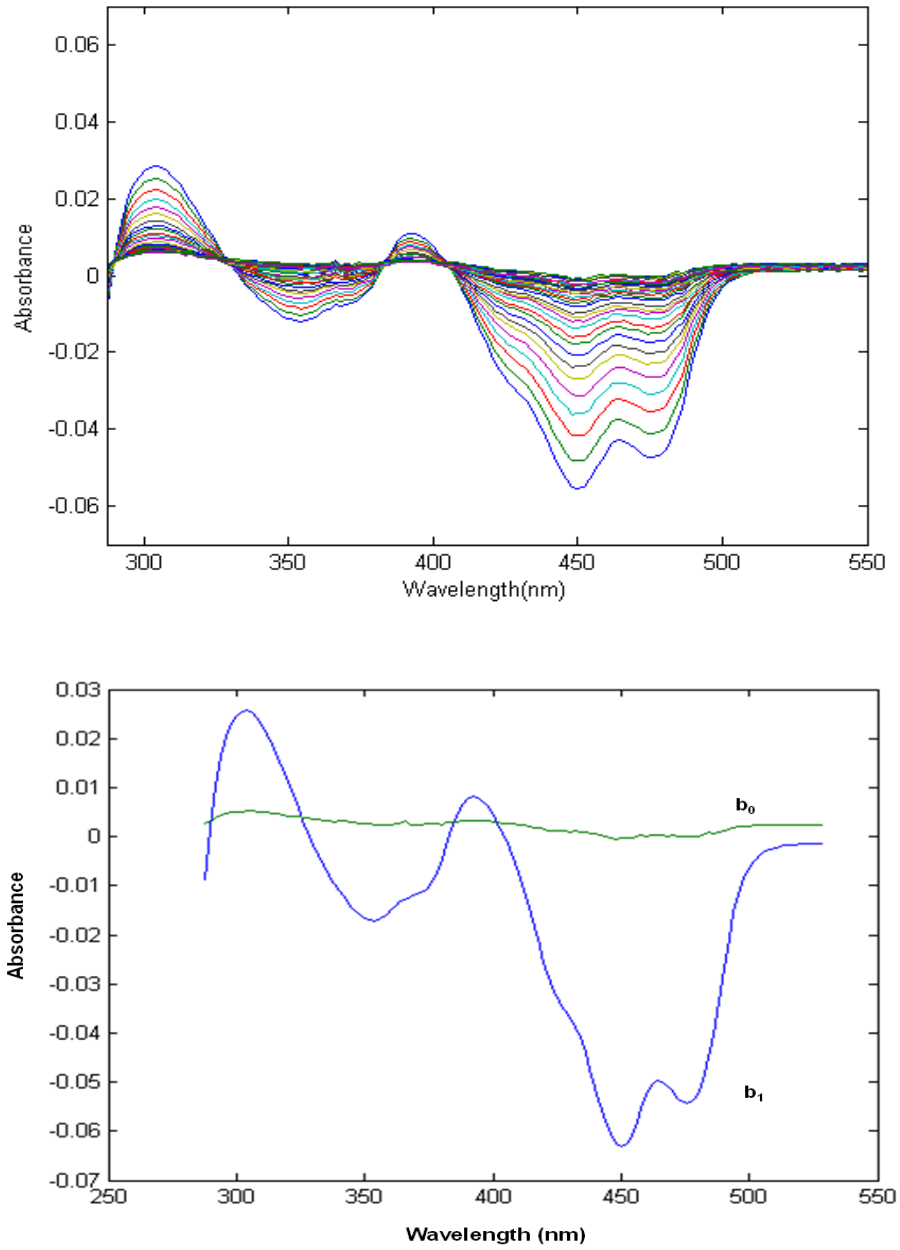

Figure 2-26 Time resolved, light induced absorption changes for EL222 in pH 6.0 buffer at room temperature. Sample was illuminated for 60 seconds and spectra were taken every 2 second for 60 seconds. Bottom figure shows b-spectra from single-exponential fitting with time constant of 14.23 sec. associated with b_1 (τ_{rec}) and b_0 is the time-independent spectra.

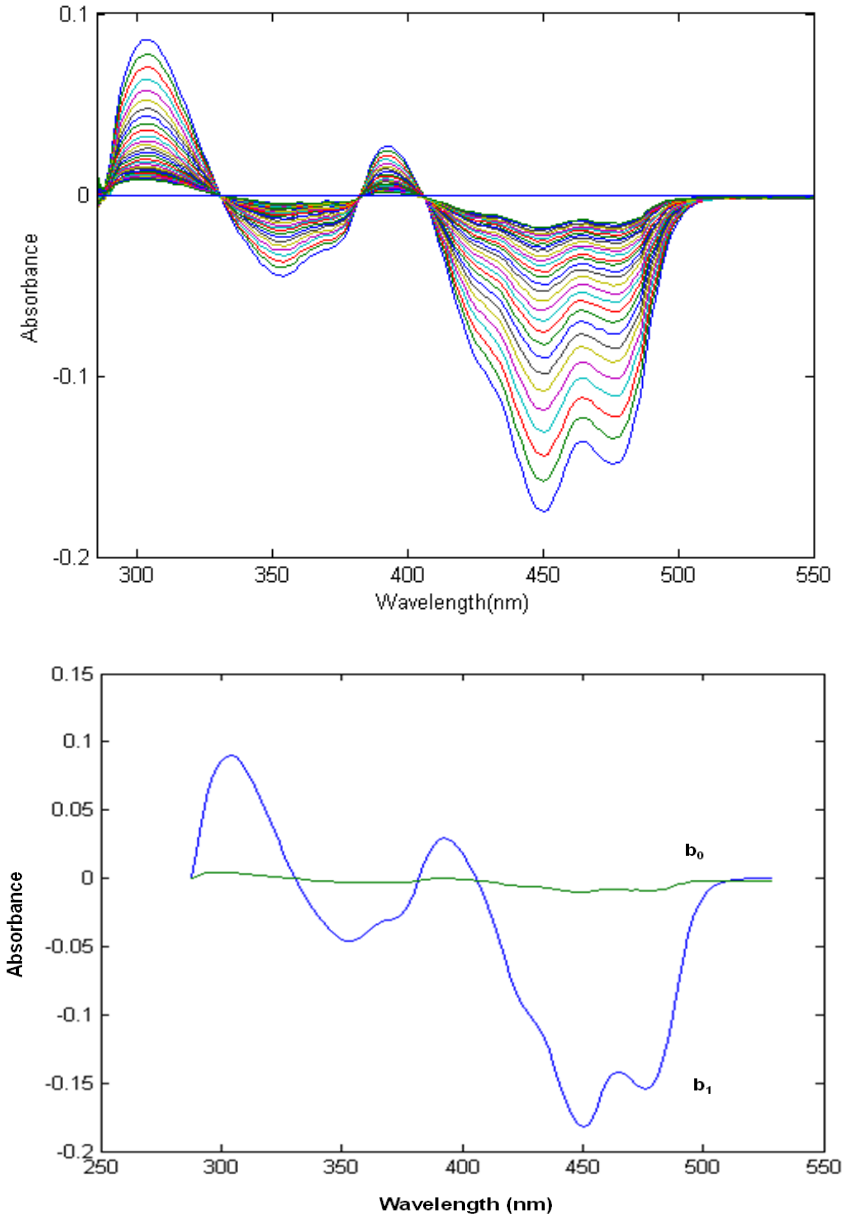

Figure 2-27 Time resolved, light induced absorption changes for EL222 in pH 8.0 buffer at room temperature. Sample was illuminated for 60 seconds and spectra were taken every 2 second for 60 seconds. Bottom figure shows b-spectra from single-exponential fitting with time constant of 19.46 sec. associated with b_1 (τ_{rec}) and b_0 is the time-independent spectra.

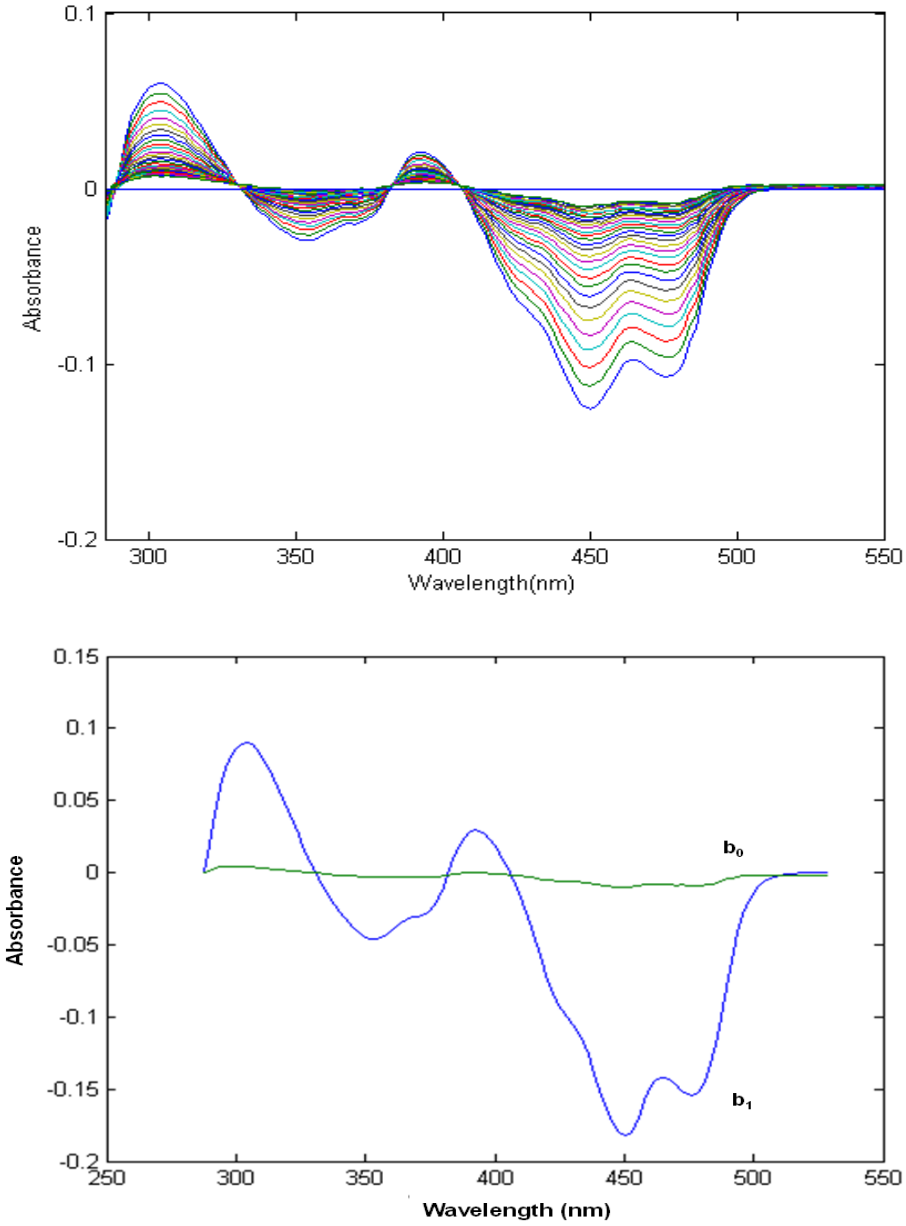

Figure 2-28 Time resolved, light induced absorption changes for EL222 in pH 9.5 buffer at room temperature. Sample was illuminated for 60 seconds and spectra were taken every 2 second for 60 seconds. Bottom figure shows b-spectra from single-exponential fitting with time constant of 19.5 sec. associated with b_1 (τ_{rec}) and b_0 is the time-independent spectra.

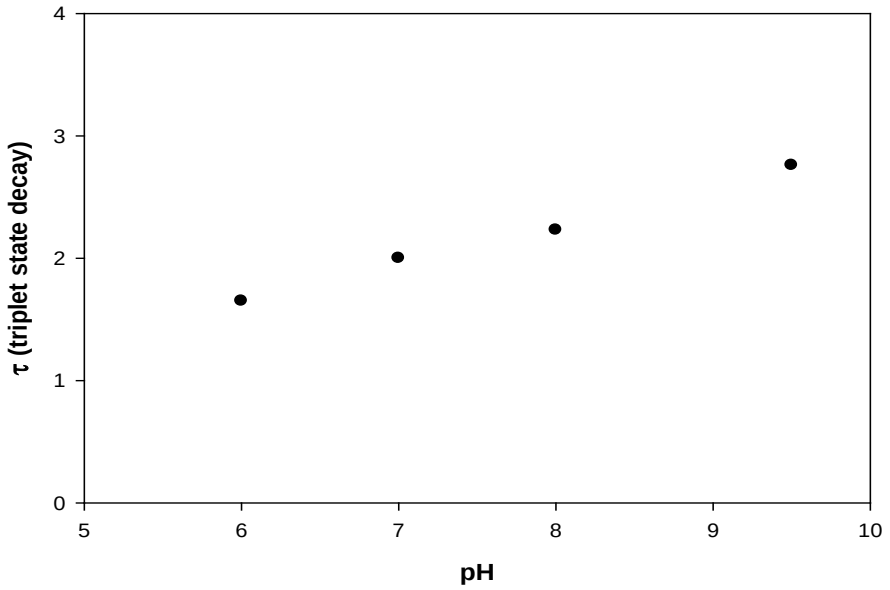

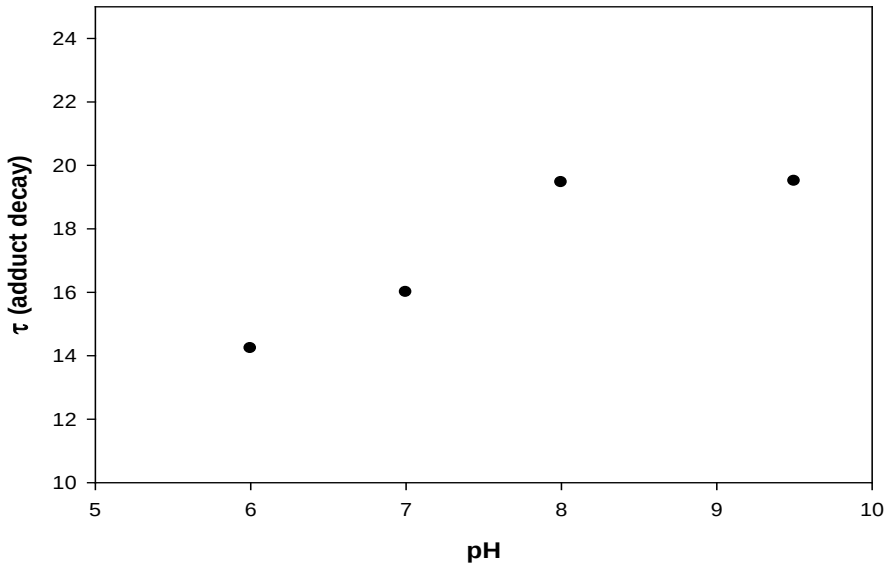

Figure 2-29 pH sensitivity of the rates of adduct formation (top graph) in μsec. and adduct decay (bottom graph) in sec.

The difference in pH sensitivities between LOV2 and EL222 can be rationalized by looking at the hydrogen bonding network around the FMN chromophore (chapter 3). Although we still believe that the back reaction of EL222 follows the mechanism of other LOV domains which involves base catalysis (due to our imidazole effect results), we realize that this might not be the only important or rate limiting process in the back reaction of EL222.

2.4 Discussion

We have presented the first detailed in vitro characterization of a light activated DNA binding domain from a marine bacterium named, *Erythrobacter litoralis.* The availability of the crystal structure data on EL222 [18] aids the mechanistic interpretation of the spectral data collected during this study. Also the comparison with the phot1-LOV2 domain which has been studied in detail [6, 19-21] facilitates understanding of the photocycle scheme in EL222. The data presented in this study shows only one transient specie preceding the formation of the adduct state $EL222^{S}_{390}$. The FMN molecule inside the LOV domain of EL222 will go to the singlet excited state upon absorption of a photon of light. The proximity of the sulfur atom from the conserved cysteine at position 75 of the protein causes intersystem crossing of the excited FMN to the triplet state ($EL222^{L}_{660}$). This study does not resolve whether the cysteine exists as a thiol (-SH) or a thiolate ($-S^{-}$) but we propose that they can be at equilibrium inside the FMN binding pocket. The N(5) of the FMN

becomes more basic and more reactive upon intersystem crossing to the triplet state from the singlet excited state. The N(5) of FMN is protonated by a proton donor group that is not yet identified but proposed to be either the cluster of water molecules around the FMN or the thiol of the cysteine. After protonation of the N(5), the N(5)-C(4a) double bond becomes a single bond which makes the newly formed C(4a) carbo-cation very reactive. This will allow the reaction with cysteine sulfide to happen on a microsecond time scale (fig 2-30). Although the possibility of adduct formation through radical pair formation as a mechanism is also possible, we believe this is unlikely (refer to the introduction). The back reaction reverses this scheme (since b_0-spectra shows a cyclic process). The proton donor now acts as an acceptor or another base removes the proton from the N(5) of the FMN inside EL222. We could not identify any amino acids close to the N(5) that can act as a base and remove the proton but we suggest structural water in the FMN binding site pocket can act as the proton acceptor. Dehydration studies on LOV2 have shown that removing these waters can affect the time constant of the recovery and eventually stops it from cycling [22]. The removal of a proton from the N(5) causes the flavin to return to a lower energy state by breaking the sulfur and C(4a) bond and regenerate the N(5)-C(4a) double bond. Upon the formation of the double bond, flavin has returned to the ground state and in doing so EL222 has returned to the dark state ($EL222^{D}_{450}$) which completes the photocycle (fig 2-30).

EL222 shows a larger D_2O effect than LOV2 in both the adduct formation and the back reaction. Deuterium transfer reactions are generally slower due to the larger

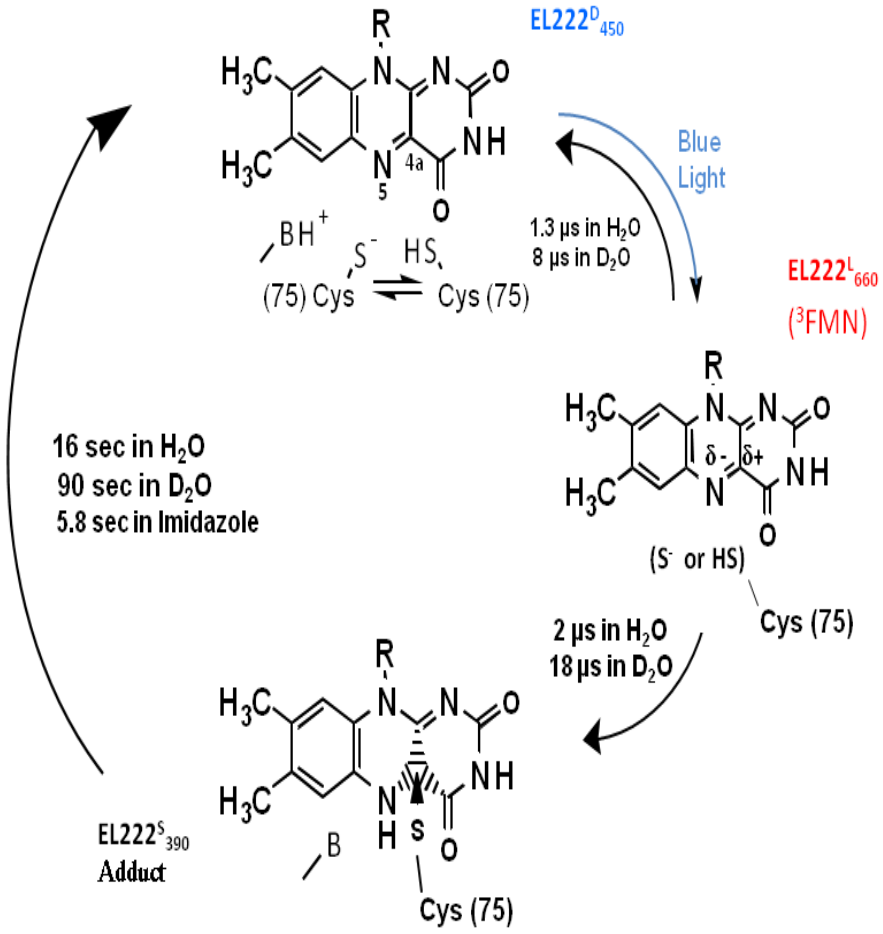

Figure 2-30 Photocycle scheme and proposed reaction mechanism for EL222. Blue light photolysis produces a triplet species which decays through a branching scheme back into the ground state and forward to the adduct state. All the time constants in this scheme are based on measurements done at room temperature which is not controlled but measured to be 20±2℃.

mass of deuterium relative to hydrogen. There are two types of deuterium effects that can contribute to this. The primary isotope effect which is the kinetics slowing of hydrogen transfer reactions in the form of breakage of a bond and formation of a new bond between the donor and the acceptor groups. The secondary isotope effects include hydrogen bonding and structural solvent effect. They are usually much smaller than the primary effects although if there are a large number of hydrogen bond alterations involved in a reaction, contribution of the secondary isotope effects can be considerable. We suspect that the secondary contributions play a major role in the adduct formation rate limiting step since the calculated activation energy barrier for adduct formation is about 22 KJ/mole which is within the energy range of a few hydrogen bonds.

The apparent pH independence of the adduct formation between pH 6.0 and 9.5 can only suggest that groups involved in the reaction have pk values outside this range. Although small, a steady increase of τ_F with increased pH (fig 2-29) can suggest that the active cysteine needs to be in the thiolate (S^-) form in the binding pocket of the FMN. As the pH increases and shifts the equilibrium toward the cysteine with a thiol (-SH), the rate of the cysteinyl-adduct formation is slower.

The data presented here suggests that back reaction is a base catalyzed reaction with a proton transfer as the rate limiting step. The small but significant effect of pH changes on the rate constant of the back reaction suggests that alteration

in hydrogen bonding can play an important role in the back reaction. We will explore this idea further in the next chapter.

References:

1. Pompeani, A.J., et al., *The Vibrio harveyi master quorum-sensing regulator, LuxR, a TetR-type protein is both an activator and a repressor: DNA recognition and binding specificity at target promoters.* Molecular Microbiology, 2008. **70**(1): p. 76-88.

2. Briggs, W., et al., *The phototropin family of photoreceptors.* PLANT CELL, 2001. **13**(5): p. 993-997.

3. Losi, A., et al., *First evidence for phototropin-related blue-light receptors in prokaryotes.* Biophys J, 2002. **82**(5): p. 2627-34.

4. Briggs, W., J. Christie, and M. Salomon, *Phototropins: A new family of flavin-binding blue light receptors in plants.* ANTIOXIDANTS & REDOX SIGNALING, 2001. **3**(5): p. 775-788.

5. Briggs, W.R., et al., *The phototropin family of photoreceptors.* Plant Cell, 2001. **13**(5): p. 993-7.

6. Swartz, T., et al., *The photocycle of a flavin-binding domain of the blue light photoreceptor phototropin.* JOURNAL OF BIOLOGICAL CHEMISTRY, 2001. **276**(39): p. 36493-36500.

7. Christie, J.M., et al., *LOV (light, oxygen, or voltage) domains of the blue-light photoreceptor phototropin (nph1): binding sites for the chromophore flavin mononucleotide.* Proc Natl Acad Sci U S A, 1999. **96**(15): p. 8779-83.

8. Müller, F., *Chemistry and biochemistry of flavoenzymes*. 1991, Boca Raton: CRC Press. v. <1-3 >.

9. Lewis, J.W. and D.S. Kliger, *Microliter flow cell for measurement of irreversible optical absorbance transients.* Review of Scientific Instruments, 1993. **64**(10): p. 2828-2833.

10. Kliger, D.S., J.W. Lewis, and C.E. Randall, *Polarized light in optics and spectroscopy*. 1990, Boston: Academic Press. x, 304.

11. Szundi, I., J.W. Lewis, and D.S. Kliger, *Deriving reaction mechanisms from kinetic spectroscopy. Application to late rhodopsin intermediates.* Biophysical Journal, 1997. **73**(2): p. 688-702.

12. Corchnoy, S.B., et al., *Intramolecular proton transfers and structural changes during the photocycle of the LOV2 domain of phototropin 1.* Journal of Biological Chemistry, 2003. **278**(2): p. 724-731.

13. Szundi, I., T.E. Swartz, and R.A. Bogomolni, *Multicolored protein conformation states in the photocycle of transducer-free sensory rhodopsin-I.* Biophys J, 2001. **80**(1): p. 469-79.

14. Crosson, S., S. Rajagopal, and K. Moffat, *The LOV domain family: Photoresponsive signaling modules coupled to diverse output domains.* BIOCHEMISTRY, 2003. **42**(1): p. 2-10.

15. Alexandre, M., et al., *A Base-Catalyzed Mechanism for Dark State Recovery in the Avena sativa Phototropin-1 LOV2 Domain.* BIOCHEMISTRY, 2007. **46**(11): p. 3129-3137.

16. Kottke, T., et al., *Phot-LOV1: Photocycle of a blue-light receptor domain from the green alga Chlamydomonas reinhardtii.* BIOPHYSICAL JOURNAL, 2002. **84**(2): p. 1192-1201.

17. Corchnoy, S., et al., *Intramolecular proton transfers and structural changes during the photocycle of the LOV2 domain of phototropin 1.* JOURNAL OF BIOLOGICAL CHEMISTRY, 2003. **278**(2): p. 724-731.

18. Nash, A.I., et al., *Structural basis of photosensitivity in a bacterial light-oxygen-voltage/helix-turn-helix (LOV-HTH) DNA-binding protein.* Proceedings of the National Academy of Sciences, 2011. **108**(23): p. 9449-9454.

19. Harper, S.M., L.C. Neil, and K.H. Gardner, *Structural Basis of a Phototropin Light Switch.* Science, 2003. **301**(5639): p. 1541-1544.

20. Christie, J.M., et al., *Phototropin LOV domains exhibit distinct roles in regulating photoreceptor function.* Plant J, 2002. **32**(2): p. 205-19.

21. Swartz, T.E., et al., *Vibration Spectroscopy Reveals Light-Induced Chromophore and Protein Structural Changes in the LOV2 Domain of the Plant Blue-Light Receptor Phototropin 1†.* Biochemistry, 2002. **41**(23): p. 7183-7189.

22. Chan, R.H. and R.A. Bogomolni, *Structural water cluster as a possible proton acceptor in the adduct decay reaction of oat phototropin 1 LOV2 domain.* The Journal of Physical Chemistry B, 2012. **116**(35): p. 10609-10616.

CHAPTER 3

MODULATION OF THE PHOTOCYCLE OF EL222 BY ALTERING THE HYDROGEN BONDING NETWORK AROUND THE CHROMOPHORE

3.1 Introduction

LOV domains are responsible for blue-light perception in all Kingdoms of life and control a wide array of responses. LOV domains are the light-sensitive components of phototropin in plants and control phototropism, chloroplast movement, and opening of the guard cells [1-2]. The discovery of LOV proteins in the bacterial world was significant since it established a new mechanism of blue-light sensing in bacteria alongside the photoactive yellow protein, PYP [3], blue light using FAD (BLUF) domains [4], and cryptochrome [5]. The function of almost all of these bacterial LOV domains remains mostly undetermined with a few exceptions. The bacterium, *Caulobacter Crescentus* contains a LOV-histidine kinase (LOVK) that through a response regulator (LOVR) regulates Cell-Cell attachment [6]. The bacterium, *Brucella Melitensis* is a human pathogen, and contains a LOV-histidine kinase (LOV-HK) that is involved in regulating virulence [7]. Among the several LOV domains that the bacterium *Erythrobacter Litoralis* contains, there is one that has a LOV domain at the N-terminus and a helix-turn-helix (HTH) DNA-binding domain at the C-terminus [8]. Recently, the dark-state crystal structure of this 222 amino acid protein (named EL222) has been solved [8] that displays interactions between the LOV and the HTH domain. It was also shown that light controls the

binding of this protein to DNA [8]. Although the crystal structure of the dark-state aids understanding and analyzing results of other biochemical and biophysical experiments, a true atomic resolution light-state structure is still missing. Absorption spectroscopy has given us a glance into the photochemistry of this LOV-domain that was covered in detail in chapter two. In the absence of the light-state crystal structure, formation of the adduct state (EL222 $^{S}_{390}$) from the triplet state needs further detailed study that will be addressed in this chapter. EL222 shows a larger D_2O effect than LOV2 in both the adduct formation and the back reaction. Since the activation energy barrier for adduct formation is about 22 KJ/mol, hydrogen bonding might play a large role in the formation of the adduct and decay of the adduct state into the dark state. The N(5) of the isoalloxazine ring of the FMN plays an important role in the photocycle of LOV-domains. D_2O studies show that protonation of N(5) is the rate limiting step in the formation [9], which is then followed by a C-S covalent bond (fig 2-30). Same studies also revealed the deprotonation of the N(5) after adduct formation, is the rate limiting step that causes the breakage C-S covalent bond and return of the EL222$^{S}_{390}$ adduct state to the dark state (EL222$^{D}_{450}$). The careful study of the available crystal structure of the EL222 (PDB ID: 3P7N) reveals that a highly conserved glutamine at position 138, can hydrogen bond with the N(5) of the FMN (fig 3-1 and 3-2).

In this chapter, we have investigated several mutations at glutamine 138 and alanine 79 (fig 3-1) with the goal of further understanding the influence of hydrogen bonding around FMN on the photocycle of EL222. We mutated a glutamine to

asparagine (Q138N) and a glutamine to leucine (Q138L). The highly conserved glutamine in the motif, NCRFL**Q,** is an alanine in the EL222 (fig 3-1) and was mutated to glutamine (A79Q) to find out what role the added hydrogen bonding of glutamine plays in photocycle of EL222. The light induced absorbance changes of EL222 mutants in the 400 ns to 1 hour time range were measured, globally analyzed, and the results are used to discuss the mechanism of adduct formation and decay in a greater detail. We observed considerable changes in the photocycle of EL222 with the slight perturbations made with the Q138N and Q138L mutants to the hydrogen bonding of the isoalloxazine ring of FMN. The A79Q also shows significant changes which highlight the effects of amino acids not directly involved in the photocycle.

3.2 Materials and Methods

3.2.1 Cloning, Mutagenesis, Protein Expression, and Purification

EL222 containing plasmids were purified from the overnight cell culture using StrataPrep plasmid mini-prep kit. The method employs the alkaline method of cell lysis and a microspin cup with a silica based fiber matrix that binds plasmids of interest. After washing the contaminants and cell debris from the microspin cup with a washer buffer, the plasmid is eluted from the fiber matrix with 10mM Tris-base pH adjusted to 8.5. The result is purified plasmid DNA that is ready for restriction digestion, PCR, and sequencing reactions. Integrated DNA technologies (San Diego, CA) synthesized the primers for the PCR reaction. The primers for the reaction: 5'-

CTATTTCCTCGGCAGCCTGGTCGAAGTCGACGACG-3' forward and 5'-CGT CGTCGACTTCGACCAGGCTGCCGAGGAAATAG 3' reverse primer for EL222 Q138L mutant and 5'-CTATTTCCTCGGCAGCAACGTCGAAGTCGACGACG-3' forward and 5'-CGTCGTCGACTTCGACGTTGCTGCCGAGGAAATAG-3' reverse primer for EL222Q138N mutant and 5'-CAATTGCCGATTCCTGCAAGGTTCCG GCACCGAGC-3' forward and 5'-GCTCGGTGCCGGAACCTTGCAGGAATCGG CAATTG-3' reverse primer for EL222A79Q mutant. Mutagenesis of the EL222 was carried out according to instructions provided by Stratagene QuickChange site-Directed mutagenesis kit. This kit allows site-specific mutation in double stranded plasmid which is less labor intensive and does not require unique restriction sites and produces mutants with greater than 80% efficiency. The key to this method is the use of *Pfu*Turbo DNA polymerase that replicates both plasmid strands with 6-fold higher fidelity in DNA synthesis than the Taq DNA polymerase. In short, this technique uses the wild type plasmid and the two primers (forward and reverse) that have the mutation of interest added. After the primers anneal to the vector, *Pfu*Turbo DNA polymerase, extends them during temperature cycling to generate complete plasmid containing the desired mutation. The product is then treated with Dpn I which digests the parental DNA template (wild type EL222), leaving only the mutation-containing synthesized DNA [10]. The mutated plasmid are then transformed into XL-1 Blue Super-competent cells and incubated at 37℃ overnight. The successful colonies were grown in Luria broth and plasmids were purified using StrataPrep plasmid mini-prep kit. Several samples of plasmids were sent to UC Berkeley DNA sequencing facility

for sequencing. The plasmids containing the targeted mutation were then transformed into *E.coli* BL21 (DE3) pLysS competent cells and grown on an Ampicillin containing plates overnight. The protein purification was carried out as previously described in the materials and methods section of chapter 2. Samples were lyophilized in dark for D_2O experiments.

3.2.2 Sequence Comparison Analysis

A dynamic programming algorithm is used to determine similar regions of phot1-LOV2 and EL222 sequences. The LALIGN sequence alignment program [11-14] from the ExPASy Proteomics Server is used and the result of the homology comparison is shown in figure 3-1.

3.2.3 UV-Visible Absorption Spectroscopy

Light induced absorption changes at short and long times were measured and analyzed as previously described (chapter 2). The delay for the probe light was moved to longer times (5.04 sec) for EL222 Q138N to observe the return of the adduct to the ground state. The long time spectra were taken at much longer times and was followed for one hour during EL222Q138L mutant measurements to observe the decay of the adduct to the dark state.

3.3 Results

The photocycle of EL222 wild type was discussed in detail in chapter 2 and the set of experiments are repeated here to establish the role of hydrogen bonding in the formation of adduct state and the spontaneous decay of the adduct to the dark state. The UV-visible dark state absorbance spectra of the mutants display the same characteristic profiles (fig 3-3) for typical LOV domains. They show maxima between 400 nm to 500 nm typical of FMN inside LOV-domains with the 450nm maximum shifted to 445 in EL222Q138Land to 452 nm in EL222A79Q mutant (fig 3-3). All mutants show loss of this absorption maximum upon illumination with light indicating the formation of $EL222^{S}_{390}$ state. The shift in the 450 nm absorbance usually indicates a change in the electronic environment surrounding the FMN [15-17]. The EL222Q138N does not show much difference from the wild type EL222 as expected since Q and N can form comparative hydrogen bonding around FMN environment. The spectroscopic data confirms that the larger change by the Q138L mutant to the environment of FMN binding pocket causes the larger change in the photocycle time constants.

```
20        30        40        50        60        70
LOV2   VITDPRLPDNPIIFASDSFLQLTEYSREEILGRNCRFLQGPETDRATVRKIRDAIDNQTE
       :..:::: ::::.:  ...: .:: ::.:: .:::::::: :  :.   . ::::.. ..
EL222  VVSDPRLADNPLIAINQAFTDLTGYSEEECVGRNCRFLAGSGTEPWLTDKIRQGVREHKP
                50        60        70        80        90       100

             80        90       100       110
LOV2   VTVQLINYTKSGKKFWNLFHLQPMRDQKGDVQYFIGVQLD
       : :...:: :.:  : :   . :. :.  .. ::.: :..
EL222  VLVEILNYKKDGTPFRNAVLVAPIYDDDDELLYFLGSQVE
              110       120       130       140
```

Figure 3-1 Sequence comparison of LOV-domains between EL222 and phot1-LOV2. The sequences show 42.0% identity in 100 residues overlap

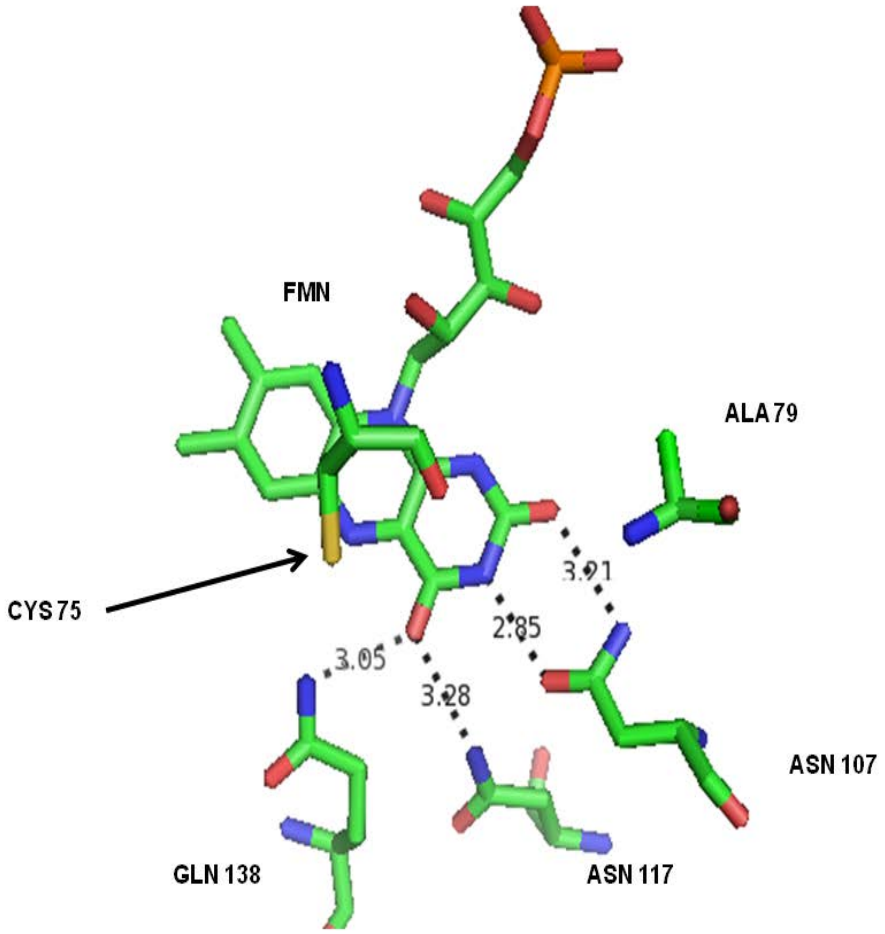

Figure 3-2 Hydrogen bonding network of EL222 in the dark state. The active cysteine is shown to represent its location compare to the hydrogen bonding residues. Alanine 79 is shown to represent its distance to the ribityl chain and N1 of the isoalloxazine ring of FMN.

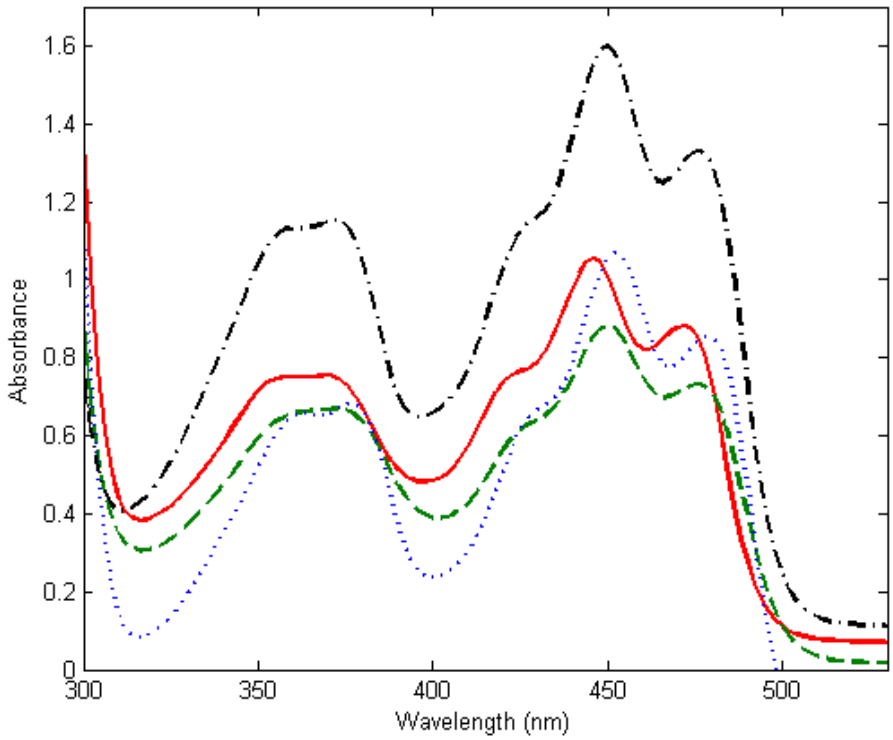

Figure 3-3 Absolute dark spectrum of the wild type EL222 (black -.-.-.), EL222A79Q (blue …..), EL222Q138L (red solid line), and EL222Q138N (green - - -). The Q138L and A79Q show shifted maxima around the 450nm.

3.3.1 Early Photocyle

In order to find an apparent rate constant of formation, we chose seven delay points of (.4, 1, 2, 4, 10, 20, 100 μs) for EL222A79Q (fig 3-4). In order to confirm that no other late process happens in the formation of adduct, delay points of 210 ms and 1.04 sec were added to the measurements of the Q138L (fig 3-5).

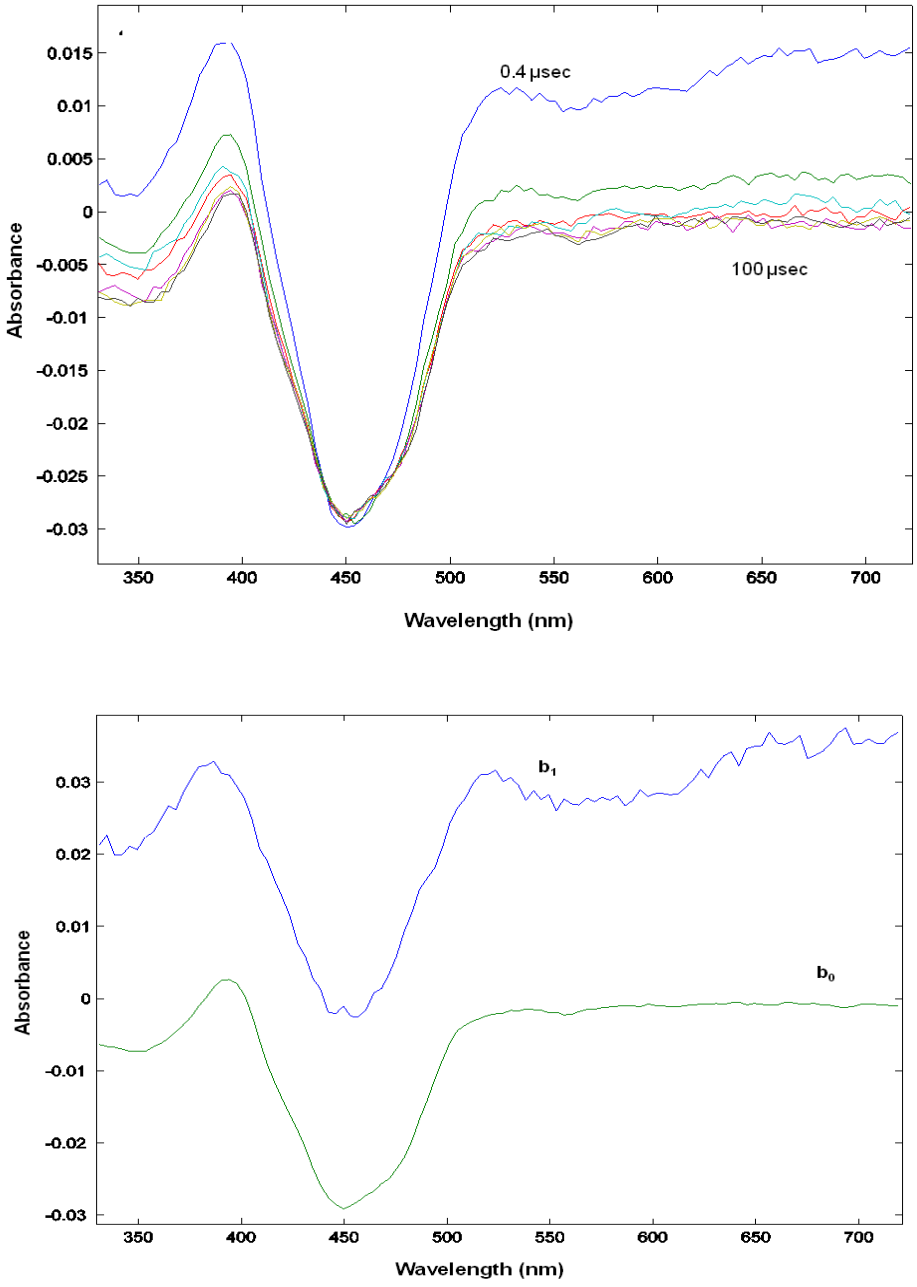

Figure 3-4 The absorption difference spectra of EL222A79Q at room temperature after excitation with a 477 nm laser pulse. Spectra were collected at 0.4, 1, 2, 4, 10, 20, 100 µs. Bottom graph shows the result of the global multi-exponential fitting of difference absorption spectra from the A79Q mutant. The b_1 is b-spectrum with an apparent rate constant of 480 ns and b_0 is the spectrum of the product formed.

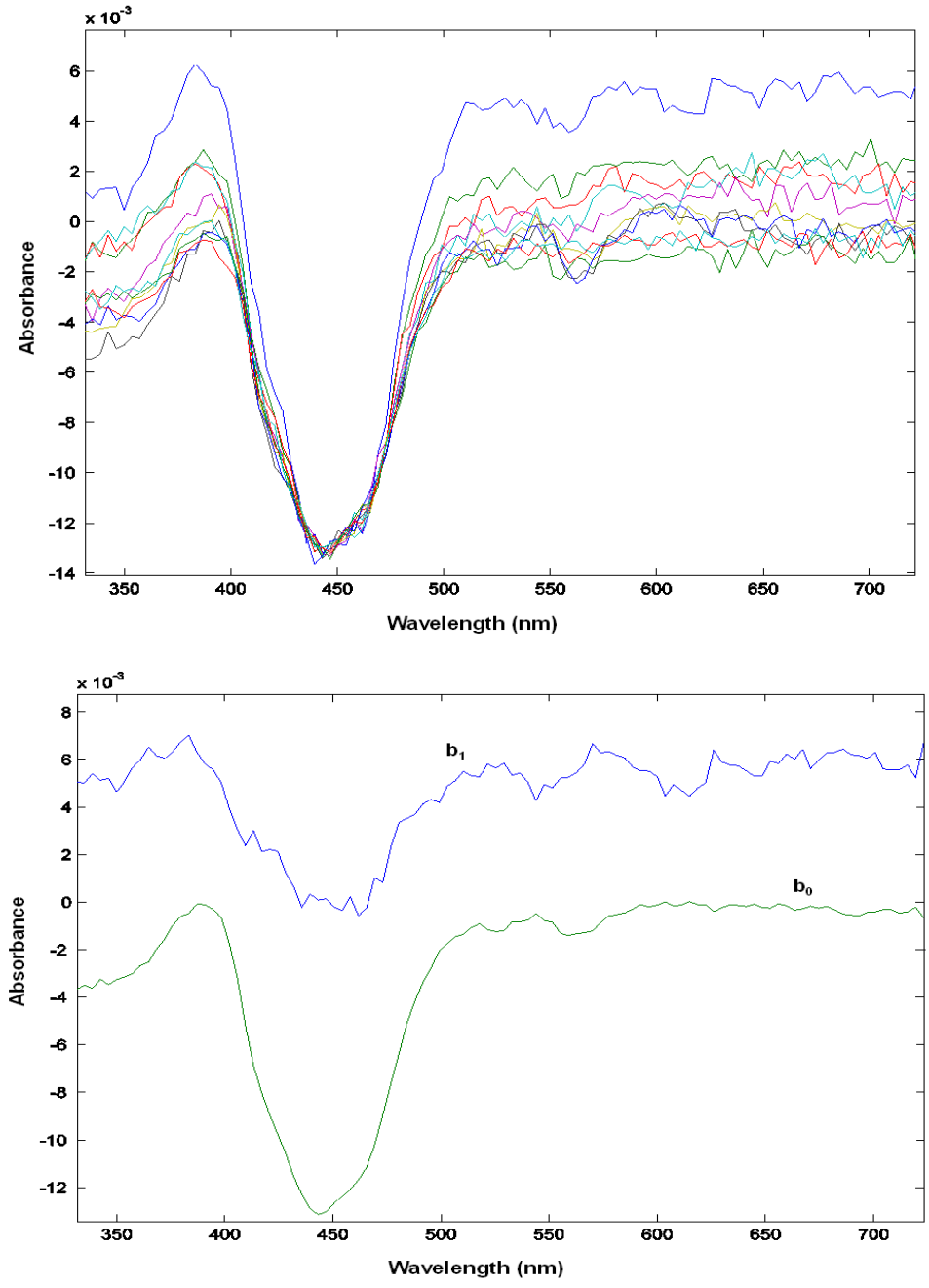

Figure 3-5 The absorption difference spectra of EL222Q138L at room temperature after excitation with a 477 nm laser pulse. Spectra were collected at 0.4, 1, 2, 4, 10, 20, 100 µs and 1, 10, 90, 210 ms, and 1.04 sec time points were added to follow any late events. Bottom graph shows the result of the global multi-exponential fitting of difference absorption spectra from the Q138L mutant. The b_1 is b-spectrum with an apparent rate constant of 2.3 µs and b_0 is the spectrum of the product formed.

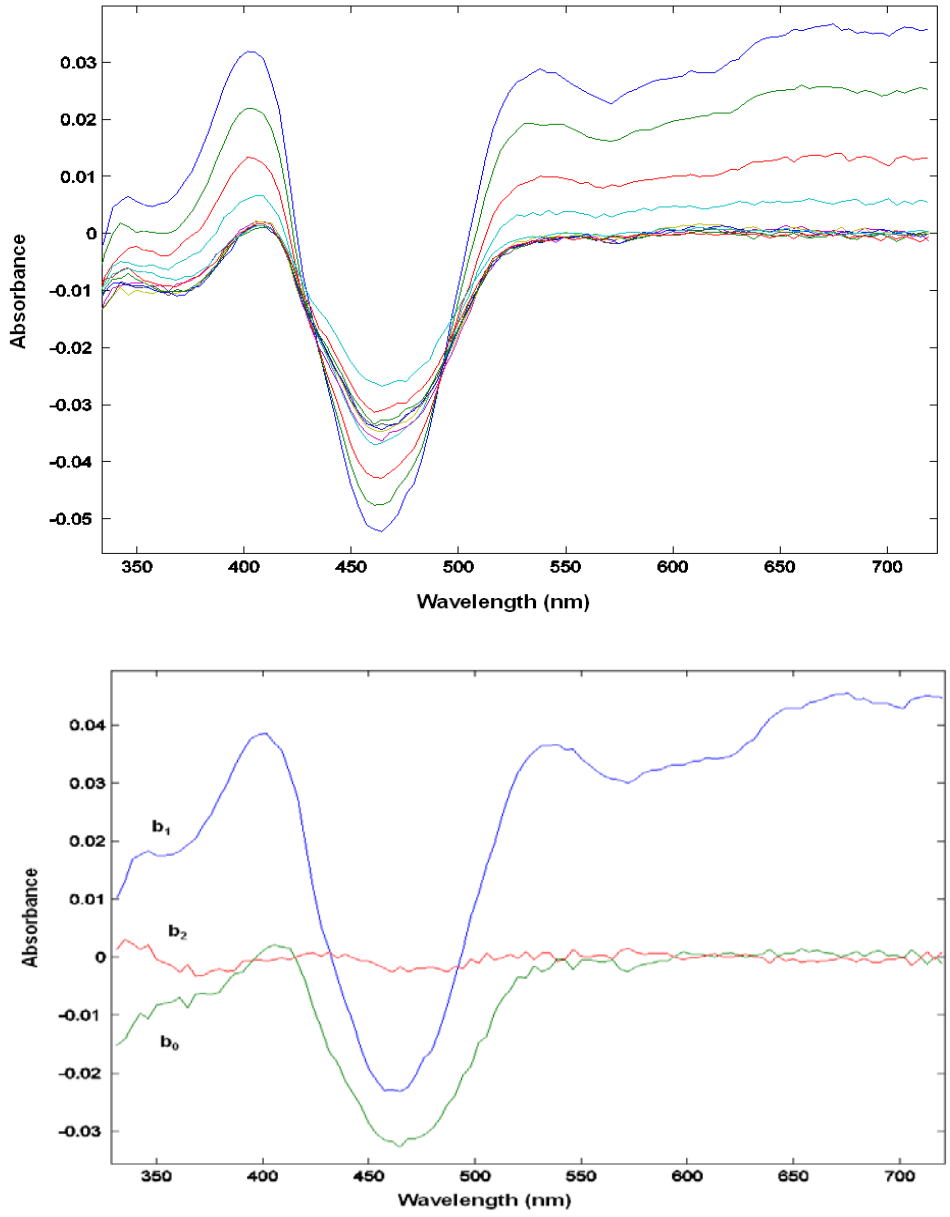

Figure 3-6 The absorption difference spectra of EL222Q138N at room temperature after excitation with a 477 nm laser pulse. Spectra were collected at 0.4, 1, 2, 4, 10, 20, 100 µs and 1, 10, 90, 210 ms, 1.04, 2.84, 5.54 sec time points were added to follow spontaneous decay of adduct to ground state. Bottom graph shows the result of the global multi-exponential fitting of difference absorption spectra from the Q138N mutant. The b_1 is b-spectrum with an apparent rate constant of 1.75 µs and b_0 is the spectrum of the product formed (adduct) and b_2 is the time independent spectra which is zero since this is a cyclic process. The return has a time constant of 3.5 seconds.

During the experiments, it was determined that EL222Q138N has a very fast back reaction that can be resolved by nanosecond flash laser spectroscopy so time delay points of 2.84 and 5.54 sec were added to the Q138N measurements to follow the decay of adduct back to the ground state (fig 3-6). All these mutants displayed apparent rate constants that were very different from EL222 wild type. The A79Q showed faster apparent rate constant at 480 ns including a change in the branching ratio of the formation with 60% going to the signaling state $EL222^{S}_{390}$ and 40% going back to $EL222^{D}_{450}$. This is a complete switch from the wild type that showed 40% going to $EL222^{S}_{390}$ and 60% back to $EL222^{D}_{450}$ from the triplet state ($EL222^{L}_{660}$). The change of alanine to glutamine (that is highly conserved in the other LOV-domains in the NCRFLQ motif), has made the formation faster and more efficient (fig 3-4). The Q138N and Q138L mutants show apparent rate constants that are slower than the wild type EL222. The Q138N mutant has apparent time constant of 1.75 μs, 2 times slower than wild type, while Q138L shows an apparent rate constant of 2.3 μs which is three times slower than wild type. More significantly, Q138L shows a large change in branching ratio compared to the wild type. In this mutant 65% of triplet state goes to $EL222^{S}_{390}$ state while 35% goes back to the ground state which makes it more efficient between all the mutants. The Q138N mutant shows 30% of triplet state, $EL222^{L}_{660}$, going to the $EL222^{S}_{390}$ state which is 70% going back to $EL222^{D}_{450}$ state which is similar to the wild type EL222. The branching ratios help us calculate the time constant for the adduct formation (τ_f) and the time constant for the return to

ground state (τ_R) from the apparent time constant (τ_{app}) using the equation 2.4. These values are reported in table 3-1 with wild type for comparison.

Temp. 20℃ in H_2O	τ_{app} (μs)	τ_R (μs)	τ_F (μs)
EL222 wild type	0.780	1.30	1.95
Q138L mutant	2.30	6.57	3.54
Q138N mutant	1.75	2.50	5.83
A79Q mutant	0.480	1.20	0.800

Table 3-1 The apparent time constant, adduct formation, and return of the triplet state to the ground state time constants of the wild type and mutants at room temperature (20℃) are calculated using the single exponential fitting and branching ratio.

Temp. 20℃ in D_2O	τ_{app} (μs)	τ_R (μs)	τ_F (μs)
EL222 wild type	5.50	7.86	18.34
Q138L mutant	2.90	4.83	7.25
Q138N mutant	8.90	14.83	22.25

Table 3-2 The apparent time constant, adduct formation, and return of the triplet state to the ground state time constants of the wild type and mutants in D_2O at room temperature (20℃) are calculated using the single exponential fitting and branching ratio.

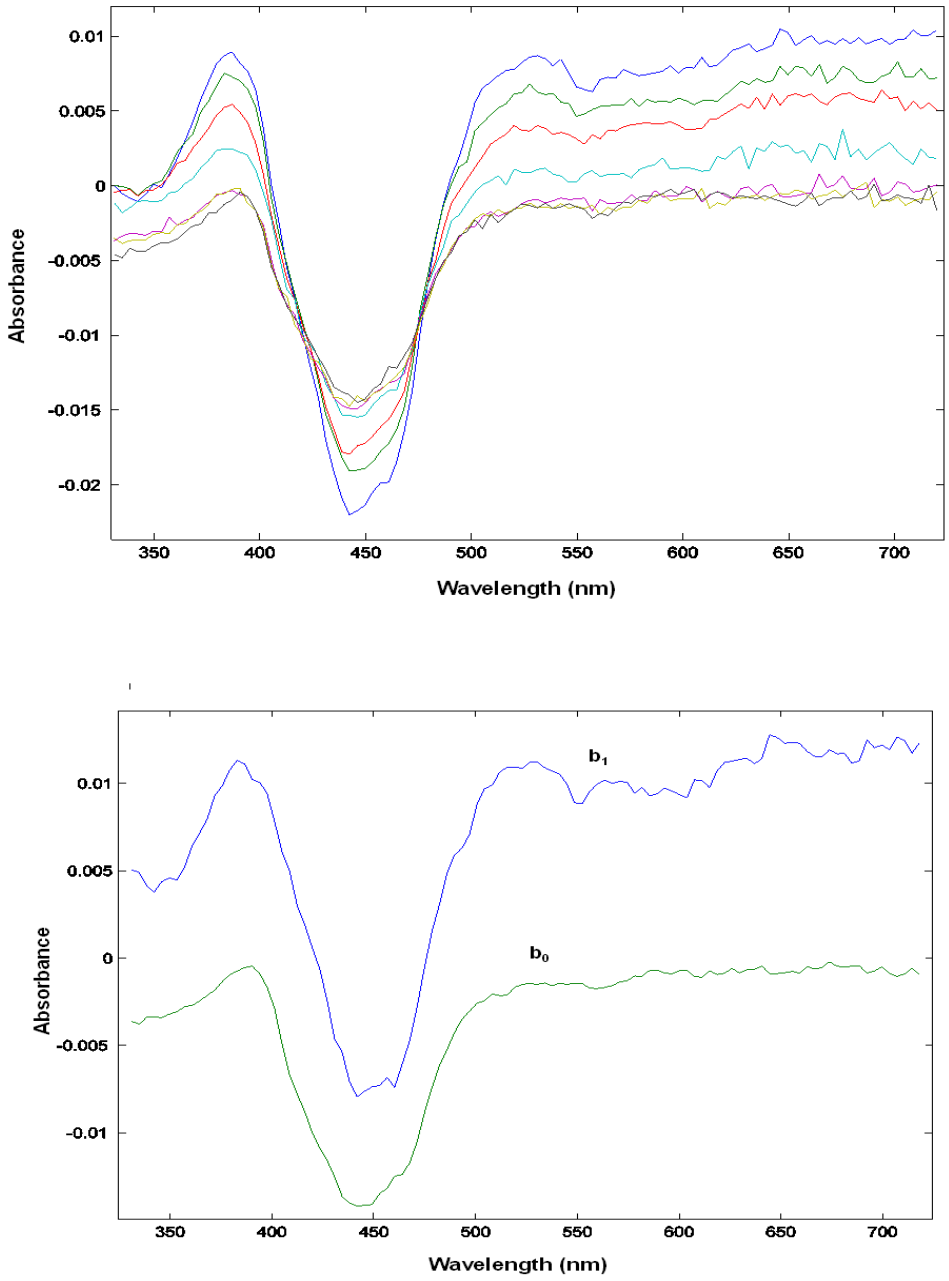

Figure 3-7 The absorption difference spectra of the Q138L mutant in D_2O at room temperature after excitation with a 477 nm laser pulse. Spectra were collected at 0.4, 1, 2, 4, 10, 20, 100 µs. Bottom graph shows the result of the global multi-exponential fitting of difference absorption spectra from the Q138L mutant. The b_1 is b-spectrum with an apparent rate constant of 2.90 µs and b_0 is the spectrum of the product formed.

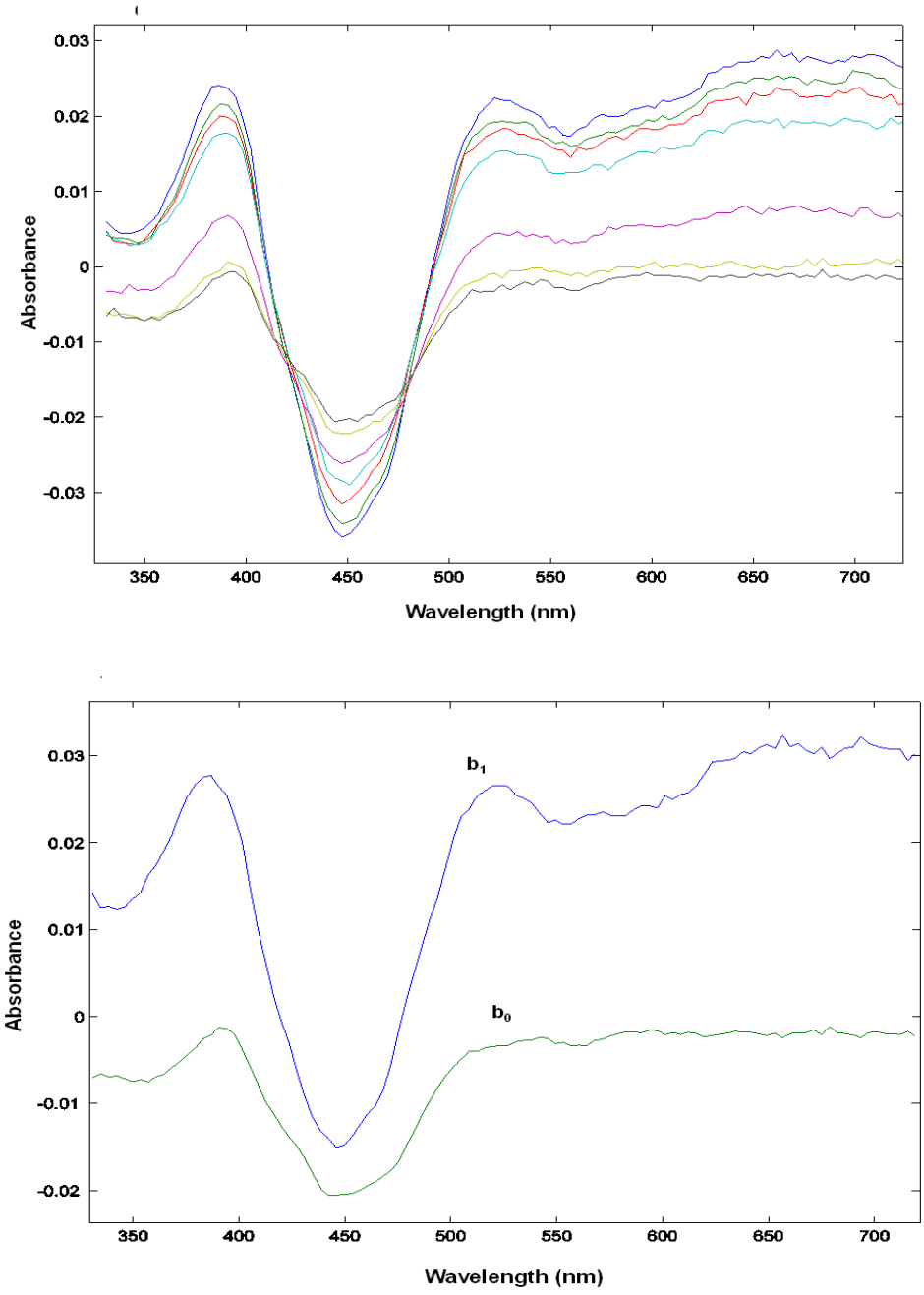

Figure 3-8 The absorption difference spectra of the Q138N mutant in D_2O at room temperature after excitation with a 477 nm laser pulse. Spectra were collected at 0.4, 1, 2, 4, 10, 20, 100 µs. Bottom graph shows the result of the global multi-exponential fitting of difference absorption spectra from the Q138N mutant. The b_1 is b-spectrum with an apparent rate constant of 8.90 µs and b_0 is the spectrum of the product formed.

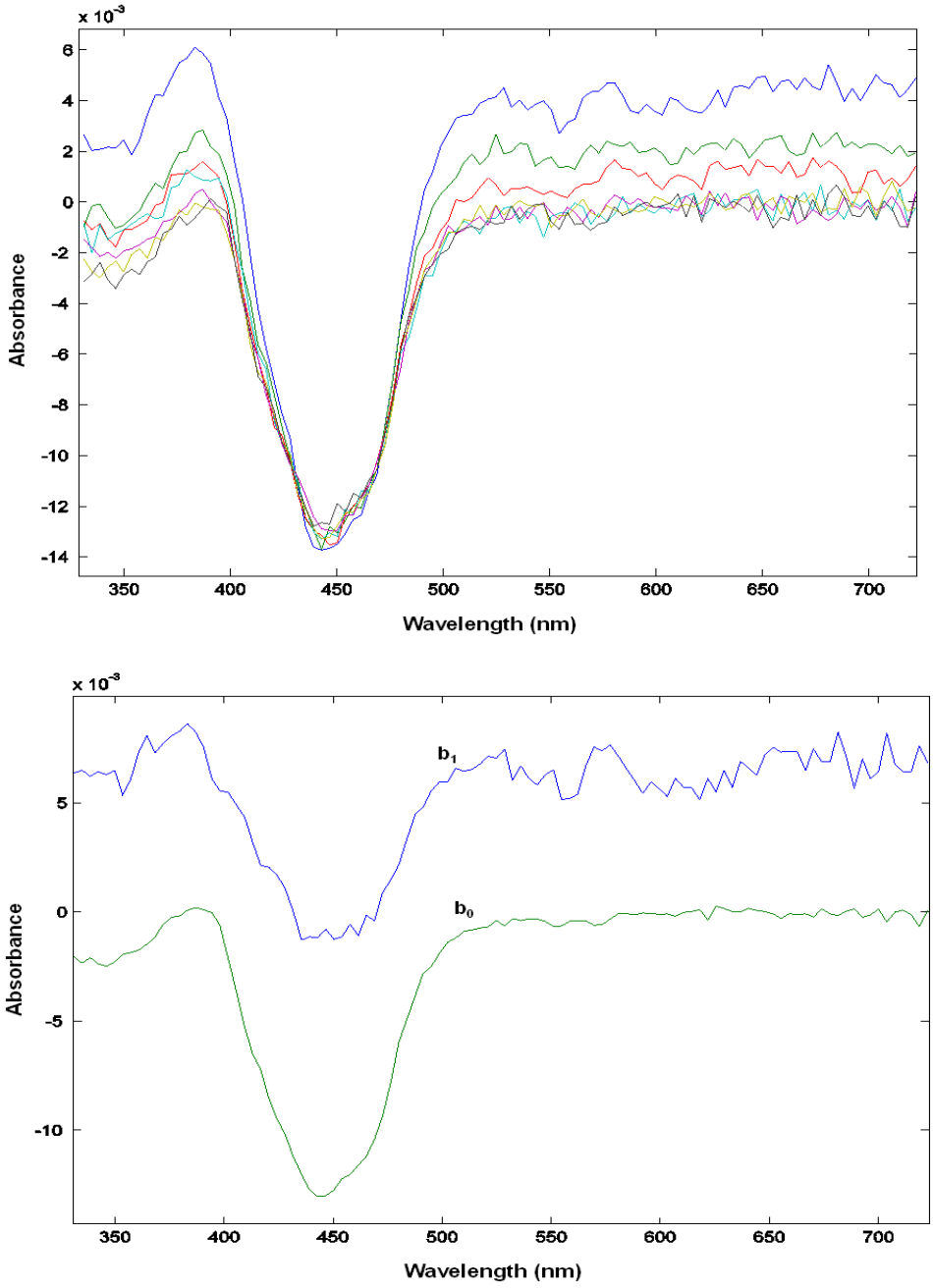

Figure 3-9 The absorption difference spectra of the Q138L mutant at 15℃ after excitation with a 477 nm laser pulse. Spectra were collected at 0.4, 1, 2, 4, 10, 20, 100 µs. Bottom graph shows the result of the global multi-exponential fitting of difference absorption spectra from the Q138L mutant. The b_1 is b-spectrum with an apparent rate constant of 1.0 µs and b_0 is the spectrum of the product formed.

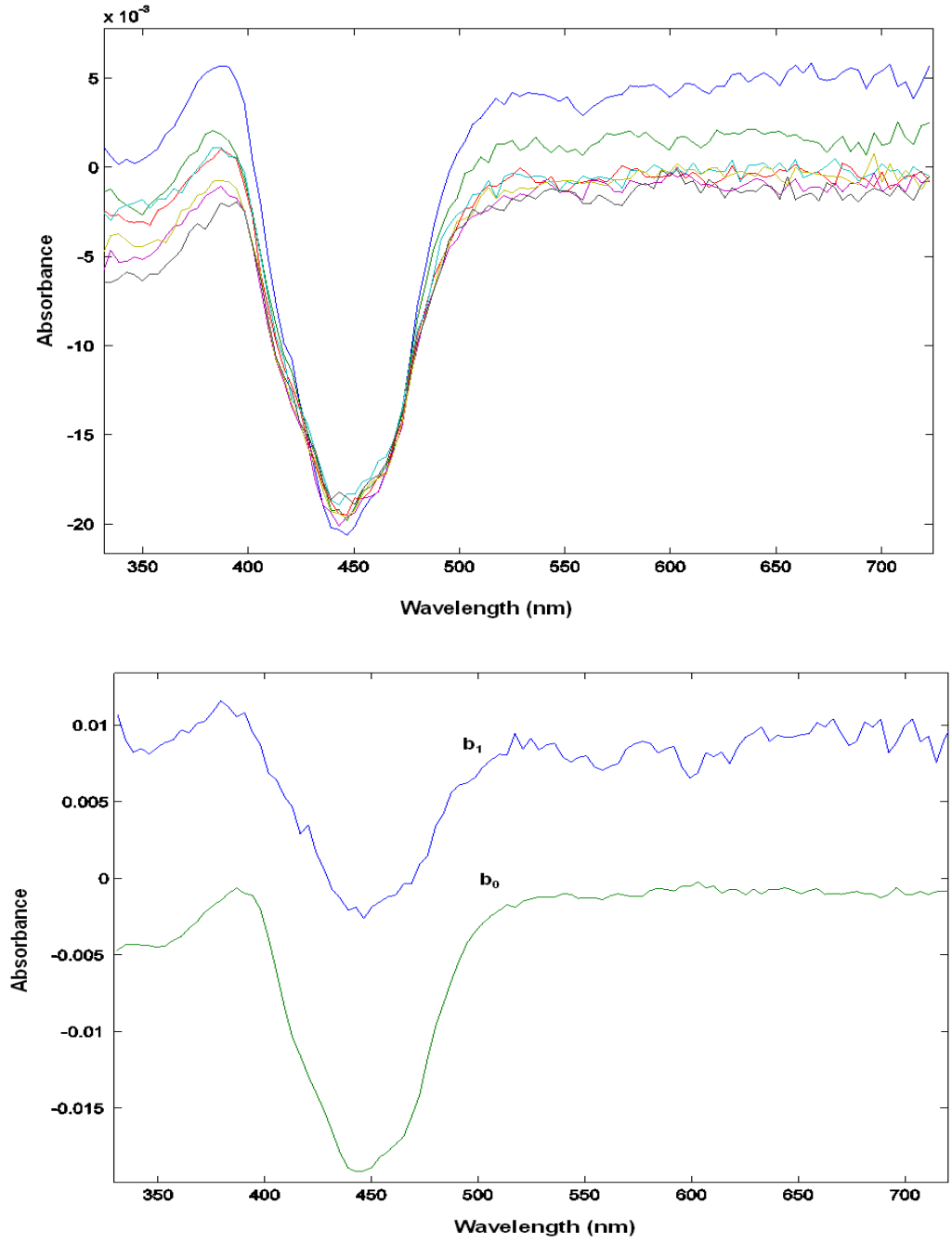

Figure 3-10 The absorption difference spectra of the Q138L mutant at 35℃ after excitation with a 477 nm laser pulse. Spectra were collected at 0.4, 1, 2, 4, 10, 20, 100 µs. Bottom graph shows the result of the global multi-exponential fitting of difference absorption spectra from the Q138L mutant. The b_1 is b-spectrum with an apparent rate constant of 800 ns and b_0 is the spectrum of the product formed.

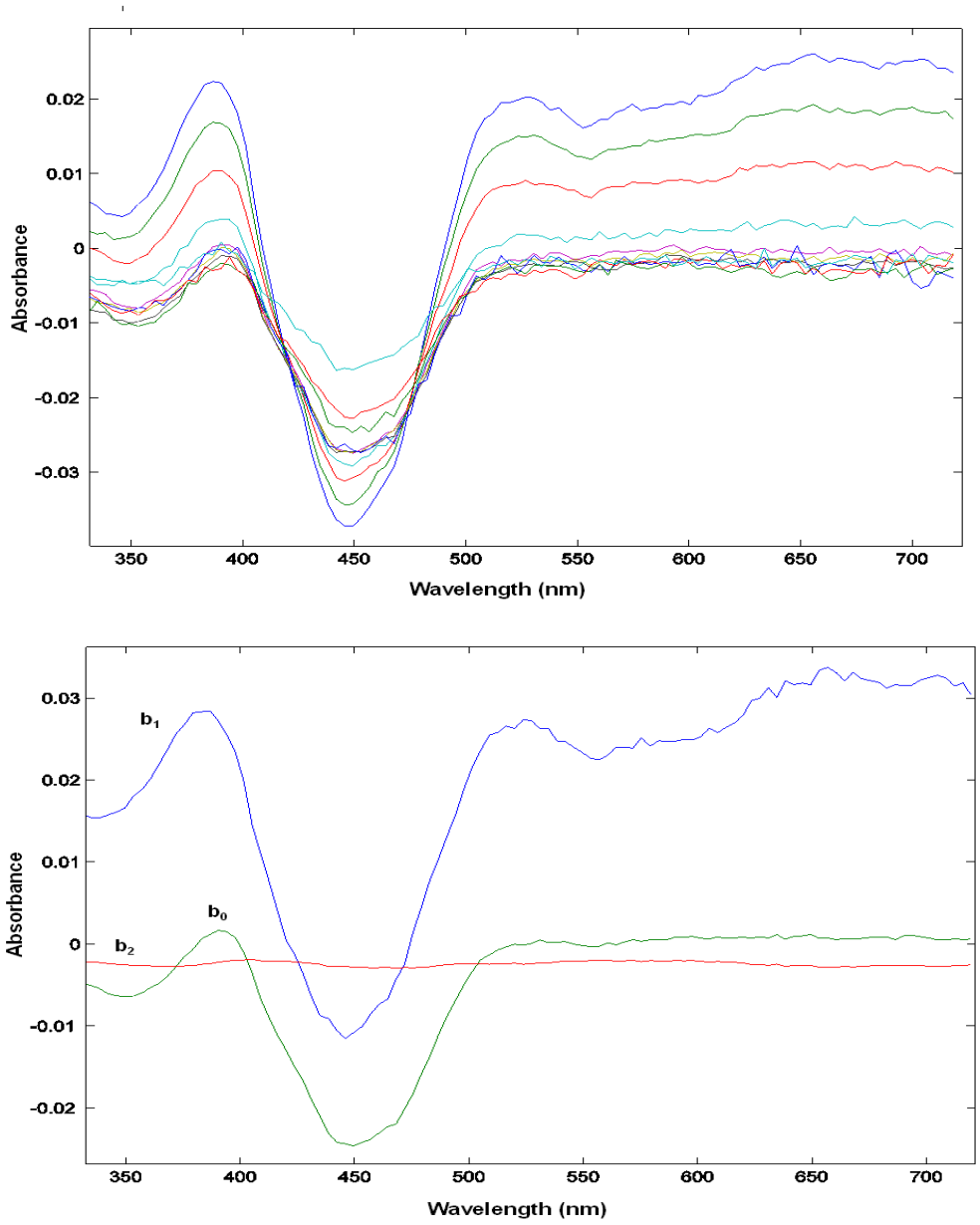

Figure 3-11 The absorption difference spectra of the Q138N mutant at 15°C after excitation with a 477 nm laser pulse. Spectra were collected at 0.4, 1, 2, 4, 10, 20, 100 µs and 1, 10, 90, 210 ms, 1.04, 2.84, 5.54 sec time points were added to follow spontaneous decay of adduct to ground state. Bottom graph shows the result of the global multi-exponential fitting of difference absorption spectra from the Q138N mutant. The b_1 is b-spectrum with an apparent rate constant of 2.20 µs and b_0 is the spectrum of the product formed (adduct) and b_2 is the time independent spectra which is zero since this is a cyclic process. The return has a time constant of 9.5 seconds.

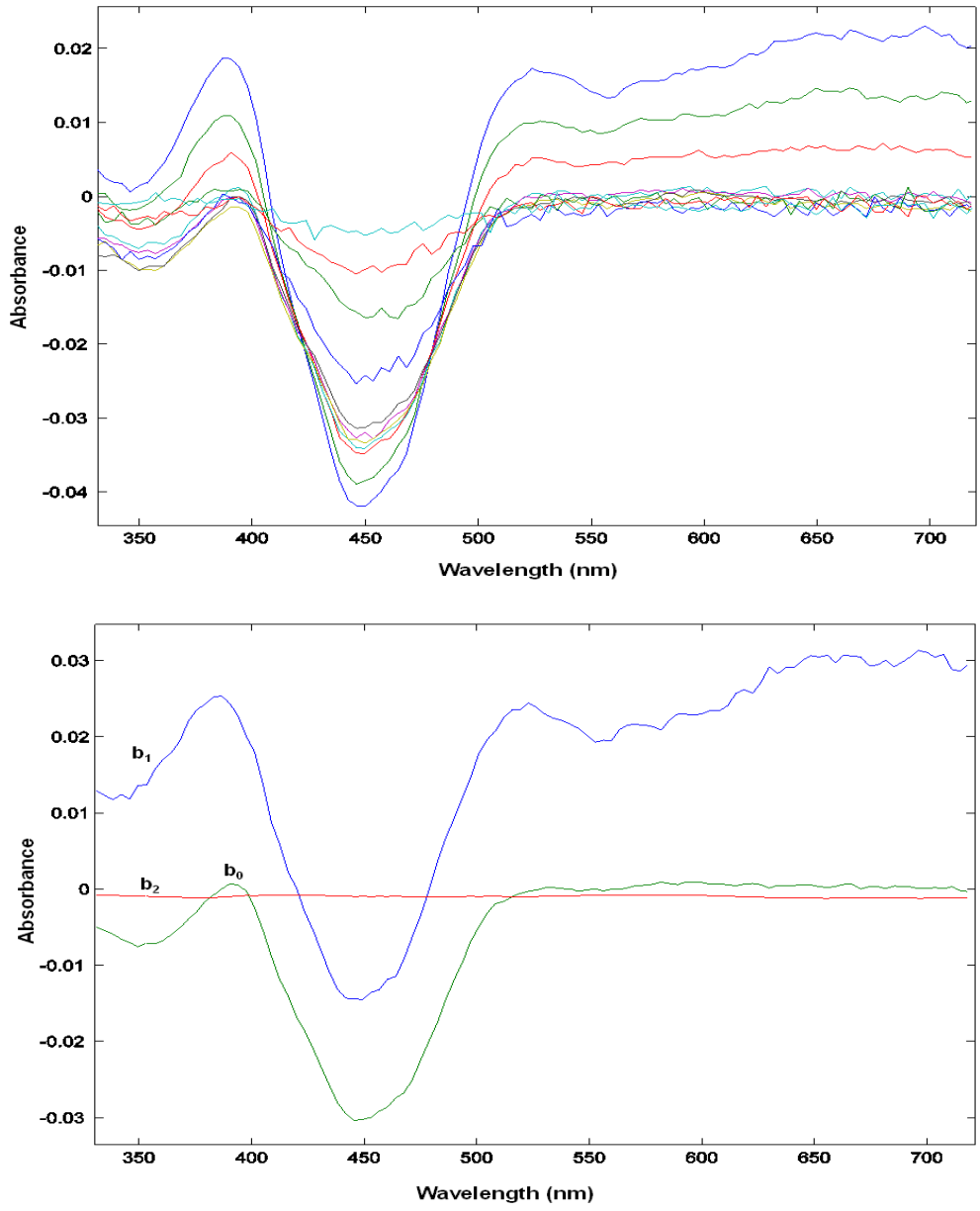

Figure 3-12 The absorption difference spectra of the Q138N mutant at 35℃ after excitation with a 477 nm laser pulse. Spectra were collected at 0.4, 1, 2, 4, 10, 20, 100 µs and 1, 10, 90, 210 ms, 1.04, 2.84, 5.54 sec time points were added to follow spontaneous decay of adduct to ground state. Bottom graph shows the result of the global multi-exponential fitting of difference absorption spectra from the Q138N mutant. The b_1 is b-spectrum with an apparent rate constant of 1.30 µs and b_0 is the spectrum of the product formed (adduct) and b_2 is the time independent spectra which is zero since this is a cyclic process. The return has a time constant of 2.20 seconds.

The wild type EL222 displays a large deuterium effect (more the seven times slower in D_2O) which is an indication of a proton or hydrogen atom transfer or alteration of hydrogen bonds as the rate limiting step in the reaction. We studied the D_2O effect on the Q138N and Q138L mutants with interesting results (table 3-2). The Q138N mutant has an apparent rate constant that is five times slower in D_2O (fig 3-8) which follows the trend of wild type EL222. This is not very surprising since asparagine and glutamine are both capable of making similar hydrogen bonding although asparagine is shorter than glutamine (by one C-C bond which is 1.5 A°). The Q138L mutant does not show much D_2O effect when we compare the apparent time constants which is 2.9 μs in D_2O versus 2.3 μs in H_2O. The closer look at the spectra reveals that D_2O causes the branching ratio to change in the Q138L mutant. This is not seen in wild type EL222 or the other mutant which causes the forward time constant (τ_f) to become 7.25 μs, more than two times slower than the Q138L in H_2O. The Q138L therefore shows a slight D_2O effect, much less than the rest.

In order to compare the energetics of the adduct formation reaction of the wild type with the mutant; the temperature effect on the formation was studied at two additional temperatures of 15℃, and 35℃. As expected, as the temperature increases, the adduct formation reaction becomes faster (table 3-3 and 3-4). The Q138L sample (fig 3-9 and 3-10) is not as stable as the wild type or the other two mutants so several samples are used in two different experimental sessions (different days) to complete the experiment, so the time constant at 20℃ does not agree with the trend. In order to overcome this problem, we have calculated and report here a range for the activation

energy value of formation for the Q138L based on adjusted time constant and experimental rate constant. According to equation 2.6, the slope of the plot (ln k) vs. (1/T) of the data will give (-Ea/R) value. The energy of activation for the $EL222^{S}_{390}$ species formation for wild type EL222 is 5.2 kcal/mole while for the Q138N mutant it is 4.57 kcal/mole and 1.96-4.36 kcal/mole for the Q138L mutant. This result indicates that the hydrogen bonding rearrangements, which needs to happen to in order to overcome and generate the transition state, are similar between the wild type and the mutants. The hydrogen bond energy usually range from 1 kcal/mole to 5 kcal/mole, which means that in both mutants, and especially in the Q138L, the activation energy values might result from the hydrogen bonding changes that we have introduced in the structure.

During the Q138N measurements, we discovered that the Q138N is a fast cycler. This is a term used in our lab for LOV-domains that show a very fast adduct decay to the dark state [18]. The longer time delay points were then added to the measurement to time resolve the back reaction. The b-spectra (fig 3-6) that resulted from the global exponential analysis [9, 19-20] show spectra that represent the difference between the spectra of the starting delay time and final delay time and they each have time constant that represents adduct formation and adduct decay to ground state. In this case the b-spectrum which represents the spectrum of the final intermediate minus the initial state is zero since it returns to the ground state within the delay time of the measurement (cyclic process).

15℃ in H_2O	τ_{app} (μs)	τ_R (μs)	τ_f (μs)
EL222 wild type	0.970	1.62	2.40
Q138L mutant	1.00	2.86	1.54
Q138N mutant	2.20	3.14	7.33

Table 3-3 The apparent time constant, adduct formation, and return of the triplet state to the ground state time constants of the wild type and mutants at 15℃ are calculated using the single exponential fitting and branching ratio.

35℃ in H_2O	τ_{app} (μs)	τ_R (μs)	τ_f (μs)
EL222 wild type	0.535	0.890	1.34
Q138L mutant	0.800	2.29	1.23
Q138N mutant	1.30	1.86	4.33

Table 3-4 The apparent time constant, adduct formation, and return of the triplet state to the ground state time constants of the wild type and mutants at 35℃ are calculated using the single exponential fitting and branching ratio.

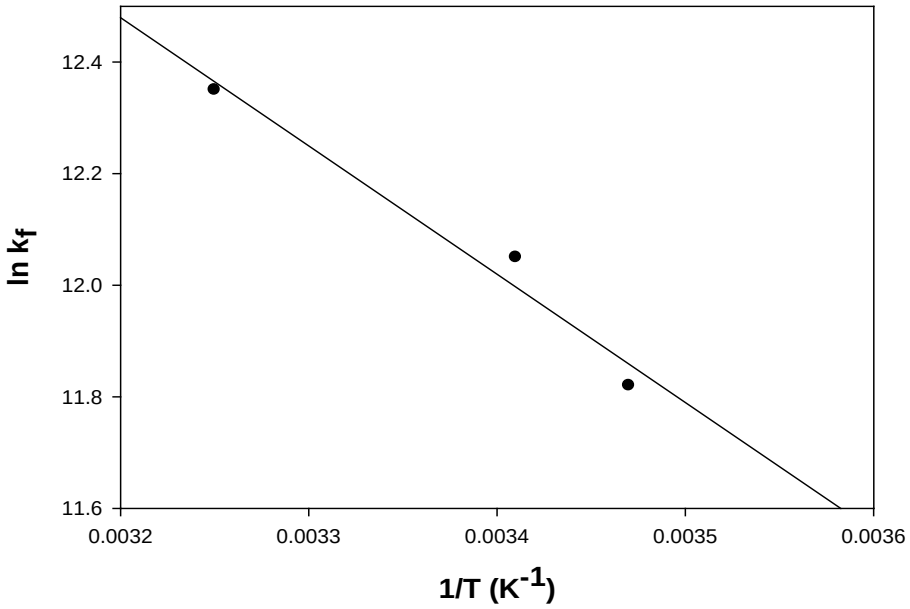

Figure 3-13 Arrhenius plot for the adduct formation kinetics of the EL222 Q138N

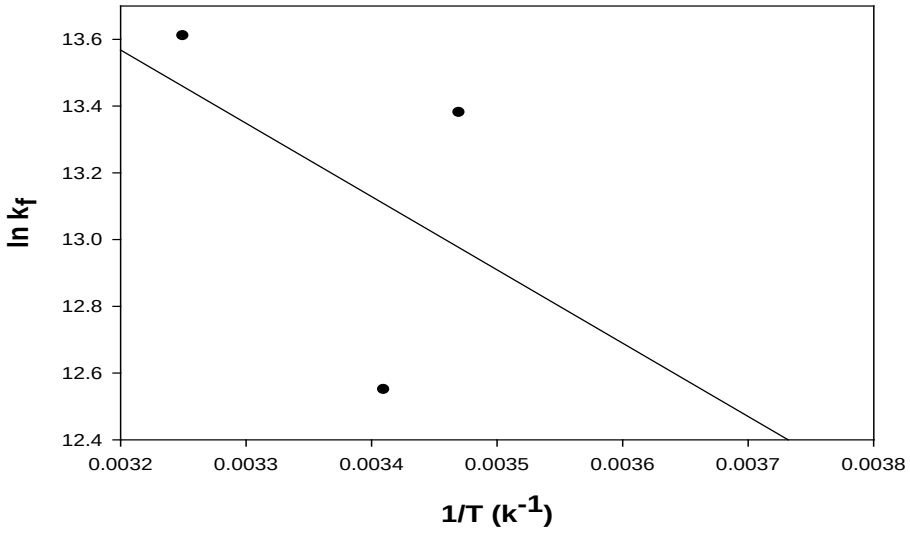

Figure 3-14 Arrhenius plot for the adduct formation kinetics of the EL222 Q138L

3.3.2 Late Photocycle

As mentioned above, the back reaction of the Q138N mutant was measured using laser flash spectroscopy apparatus with longer delay times (fig 3-6). The analysis of data revealed only one apparent time constant of 3.5 sec for back reaction at room temperature. Since we performed the temperature control experiment to find the activation energy of the formation for this mutant, we also collected data for the back reaction at various temperatures. It is therefore possible to calculate the activation energy for the back reaction of the Q138N mutant (fig 3-15). We report 49 kJ/mole (12 kcal/mol), as the value of activation energy for the back reaction of Q138N. This value is comparable to the activation energy of LOV2 back reaction, which was reported as 55 KJ/mole [21]. The difference in the value is within one or more hydrogen bonding difference which is expected since we have slightly perturbed the hydrogen bonding through this mutation. The back reaction of the Q138N was also studied using the Hewlett Packard 8452A diode array spectrometer (fig 3-16). The spectra were taken every second for 30 seconds and gave a time constant of 1.54 seconds for the back reaction. Due to the limitation of the spectrometer for fast cycling mutants (delays between switching off the light and the start of the scan), values for the time constant that were determined during the early photocycle studies from nanosecond to seconds, are more accurate results for fast cycling mutant. Although it should be noted that the temperature difference can also be partially responsible for the difference between measured values, since reaction rates are temperature dependent. The deuterium effect on the back reaction of the

Q138N mutant was also studied (fig 3-17). The Q138N mutant shows a time constant of 9.77 sec for back reaction which is almost three times slower than the wild type. The deuterium effect is bigger for the wild type in both the formation and back reaction.

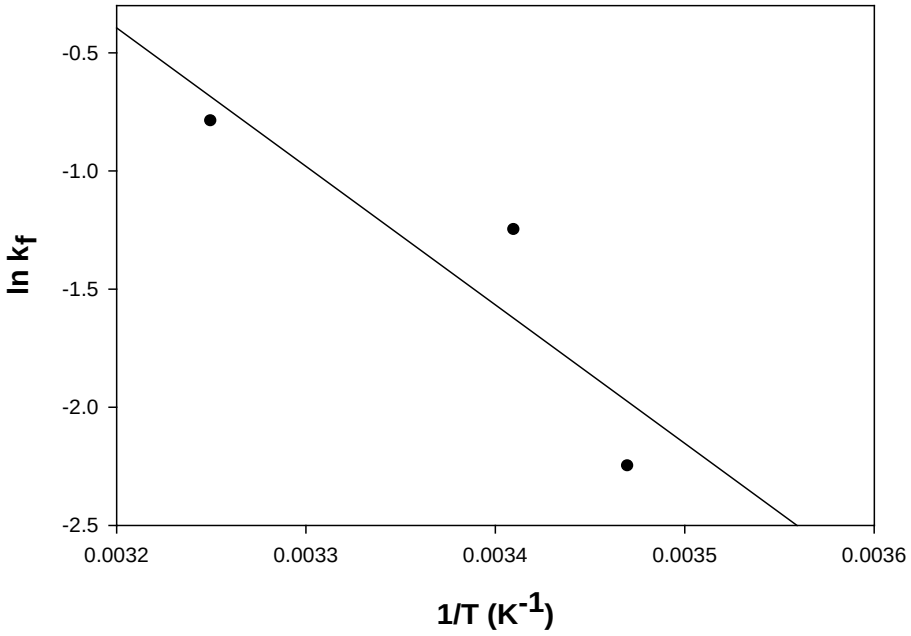

Figure 3-15 Arrhenius plot for the back reaction kinetics of the EL222 Q138N

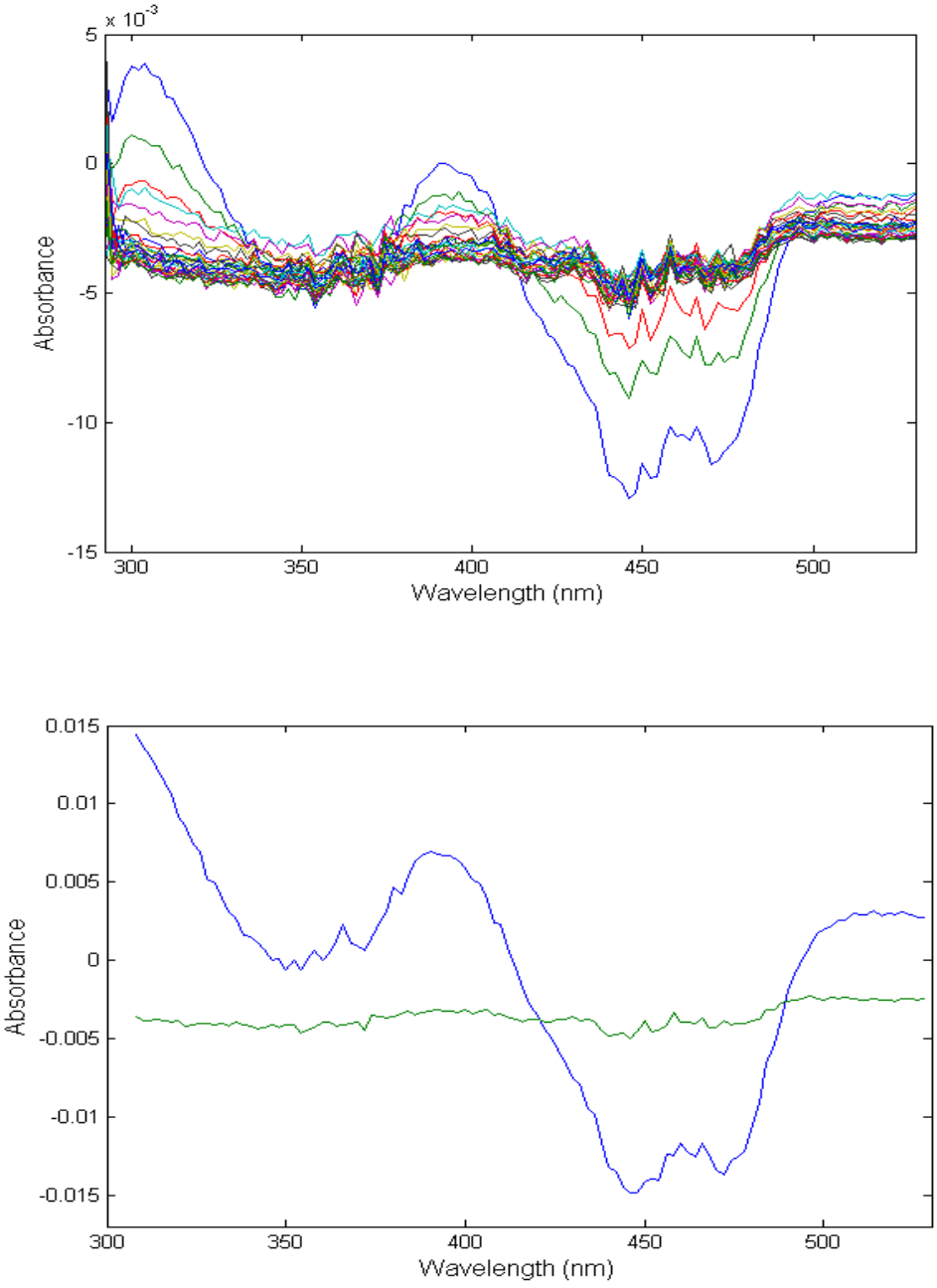

Figure 3-16 Time-resolved, light induced absorption changes for the Q138N mutant at room temperature. Sample was illuminated for 60 seconds and spectra were taken every second for 30 seconds. Bottom figure shows the b-spectra from single-exponential fitting with time constant of 1.54 sec. associated with b_1 (blue) and b_0 is the time independent spectra which is zero because it is a cyclic process.

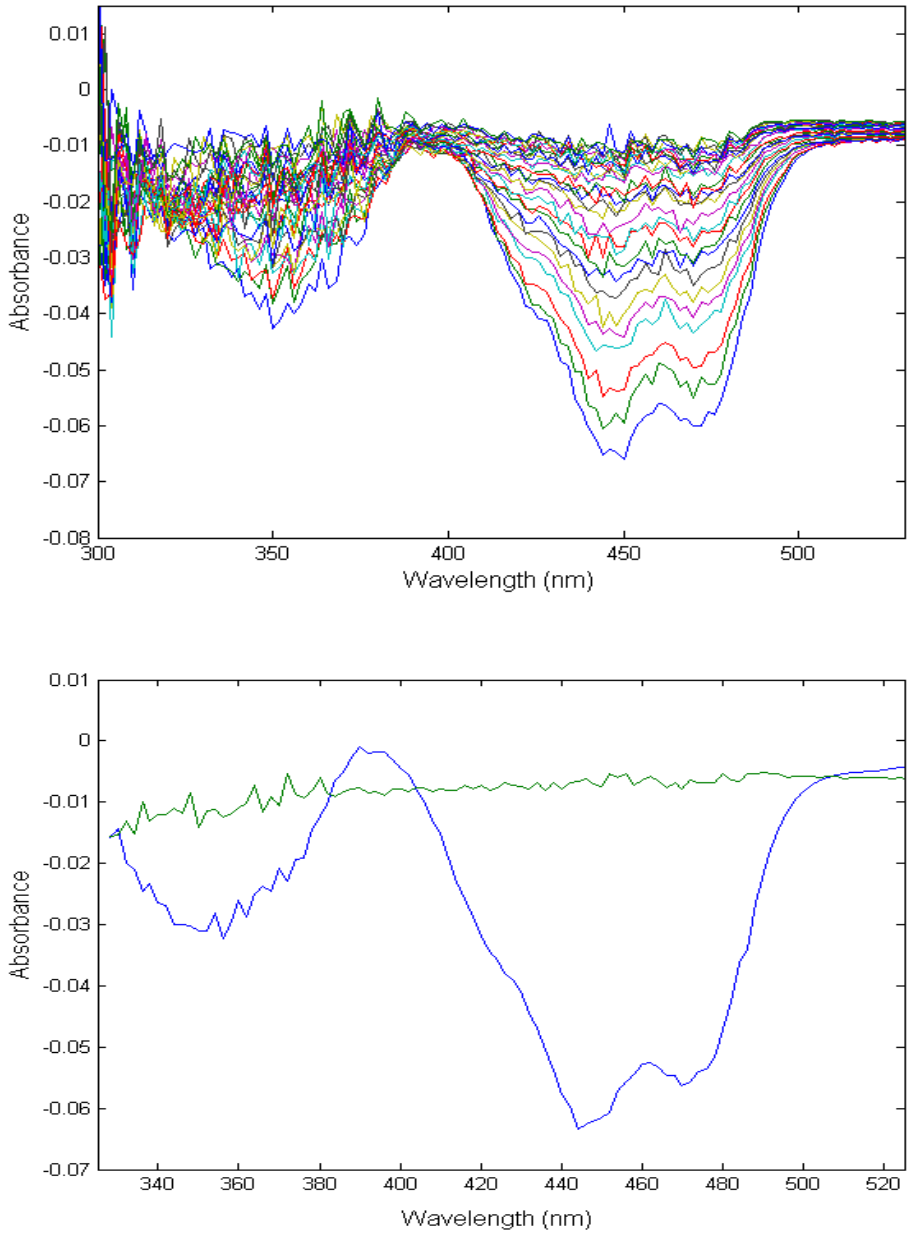

Figure 3-17 Time-resolved, light induced absorption changes for the Q138N mutant in D_2O at room temperature. Sample was illuminated for 60 seconds and spectra were taken every second for 30 seconds. Bottom figure shows the b-spectra from single-exponential fitting with time constant of 9.77 sec. associated with b_1 (blue) and b_0 is the time independent spectra which is zero because it is a cyclic process.

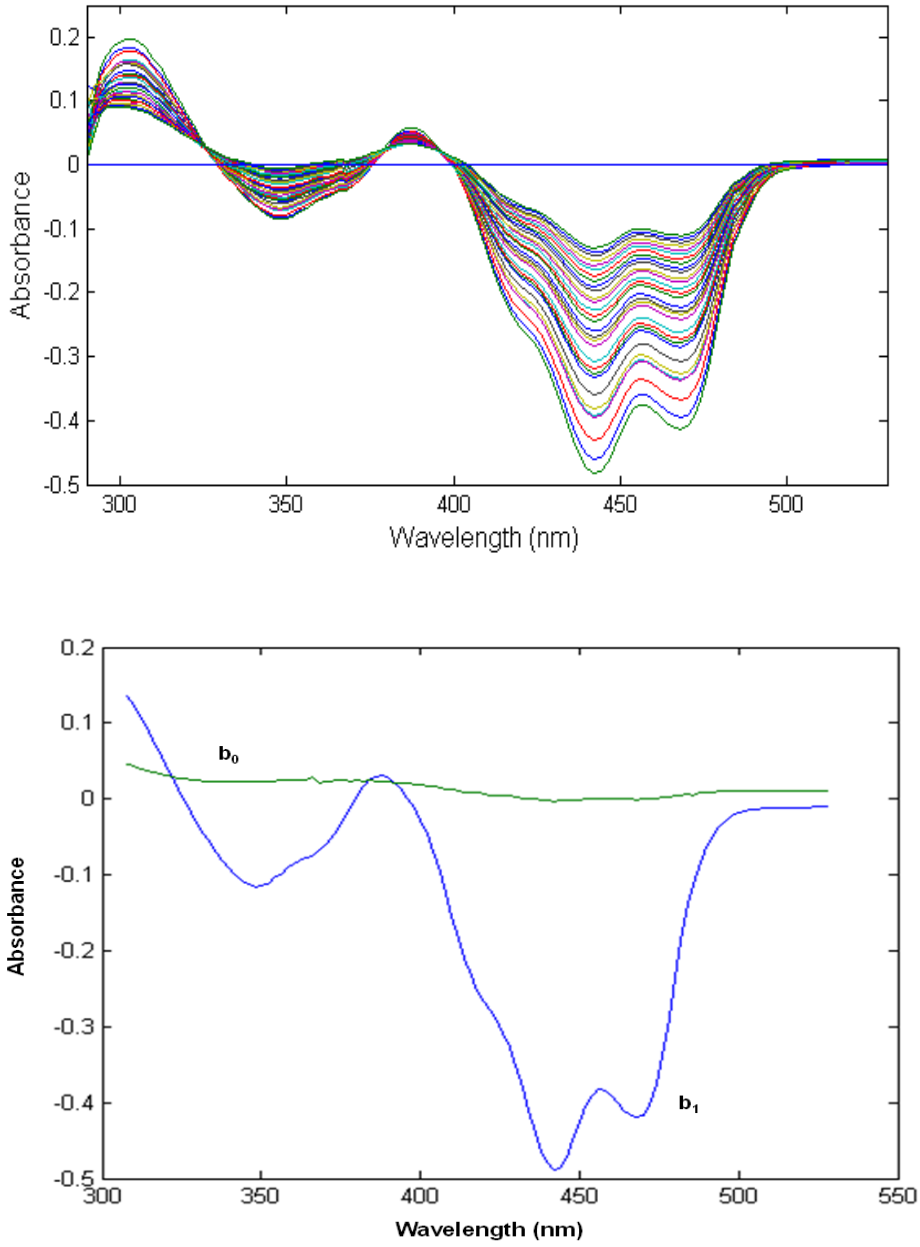

Figure 3-18 Time-resolved, light induced absorption changes for the Q138L mutant at room temperature. Sample was illuminated for 60 seconds and spectra were taken every 2 minutes for 60 minutes. Bottom figure shows the b-spectra from single-exponential fitting with time constant of 45.5 min. associated with b_1 and b_0 is the time independent spectra which is zero because it is a cyclic process.

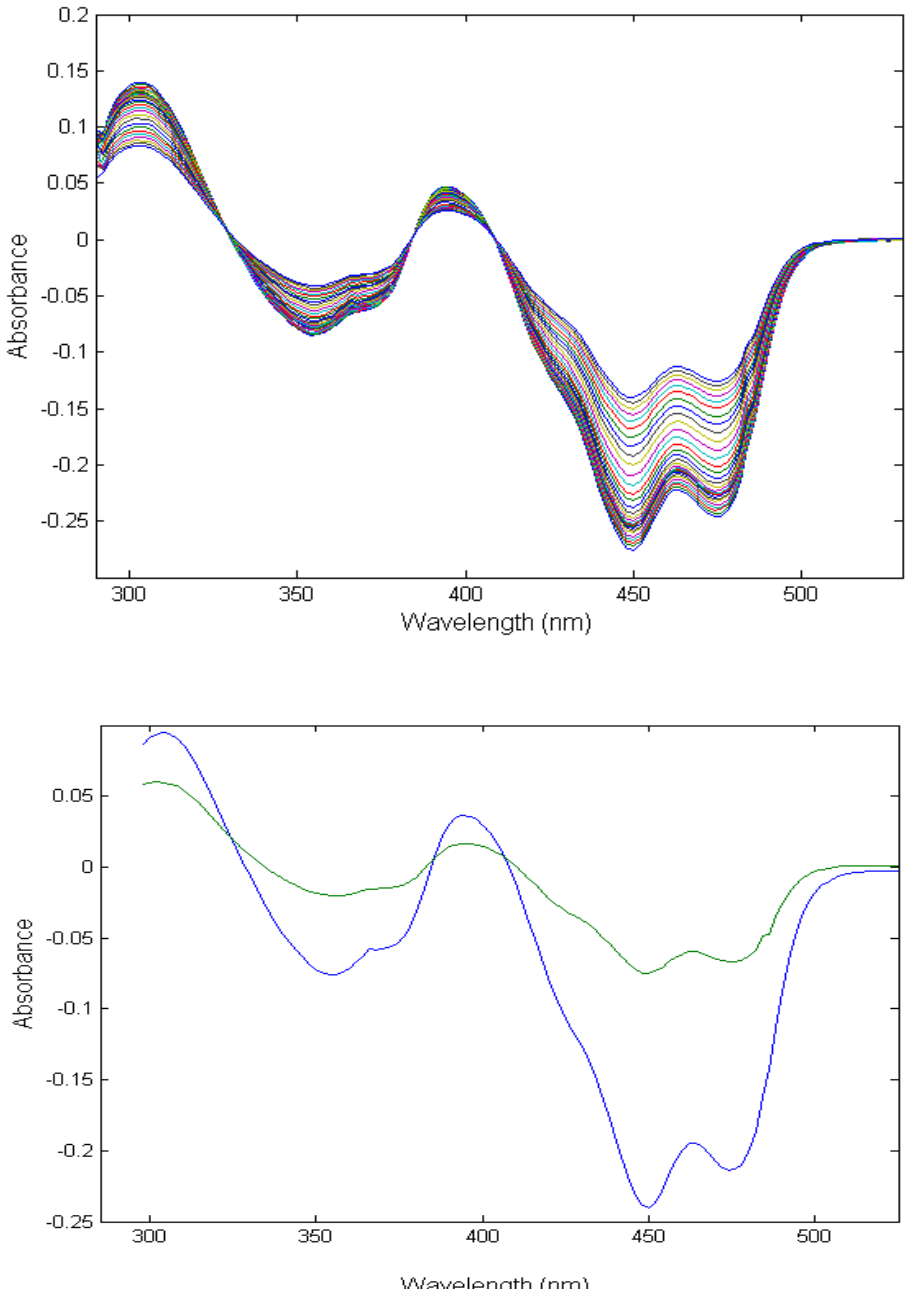

Figure 3-19 Time-resolved, light induced absorption changes for the A79Q mutant at room temperature. Sample was illuminated for 60 seconds and spectra were taken every 2 seconds for 60 seconds. Bottom figure shows the b-spectra from single-exponential fitting with time constant of 60 sec. associated with b_1 (blue) and b_0 (green) is the time independent spectra.

There is a considerable change that is seen in the back reaction of the Q138L mutant (fig 3-18). The adduct decay to the dark side has a time constant of 45.5 minutes which is 170 fold slower than the wild type. These data indicates that the loss of hydrogen bonding with the FMN contribute to a larger change in the back reaction of the Q138L than the Q138N mutant. The deuterium effect experiment for the Q138L could not be performed due to instability of the protein (loss of chromophore) in the long experimental time needed to collect the data (between one to two hours).

The A79Q mutant also showed a slowing of the back reaction. The adduct decay into the dark state slowed down almost 4 fold with a time constant of 60 seconds (fig 3-19). The b_1-spectrum of the A79Q mutant should be zero since this is a cyclic process but it is not since in the times that the spectra are taken (every 2 seconds for 60 seconds), there was not enough for the adduct to completely decay back into the dark state. Structural manipulations using Pymol program show that the glutamine at position 79 (fig 3-20) can hydrogen bond with the C(2)=O of the isoalloxazine ring of the FMN. This position of the FMN is not predicated to be involved directly in the photocycle process but it is involved in the conjugated double bonding on the polar side of the isoalloxazine ring that also involves the N(5). It is also possible that the glutamine at position 79 can hydrogen bond with N(1) or the N(3) of the FMN. This result seems to indicate that any changes made to the electronic environment of the FMN either directly or indirectly, can affect the photocycle of the EL222.

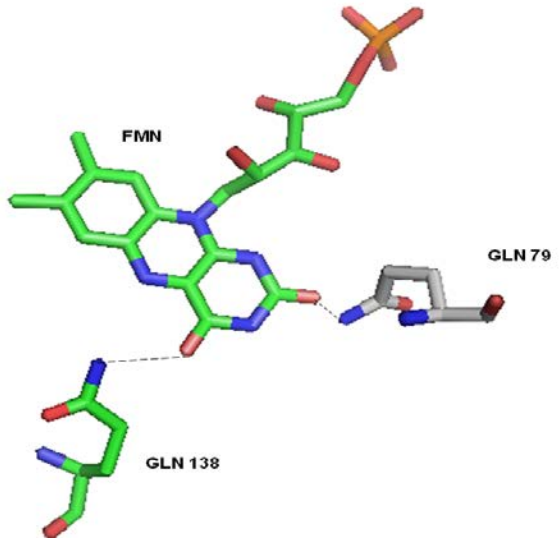

Figure 3-20 The newly introduced hydrogen bonding in the binding pocket of FMN inside EL222. The glutamine at position 79 was originally an alanine. The glutamine at position 138 is shown for clarity.

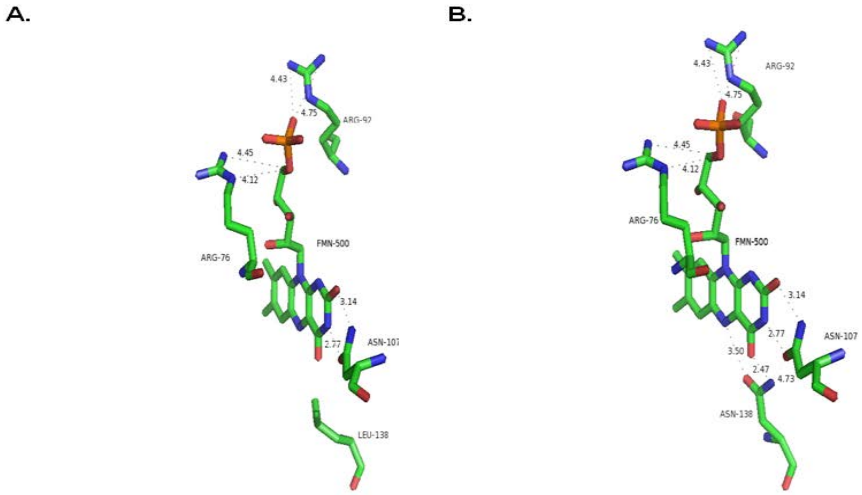

Figure 3-21 The substitution of the glutamine at position 138 with Asparagine and Leucine leads to altered or loss of hydrogen bonding.

3.4 Discussion

In this study, we have presented several mutants that highlight the importance of hydrogen bonding in the photocycle of EL222. Due to the pH effect experimental results in chapter two, we proposed that hydrogen bonding can be a large contributor to the back reaction of EL222. Although several mutational studies on LOV domains [16, 22] have suggested residues around FMN that can change the electron density around the isoalloxazine ring of FMN, can affect the photocycle. There are also studies that show the conserved glutamine 513 in phot1-lov2 [16] and the glutamine 123 in YtvA [23] can affect the recovery reaction kinetics. Additionally, it has been shown in *A.capillus-veneris* neochrome1 LOV2 domain that mutating Q1029 to a leucine [15] can reduce the magnitude of light-induced protein structural changes. In vivo, light induced activity of VIVID fungal photoreceptor shows that mutation of the glutamine residue to leucine attenuated the activity [24]. It is suggested that in LOV2 illumination causes the glutamine that is in hydrogen bonding with the C(4)=O of FMN, to rotate and hydrogen bond with the protonated N(5) atom of FMN [16, 25-26]. Time-resolved FTIR spectroscopy has demonstrated that this rotation is done within a few microseconds, which is in the time scale of the adduct formation [27]. This hydrogen bond switching is also observed in blue light sensing using FAD (BLUF) domains [28] followed by radical-pair recombination.

Most of these studies focus on structural changes that happen through glutamine hydrogen bonding with emphasis on back reaction changes. The aim of

our study is to understand the role of hydrogen bonding in the formation and the back reaction. Both glutamine mutants that disrupt the hydrogen bonding of the glutamine amide and the O(4) carbonyl oxygen of FMN, show slowing of the $EL222^{S}{}_{390}$ adduct formation (in case of the Q138L mutant by 2 fold and the Q138N mutant by 3 fold). The addition of a glutamine to position 79 creates the possibility of the hydrogen bonding to the C(2)=O as well as the N(1), accelerates the adduct formation by more than 2 fold. The N (1), N (3), N (5) side of the isoalloxazine ring of FMN, is the polar side of the molecule. Our results show that changes in the hydrogen bonding at various position of the polar site of the isoalloxazine ring, can lead to changes in photochemistry and even the absolute spectral properties of the molecule.

The deuterium effect experiment also reveals the importance of this hydrogen bonding on the formation of the adduct. The wild type EL222 shows 9 fold slowing with the D_2O but only 2 fold slowing in the Q1138L where hydrogen bonding possibility has been removed. The Q138N where hydrogen bonding has been altered but still possible, formation has been slowed 5 fold which is more similar to the wild type.

The back reaction experiments show more pronounced results. The Q138L mutual shows 170 fold slowing of the recovery time constant. This is more than one order of magnitude greater than the change seen in LOV2Q513L and is significant. The increased stability of the adduct can be rationalized in the following way. The spontaneous breakage of the C-S bond occurs after the deprotonation of the N(5) of

the FMN. The Q138L mutant lacks hydrogen bonding with the protonated N(5) and that seems to stabilize the adduct. The Q138N mutant results can further support this idea. The effect of temperature and hydration on the light-triggered single propagation in the phot1-LOV2 domain using FTIR reveals that C(4)=O exists in two conformer populations (fig 3-22) of a one or two hydrogen bonding arrangement [29]. The asparagines substitution is suggested to enhance this flexibility at that region [30] which can further destabilize the N(5) proton by hydrogen bond switching during the adduct state (much like glutamine asparagines can switch hydrogen bonding from C(4) =O to N(5)-H during adduct formation). The Q138N mutation therefore can accelerate the adduct decay to the dark state by destabilizing the N(5)-H bond. We measured the back reaction of the Q138N to be almost 5 fold faster than wild type and calculated an activation energy of 49 KJ/Mole which is lowered compared to the reported 55 KJ/mol value for LOV2 [21] accounting for a much faster adduct decay reaction. It should be noted that in phot1-LOV2, an approximately 14.5 Kcal/mol difference is reported between the light and dark state [31]. The back reaction happens through spontaneous relaxation, which suggests that the light state is conformationally strained and energetically less favorable. In conclusion, the hydrogen bonding network around the polar side of the isoalloxazine ring of the FMN appears to modify the velocity and efficiency of the photocycle by either destabilizing the adduct state or destabilizing the transition state to the response needed. The details of affects to the adduct formation has not been reported for any of the LOV-domains and it is the first report of any changes to the EL222 photocycle.

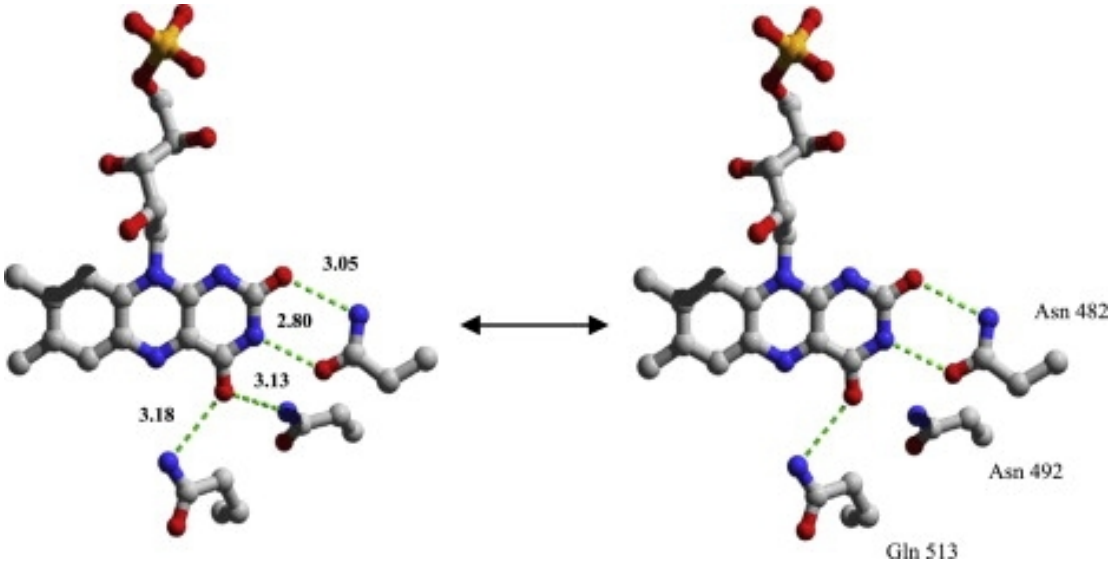

Figure 3-22 Hydrogen bonding in the binding pocket of FMN inside LOV2. The potential H-bond partners of the FMN isoalloxazine moiety are Asn-482 at 2.8 A° of FMN-N(3) and 3.05 A° of FMN-C(2)=O, Asn-492, and Gln-513 at 3.13 A° and 3.18 A° of FMN-C(4)=O. C(4)=O is in equilibrium between double H-bonded by Asn-492 and Gln-513 (left) and single H-bonded to Gln-513 (right).

The modification of the photocycle of EL222 might also have biotechnological applications. The ability to regulate a cellular function with blue light through LOV-domains has gained much interest recently. LOV-domains are now modified and used as fluorescence reporters [32], and fusion proteins involving LOV-domains are designed to activate DNA transcription [33-34]. A fusion protein of LOV2 and RAC protein has recently been shown to function as a regulator of the motility and migration of the living cells [35]. As more fusion proteins are designed, modulation of the photocycle will be a very important aspect of research in this field to modify the kinetics and the efficiency of the activated LOV-domain in the reaction

of interest. In this chapter, we demonstrated that the modification of a single amino acid can change the lifetimes of EL222 by several folds which will be of great interest to the researchers in this field.

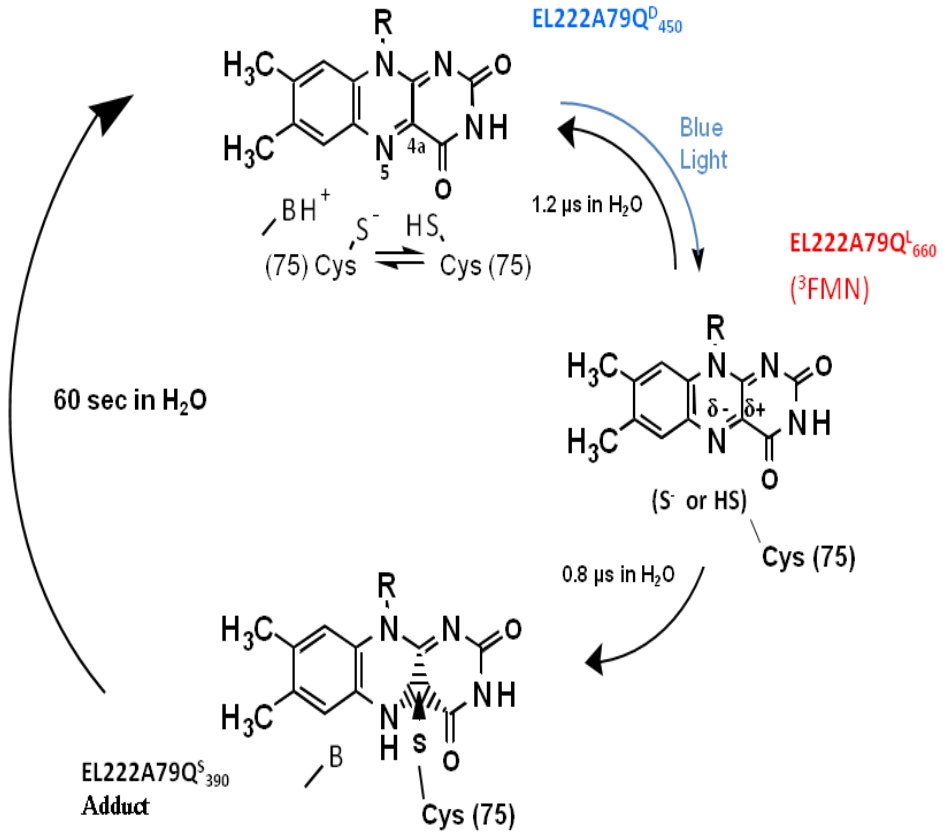

Figure 3-23 Photocycle scheme and proposed reaction mechanism for EL222A79Q mutant.

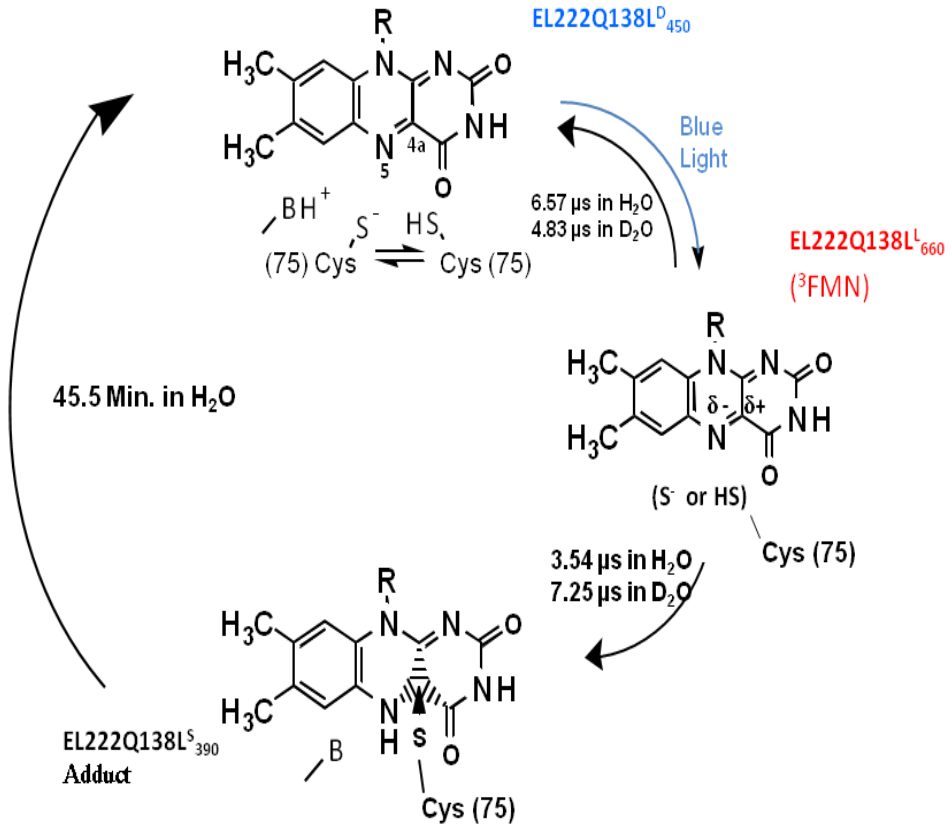

Figure 3-24 Photocycle scheme and proposed reaction mechanism for EL222Q138L mutant.

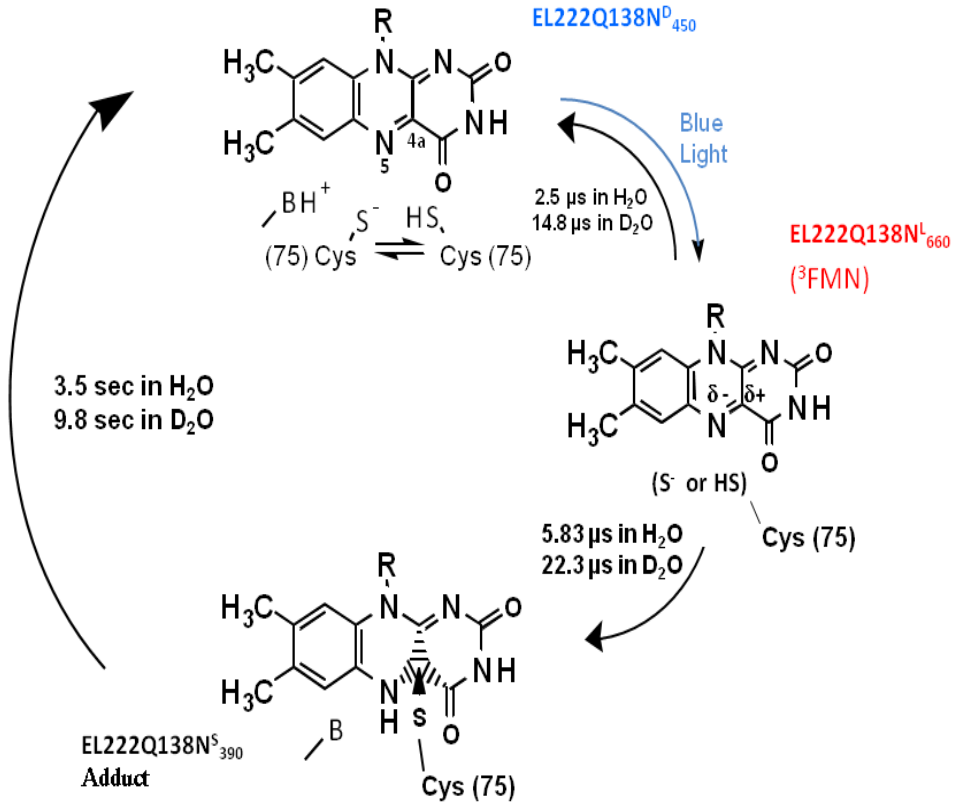

Figure 3-25 Photocycle scheme and proposed reaction mechanism for EL222Q138N mutant.

References:

1. Christie, J.M. and W.R. Briggs, *Blue light sensing in higher plants. [Erratum In: J Biol Chem 2001 May 18;276(20):17620].* Journal of Biological Chemistry, 2001. **276**(15): p. 11457-60.

2. Briggs, W. and J. Christie, *Phototropins 1 and 2: versatile plant blue-light receptors.* TRENDS IN PLANT SCIENCE, 2002. **7**(5): p. 204-210.

3. Baca, M., et al., *Complete Chemical Structure of Photoactive Yellow Protein: Novel Thioester-Linked 4-Hydroxycinnamyl Chromophore and Photocycle Chemistry.* Biochemistry, 1994. **33**(48): p. 14369-14377.

4. Gomelsky, M. and G. Klug, *BLUF: a novel FAD-binding domain involved in sensory transduction in microorganisms.* Trends in Biochemical Sciences, 2002. **27**(10): p. 497-500.

5. Cashmore, A.R., et al., *Cryptochromes: Blue light receptors for plants and animals.* Science (Washington D C), 1999. **284**(5415): p. 760-765.

6. Purcell, E.B., et al., *A photosensory two-component system regulates bacterial cell attachment.* Proceedings of the National Academy of Sciences of the United States of America, 2007. **104**(46): p. 18241-18246.

7. Swartz, T.E., et al., *Blue-light-activated histidine kinases: Two-component sensors in bacteria.* Science, 2007. **317**(5841): p. 1090-1093.

8. Nash, A.I., et al., *Structural basis of photosensitivity in a bacterial light-oxygen-voltage/helix-turn-helix (LOV-HTH) DNA-binding protein.* Proceedings of the National Academy of Sciences, 2011. **108**(23): p. 9449-9454.

9. Swartz, T., et al., *The photocycle of a flavin-binding domain of the blue light photoreceptor phototropin.* JOURNAL OF BIOLOGICAL CHEMISTRY, 2001. **276**(39): p. 36493-36500.

10. Nelson, M. and M. McClelland, *[25] Use of DNA methyltransferase/endonuclease enzyme combinations for megabase mapping of chromosomes*, in *Methods in Enzymology*, W. Ray, Editor. 1992, Academic Press. p. 279-303.

11. Arnold, K., et al., *The SWISS-MODEL workspace: a web-based environment for protein structure homology modelling.* Bioinformatics, 2006. **22**(2): p. 195-201.

12. Bordoli, L., et al., *Protein structure homology modeling using SWISS-MODEL workspace.* Nat. Protocols, 2008. **4**(1): p. 1-13.

13. Schwede, T., et al., *SWISS-MODEL: an automated protein homology-modeling server.* Nucleic Acids Research, 2003. **31**(13): p. 3381-3385.

14. Huang, X. and W. Miller, *A time-efficient, linear-space local similarity algorithm.* Advances in Applied Mathematics, 1991. **12**(3): p. 337-357.

15. Nozaki, D., et al., *Role of Gln1029 in the Photoactivation Processes of the LOV2 Domain in Adiantum Phytochrome3†.* Biochemistry, 2004. **43**(26): p. 8373-8379.

16. Nash, A.I., et al., *A Conserved Glutamine Plays a Central Role in LOV Domain Signal Transmission and Its Duration†.* Biochemistry, 2008. **47**(52): p. 13842-13849.

17. Jones, M.A., et al., *Mutational Analysis of Phototropin 1 Provides Insights into the Mechanism Underlying LOV2 Signal Transmission.* Journal of Biological Chemistry, 2007. **282**(9): p. 6405-6414.

18. Christie, J.M., et al., *Steric interactions stabilize the signaling state of the LOV2 domain of phototropin 1.* Biochemistry, 2007. **46**(32): p. 9310-9319.

19. Szundi, I., J.W. Lewis, and D.S. Kliger, *Deriving reaction mechanisms from kinetic spectroscopy. Application to late rhodopsin intermediates.* Biophysical Journal, 1997. **73**(2): p. 688-702.

20. Szundi, I., T.E. Swartz, and R.A. Bogomolni, *Multicolored protein conformation states in the photocycle of transducer-free sensory rhodopsin-I.* Biophys J, 2001. **80**(1): p. 469-79.

21. Corchnoy, S., et al., *Intramolecular proton transfers and structural changes during the photocycle of the LOV2 domain of phototropin 1.* JOURNAL OF BIOLOGICAL CHEMISTRY, 2003. **278**(2): p. 724-731.

22. Miller, S.M., et al., *Use of a site-directed triple mutant to trap intermediates: demonstration that the flavin C(4a)-thiol adduct and reduced flavin are kinetically competent intermediates in mercuric ion reductase.* Biochemistry, 1990. **29**(11): p. 2831-41.

23. Avila-Pérez, M., et al., *In Vivo Mutational Analysis of YtvA from Bacillus subtilis.* Journal of Biological Chemistry, 2009. **284**(37): p. 24958-24964.

24. Zoltowski, B.D., et al., *Conformational Switching in the Fungal Light Sensor Vivid.* Science, 2007. **316**(5827): p. 1054-1057.

25. Crosson, S. and K. Moffat, *Photoexcited structure of a plant photoreceptor domain reveals a light-driven molecular switch.* Plant Cell, 2002. **14**(5): p. 1067-1075.

26. Freddolino, P.L., M. Dittrich, and K. Schulten, *Dynamic Switching Mechanisms in LOV1 and LOV2 Domains of Plant Phototropins.* Biophysical journal, 2006. **91**(10): p. 3630-3639.

27. Pfeifer, A., et al., *Time-Resolved Fourier Transform Infrared Study on Photoadduct Formation and Secondary Structural Changes within the Phototropin LOV Domain.* Biophysical journal, 2009. **96**(4): p. 1462-1470.

28. Gauden, M., et al., *Hydrogen-bond switching through a radical pair mechanism in a flavin-binding photoreceptor.* Proceedings of the National Academy of Sciences, 2006. **103**(29): p. 10895-10900.

29. Alexandre, M.T.A., et al., *Conformational Heterogeneity and Propagation of Structural Changes in the LOV2/J± Domain from Avena sativa Phototropin 1 as Recorded by Temperature-Dependent FTIR Spectroscopy.* Biophysical journal, 2009. **97**(1): p. 238-247.

30. Losi, A. and W. Gärtner, *Old Chromophores, New Photoactivation Paradigms, Trendy Applications: Flavins in Blue Light-Sensing Photoreceptors†.* Photochemistry and Photobiology, 2011. **87**(3): p. 491-510.

31. Harper, S.M., et al., *Conformational changes in a photosensory LOV domain monitored by time-resolved NMR spectroscopy.* Journal Of The American Chemical Society, 2004. **126**(11): p. 3390-3391.

32. Chapman, S., et al., *The photoreversible fluorescent protein iLOV outperforms GFP as a reporter of plant virus infection.* Proceedings of the National Academy of Sciences, 2008. **105**(50): p. 20038-20043.

33. Strickland, D., K. Moffat, and T.R. Sosnick, *Light-activated DNA binding in a designed allosteric protein.* Proceedings of the National Academy of Sciences, 2008. **105**(31): p. 10709-10714.

34. Morgan, S.-A., S. Al-Abdul-Wahid, and G.A. Woolley, *Structure-Based Design of a Photocontrolled DNA Binding Protein.* Journal of Molecular Biology, 2010. **399**(1): p. 94-112.

35. Wu, Y.I., et al., *A genetically encoded photoactivatable Rac controls the motility of living cells.* Nature, 2009. **461**(7260): p. 104-108.

CHAPTER 4

CHARACTERIZATION AND PHOTOCYCLE OF TWO LIGHT REGULATED LOV HISTIDINE KINASES FROM MARINE BACTERIUM ERYTHROBACTER LITORALIS HTCC2594

4.1 Introduction

The visible and infrared regions of solar radiation not only support life on earth but also contain information essential for each living organism. Not long ago, bacteria were considered insensitive to light, except for some phototrophs that use the light as a source of energy. Since most of the photoreceptors that were first discovered and analyzed, were found in phototrophs, it was thought that these photosensory proteins were a specialized adaption of these bacteria [1]. Discovery and characterization of blue-light sensing LOV-domains (Light, Oxygen, Voltage), and red light sensing bacteriophytochromes in nonphototrophic bacteria changed this view [2-4]. As of the completion of this chapter, LOV-domains are found in 227 bacteria species and out of 322 LOV-domains among them, 171 (53%) have kinase as an effector domain (updated by Dr. Aba Losi, private communication). The flavin-binding photosensory LOV-domains found in bacteria are coupled to diverse output domains but so far only a few have been linked to cellular function. Among the several that have been studied in detail, two have histidine kinases (HK) as an effector domain. The mammalian pathogen *Brucella Abortus* uses light and LOV-HK for virulence [2] and LOV-HK from *Caulobacter Crescentus* is involved in the

positive regulation of cell attachment [5]. Histidine kinases in prokaryotes are a part of a two-component signal transduction pathway that sense, respond, and adapt to environmental stimuli. Two-component signal transduction pathways have a sensor histidine kinase and a response regulator [6]. In the case of LOV-HK, blue light sensed by LOV-domain, activates the kinase resulting in auto-phosphorylation of a conserved histidine in the histidine kinase domain. Transfer of this phosphate to a conserved aspartate in the targeted response regulator (RR) activates a response [4]. Two component signal transduction pathways are not present in mammals and therefore are the target of much study in antibacterial drug development as well as understanding the various cellular processes that they control [7].

The full genome of a marine bacterium named, *Erythrobacter Litoralis*, has been sequenced [8]. The sequence analysis predicts that the genome of this bacterium codes for two histidine kinases that contain a LOV domain at their N-terminus. They were named EL346 and EL368 based on the number of amino acids they contained. These two LOV-HK proteins show the conserved GRNCRFLQ motif so they were predicted to bind a flavin and they both contain a conserved cysteine approximate to the flavin necessary for cysteinyl adduct formation. The genes encoding EL346-LOV-HK, and EL368-LOV-HK were cloned and expressed in *Escherichia coli* and purified [2]. Both proteins show characteristic LOV-domain 450nm and 370nm absorption with vibronic bands around them indicating interaction of the flavin with the chromophore binding pocket of the protein [2]. The chromophore extraction and analysis by thin-layer chromatography (TLC) showed that FMN is the flavin

chromophore inside both proteins. Light induced absorption changes showed that both proteins complete a photocycle and spontaneously relaxes back to the ground state after blue light activation [2]. The addition of [γ-^{32}P] ATP (adenosine tri-phosphate) to samples after illumination, showed that both LOV-HKs function as light-activated kinases and therefore are part of the two component system in *Erythrobacter litoralis*.

A typical histidine kinase contains two parts: a sensory domain and a conserved C-terminal histidine kinase (HK) domain that has two subunits, the dimerization and histidine phosphotransfer (DHp) domain and the catalytic and ATP binding (CA) domain (fig 4-1). Histidine kinases are divided into two classes based on the position of the conserved histidine containing region with respect to the kinase domain (which contains the N, G1, F, and G2 conserved boxes), which is identified based on unique sequences in the primary sequence (fig 4-2). In class I (EnvZ-like) histidine kinases, the conserved His residue in the H box of the DHp domain is the primary auto-phosphorylation site but in class II (CheA-like) histidine kinases, the conserved His residue is in the H box of the Histidine-containing phosphotransfer (Hpt) domain [9]. It is important to mention that the Hpt and DHp domains are significantly different from each other which might reflect differences in functional and regulatory mechanisms.

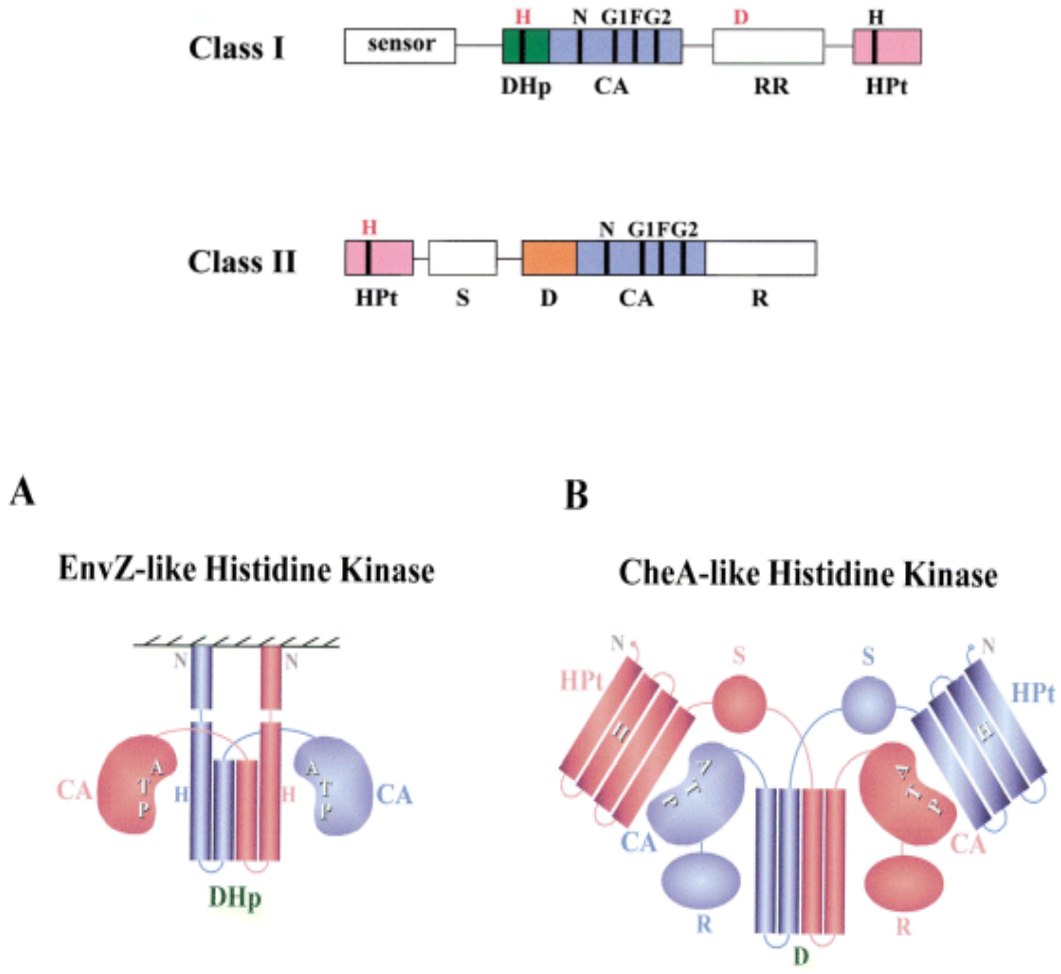

Figure 4-1 Class I and class II histidine kinases. A schematic diagram of two classes of histidine kinases is presented. This classification is based on the position of the conserved histidine containing region with respect to the kinase domain (which contains the N, G1, F and G2 conserved boxes) in the primary sequence. Bottom figure shows models of domain organization of class I (EnvZ-like) and class II (CheA-like) histidine kinases. They are both in form of dimers and two monomers are shown by different colors.

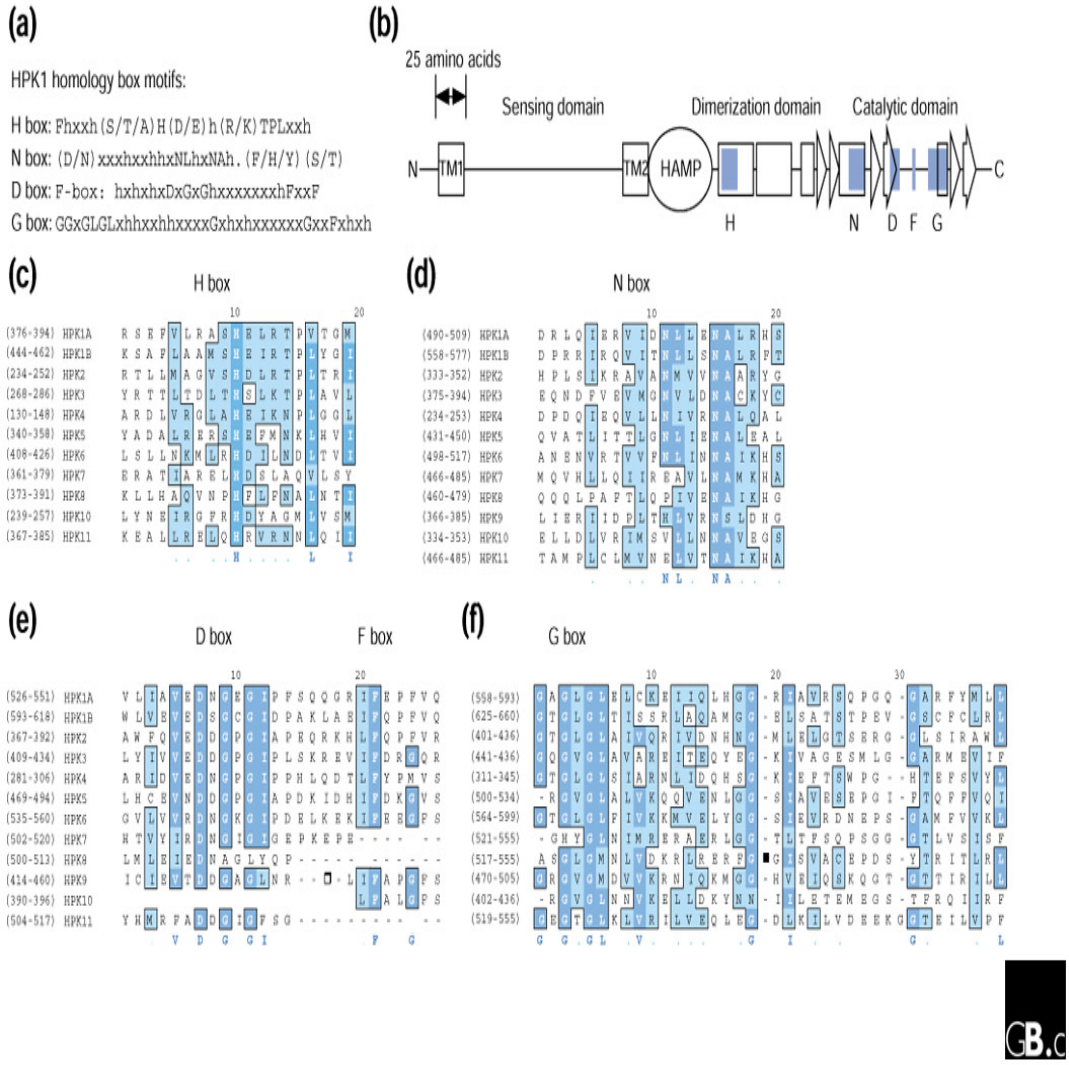

Figure 4-2 Conserved sequence motifs in the 11 histidine protein kinase (HPK) subfamilies from the class I (*E. coli* EnvZ) family, which includes a majority of all HPKs. The conserved regions that make up the HPK core designated the H, N, D, F and G boxes (shown in blue), spans approximately 200 residues in total. Sequence alignments of **(c)** the H box, **(d)** the N box, **(e)** the D and F boxes, and **(f)** the G box for one representative member of each of the 11 HPK subfamilies are shown. Some members of the HPK subfamily do not contain an F box and some members of HPK 11 subfamily contain a partial F box.

In this study, we will discuss the classification of LOV-containing histidine kinases in *Erythrobacter litoralis* based on sequence alignment, and present a detailed study of the photocycle of the LOV-domains from these proteins that show different time constants than the studied EL222 from the same organism (chapter 2) and the previously studied LOV2 [10].

4.2 Materials and Methods

4.2.1 Sequence Comparison, Modeling, and Chromophore Analysis

A dynamic programming algorithm is used to determine similar regions of phot1-LOV2, EL346, and EL368 sequences. The LALIGN sequence alignment program [11-13] from the ExPASy Proteomics Server is used and the result of the homology comparison is shown in figure 4-3 and 4-4. The computation of various physical and chemical parameters was performed using ProtParam tool from ExPASy bioinformatics resource portal [13]. The Blast (Basic Local Alignment Search Tool, NCBI Servers) search was used to align and classify the histidine kinases and this work was further followed by using the pfam database [14-15] from Sanger Institute that is used to classify protein families. Structure modeling of the LOV-domains from both EL-LOV-kinase domains was done using the SWISS-MODEL Template Library [12]. For EL368 model, a crystal structure of the LOV-domain from EL222 was used as a template and for EL346 model, a crystal structure of the LOV-domain from *Chlamydomonas Reinhardtii* was used as a template. Chromophore analysis

was performed by thin layer chromatography using the following protocol. Protein samples were buffer exchanged by dialyzing against 2 liters of distilled water twice (12 hours each time) before analysis. The chromophore was released by boiling in 70% ethanol for 2 min. Samples were then chilled on ice and centrifuged at 10K for 10 min. The flavin-containing supernatants were lyophilized to dryness and resuspended in 35% ethanol (5–10 ml). TLC (Thin Layer Chromatography) was performed with *n*-butanol/acetic acid/water, 3:1:1 (vol/vol), as the solvent [16].

4.2.2 Cloning, Protein Expression, and Purification

The genes of both LOV-HKs were PCR-amplified and cloned into the pET/100D TOPO plasmid according to the manufacturer's instructions for TOPO directional cloning. This plasmid generates a fusion protein with the protein of interest and an N-terminal 5xHis tag. The protein was expressed in *E. coli* BL21(DE3)pLysS as discussed in chapter 2. The protein was affinity purified using the TALON metal affinity resin (BD Biosciences Clontech) following the manufacturer's procedure. Cell growth, cell harvesting, and protein purification were done under dim red light. Protein samples were then buffer exchanged into a low salt buffer (5mM Tris/5mM NaCl pH8.0) using a Sephadex G25 PD-10 ml gravity desalting column (GE Healthcare). Samples of the purified protein were lyophilized in the dark for D_2O experiments.

4.2.3 UV-Visible Absorption Spectroscopy

Light-induced absorption changes at short times were measured using the laser flash photolysis spectrometer with a microflow system [17]. Difference spectra in the 30-ns to 1-ms time window were collected. In brief, a dye laser pumped by the third harmonic of an Nd:Yag laser provided a 10 ns, 80 μJ/mm^2 light pulse at 477 nm with an optical path length of 2 mm. The room temperature for all measurements was about 20 °C which was not controlled. Light used to probe absorbance was polarized linearly to the magic angle (54.7°) relative to the laser polarization axis to prevent rotational diffusion artifacts [18]. Light-induced absorption changes at long times were measured using a Hewlett Packard 8452A diode array spectrometer. Difference spectra were collected every 10 minutes with an optical pathlength of 0.5 cm. The light source was a continuous beam provided by a fiber optic illuminator (V-LUX 1000, Volpi Manufacturing, USA) and samples were illuminated for one minute prior to data collection. Control of data acquisition was automated with software written in LabVIEW (National Instruments, Austin, TX) and all the data were collected at room temperature.

4.3 Results

4.3.1 Sequence Analysis of EL346 and EL368

Figures 4-3 to 4-6, show the full sequence analysis of the EL346 and EL368 using ProtParam and LALIGN tools from ExPASy bioinformatics resource portal [11-12]. Much like other LOV-domains, the highly conserved motif of NCRFLQ, is

seen in both proteins with the active cysteine at position 55 for EL346 and position 93 for EL368 capable of forming the cysteinyl adduct with the FMN chromophore molecule associated with it. Although there is no structural information available for these proteins, they are members of the PAS (Per-ARNT-Sim) family of sensory domains that have very similar folds. LOV-domains belong to the PAS family sensory domains, and since EL346 and EL368 are more than 40% homologous to the LOV2-domain, we expect a similar fold to the LOV2 for both proteins. Both *Erythrobacter* LOV-kinases also show complete conservation of residues whose side chains interact with the FMN chromophore of the LOV-domain.

The pfam (Sanger Institute, UK) analysis of the EL368 protein sequence shows an alignment with the LOV-domain from residue 70 to 162 with a special class of histidine kinases, named HWE HK, spanning from residue 178 to 262. Members of this sensor HK family differ from most others by the absence of a recognizable F box and the presence of several conserved residues, especially a histidine in the N box and a WXE sequence in the G1 box, which was used to define the family (HWE). The catalytic and ATP binding (CA) domain of EL368 spans from residues 268 to 311. It is therefore concluded that EL346 HK is a member of class I histidine kinase.

The pfam analysis of the EL346 protein sequence shows the LOV-domain alignment for residue 34 to 121 with kinase form residues 139 to 229. The domain architecture shows that EL346 belongs to class I histidine kinase and the subfamily 11 of the HK [19]. The BLAST search of the sequence identifies the kinase as a

HWE kinase even though the conserved WXE sequence is missing. Their identification of the kinase as HWE is because of the missing F box in this kinase, although that is also seen in the subfamily 11 of the HK. The CA domain of EL346 HK follows next and spans from residues 235 to 333.

A major problem in studying the full length histidine kinase structure is that the majority of histidine kinases are membrane-bound or membrane associated. This makes biophysical studies of the full length HK very challenging, since it is difficult to purify soluble and homogenous protein samples needed for studies. EL346 and El368 are both cytosolic histidine kinases and show remarkable stability and solubility, which make them great targets for biophysical studies. Swartz et al [2] has previously demonstrated that both proteins display the signature LOV-domain UV-Visible absorption at 370 and 450 nm and that both kinases function as light activated kinases. Due to this result, it was important to study the photocycle of both proteins.

```
        10         20         30         40         50         60
MTDGDGRDLP LKGEISAQAG REFDTSRLDL RAIIDPRDLR VDPTRLFLET TQQTRLAICI

        70         80         90        100        110        120
SDPHQPDCPV VYVNQAFLDL TGYAREEIVG RNCRFLQGAD TDPEQVRKLR EGIAAERYTV

       130        140        150        160        170        180
VDLLNYRKDG IPFWNAVHVG PIYGEDGTLQ YFYGSQWDIT DIVAERRKAE TQRRIAAELR

       190        200        210        220        230        240
HRTGNIFAVL NAIIGLTSRR ERDVSEFADK LSERVSALAS AHRMTIMDEP DQEAVAIDDL

       250        260        270        280        290        300
VTGVMKPYRN RFAERVTTSG PKIELGPRSV TALGLALHEL ATNAVKYGAL SVDAGRVEIS

       310        320        330        340        350        360
WSREDGDVTL VWQEQGGPTV SQEQSEPVKG NGTMLIDGMI ASLTGSIERD FAAAGLQAKI


TLPVHQPE
```

Number of amino acids: 368
Molecular weight: 40804.9
Theoretical pI: 5.09

Amino acid composition:

Ala (A)	34	9.2%
Arg (R)	33	9.0%
Asn (N)	9	2.4%
Asp (D)	29	7.9%
Cys (C)	3	0.8%
Gln (Q)	17	4.6%
Glu (E)	27	7.3%
Gly (G)	29	7.9%
His (H)	6	1.6%
Ile (I)	23	6.2%
Leu (L)	32	8.7%
Lys (K)	10	2.7%
Met (M)	6	1.6%
Phe (F)	10	2.7%
Pro (P)	17	4.6%
Ser (S)	18	4.9%
Thr (T)	25	6.8%
Trp (W)	4	1.1%
Tyr (Y)	9	2.4%
Val (V)	27	7.3%

Total number of negatively charged residues (Asp + Glu): 56
Total number of positively charged residues (Arg + Lys): 43
Formula: $C_{1784}H_{2853}N_{519}O_{559}S_9$
Total number of atoms: 5724

Figure 4-3 Sequence of EL368 and computation of various physical and chemical parameters.

```
        10         20         30         40         50         60
MAVGLAEHDK EAWGRLPFSL TIADISQDDE PLIYVNRAFE QMTGYSRSSV VGRNCRFLQG

        70         80         90        100        110        120
EKTDPGAVER LAKAIRNCEE VEETIYNYRA DGEGFWNHLL MGPLEDQDEK CRYFVGIQVD

       130        140        150        160        170        180
MGQSESPDRA TELDRQLAEV QHRVKNHLAM IVSMIRIQSS QAGGVGSQFD SLSRRVEALQ

       190        200        210        220        230        240
LLYQEMDIAG AAKATDKIIP LGAYLGRIAS AINHIDGRGA IKVNVQADTV DVPVETAGRI

       250        260        270        280        290        300
GLLVSEVLTN ALQHAFSDRA SGVVQLRSSV MSGEQLRVTV EDDGRGIPED CDWPNEGNLG

       310        320        330        340
SRIVRQLVQG LGAELNVTRG GTGTIVNIDI PLSQQKTLIA DERTKD
```

Number of amino acids: 346
Molecular weight: 37947.7
Theoretical pI: 4.94

Amino acid composition:

Ala (A)	29	8.4%
Arg (R)	26	7.5%
Asn (N)	13	3.8%
Asp (D)	25	7.2%
Cys (C)	4	1.2%
Gln (Q)	21	6.1%
Glu (E)	26	7.5%
Gly (G)	32	9.2%
His (H)	**6**	**1.7%**
Ile (I)	23	6.6%
Leu (L)	30	8.7%
Lys (K)	10	2.9%
Met (M)	8	2.3%
Phe (F)	7	2.0%
Pro (P)	10	2.9%
Ser (S)	22	6.4%
Thr (T)	15	4.3%
Trp (W)	3	0.9%
Tyr (Y)	7	2.0%
Val (V)	29	8.4%

Total number of negatively charged residues (Asp + Glu): 51
Total number of positively charged residues (Arg + Lys): 36
Formula: $C_{1640}H_{2647}N_{483}O_{527}S_{12}$
Total number of atoms: 5309

Figure 4-4 Sequence of EL346 and computation of various physical and chemical parameters.

```
           10        20        30        40        50        60
LOV2   TLERIEKNFVITDPRLPDNPIIFASDSFLQLTEYSREEILGRNCRFLQGPETDRATVRKI
       : .. .  . :.::. :: :.......::.:: :.::::.:::::::::: .::   :::.
EL368  TTQQTRLAICISDPHQPDCPVVYVNQAFLDLTGYAREEIVGRNCRFLQGADTDPEQVRKL
      50        60        70        80        90       100

           70        80        90       100       110       120
LOV2   RDAIDNQTEVTVQLINYTKSGKKFWNLFHLQPMRDQKGDVQYFIGVQLDGTEHVRDAAER
       :..:  .  ..:.:.:: :.:  ::: :. :.  . : .::: : : : :. : .  .
EL368  REGIAAERYTVVDLLNYRKDGIPFWNAVHVGPIYGEDGTLQYFYGSQWDITDIVAERRKA
     110       120       130       140       150       160


LOV2   E
       :
EL368  E
     170
```

Figure 4-5 Sequence comparison of LOV-domains between EL368 and phot1-LOV2. The sequences show 43.8 % identity in 121 residues overlap.

```
         10        20        30        40        50        60
LOV2   RIEKNFVITDPRLPDNPIIFASDSFLQLTEYSREEILGRNCRFLQGPETDRATVRKIRDA
       :.  ...:.:    :.:.:... .: :.: :::  ..:::::::::: .:: ..:...  :
EL346  RLPFSLTIADISQDDEPLIYVNRAFEQMTGYSRSSVVGRNCRFLQGEKTDPGAVERLAKA
           20        30        40        50        60        70

         70        80        90       100       110
LOV2   IDNQTEVTVQLINYTKSGKKFWNLFHLQPMRDQKGDVQYFIGVQLD
       : :  ::   . ::  .:. ::: . . :..::    .::.:.:.:
EL346  IRNCEEVEETIYNYRADGEGFWNHLLMGPLEDQDEKCRYFVGIQVD
           80        90       100       110       120
```

Figure 4-6 Sequence comparison of LOV-domains between EL346 and phot1-LOV2. The sequences show 40.6 % identity in 106 residues overlap.

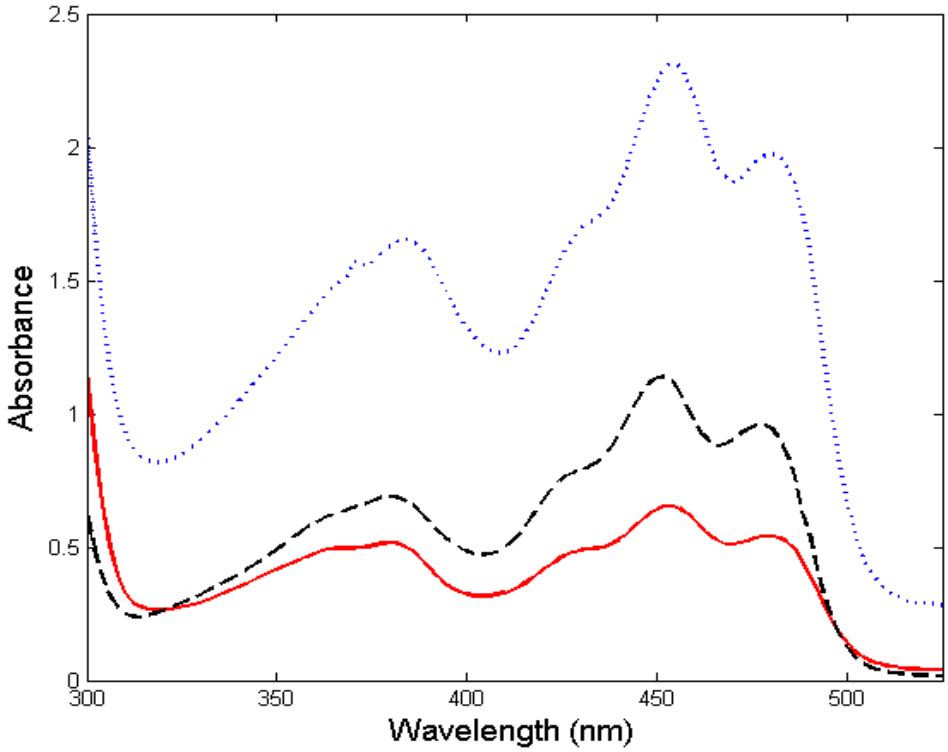

Figure 4-7 Absolute dark spectrum of the wild type LOV2 (black- - -), EL368 (blue …..), and EL346 (red solid line)

4.3.2 UV-Visible Spectroscopy

The UV-Visible dark state absorbance spectra of the EL346 and EL368 display the same characteristic profiles of the LOV2-domain (fig 4-7). They both show a maximum at 450 nm, which is the $S_0 \rightarrow S_1$ transition of the FMN and the absorption maximum at 370 nm, which is the $S_0 \rightarrow S_2$ transition of the FMN chromophore. Both proteins display the loss of blue-light absorption upon illumination like the other studied LOV-domains [10, 16] and recover to their dark state profile when left in the dark. Based on the sequence alignment that shows a high similarity between EL

LOV-domains and the LOV2-domain, especially with all the residues that interact with FMN, we predict that the time constants for the adduct formation should be very similar.

In order to find an apparent rate constant of the adduct formation, nine delay points of (0.3, 1, 2, 5, 10, 100, 200, 500, and 1000 μs) were chosen. The late delay points were added to follow the reaction and confirm that we are not missing any late processes. Since we expect the slowing of the adduct formation in D_2O, we added delay time points of 20 and 50 μs to the D_2O measurements. EL346 and EL368 both showed a very similar apparent time constant (τ_{app}), which is 2.33 μs for EL346 and 2.32 μs for EL368 at room temperature (20±2℃) at pH 8.0. The singular-value decomposition approach (SVD) provides a very efficient way to speed up the fitting procedure of our data and to determine the number of spectrally distinct intermediates. It can also be used to eliminate random noise from the data. The apparent time constants are the result of a global exponential fitting analysis of the data which follows the SVD treatment of the data [20].

From the spectra, we can calculate the branching ratio of the amount that decays to the adduct (forward reaction from the triplet) and the ratio of the amount that returns to the ground state from the triplet state (return reaction). The branching ratio calculation is very important since the apparent rate constant value by itself does not give us the rate constant value for the formation of the adduct and the efficiency by which the adduct is formed (ratio of the forward reaction vs. the return reaction). The data (fig 4-8 and 4-9) show the formation of an intermediate species at 660 nm,

which is the triplet state of the FMN [10, 21]. The triplet state is the excited state of the FMN that has happened through intersystem crossing from a singlet state due to a heavy atom effect. The probability of a reaction happening between the FMN and the surrounding protein is three orders of magnitude higher via a triplet state than a singlet state [10]. The formation of the triplet state is reported to be around 2-3 ns [10] and this rate is believed to have been enhanced because of the proximity of a sulfur atom of the conserved cysteine.

The EL346 protein shows the formation of the triplet state, indicated by a broad absorption band beginning close to 600 nm and continuing to 725 nm with a maximum around 660 nm. The 660 nm absorption is seen at the time delay points of 0.3, 1, 2, and 5 μs, which means after 5 μs time delay, most of the triplet state had either decayed to the adduct state, named $EL346^{S}_{390}$ (S is for signaling state and 390 nm is the absorption if the adduct intermediate) or it has returned to the ground state, named $EL346^{D}_{450}$ (D is for the dark state that has an absorption of 450 nm). From the absorption difference spectra, we have calculated the branching ratio to be 70% for the forward reaction and 30% back to the ground state (for detailed explanation of branching ratio determination, please refer to figure 2-6). This ratio for the forward reaction is higher than reported for the LOV2, which is 50% ( ) and EL222, which is 40% (chapter 2).

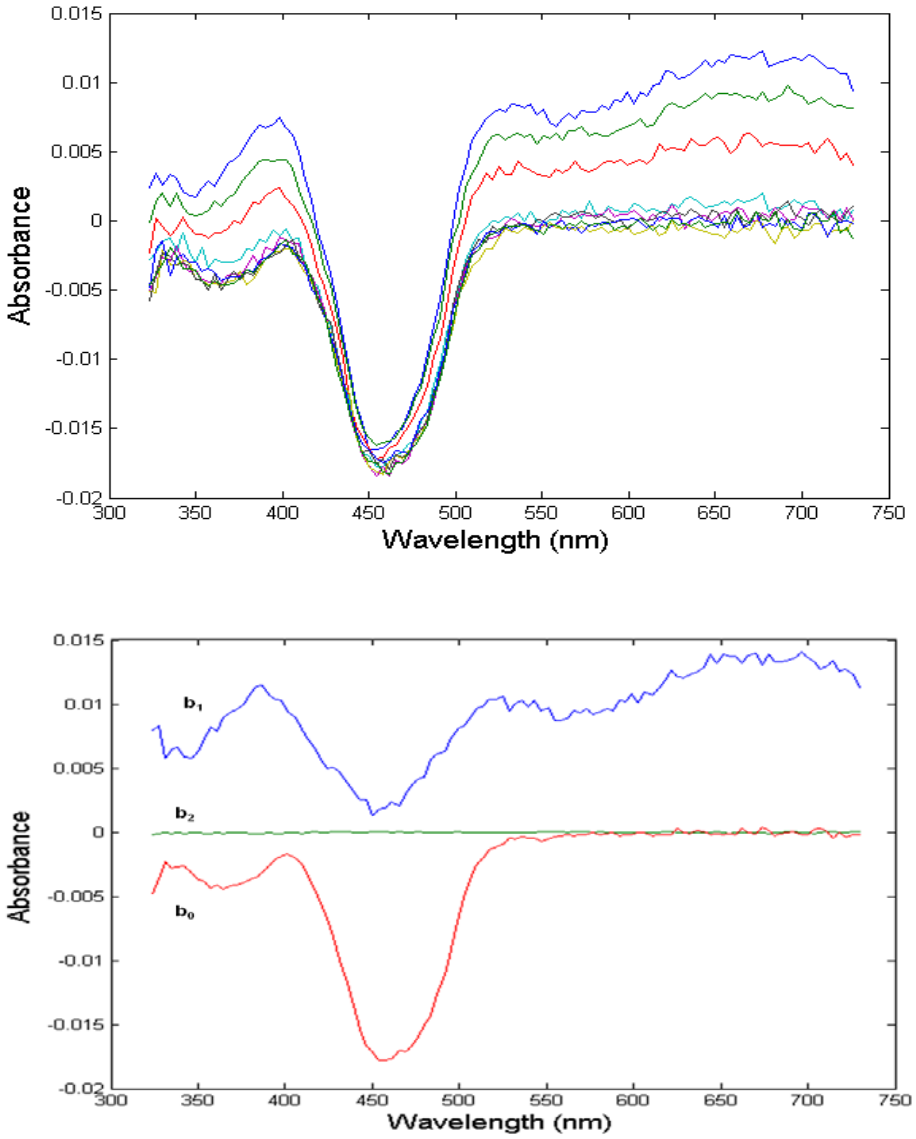

Figure 4-8 The absorption difference spectra of EL346 at room temperature after excitation with a 477nm laser pulse. Spectra were collected at 0.3, 1, 2, 5, 10, 100, 200, 500, 1000 µs. Bottom graph shows the results of global multi-exponential fitting of difference absorption spectra from EL346. The b_1 is the b-spectrum with an apparent rate constant of 2.33 µs, and b_0 is the spectrum of the product formed. The b_2 spectrum is zero meaning that there is not a second component observed.

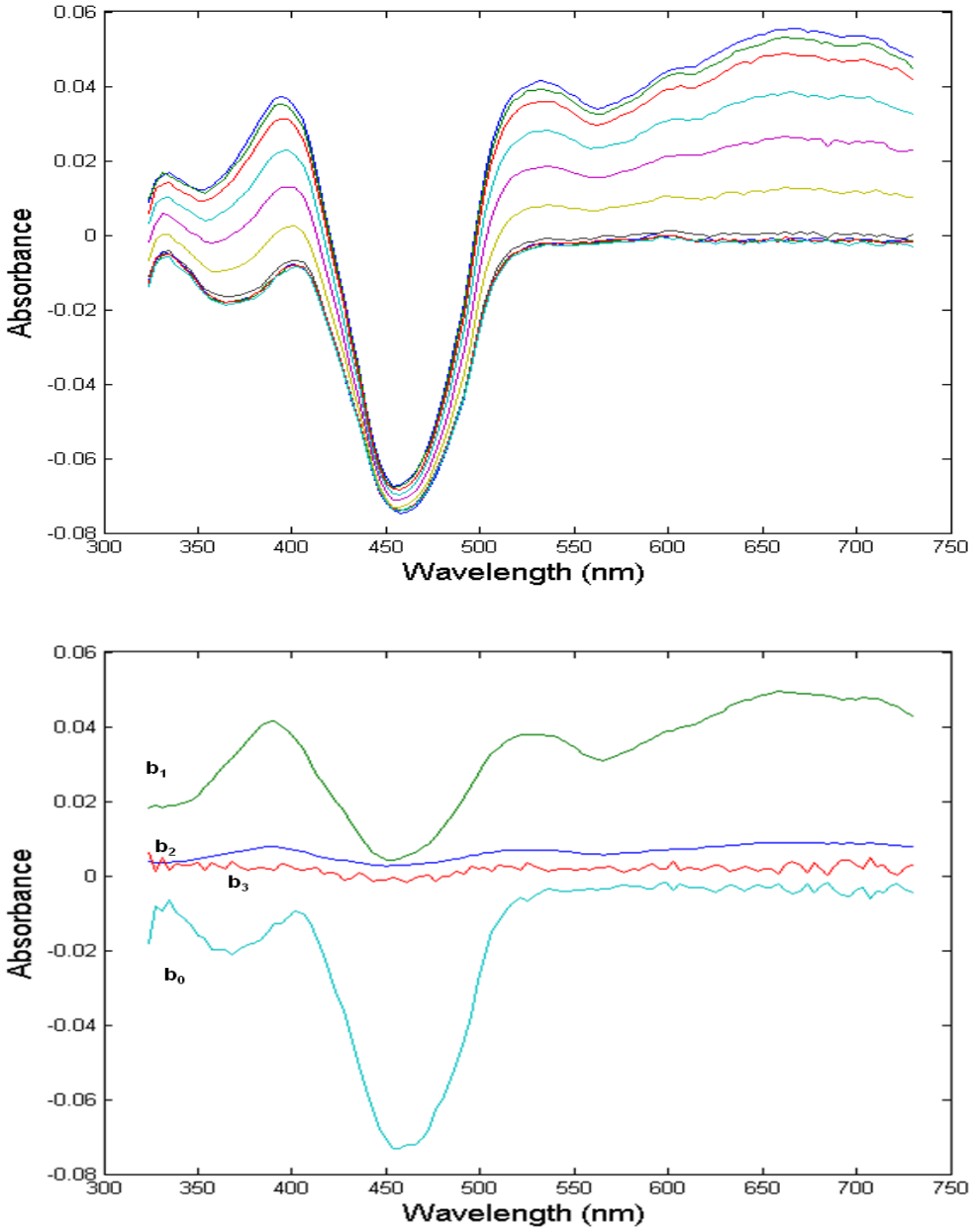

Figure 4-9 The absorption difference spectra of EL346 in D_2O at room temperature after excitation with a 477nm laser pulse. Spectra were collected at 0.3, 1, 2, 5, 10, 20, 50, 100, 200, 500, 1000 µs. Bottom graph shows the results of global multi-exponential fitting of difference absorption spectra from EL346. The b_1 is the b-spectrum with an apparent rate constant of 13.5 µs, and b_0 is the spectrum of the product formed. The b_2 spectrum has an apparent rate constant of 2.5 ms and $b_3$does not have a shape and seems zero meaning that there is not a third component observed.

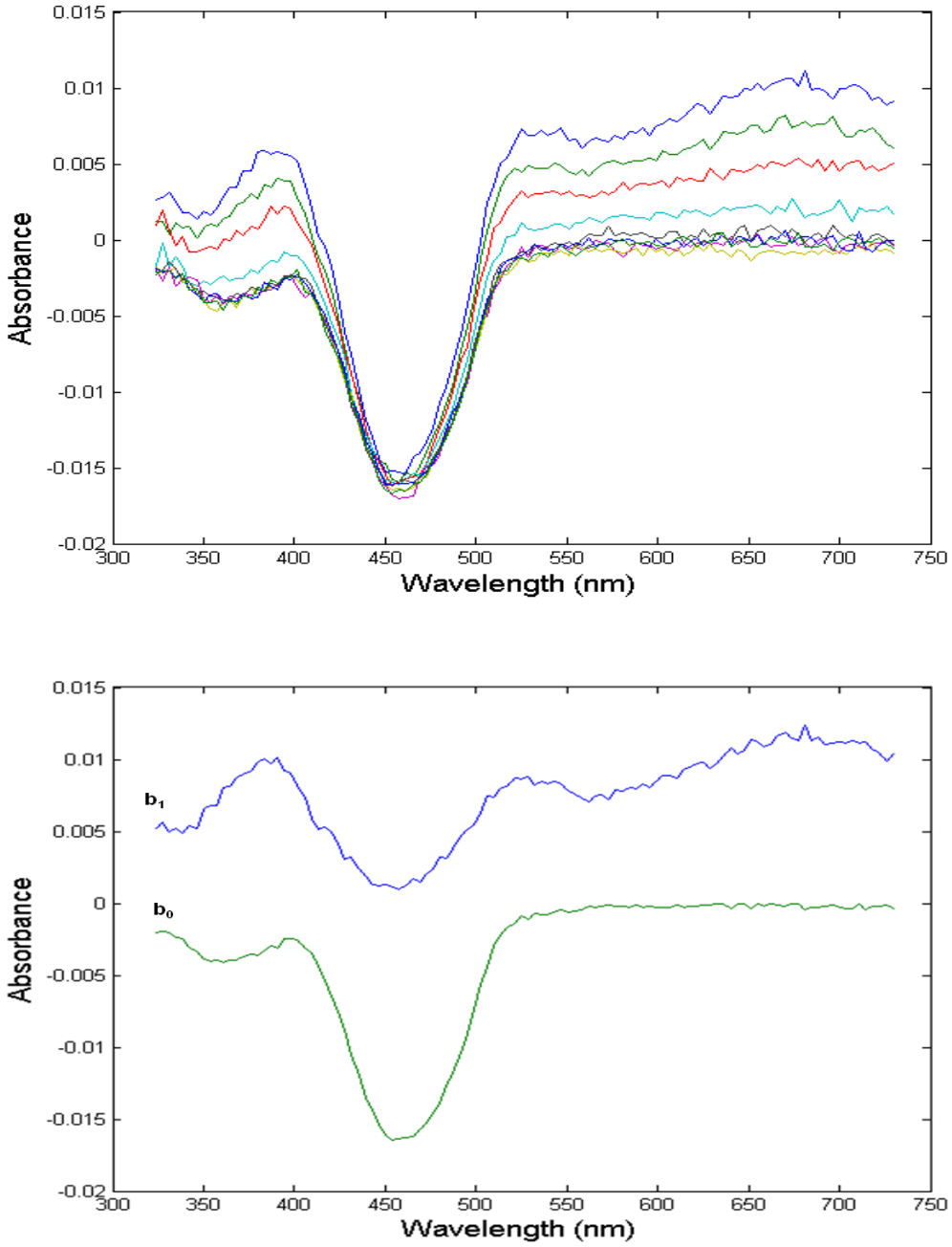

Figure 4-10 The absorption difference spectra of EL346 at 15℃ after excitation with a 477nm laser pulse. Spectra were collected at 0.3, 1, 2, 5, 10, 100, 200, 500, 1000 µs. Bottom graph shows the results of global multi-exponential fitting of difference absorption spectra from EL346. The b_1 is the b-spectrum with an apparent rate constant of 2.7 µs, and b_0 is the spectrum of the product formed.

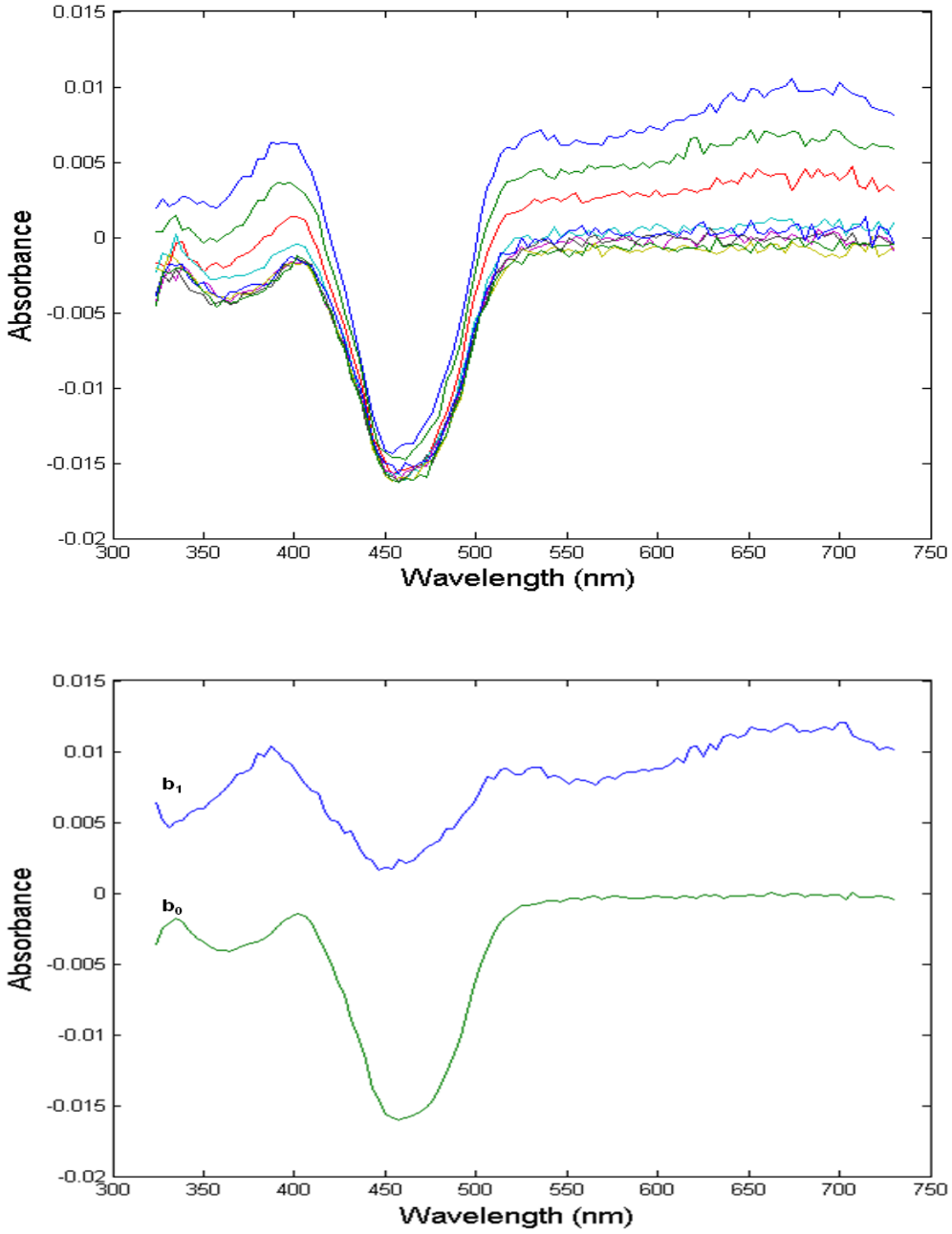

Figure 4-11 The absorption difference spectra of EL346 at 25℃ after excitation with a 477nm laser pulse. Spectra were collected at 0.3, 1, 2, 5, 10, 100, 200, 500, 1000 µs. Bottom graph shows the results of global multi-exponential fitting of difference absorption spectra from EL346. The b_1 is the b-spectrum with an apparent rate constant of 1.95 µs, and b_0 is the spectrum of the product formed.

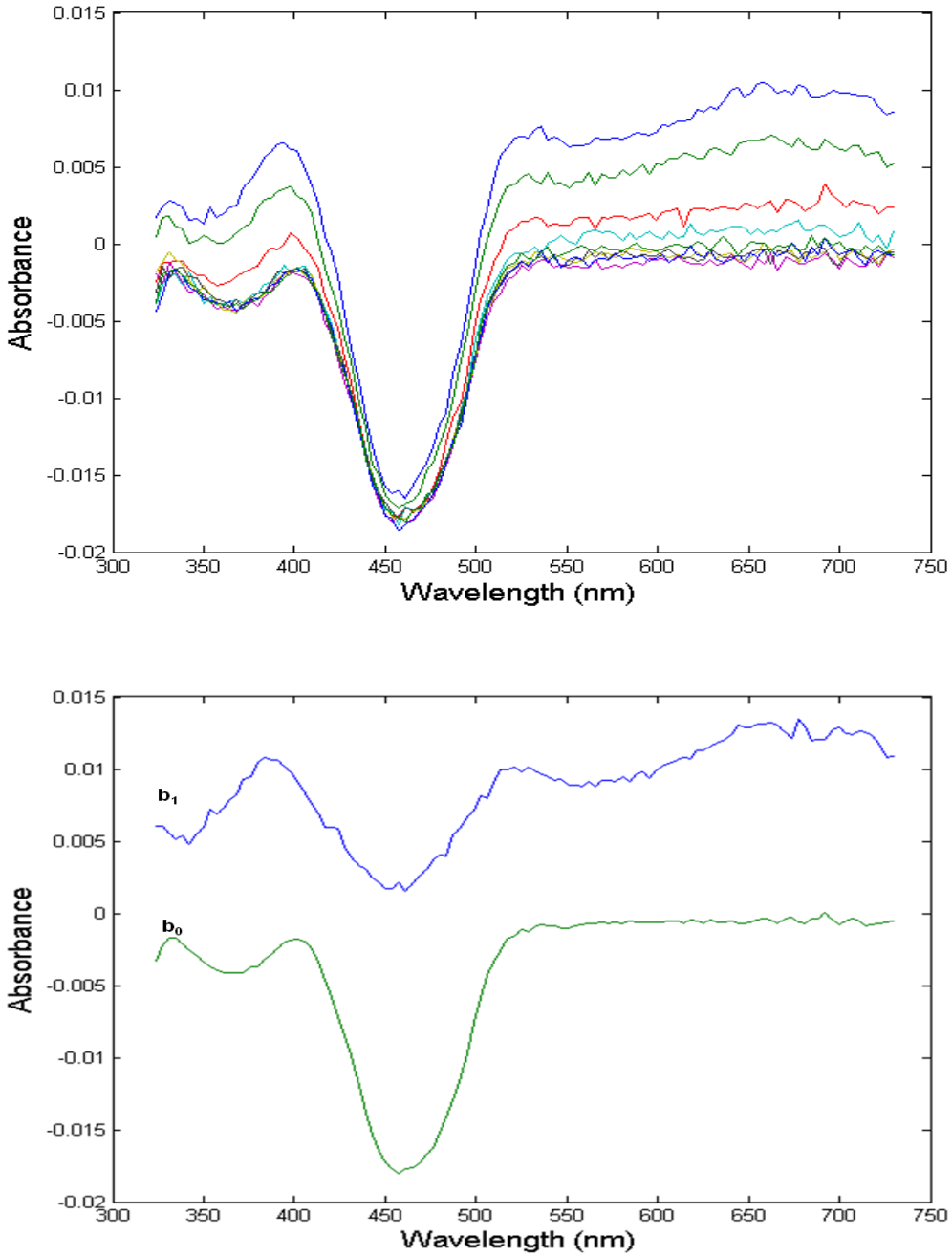

Figure 4-12 The absorption difference spectra of EL346 at 35℃ after excitation with a 477nm laser pulse. Spectra were collected at 0.3, 1, 2, 5, 10, 100, 200, 500, 1000 µs. Bottom graph shows the results of global multi-exponential fitting of difference absorption spectra from EL346. The b_1 is the b-spectrum with an apparent rate constant of 1.6 µs, and b_0 is the spectrum of the product formed.

EL346	τ_{app} (μs)	τ_F (μs)	τ_R (μs)
15℃	2.70	3.86	9.00
20℃	2.33	3.33	7.77
25℃	1.95	2.79	6.50
35℃	1.60	2.29	5.33
D_2O	13.50	22.50	33.75

Table 4-1 The apparent time constant, adduct formation, and return of the triplet to ground state time constants at various temperature and D_2O calculated using single exponential fitting and branching ratios.

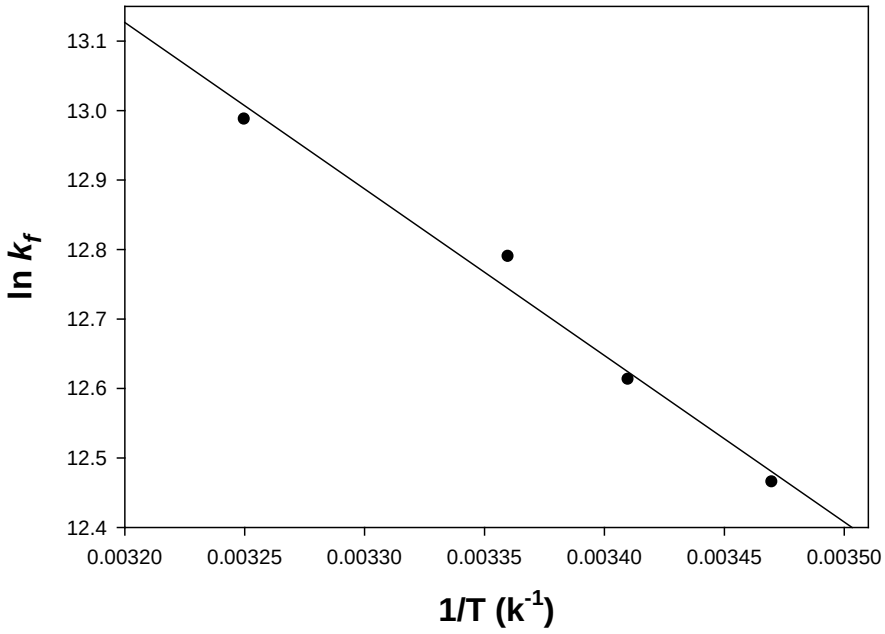

Figure 4-13 Arrhenius plot for the adduct formation kinetics of the EL346.

Based on the branching ratio, we calculated the rate constant for the formation (τ_F) of EL346, to be 3.33 μs and the return reaction from the triplet to the ground state (τ_R) to be 7.77 μs. The τ_F of the EL346 is very close to the reported value for LOV2, which is reported as 4 μs [10]. Analysis of the data shows that a single exponential fit of data can explain it. The b-spectra shows two spectra (b_1 and b_0), with the b_1 spectrum representing the difference between the starting delay time (0.3 μs) and the final delay time (100 μs), which is an intermediate with the apparent time constant that we reported here. The b_0 spectrum is the difference spectrum of the final intermediate ($EL346^{S}_{390}$) and the ground state ($EL346^{D}_{450}$). Addition of a second exponential did not improve the fitting quality and shows a b_2 spectrum that is zero, meaning that single exponential fit was enough to explain the data. We can explain the data with a linear scheme in the following way.

$$EL346^{D}_{450}\ (\tau_R) \leftarrow EL346^{L}_{660} \rightarrow (\tau_F)\ EL346^{S}_{390}$$

LOV2-domain shows slowing of the formation in D_2O [22], which indicates that proton transfer to the N5 atom of the FMN is the rate limiting step in the adduct formation reaction. This D_2O effect was also observed in EL222 to even greater degree (chapter 2) and was also measured for both EL LOV-HK proteins. EL346 shows (fig 4-9) almost seven times slowing of the adduct formation (τ_F =22.5 μs in D_2O), which again indicated that a proton transfer is the rate limiting step in this reaction. Unlike LOV2 and EL222, branching ratio change was seen in EL346 in D_2O. The ratio of the triplet state going to $EL346^{S}_{390}$ changed from 70% to 60% and this change was considered when calculating the τ_F of EL346 in D_2O. There is also a

change in data fitting of this protein from LOV2 and EL222. In order to better fit the data during analysis, bi-exponential fitting was used (fig 4-9) which adds a time constant of 2.5 ms. The shape of this spectrum resembles semiquinone of free FMN, which was observed before (fig 2-19). The D_2O effect experiments are performed when measured amount of D_2O is added to the lyophilized sample. Since not all the sample usually dissolves in D_2O (samples are clarified by centrifugation before each experiment) and are not as stable as samples in H_2O, therefore are free FMN present in the sample. It is important to mention that there is always free FMN in the sample since flavin is in the equilibrium state of the bound to protein and free in our samples and free FMN under our experimental conditions can form semiquinone [23], which is a radical form due to addition of one hydrogen atom.

In order to study and compare the energetics of the adduct formation reaction, the temperature effect on the formation was studied at three additional temperatures of 15, 25, and 35^0C (fig 4-10, 4-11, and 4-12). As we have seen before in the EL222 (chapter2), when the temperature increases, the adduct formation reaction becomes faster, which goes from 3.86 µs at 15^oC to 2.29 µs at 35^0C. The τ_F at different temperatures were calculated from the measured apparent time constants (τ_{app}) using the same branching ratio for each temperature since the ratio remained the same (table 1-1). The equation 2.6 is used and the data are plotted as (lnk) vs. (1/T) and the slope of the line was measured, which gives us the value for activation energy. The value for the formation of $EL346^S_{390}$ is 20 KJ/mole (4.8 kcal/mole) and the entropy of the adduct formation is -135.65 J/mole.K (-32.4 cal/mole.K) at room temperature

(295 K was used in calculations). The enthalpy of activation for the $EL346^{S}_{390}$ is similar compared to the EL222 molecule and the negative entropy value suggests that the reaction is entropically unfavorable. This suggests that changes in the FMN binding pocket of the protein needs to happen, including hydrogen bonding rearrangements, in order to overcome the unfavorable nature of this reaction and generate the transition state.

The EL368 protein shows similar values for the time constant as the EL346 did. All the experiments performed on the EL346 including the D_2O effect and the temperature control of the adduct formation, has been performed for this protein as well. From the absorption difference spectra, we calculated the branching ratio to be 65% forward from the triplet state to the adduct state ($EL368^{S}_{390}$) and 35% back to the ground state ($EL368^{D}_{450}$). While this ratio did not change at different temperatures it did change to a 1:1 ratio in D_2O containing samples. The EL368 shows (fig 4-14) almost seven times slowing of the adduct formation (τ_F =24.2 μs in D_2O versus 3.57 μs in H_2O both at room temperature). This result indicates that like EL346, a proton transfer reaction to N5 of the isoalloxazine ring of the FMN is the rate limiting step in the formation reaction. In EL368, a three exponential fit was used to fit the D_2O effect experimental data (fig 4-15). The added time constants of 2 μs and 200 μs are associated with the two spectra (b_2 and b_3) of the fit.

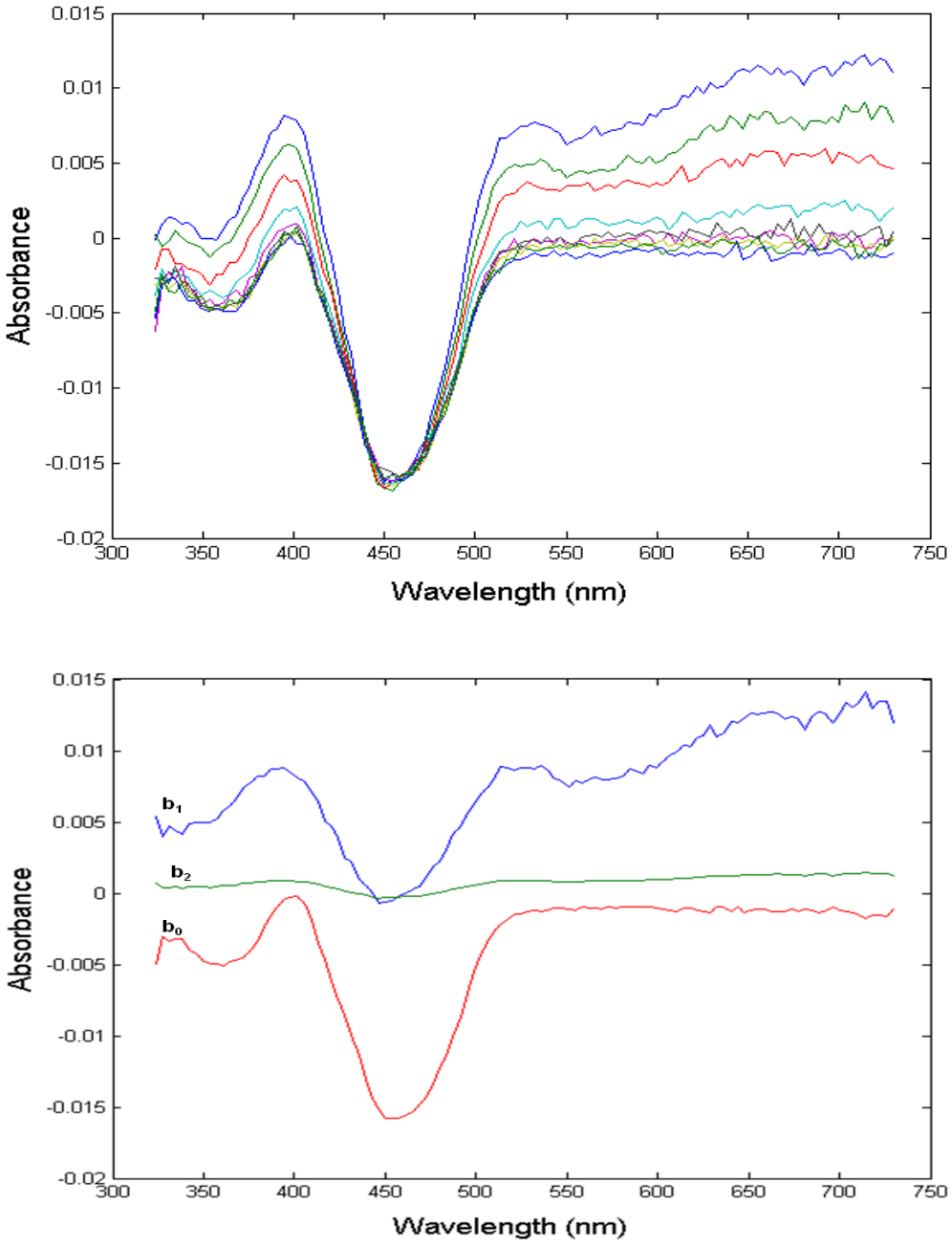

Figure 4-14 The absorption difference spectra of EL368 at room temperature after excitation with a 477nm laser pulse. Spectra were collected at 0.3, 1, 2, 5, 10, 100, 200, 500, 1000 µs. Bottom graph shows the results of global multi-exponential fitting of difference absorption spectra from EL368. The b_1 is the b-spectrum with an apparent rate constant of 2.32 µs, and b_0 is the spectrum of the product formed. The b_2 spectrum shows an apparent time constant of 1ms.

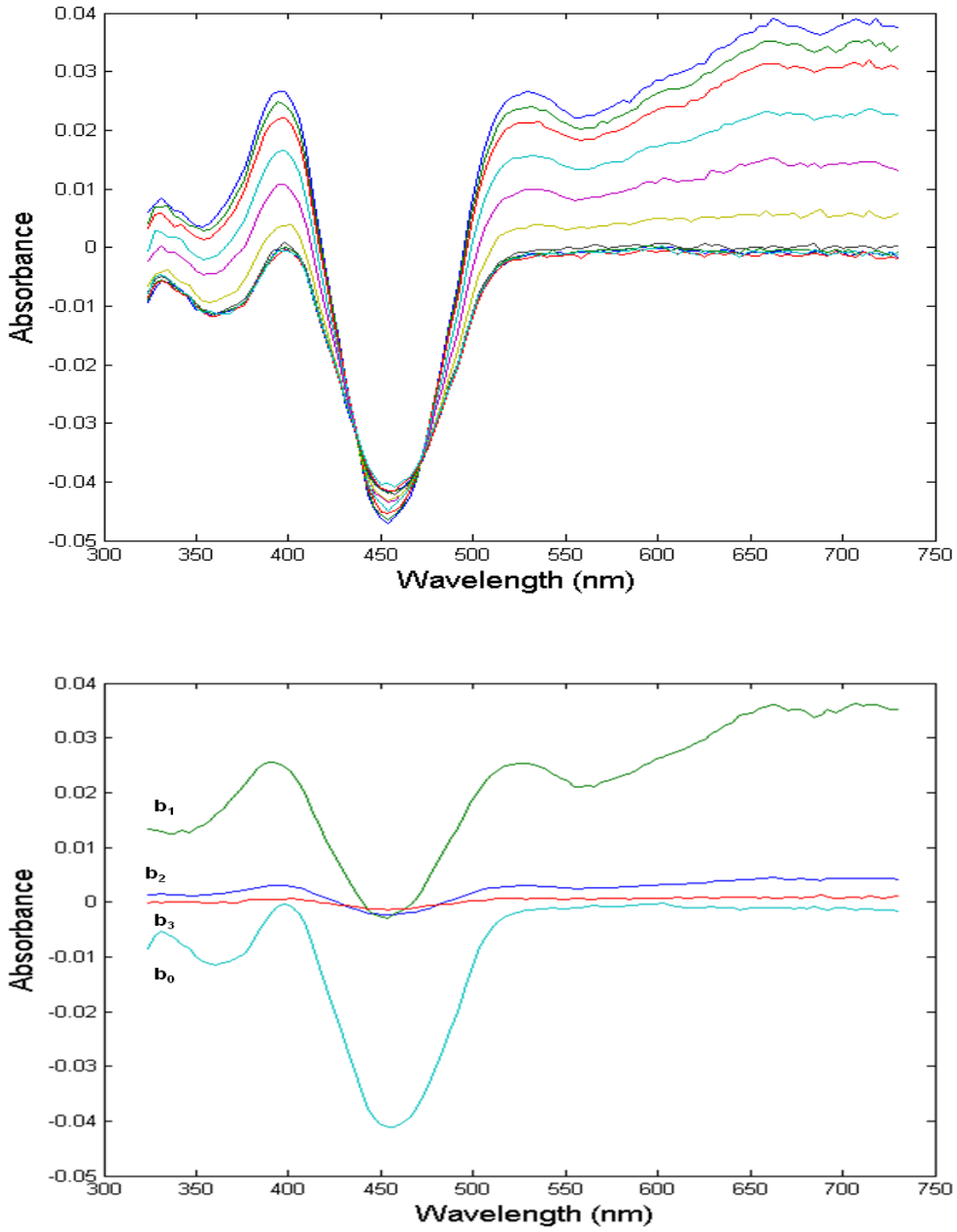

Figure 4-15 The absorption difference spectra of EL368 in D_2O at room temperature after excitation with a 477nm laser pulse. Spectra were collected at 0.3, 1, 2, 5, 10, 20, 50, 100, 200, 500, 1000 µs. Bottom graph shows the results of global multi-exponential fitting of difference absorption spectra from EL368. The b_1 is the b-spectrum with an apparent rate constant of 12.1 µs, and b_0 is the spectrum of the product formed. The b_2 spectrum has an apparent rate constant of 2 µs and b_3 200 µs.

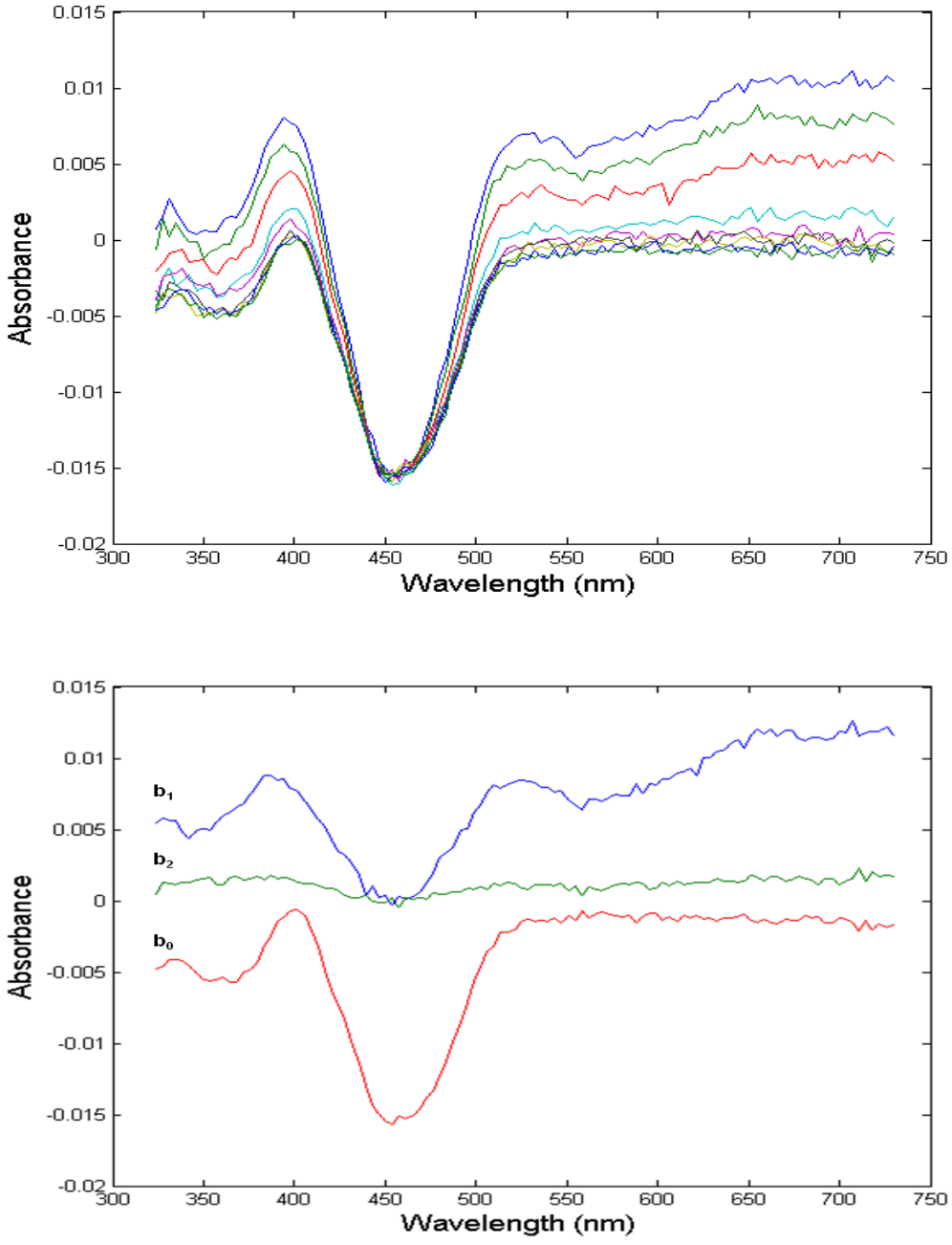

Figure 4-16 The absorption difference spectra of EL368 at 15℃ after excitation with a 477nm laser pulse. Spectra were collected at 0.3, 1, 2, 5, 10, 100, 200, 500, 1000 µs. Bottom graph shows the results of global multi-exponential fitting of difference absorption spectra from EL368. The b_1 is the b-spectrum with an apparent rate constant of 2.44 µs, and b_0 is the spectrum of the product formed. The b_2 spectrum shows an apparent time constant around 1ms.

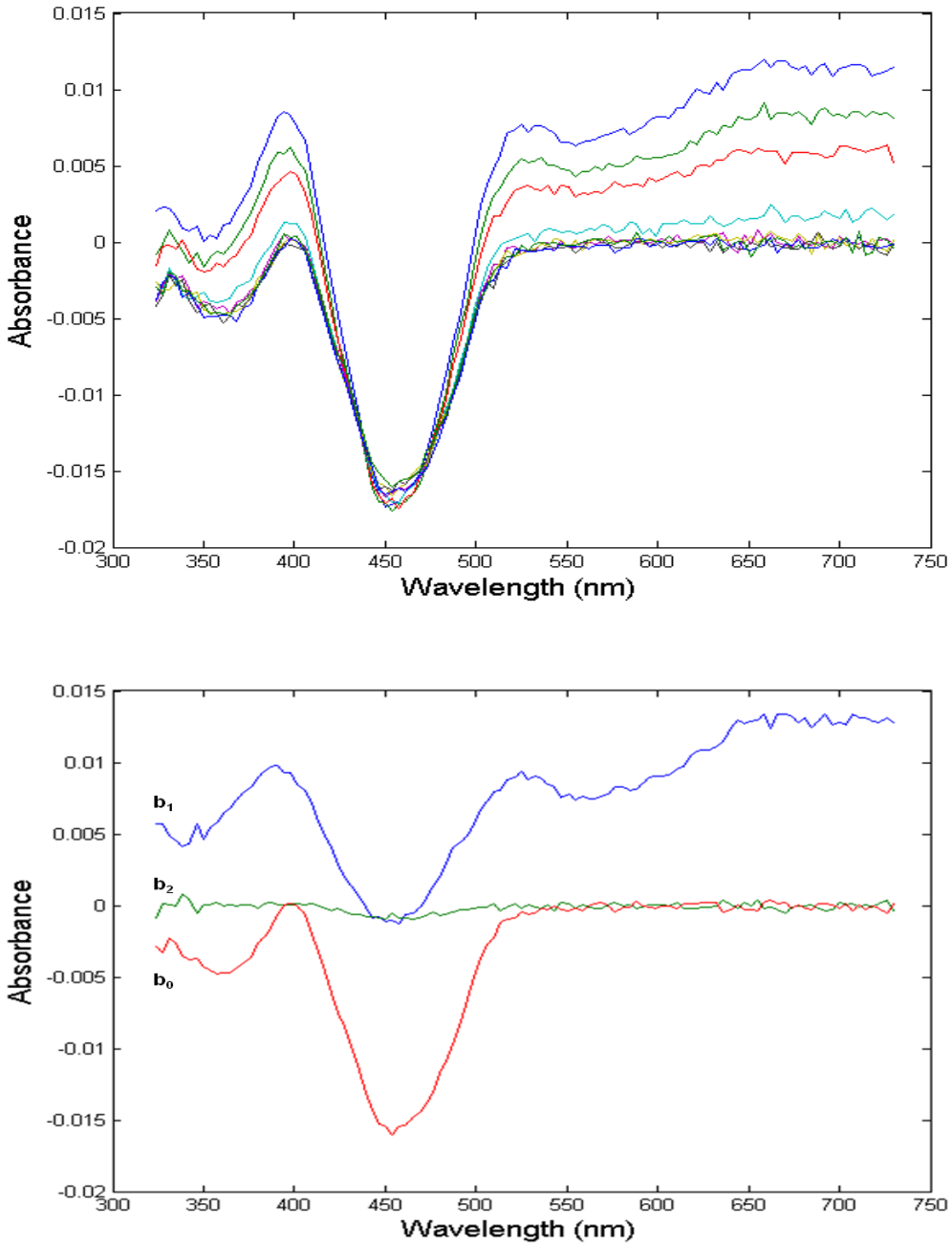

Figure 4-17 The absorption difference spectra of EL368 at 25℃ after excitation with a 477nm laser pulse. Spectra were collected at 0.3, 1, 2, 5, 10, 100, 200, 500, 1000 µs. Bottom graph shows the results of global multi-exponential fitting of difference absorption spectra from EL368. The b_1 is the b-spectrum with an apparent rate constant of 1.93 µs, and b_0 is the spectrum of the product formed. The b_2 spectrum shows an apparent time constant around 1ms.

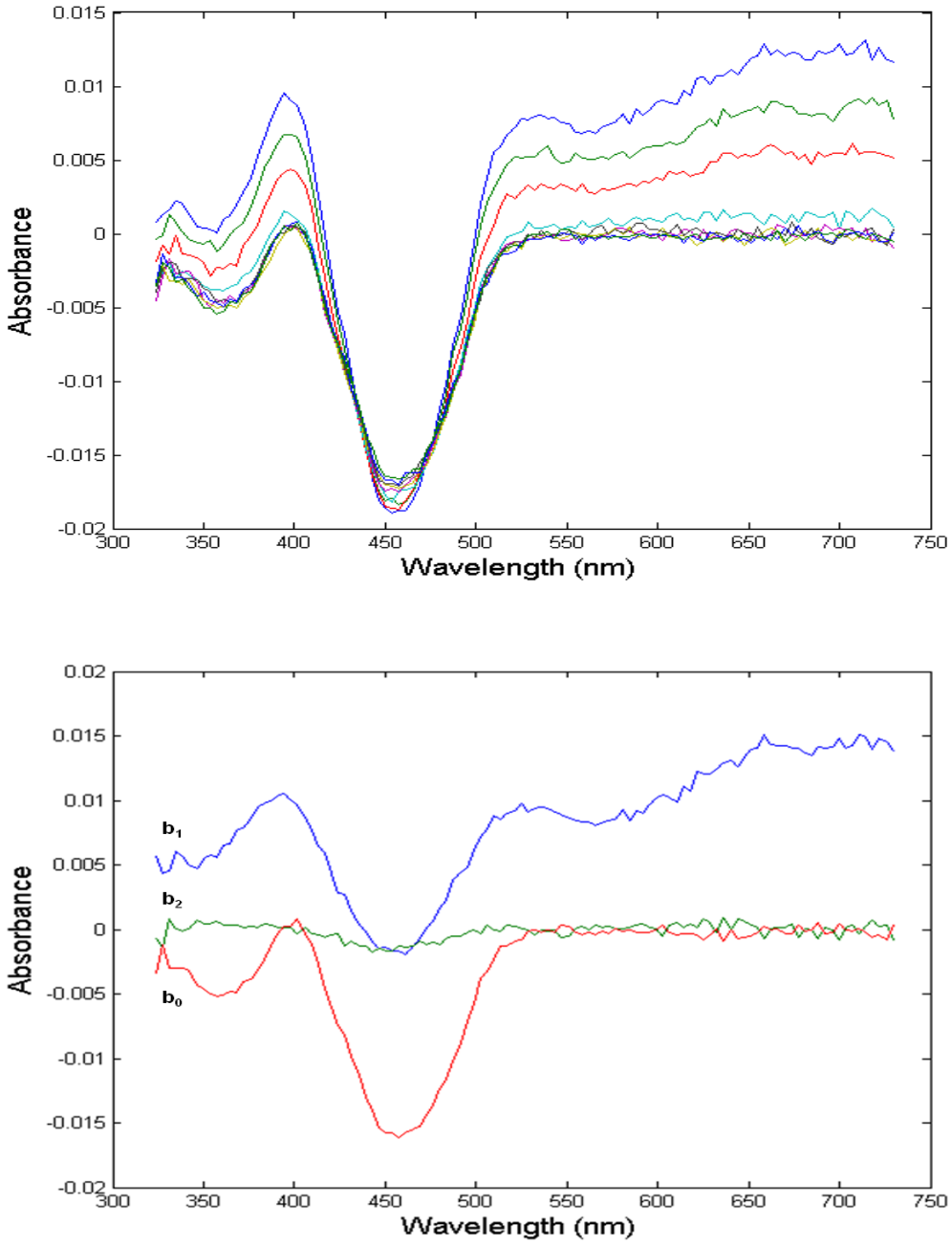

Figure 4-18 The absorption difference spectra of EL368 at 35℃ after excitation with a 477nm laser pulse. Spectra were collected at 0.3, 1, 2, 5, 10, 100, 200, 500, 1000 µs. Bottom graph shows the results of global multi-exponential fitting of difference absorption spectra from EL368. The b_1 is the b-spectrum with an apparent rate constant of 1.57 µs, and b_0 is the spectrum of the product formed. The b_2 spectrum shows an apparent time constant around 1ms.

EL368	τ_{app} (μs)	τ_F (μs)	τ_R (μs)
15℃	2.44	3.75	6.97
20℃	2.32	3.57	6.63
25℃	1.93	2.97	5.51
35℃	1.57	2.42	4.49
D_2O	12.1	24.2	24.2

Table 4-2 The apparent time constant, adduct formation, and return of the triplet to ground state time constants at various temperature and D_2O calculated using single exponential fitting and branching ratios.

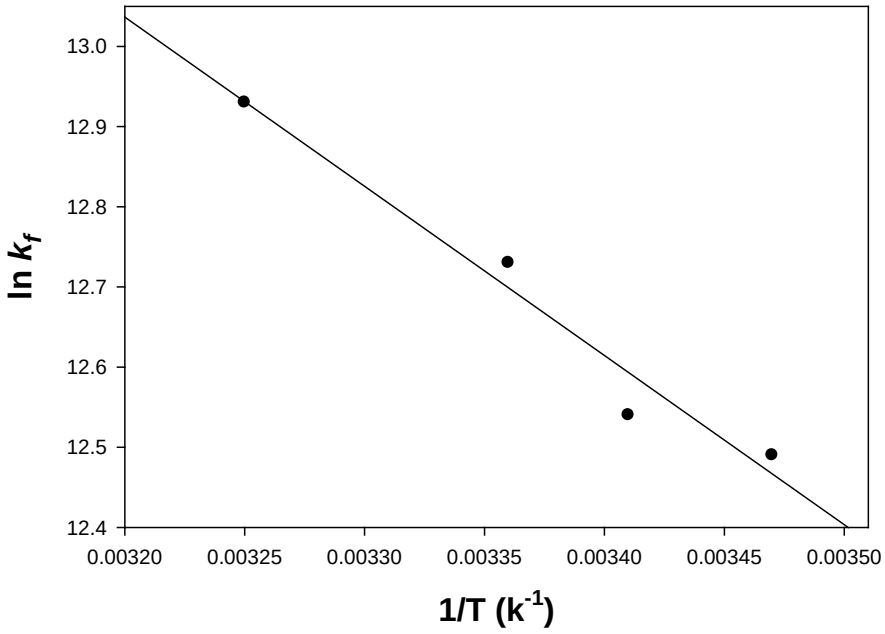

Figure 4-19 Arrhenius plot for the adduct formation kinetics of the EL368.

The additional time constants that are observed in the D_2O affect and the temperature experiments are expected from the free FMN in solution (fig 2-19) that can form semiquinone. We therefore conclude that the single exponential fit can explain the data and that additional time constants do not represent late processes. Bases on these results, we can explain the data with a linear scheme much like the EL346 adduct formation in the following way.

$$EL368^{D}{}_{450}\ (\tau_R) \leftarrow EL368^{L}{}_{660} \rightarrow (\tau_F)\ EL368^{S}{}_{390}$$

The values of τ_R and τ_F are given in table 4-2, which also includes the values for the temperature experiments. The temperature effect on the formation was studied at three additional temperatures of 15, 25, and 35℃ (fig 4-16, 4-17, and 4-18). For EL368, the adduct formation time constants changes from 3.75 µs at 15℃ to 2.42 µs at 35℃. In order to find the enthalpy of activation, data were plotted as (lnk) vs. (1/T) and the slope of the line was calculated. The activation energy value for the formation of $EL368^{S}{}_{390}$ species is 18 kJ/mole (4.2 kcal/mole.K) and the entropy of the adduct formation is -135.65 J/mole.K (-32.4 cal/mole.K) at room temperature. The comparable values for the enthalpy of formation between El346 and El368 indicates a similar mechanism of the adduct formation.

4.4 Discussion

EL346 and EL368 were identified as light activated histidine kinases before [2, 24] and we report a detailed photocycle study for these LOV containing histidine kinases. In the absence of any structural information, absorption spectroscopy is a

great tool to study these flavin containing molecules. Swartz el al. provided evidence that a LOV-domain regulated the HK domain in both of these molecules [2] and they demonstrated by light induced absorption difference spectra that a cysteinyl adduct is formed and then relaxes back to the dark state. The EL346 half life is reported as 28 min. (τ =40.4 min.) and the half life for EL368 is reported as 32 min. (τ =46.2 min.). High concentrations of imidazole accelerated the back reaction (data not shown), which indicates that the back reactions in these LOV-domains are based catalyzed. Additionally, there is evidence that the addition of ATP (Adenosine triphosphate) can accelerate the back reaction by two folds (private communication with Dr. Gardner's group). This is the first time that we observe other factors outside of LOV-domain can affect the recovery rate of the adduct. There is also some evidence that shows constructs of EL346, that contain mostly LOV-domains, have different back reaction time constants (back reaction becomes slower). These results are completely different than others, where we have demonstrated that in EL222 (chapter 2), and in *Brucella Melitensis* LOV-HK (private communications with Dr. Swartz), light activation and photocycle are the intrinsic properties of the LOV-domain. Although more studies need to be done, including the design of more mutants and constructs to address this in detail, it seems that at least for these two molecules, accessory domains and small molecules can affect the photocycle of their LOV-domains. We can find support for this idea through building a model for EL346 (based on LOV-domain from *Chlamydomonas Reinhardtii* as template) and EL368 (based on LOV-domain from *Erythrobacter Litoralis* as template) using the SWISS-MODEL

Workspace which is a structure homology modeling from ExPASy Bioinformatics Resource Portal [11-13]. Although we need to be careful in drawing conclusions based on theoretical modeling of the structure since they may contain significant errors, it can still provide us with useful information. Sequence alignment and modeling shows that the FMN binding pocket of EL368 and its interactions with the chromophore is similar to LOV2 (fig 4-5), yet the back reaction time constant has changed from 60 sec. in LOV2 to 46.2 min. in EL368. Our close inspection of the differences in their LOV-domain sequence did not reveal any obvious amino acids that could be responsible for such a large change. We have demonstrated that even a single change in the hydrogen bonding interactions between FMN and the binding pocket amino acids can cause major changes in back reaction time constants (chapter 3). It is therefore possible that in the EL368, other factors are contributing to the photocycle. The sequence alignment between EL346 and LOV2 (fig 4-6) and between EL346 and EL368 (fig 4-20) shows one major difference at position 72 of the EL346. An argenine that interacts with the ribityl chain of FMN is replaced with an alanine that does not hydrogen bond. This residue should be explored in future studies to see what affect it might have on the photocycle. Based on the function that these two LOV-HKs might be serving, it is possible that they are partly regulated by their effector domains through ATP molecules that interact with the CA domain of the HK. These results highlight the importance of studying full length LOV-effector domains versus the isolated LOV-domains in order to fully understand the details of

the activation mechanism, the regulation of the photocycle, and the downstream effects of these light sensory molecules.

Another interesting result of these experiments that needs to be discussed here is the additional time constant that was persistent in all EL368 measurements. LOV-domains exhibiting two time constants have been reported before [25]. The *chlamydomonas* phot-LOV1 contains intermediates similar to phot1-LOV2 but its triplet stare decays to the adduct state with two time constants of 800 ns and 4 μs. It should be mentioned that unlike LOV2 and the LOV-domains in this study, *Chlamydomonas* phot-LOV1 does not show any considerable return to the ground state from the triplet state (τ_R =27 μs). As discussed in the result section, FMN in the solution can also show these times constants and therefore the additional time constants seen might be due to free FMN in our sample. Experiments can be designed to address this question including performing the experiments under nitrogen (remove the oxygen that can re-oxidize the reduced flavin) to see if the time constants change. There are several important questions that remain and will be explored in future studies of these LOV-HK domains. Why is the back reaction for these proteins so slow? What are the light induced activation mechanisms of the kinase domain? Finally, what are the downstream effects of this activation? There are total of 23 response regulators identified in *Erythrobacter Litoralis*, so identification of the response regulator and therefore the function for these two LOV-HKs are possible in future studies.

```
             20        30        40        50        60        70
EL346  IYVNRAFEQMTGYSRSSVVGRNCRFLQGEKTDPGAVERLAKAIRNCEEVEETIYNYRADG
       .:::.:: ..::::.:  .:::::::::::  :::  :..: ..:    . .    . ::: ::
EL368  VYVNQAFLDLTGYAREEIVGRNCRFLQGADTDPEQVRKLREGIAAERYTVVDLLNYRKDG
              10        20        30        40        50        60

             80        90       100
EL346  EGFWNHLLMGPLEDQDEKCRYFVGIQVD
         ::: . .:::.  .:   .:: : : :
EL368  IPFWNAVHVGPIYGEDGTLQYFYGSQWD
              70        80
```

Figure 4-20 Sequence comparison of LOV-domains between EL346 and EL368. The sequences show 46.6 % identity in 88 residues overlap.

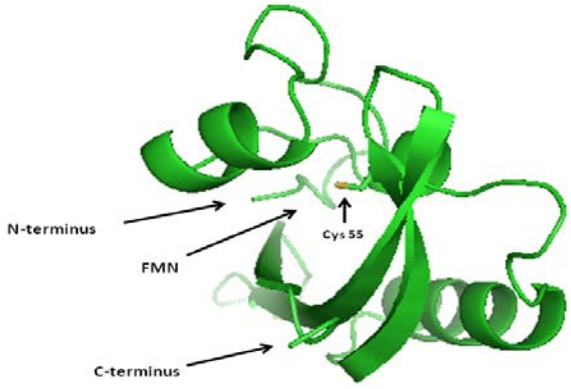

Figure 4-21 Model for EL346 (based on LOV-domain from *Chlamydomonas Reinhardtii* as template) showing active cysteine at position 55. The arrows show the N-terminus and C-terminus of the protein and the location of the FMN that is missing in this model due to differences in conserved binding pocket of FMN.

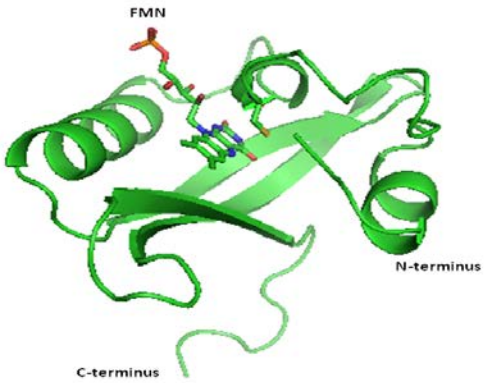

Figure 4-22 Model for EL368 (based on LOV-domain from *Erythrobacter Litoralis* as template) showing active cysteine at position 93. The N-terminus, C-terminus, and FMN of the protein are shown in the figure.

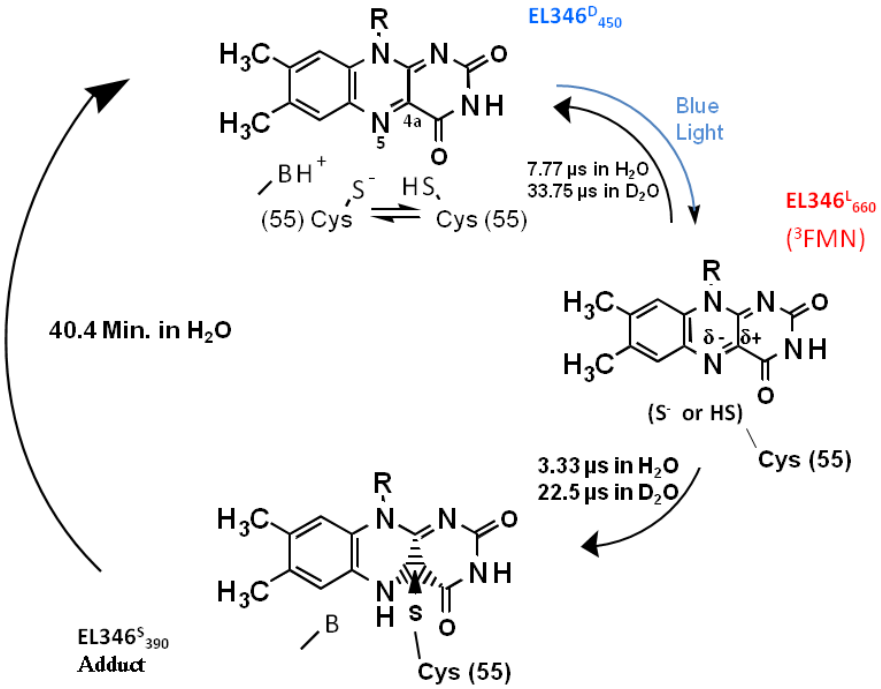

Figure 4-23 Photocycle scheme and proposed reaction mechanism for EL346.

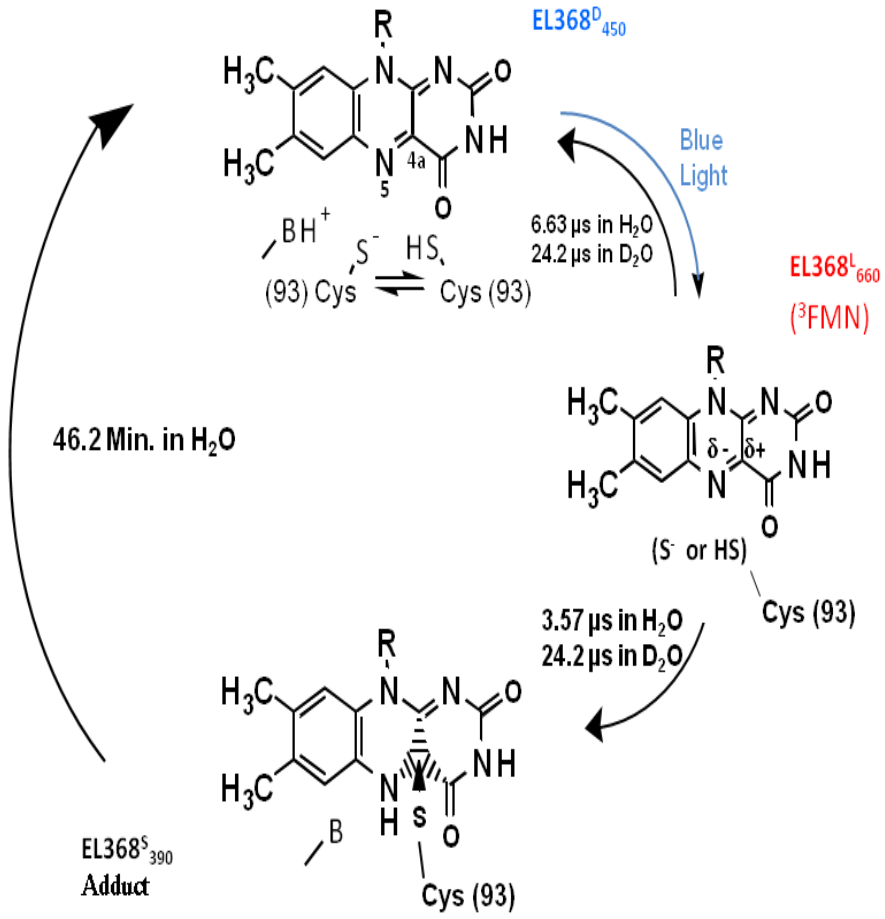

Figure 4-24 Photocycle scheme and proposed reaction mechanism for EL368.

References:

1. Van der Horst, M.A. and K.J. Hellingwerf, *Photoreceptor proteins, "star actors of modern times": A review of the functional dynamics in the structure of representative members of six different photoreceptor families.* Accounts of Chemical Research, 2004. **37**(1): p. 13-20.

2. Swartz, T.E., et al., *Blue-light-activated histidine kinases: Two-component sensors in bacteria.* Science, 2007. **317**(5841): p. 1090-1093.

3. Losi, A., *The bacterial counterparts of plant phototropins.* Photochemical & Photobiological Sciences, 2004. **3**(6): p. 566-574.

4. Crosson, S., S. Rajagopal, and K. Moffat, *The LOV domain family: Photoresponsive signaling modules coupled to diverse output domains.* BIOCHEMISTRY, 2003. **42**(1): p. 2-10.

5. Purcell, E.B., et al., *A photosensory two-component system regulates bacterial cell attachment.* Proceedings of the National Academy of Sciences of the United States of America, 2007. **104**(46): p. 18241-18246.

6. West, A.H. and A.M. Stock, *Histidine kinases and response regulator proteins in two-component signaling systems.* Trends In Biochemical Sciences, 2001. **26**(6): p. 369-376.

7. Barrett, J.F. and J.A. Hoch, *Two-component signal transduction as a target for microbial anti-infective therapy.* Antimicrobial agents and chemotherapy, 1998. **42**(7): p. 1529-1536.

8. Oh, H.-M., et al., *Complete Genome Sequence of Erythrobacter litoralis HTCC2594.* J. Bacteriol., 2009. **191**(7): p. 2419-2420.

9. Dutta, R., L. Qin, and M. Inouye, *Histidine kinases: diversity of domain organization.* Molecular Microbiology, 1999. **34**(4): p. 633-640.

10. Swartz, T., et al., *The photocycle of a flavin-binding domain of the blue light photoreceptor phototropin.* JOURNAL OF BIOLOGICAL CHEMISTRY, 2001. **276**(39): p. 36493-36500.

11. Arnold, K., et al., *The SWISS-MODEL workspace: a web-based environment for protein structure homology modelling.* Bioinformatics, 2006. **22**(2): p. 195-201.

12. Bordoli, L., et al., *Protein structure homology modeling using SWISS-MODEL workspace.* Nat. Protocols, 2008. **4**(1): p. 1-13.

13. Schwede, T., et al., *SWISS-MODEL: an automated protein homology-modeling server.* Nucleic Acids Research, 2003. **31**(13): p. 3381-3385.

14. Bateman, A., et al., *The Pfam protein families database.* Nucleic Acids Research, 2004. **32**(suppl 1): p. D138-D141.

15. Finn, R.D., et al., *The Pfam protein families database.* Nucleic Acids Research, 2010. **38**(suppl 1): p. D211-D222.

16. Christie, J.M., et al., *LOV (light, oxygen, or voltage) domains of the blue-light photoreceptor phototropin (nph1): binding sites for the chromophore flavin mononucleotide.* Proc Natl Acad Sci U S A, 1999. **96**(15): p. 8779-83.

17. Lewis, J.W. and D.S. Kliger, *Microliter flow cell for measurement of irreversible optical absorbance transients.* Review of Scientific Instruments, 1993. **64**(10): p. 2828-2833.

18. Kliger, D.S., J.W. Lewis, and C.E. Randall, *Polarized light in optics and spectroscopy*. 1990, Boston: Academic Press. x, 304.

19. Grebe, T.W. and J.B. Stock, *The Histidine Protein Kinase Superfamily*, in *Advances in Microbial Physiology*, R.K. Poole, Editor. 1999, Academic Press. p. 139-227.

20. Szundi, I., J.W. Lewis, and D.S. Kliger, *Deriving reaction mechanisms from kinetic spectroscopy. Application to late rhodopsin intermediates.* Biophysical Journal, 1997. **73**(2): p. 688-702.

21. Stanley, R.J., *Advances in flavin and flavoprotein optical spectroscopy.* Antioxidants & Redox Signaling, 2001. **3**(5): p. 847-866.

22. Corchnoy, S., et al., *Intramolecular proton transfers and structural changes during the photocycle of the LOV2 domain of phototropin 1.* JOURNAL OF BIOLOGICAL CHEMISTRY, 2003. **278**(2): p. 724-731.

23. Tseng, T.-S., et al., *Light-activated bacterial LOV-domain histidine kinases.* Methods in enzymology, 2010. **471**: p. 125-134.

24. Correa, F., et al., *Blue Light regulated two-component systems: Enzymatic and functional analyses of Light-Oxygen-Voltage (LOV)-histidine kinases and downstream response regulators.* Biochemistry, 2013. **52**(27): p. 4656-4666.

25. Kottke, T., et al., *Phot-LOV1: Photocycle of a blue-light receptor domain from the green alga Chlamydomonas reinhardtii.* BIOPHYSICAL JOURNAL, 2002. **84**(2): p. 1192-1201.